50X1

206

PROGRAM REPORT

VOLUME

21

APPENDIXES 40 AND 41

206

PROGRAM REPORT

VOLUME

21

APPENDIXES 40 AND 41

CONTENTS

APPENDIX 40

AIR FORCE, GENERAL SYSTEM ENGINEERING/TECHNICAL

DIRECTION AND ASSOCIATE CONTRACTOR RESPONSIBILITIES

(AF EXHIBIT 61-10)

APPENDIX 41

FINAL FLIGHT EVALUATION REPORT

i

APPENDIX 40

AIR FORCE, GENERAL SYSTEM ENGINEERING/TECHNICAL

DIRECTION AND ASSOCIATE CONTRACTOR RESPONSIBILITIES

(AF EXHIBIT 61-10)

This document contains 17 pages.

SAFSP-206 Exhibit 61-10
Dated 18 Feb 1963
Supercedes Exhibit
Dated 27 July 1962

AIR FORCE, GENERAL SYSTEM ENGINEERING/TECHNICAL DIRECTION AND ASSOCIATE CONTRACTOR RESPONSIBILITIES FOR PROGRAM 206

1.0 PURPOSE

This document defines the general area of coordination and integration responsibilities for the various contractors. The requirements resulting therefrom will be itemized and priced against the basic work specification for each associate contractor. Specific responsibilities are delineated in contract work specifications and take precedence over this document.

2.0 MANAGEMENT

The Program Office, SAFSP-206, is responsible for providing the necessary management control.

3.0 DIVISIONS OF RESPONSIBILITIES

3.1 Aerospace Corporation

Aerospace Corporation, has responsibility for general system engineering as defined in its basic contract. The scope of these responsibilities shall include:

3.1.1 System analysis and preparation of system specifications. Review of environmental design criteria and environmental test levels.

3.1.2 Review of interface specification for the Atlas/Agena D, and Satellite Vehicle. Review of associate contractor specifications to assure compliance with system requirements.

Din 63REHPGE9986

SAFSP-206-0-55

1

3.1.3 Definition of interface requirements between flight vehicle TT&C subsystem, and ground environment.

3.1.4 Definition and preparation of requirements for program peculiar ground support including TT&C environment, MAB, and launch operations, on-orbit operation, and re-entry.

3.2 Aerospace Corporation

Aerospace Corporation, with coordination and approval of the Air Force will execute technical directions for the following:

3.2.1 Satellite Vehicle configuration and its interfaces.

3.2.2 The Atlas D/Agena D mission peculiar equipment. The technical directions will include the isolation of technical weaknesses and applications of new data, new developments, and modified requirements.

3.3 Associate Contractors

The following is a list of the associate contractors and their physical responsibilities.

3.3.1 The Astronautics Division of General Dynamics is responsible for manufacture, test, and delivery of Atlas D boosters, and AGE. GD/A will also provide launch services for the Atlas D booster; the required support in engineering, PALC II Maintenance, test, launch planning, launch, test evaluation; and other services defined in contracts AF 04(647)-699, AF 04(647)-47, and AF 04(694)-185. In addition, GD/A will prepare powered flight guidance equations for the Atlas D/Agena D launch vehicle. GD/A will accomplish installation and checkout services as defined in the PALC II Activation effort under contract AF 04(647)-188 as modified to incorporate GE Interface Specification SVS 4206.

63REHPGE9986
SAFSP-206-0-55

2

3.3.1.1 GE-BSD will be responsible for providing to GD/A the Mark II Airborne Guidance Equipment for the Atlas D Booster in accordance with Air Force Contract AF 04(647)-872 and assisting the 6595th Aerospace Test Wing personnel operating the Mark II Sergeant Ground Station at Vandenberg AFB in accordance with Contract AF 04(647)-152.

3.3.1.2 The Burroughs Corporation will be responsible for providing technical advice for the 6595th ATW personnel (operating the modified MARK II SGTS Ground Station at Vandenberg AFB) and the wiring computer programs in accordance with Air Force Contract AF 04(647)-282.

3.3.2 The Lockheed Missile & Space Company will be responsible for manufacture, test, and delivery of Agena D boosters and modifications to 206 configurations and AGE. LMSC will also provide launch services for the Agena D booster; the required support in engineering, test planning, test, launch planning, launch, test evaluation; and other services defined in Contracts AF 04(695)-68, AF 04(695)-92, and AF 04(695)-52. LMSC will accomplish installation and checkout services as defined in the PALC II Activation effort under Contract AF 04(695)-131 as modified to incorporate GE Interface Specifications SVS 4206.

3.3.3 The Advanced Space Projects Department of the General Electric Company (GE-ASPD), is responsible for design, development, manufacture, test, and delivery of the Satellite Vehicle and associated AGE. This contractor will also provide launch, on-orbit and retrieval services for the satellite vehicle; required support in engineering, test, launch planning, launch, and test evaluation; and other services defined in Contracts AF 04(695)-76 and AF 04(695)-155.

3.3.4 Space Technology Laboratories is responsible for development of procedures and computer programming providing for orbit selection, on-orbit planning, and shall support on-orbit operations as required.

63REHPGE9986
SAFSP-206-0-55

3

3.4 Associate Air Force Agencies

3.4.1 SSV/SSVZ (Atlas Booster Program Office)

Responsible for procurement and production surveillance of the Atlas Booster. Atlas Launch Services and PALC II Activation as indicated in paragraph 3.3.1.

3.4.2 SSD (Agena D Program Office)

Responsible for procurement and production surveillance of the Agena D Booster, Agena D Launch Services and PALC II Activation contracts as indicated in paragraph 3.3.2.

3.4.3 SSO Satellite Vehicle Operations (SSOC, SSOQ, SSOT)

Responsible for all contractor actions required of specific supporting contractor contributing to the common TT&C ground network support of Program 206.

Specific Contractor partial list.

Aerospace System Development Corporation, Lockheed Missile & Space Company, and Philco.

3.4.3.1 Aerospace Corporation is responsible for system engineering and technical direction for Satellite Control Facility implementation, standarization and augmentation.

3.4.3.2 System Development Corporation is responsible for computer program integration and computer program utility systems.

3.4.4 SSN (Facilities Office)

Responsible for procurement and constructions surveillance of all facilities and facility hardware requirements as determined by the respective program offices.

63REHPGE9986
SAFSP-206-0-55

4

3.4.5 The 6595th ATW will be responsible for launch base integration, operation, and evaluation of Program 206 through satellite vehicle injection.

3.4.6 The 6594th ATW will be responsible for the SCF readiness for on-orbit operation commencing at satellite vehicle injection and for retrieval operation through termination.

4.0 DEFINITION OF RESPONSIBILITIES

4.1 Interface Responsibilities

Interface specifications and appropriate technical data will be forwarded to the respective Air Force Program Office for review, coordination and approval.

4.1.1 Atlas/Agena D. LMSC has over-all responsibility.
GD/A will provide support to LMSC.

4.1.2 Agena D/Satellite Vehicle. The Satellite Vehicle Contractor (GE-ASPD) has over-all responsibility. LMSC will provide technical support to the Satellite Vehicle Contractor.

4.1.3 The respective associate contractors will respond to and support Aerospace Corporation meetings as required by the fulfillment of their GSE/TD responsibilities.

4.1.4 Technical Interface coordination and surveillance between the Launch MAB facilities and the SCF will be the responsibilities of the Aerospace Corporation.

63REHPGE9986
SAFSP-206-0-55

5

4.2 Tracking, Telemetry, and Control (TT&C)

4.2.1 Aerospace Corporation

Aerospace Corporation will accomplish General Systems Engineering and Technical Direction of the TT&C equipment and its interfaces with the ground environment. This will include, but will not be limited to, the following work:

4.2.1.1 Prepare and/or review studies defining program requirements.

4.2.1.2 Review the associate contractor's vehicle TT&C configuration and insure its compatibility with the ground environment.

4.2.1.3 Prepare or review ground environment studies and data, and assist the Air Force to establish requirements by preparation of suitable documentation and specifications. Monitor and review associate contractor's TT&C tests.

4.2.1.4 Monitor and review the associate contractor's computer program development.

4.2.2 General Electric - ASPD

The General Electric - ASPD will provide technical and administrative effort in support of the satellite vehicle, its test, launch and on-orbit operation, and re-entry operation as follows:

4.2.2.1 Design, develop, manufacture, test, and integrate TT&C equipment, into the Satellite Vehicle in accordance with approved specification requirements.

4.2.2.2 Conduct studies and prepare technical data in the form of specification, reports, etc., to provide for TT&C compatibility of the vehicle and ground environment.

63REHPGE9986
SAFSP-206-0-55

6

4.2.2.3 Provide system technical data as necessary and assist the Air Force in planning for the integrated operation of the Satellite Test Annex and tracking stations.

4.2.2.4 Define data processing requirements in accordance with approved plans and submit same to the Air Force/Aerospace Program Office for review and approval. This effort includes:

4.2.2.4.1 Prepare computer programming for post pass data collection and post flight data processing.

4.2.2.4.2 Prepare operational computer programs for vehicle control.

4.3 Vandenberg Air Force Base/Missile Assembly Building (MAB)

4.3.1 The 6595th Aerospace Test Wing will:

4.3.1.1 Be responsible for MAB operations to include necessary integration of MAB functions.

4.3.1.2 Provide vehicle and Pad readiness certification to the SAFSP Program Director for all elements of the Aerospace vehicle (Atlas/Agena/Satellite Vehicle).

4.3.1.3 Prepare and/or coordinate operating security plans.

4.3.2 Aerospace Corporation will:

4.3.2.1 Serve as technical advisor to the Air Force for assembly, subsystem tests and systems runs. (In the exercise of GSE/TD responsibilities, Aerospace will utilize normal management procedures as established for the basic program.)

63RE HPGE9986
SAFSP-206-0-55

7

4.3.2.2 Observe in tests and validation operations as deemed necessary in the fulfillment of GSE/TD responsibilities.

4.3.2.3 Review over-all system run data against performance specifications and present the results and recommendations to the Air Force.

4.3.3 The General Electric - ASPD will:

4.3.3.1 Provide and distribute a coordinated up-dated milestone schedule of all Program 206 activities at Vandenberg AFB, incorporating inputs to be provided by GD/A and LMSC, to include the time period of apprival of S.V. and booster until launch.

This schedule will include day-to-day activities in MAB and Total R-Day work at the launch complex.

4.3.3.2 Deliver the S.V. to the MAB for assembly, subsystem tests, and systems run prior to movement to the launch complex.

4.3.3.3 Provide test conductor and perform the necessary tests on S.V. Also GE will be responsible for the provision of coordinated test procedures to the VTS for open loop testing.

4.3.3.4 Submit all test procedures and support requirements to SAFSP-206 for review and approval.

4.3.3.5 Conduct systems test data review meetings where test results will be presented to Aerospace Corporation and the 6595th ATW.

4.3.3.6 Be responsible for over-all program security in the 206 MAB and VSP.

63REHPGE9986
SAFSP-206-0-55

8

4.4 Launch Operations

4.4.1 The 6594th Aerospace Test Wing will:

4.4.1.1 Be responsible for Launch Operations and provide the Launch Test Controller.

4.4.1.2 Be responsible for integration of associate contractors' effects in preparation for launch.

4.4.1.3 Be responsible for preparation, coordination, publication and distribution of all joint test procedures including the countdown manual. (6595th ATW may designate one of the associate contractors to be responsible for editing, printing and publication.)

4.4.1.4 Conduct data review meetings of all validation tests.

4.4.1.5 Be responsible for launch readiness determination.

4.4.1.6 Provide detailed coordination of launch complex activities. (6595th ATW may select personnel assistance from associate contractors in the accomplishment of this responsibility.)

4.4.1.7 Prepare and/or coordinate security plans.

4.4.2 Each associate contractor will:

4.4.2.1 Be responsible for the necessary security measures to protect his own equipment.

4.4.2.2 Be responsible for installation and checkout of his equipment and for the preparation of test procedures concerning only his equipment.

63REHPGE9986
SAFSP-206-O-55

9

4.4.2.3 Be required to man consoles controlling his equipment, furnish associate test conductors and assist in the preparation of joint test procedures.

4.4.2.4 Provide a responsible individual at the launch complex during any working hours when his vehicle or booster is at the complex.

4.4.2.5 Provide evaluation of data from each validation test for presentation at the data review meetings. These data will be evaluated by a segment of the contractor's organization that is separate from that performing the tests.

4.4.3 General Electric – ASPD will:

4.4.3.1 Continue to provide the up-dated milestone schedule as outlined in paragraph 4.3.3.1 above.

4.4.3.2 Be responsible for all operations in the Vehicle Service Building.

4.4.3.3 Be responsible for S/V system tests at the launch site.

4.4.4 Lockheed Missiles & Space Company will:

4.4.4.1 Provide inputs to the hour-by-hour detailed coordinated launch complex schedule.

4.4.5 General Dynamics/Astronautics will:

4.4.5.1 Provide maintenance and common AGE support for the launch complex.

4.4.5.2 Provide inputs to the hour-by-hour detailed coordinated launch complex.

63REHPGE9986
SAFSP-206-O-55

10

4.4.6 Aerospace Corporation will:

4.4.6.1 Support the 6595th ATW as required.

4.5 On-Orbit Operations

4.5.1 The 6594th Aerospace Test Wing will:

4.5.1.1 Be responsible for the on-orbit test operation of satellite vehicle and the collection and analysis of specified data associated with this phase of operation.

4.5.1.2 Be responsible for the over-all management and operational control of all Satellite Control Facilities (SCF) utilized in on-orbit operations, and will provide the orbit test controller.

4.5.1.3 Be responsible for preparation, approval, publication and distribution of all operational test documentation required by the SCF for determining the readiness of the SCF to support launch and orbital operations, including participation in the acceptance of new SCF equipments required by this program.

4.5.1.4 Be responsible for determining the readiness of the SCF to support launch and orbital operations, including participation in the acceptance of new SCF equipments required by this program.

4.5.1.5 Determine and submit to the Program Director, SAFSP-206, associate contractor support requirements for documentation, technical meetings or training required by the 6594th Aerospace Test Wing.

63REHPGE9986
SAFSP-206-O-55

11

4.5.1.6 Prepare and/or coordinate security plans.

4.5.2 Associate Contractors will:

4.5.2.1 Furnish adequate information and sufficient formal training, as approved by SAFSP-206, to familiarize 6594th Aerospace Test Wing personnel with new or unique equipments, computer programs or specialized equipment operational procedures.

4.5.2.2 Will comply with current agreements between SSD and ground station Integration Contractors. This will include but not be limited to helping the Integrating Contractors with the following:

4.5.2.2.1 Preparation of an Activation Plan and a Detailed Integrated Activation Schedule.

4.5.2.2.2 Submission of a weekly status report based upon the Activation Schedule.

4.5.2.2.3 Preparation of Phase IV equipment acceptance tests procedures to be submitted to SSD/6594th Aerospace Test Wing prior to start of Phase IV Activity.

4.5.2.3 Provide technical support to the Test Controller through the technical staff.

4.5.2.4 Provide representation within the Test Controllers supporting structure.

4.5.2.5 Perform data analysis and interpretation which will be used to provide recommendation for action during orbit operations to the Test Controller through the Test Advisor.

4.5.2.6 Participate Orbital Test Working Group meetings.

63REHPGE9986
SAFSP-206-O-55

12

4.5.2.7 Provide data inputs for specified flight evaluation reports in accordance with instruction from Test Advisor.

4.5.2.8 Rewrite as Follows: Provide support to the 6594th ATW for preparation of the Program Test Operations Order as required by the Program Office.

4.5.3 Aerospace Corporation will:

4.5.3.1 Assume the technical direction function and will provide the technical advisor staff.

4.5.3.2 Coordinate the activities of technical staff composed of the satellite vehicle contractor and associate contractors to perform real-time analysis of satellite vehicle functions.

4.5.3.3 Provide approved test plans and objectives to SAFSP-206 to enable 6594th ATW operational directives to be generated preceding each flight.

4.5.3.4 Prepare and submit to SAFSP-206 a 7-day Preliminary Flight Report and 45-day Final Flight Evaluation Report which will include associate contractor data inputs.

4.5.4 Computer Programming Associate Contractor will:

4.5.4.1 Provide a minimum of personnel at the STA, in an on-call status, to support the program peculiar computer programming effort.

4.5.4.2 Exercise the support function as members of the Test Director Staff.

63REHPGE9986
SAFSP-206-O-55

13

4.6 Retrieval Operations

4.6.1 6594th Aerospace Test Wing will:

4.6.1.1 Operate, maintain and support the Satellite Control Facility (SCF) for tracking, control, impact prediction data acquisition, data processing (Data reduction), and is responsible for all facets of the retrieval operation. This responsibility includes the operational control of all retrieval forces until termination.

4.6.1.2 Prepare and/or coordinate security plans.

4.6.2 General Electric Company will:

4.6.2.1 Over water operation

4.6.2.1.1 Be responsible for providing engineering representation at Hickam AFB to the 6594th Recovery Control Group. The support shall consist of one representative to provide liaison services to the 6594th RCG for Program 206 activity.

4.6.2.1.2 Be responsible for furnishing adequate information and sufficient formal training to familiarize the 6594th ATW personnel and others with new or unique equipment or specialized equipment operational procedures.

4.6.3 The Aerospace Corporation will:

4.6.3.1 Provide technical assistance in the form of studies, evaluations and guidance in the establishment of general requirements of retrieval operations.

63RE HPGE9986
SAFSP-206-O-55

14

4.7 Flight Configuration Control

Configuration control of flight vehicle and facilities will be maintained by the individual agency providing the vehicle or complex. The following agencies have application within Program 206. Atlas booster SSVZC, Agena booster SSZA, Satellite Vehicle GE-ASPD, Satellite Control Facility SSOC, Launch facility SSVZO, and SSZAK.

4.8 Test Evaluation and Reporting

To assist the SPO in accomplishing its test evaluation and reporting responsibility, Aerospace will provide the preparation of required reports for the area of launch, on-orbit operation, retrieval, and technical test evaluation. The 6595th and 6594th Aerospace Test Wings will issue the launch reports and orbit/retrieval reports respectively.

63REHPGE9986
SAFSP-206-O-55

15

SAFSP-206 Exhibit 61-10
Addendum No. 1
6 August 1963

AIR FORCE, GENERAL SYSTEM ENGINEERING/TECHNICAL DIRECTION AND ASSOCIATE CONTRACTOR RESPONSIBILITIES FOR PROGRAM 206

Addendum No. 1

Revise Paragraph 4.5.1.3 as follows:

Delete all after "by the SCF for"

Add after "by the SCF for" – "conduct of the orbital operations."

16

Exhibit 61-10
Addendum No. 2
6 December 1963

AIR FORCE, GENERAL SYSTEM ENGINEERING/TECHNICAL DIRECTION AND ASSOCIATE CONTRACTOR RESPONSIBILITIES FOR PROGRAM 206

1, Change "SAFSP-206 to [   ] throughout Exhibit 61-10.

2. Change Paragraph 4.2.2.4.1 to read:

"Maintain computer programming for post pass data collection and post flight

data processing."

3. Change Paragraph 4.5.2.7 to read:

"Provide flight summary inputs into Aerospace Post Flight Report."

4. Delete Paragraph 4.6.2.1.1

5. Delete Paragraph 4.6.2.1.2

6. Add Paragraph 4.6.2.1.3

"Provide technical assistance in the form of studies, evaluation and guidance

for the accomplishment of retrieval operations."

APPENDIX 41

FINAL FLIGHT EVALUATION REPORT

DIN 64SD4760
26 September 1964

This document contains 236 pages.

FINAL FLIGHT EVALUATION REPORT (S)

SV 960

CONTRACT NO. AF 04(695)-155

Approved By: _M. Binegar_ for

L. Binegar, Manager
206 Program

GENERAL ⟨GE⟩ ELECTRIC

MISSILE AND SPACE DIVISION
ADVANCED SPACE PROJECTS DEPARTMENT
P.O. BOX 8661, PHILADELPHIA 1, PA.

LIST OF EFFECTIVE PAGES

The total number of pages in this publication is 236 consisting of the following:

Title

A

i thru xvi

1-1 thru 1-24

2-1 thru 2-54

3-1 thru 3-132

4-1 thru 4-6

R-1 to R-2

A

FOREWORD

This Final Flight Evaluation Report on the flight of Vehicle 960 is prepared in response to the USAF Requirement Paragraph 6.4.3.1.4 of the Program 206 Work Specification, Phase B, dated 7 March 1963, SAFSP-206 Exhibit 63-2, Contract AF 04(695)-155.

64SD4760

PROGRAM SUMMARY

Program 206 is directed toward the launching of precisely controlled, near-space, orbiting platforms with orbit adjust and recovery capability. Ten Satellite Vehicles have repeatedly demonstrated operational feasibility and have proven the basic design philosophies by partially or totally accomplishing mission objectives on every flight. Major program decisions in the selection of the Satellite Re-entry Vehicle (SRV), the restartable ablative orbit adjust engines, the gimballed attitude reference and integral three-axis rate sensing systems, and the digital command system with four selective storage lines have been justified.

Excellence of the design has been shown by such capabilities as performing at perigees below 70 nautical miles, recovery to preplanned conditions from anomalous injection into a 57 nautical mile perigee orbit, and "ten for ten" successful air snatches of the SRV capsule. "State-of-the-art" advancements have accrued including identification of magnitudes of seasonal and geoegraphic variations in the earth's infrared radiation levels, detection of significant westerly winds at orbital altitudes and independent confirmation of the U. S. Standard Atmosphere, 1962, between 57 and 90 nautical miles by an operational system.

64SD4760

iii/iv

SV 960 SUMMARY AND CONCLUSIONS

An analysis of the flight of Satellite Vehicle (SV) 960 has been made by the General Electric Company.

Normal performance was realized through rev 9. There were intermittent stored command loading problems from revs 10 to 18, and none were accepted by the vehicle after rev 18. All stored command sequences that were accepted were properly executed, including the last one on rev 28. BUSS was used to initiate successful deorbit; subsequent air snatch of the SRV capsule occurred approximately 17 nautical miles south of the intended impact point.

The most probable cause of the command loading problem was a random part failure in the command decoder or programmer or one of the interconnecting coaxial cables. Major corrective actions included a comprehensive review of module piece-part assembly and testing, and a review of the assembly, test and handling of the coaxial cable to determine what changes were required to upgrade command system reliability. These measures, together with other corrective actions presented throughout the following text, are considered to represent that effort required to optimize operational assurance of subsequent flight vehicles.

64SD4760

INTRODUCTION

A program (reference 1) aimed at operational utilization of the Program 206 Satellite Vehicle was initiated with the launch of SV 951 on July 12, 1963. Test 3802 successfully placed the tenth vehicle, SV 960, in orbit from Pad 4 PALC II, Point Arguello, on August 14, 1964.

This report presents a comprehensive post-flight analysis of the SV 960 flight. Special emphasis is placed in evaluating malfunctions in the Telemetry, Tracking, and Command Subsystems, and identifying corrective action required to improve operational assurance of the next vehicle. Information given herein supersedes all prior releases by the General Electric Company concerning the flight of SV 960 for example, references 2 through 4.

General Electric has also taken the opportunity in this document to publish summaries of all significant malfunctions including corrective action, and system operational capabilities covered in the Program 206 Final Evaluation Reports to date (references 5 through 13).

64SD4760

vii/viii

TABLE OF CONTENTS

TABLE OF CONTENTS (Cont)

●

TABLE OF CONTENTS (Cont)

64SD4760

TABLE OF CONTENTS (Cont)

LIST OF ILLUSTRATIONS

LIST OF ILLUSTRATION (Cont)

LIST OF TABLES

SECTION 1
FLIGHT SUMMARY AND VEHICLE DESCRIPTION

This Flight Summary and Vehicle Description is historical in nature in that it provides a concise summary of Program 206 Satellite Vehicle flight performance to date, a physical description of the vehicles, a graphical portrayal of each flight profile, and a typical set of ascent parameters. A flight analysis of SV 951 to SV 959 is documented at length in the respective Final Flight Evaluation Report (reference 1 through 9).

The flight summary in table 1-1 is a concise history of the Program 206 Satellite Vehicle flight accomplishments including objectives, results, achievements, deficiencies, and corrective actions pertaining to each flight. Many details have been omitted from this summary, since all relevant information is presented in detail in Sections 2 and 3.

A vehicle description is provided by the inboard profiles. For Block I vehicles (SV 951 through SV 953), see figure 1-1; for Block II vehicles (SV 954 through SV 960), see figure 1-2. Standard axes definitions and mass property summaries for individual vehicles are given in figure 1-3 and table 1-2, respectively. These diagrams and data are provided as a necessary adjunct to the discussions of performance in Sections 2 and 3, as well as for their historical value.

Figure 1-4 (sheets 1 to 5) contains the histories of the significant vehicle orbital parameters, with the occurrence of major flight events noted for quick reference. This serves to correlate in time the important aspects of each flight. Table 1-3 presents the initial orbital parameters for the first ten vehicles.

The first ten Atlas booster vehicles all used a pitch attenuation coefficient of 0.92; therefore ascent parameters through booster-engine cutoff (BECO) have not varied significantly from flight to flight. A typical set of these ascent parameters is shown in figure 1-5.

64SD4760

1-1

Table 1-1. Flight Summary (Sheet 1 of 8)

Satellite Vehicle	FLIGHT			VEHICLE IMPROVEMENT	
	Objectives	Results	Engineering Achievements *	Deficiencies	Corrective Action
SV 951 (FTV 1467) Launched 1344 hrs PDT, 12 July 1963. First in a series of vehicles directed toward the launching of precisely-controlled, near-space orbiting platforms with recovery capability.	Primary: Terminate the Hitch-Up flight phase with successful recovery of the SRV Secondary: Demonstrate the OCV primary mission capability unhitched from the Agena during "Solo" operation.	Primary: SRV recovery, initiated by the Agena Back-Up Stabilization Subsystem (BUSS), was completed by air snatch on rev 18. Secondary: Acquisition of IR & subsequent control was obtained in spite of abnormal booster attitudes and rates at separation. Subsequent performance was compromised by spurious command executions. Stable operation was maintained between revs 18 and 25 and again on rev 34.	Operational feasibility was proven and the basic design philosophies of the Program 206 Satellite Vehicle System and associated software programs were verified. Use of gimballed attitude reference system and integral three-axis rate sensing system in a near-earth orbit were demonstrated.	Secondary: Large spurious voltage transients caused the command decoder +6 volt input to be removed leading to inadvertent commanding of other vehicle subsystems.	Secondary: The power sequencer logic was modified to incorporate an additional +6 volt input to the final output of the sequencer which would override noise effects on the continuous +28 and +6 volt power supplies Mission critical commands that could be caused by spurious signals were "safe-armed" to prevent catastrophic failures.

*All engineering achievements herein are advances in the state-of-the-art as known to the General Electric Company

64SD4760

Table 1-1. Flight Summary (Sheet 2 of 8)

Satellite Vehicle	FLIGHT			VEHICLE IMPROVEMENT	
	Objectives	Results	Engineering Achievements*	Deficiencies	Corrective Action
SV 952 (FTV 1947) Launched 1230 hrs PDT, 6 September 1963. The SV 951 configuration, except that a V-clamp was used to separate the SV from the Agena instead of a shaped charge.	Identical to those of SV 951	Primary: SRV recovery initiated by the Agena primary system was completed by air snatch on rev 34. Secondary: Full demonstration of Stabilization Subsystem capability was limited by a rapid loss of stabilization gas following pneumatic system pressurization at OCV-Agena separation. Except as limited by gas depletion, the Stabilization Subsystem performance and response to commands was normal.		Secondary: The rapid loss of pneumatic gas has been attributed to venting from an open secondary charge valve in the high pressure line.	Secondary: All field pneumatics procedures were reviewed in detail and modified to insure against recurrence of human error.

1-3

*All engineering achievements herein are advances in the state-of-the-art as known to the General Electric Company

64SD4760

Table 1-1. Flight Summary (Sheet 3 of 8)

| Satellite Vehicle | FLIGHT | | | VEHICLE IMPROVEMENT | |
	Objectives	Results	Engineering Achievements*	Deficiencies	Corrective Action
SV 953 (FTV 2196) Launched 1159 hrs PDT, 25 October 1963. The SV 952 configuration, except that orbit adjust propellants were loaded for the first time.	Primary: Terminate the Hitch-Up flight phase with successful capsule recovery and subsequent demonstration of the OCV stabilization capability during "Solo" operation. Secondary: Demonstrate the SV orbit adjust and five-day operational mission capabilities.	Primary: SRV recovery, initiated by the Agena primary system was completed by air snatch on rev 34. OCV separation from the Agena and subsequent repeated exercising of the Stabilization Subsystem were normal. Secondary: Two-engine and single-engine firings demonstrated normal orbit adjustments. A second two-engine firing provided a controlled OCV deorbit. The electrical and pneumatic expendable usage rates indicated a capability of supporting a full five-day mission.	Controlled "Clearing of near-space" was demonstrated by deorbit of the OCV into the South Pacific. Multi-restartable, selectively-controlled, ablatively-cooled engines were successfully applied to an operational space mission.		

*All engineering achievements herein are advances in the state-of-the-art as known to the General Electric Company

1-4

Table 1-1. Flight Summary (Sheet 4 of 8)

64SD4760

Satellite Vehicle	FLIGHT			VEHICLE IMPROVEMENT	
	Objectives	Results	Engineering Achievements*	Deficiencies	Corrective Action
SV 954 (FTV 2372) Launched 1346 hrs PST, 18 December 1963. This was the first Block II vehicle. It carried the Back-Up Stabilization Subsystem (BUSS) and a voltage step down module (eliminating need for pre-discharge of batteries)to protect voltage sensitive components.	Primary: Provide a two-day SV operational mission terminated by successful capsule recovery. Demonstrate OCV functional capability including OA and BUSS. Establish environmental conditions and system operational feasibility at lower altitudes during "Solo". Secondary: Demonstrate the five-day SV operational mission capability.	Primary: Separation from Agena, SV earth acquisition and the first four revs were normal. A failure occurred in the rate gyro system (RAGS) heater circuit which resulted in total depletion of the pneumatic gas supply by rev 5. SRV recovery, initiated by the SV BUSS, was accomplished by air snatch on rev 18, terminating the mission.		Primary: RAGS malfunction apparently was caused by a failed temperature controller which applied full heater power (100% duty cycle) to the component.	Primary: A series thermostat was bonded to the gyro block, which would cut power to the heaters if gyro temperature reached 172° F. MAB, VSB, and PAD test procedures were modified to assure that proper operation of the temperature controllers would be verified before each flight.

*All engineering achievements herein are advances in the state-of-the-art as known to the the General Electric Company

Table 1-1. Flight Summary (Sheet 5 of 8)

64SD4760

Satellite Vehicle	FLIGHT			VEHICLE IMPROVEMENT	
	Objectives	Results	Engineering Achievements*	Deficiencies	Corrective Action
SV 955 (FTV 2423) Launched 1100 hrs PST, 25 February 1964. Essentially identical to SV 954.	Primary: Provide a three-day SV operational mission terminated by successful capsule recovery. Demonstrate OCV functional capability including OA and BUSS. Establish environmental conditions and system operational feasibility at lower altitudes during "Solo". Secondary: Demonstrate the five-day SV operational mission capability	Primary: A roll coarse rate monitor, known to be inoperative, coupled with a faulty "Augie" roll fine-rate printout erroneously indicated that the roll and pitch gyros did not uncage. Uncage commands, sent in rev 2, inadvertently lost SV yaw attitude reference. The yaw anomaly was diagnosed and corrected on rev 18. Normal performance through rev 34 was successfully concluded with air snatch of the SRV. Three OA's and a controlled OCV de-orbit demonstrated the excellent OCV orbit adjust capability and established operational feasibility at a 70 n mi perigee. Demonstration of the BUSS was precluded by a component failure. Secondary: The system indicated a full five-day mission capability.	Successful operation over an extended period of time by the system was realized in an orbit with a perigee of 70 n mi.	Primary: Incomplete gyro uncaging commands on rev 2 caused the gyro compassing input of the yaw torquing amplifier to be removed, which resulted in a vehicle yaw rate of ≈ 2.5 degrees/hr. Failure of either relay K3 or K9 in the BUSS "J" box precluded orientation of the OCV by the BUSS following OCV de-orbit engine cutoff.	Primary: The GCOMPAT software program was modified to provide an error print whenever an RPGU command occurs without an F+ or F- following within 600 seconds. The BUSS manufacturer indicated that this was a random delay failure requiring no corrective action.

1-6

*All engineering achievements herein are advances in the state-of-the-art as known to the General Electric Company

C05099047

64SD4760

Table 1-1. Flight Summary (Sheet 6 of 8)

Satellite Vehicle	FLIGHT			VEHICLE IMPROVEMENT	
	Objectives	Results	Engineering Achievement *	Deficiencies	Corrective Action
SV 956 (FTV 3435) Launched 1214 hrs PST, 11 March 1964. Essentially identical to SV 954.	Identical to those of SV 955.	Primary: Three days of normal operational mission were success-fully concluded with air snatch of the SRV. Three OA's and a con-trolled OCV de-orbit demonstrated the ex-cellent OCV orbit adjust capability and esta-blished operational feasibility at 70 n mi perigee. Demonstration of the BUSS was pre-cluded by a component failure. Secondary: The system indicated a five-day mission capability.		Primary: BUSS Solenoid Valve No. 4 was inopera-tive precluding orienta-tion of the vehicle by the BUSS following OCV deboost engine cutoff. The valve had most pro-bably burned out prior to launch due to improper testing.	Primary: Modifications were incorporated in test procedures to insure adequate cool-ing of solenoids during field checkouts.
SV 957 (FTV 3743) Launched 1048 hrs PST, 23 April 1964. Essentially identical to SV 954	Primary: Provide a three-day SV operational mission terminated by success-ful capsule recovery. Establish environ-mental conditions and total system operational feasibility at lower altitudes. Secondary: Demon-strate the five-day SV operational mission capability.	Primary: Four days of normal operational mission, including two days at a 72 n mi peri-gee, were successfully concluded with air snatch of the SRV. Secondary: The system indicated a full five-day mission capability.		Primary: The IR horizon sensing system (IRHSS) developed a stable 4 to 6 degree negative pitch offset from the local vertical between revs 42 and 46 which remained throughout the flight.	Primary: The offset was traced to a relay failure in the inhibit circuit of the IRHSS. Modifications were incorporated to enhance the relay reliability.

1-7

*All engineering achievements herein are advances in the state-of-the-art as known to the General Electric Company

Table 1-1. Flight Summary (Sheet 7 of 8)

Satellite Vehicle	FLIGHT			VEHICLE IMPROVEMENT	
	Objectives	Results	Engineering Achievement *	Deficiencies	Corrective Action
SV 958 (FTV 3592) Launched 1221 hrs PDT, 19 May 1964. Essentially identical to SV 954.	Primary: Provide a four-day SV operational mission terminated by successful capsule recovery. Establish environmental conditions and total system operational feasibility at lower altitudes. Secondary: Demonstrate the five-day SV operational mission capability.	Primary: At injection, the SV was placed in an orbit with a perigee of 57 n mi, and was coning with a roll rate of ≈−19 deg/sec after separation. Stabilized attitude was achieved before the first station contact and OA capability was used on rev 2 to add energy and raise perigee to the planned injection condition. Nominal performance was realized until attitude reference was lost on rev 15, followed by an inability to command roll on rev 16. Attitude reference was regained on rev 25 which allowed use of the primary system to initiate successful de-orbit and subsequent air snatch of the SRV on rev 34.	Survived 57 nautical mile perigee after injection. Corrected and proceeded with partial mission in spite of encountering densities 17 times greater than that previously seen. The U.S. Standard Atmosphere, 1962 was substantiated by aerodynamic data obtained between 57 and 90 n mi. Above 90 n mi the 1962 standard was found to specify higher densities than measured and which diverged with increasing altitude. The existence of significant westerly winds at orbital altitudes was also substantiated. Successful de-orbit of the SRV was accomplished from an altitude of 72 n mi.	Primary: The abnormal SV injection ripped and dislodged portions of the rear bulkhead thermal blankets which intermittently blocked and/or reflected energy to the scanner heads. This, in conjunction with lower than normal IR stimuli in the South Polar region and/or high IRHSS inhibit level, caused the loss of IR lock. The 10 pps time generator module in the command decoder failed on rev 16 because of the temperature cycling caused by the low altitude on rev 1 and 2 and by the tumbling vehicle on rev 16. This failure caused loss of the roll maneuver command capability.	Primary: Mounting boards in the 10 pps module made of thermally sensitive Photose ran were changed to thermally insensitive Epoxyglass.

64SD4760

1-8

Table 1-1. Flight Summary (Sheet 8 of 8)

| Satellite Vehicle | FLIGHT | | | VEHICLE IMPROVEMENT | |
	Objectives	Results	Engineering Achievement *	Deficiencies	Corrective Action
SV 959 (FTV 3684) Launched 1151 hrs PDT, 6 July 1964. Essentially identical to SV 954.	Identical to those of 958.	Primary: The vehicle experienced intermittent IR lock to the horizon reference throughout flight. BUSS was used to initiate successful de-orbit and subsequent air snatch of the SRV on rev 34.		Primary: Study of SV 959 and previous flights indicated the most probable cause of loss of IR lock to be IRHSS inhibit in the South Polar region because of the low IR energy level associated with the "winter" season.	Primary: Operational changes were made to to provide capability of flying inertial by disabling the IR reference over th South Polar region during the "winter" season. Hardware was added to reduce vehicle rates to less than 2.5 degree/hr while flying inertial.
SV 960 (FTV 3802) Launched 1500 hrs PDT, 14 August 1964. Essentially identical to SV 954. Booster was first use of an Atlas Standard Launch Vehicle, (SLV-3).	Primary: Provide a five-day SV operational mission terminated by successful capsule recovery. Establish environmental conditions and system operational feasibility at lower altitudes.	Primary: Normal performance was realized through rev 9. There were intermittent stored command loading problems from rev 10 to 18 and none would be accepted by the vehicle after Hula 18. The last stored command sequence was executed during rev 28. BUSS was used to initiate successful de-orbit and subsequent air snatch of the SRV in rev 66.	Seasonal and geographical variability of the earth's equivalent black body temp, in the scanner's IR frequency spectrum, was determined and found to have significant effects on IRHSS performance. The high reliability of the SRV Subsystem was demonstrated by the tenth successive recovery by air snatch.	Primary: Prime mission capability was lost because of the inability to load stored commands. The malfunction was most probably due to a random piece-part failure in the command decoder or programmer or one of the interconnecting coaxial cables.	Primary: Comprehensive reviews of module piece part assembly and test and assembly, test, and handling of the coaxial cable were made to indicate changes required to upgrade system reliability.

*All engineering achievements herein are advances in the state-of-the-art as known to the General Electric Company

64SD4760

1-9
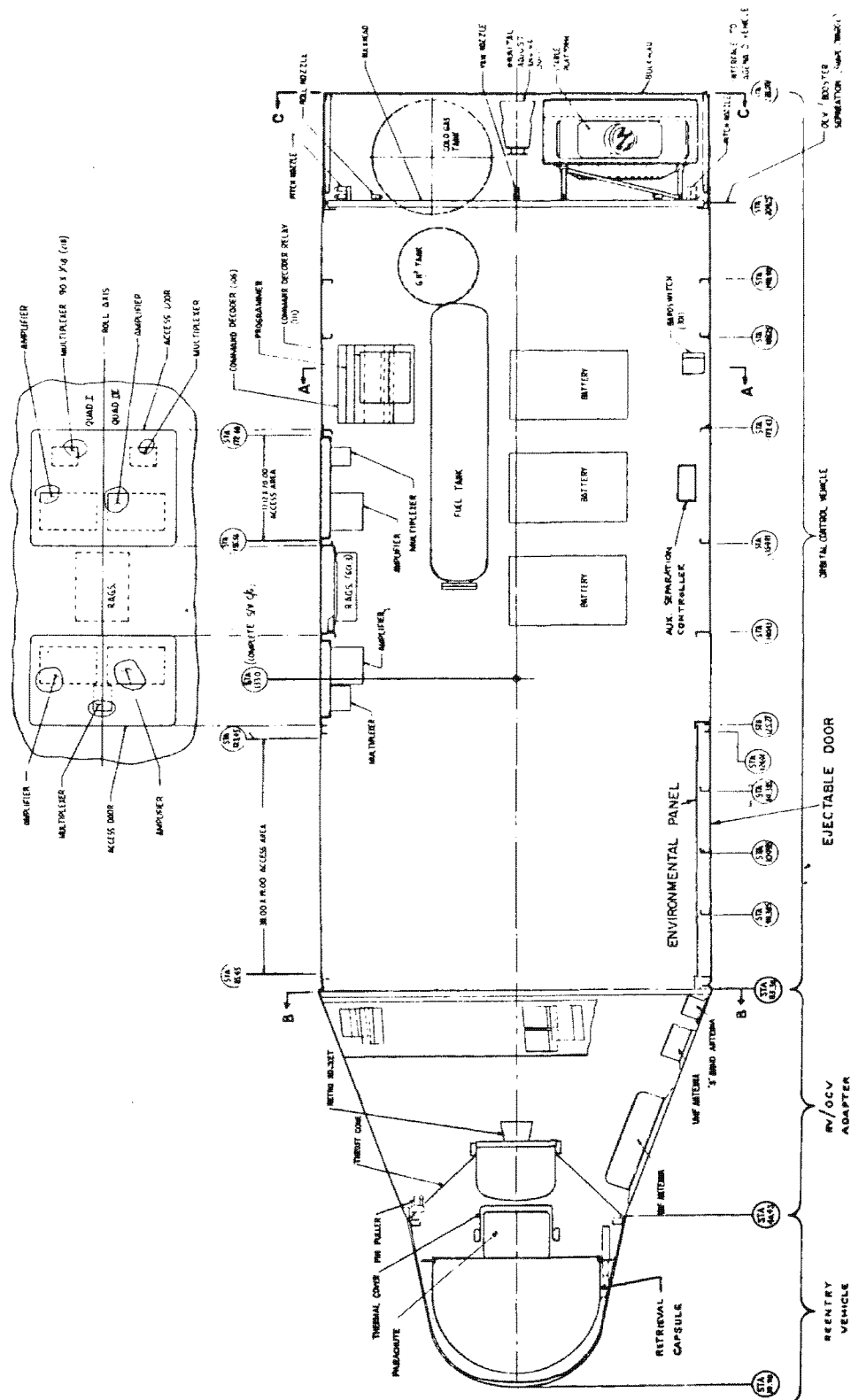
CROSS SECTION ALONG YAW AXIS, SHOWING QUADS I AND II

Figure 1-1. Satellite Vehicle Inboard Profile (Block I Vehicles)
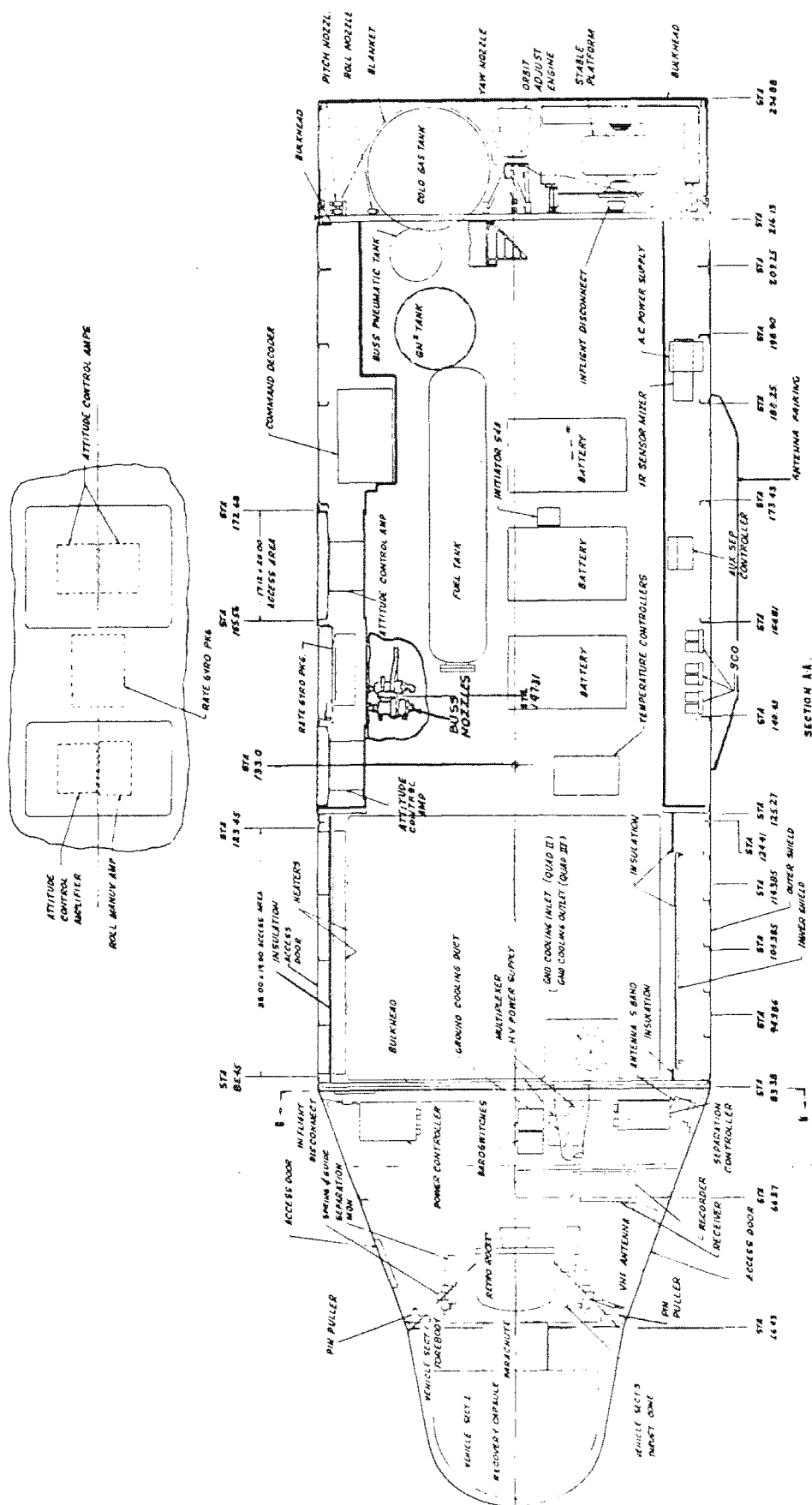
Figure 1-2. Satellite Vehicle Inboard Profile (Block II Vehicles)

64SD4760

TOP VIEW

☐ – ROLL NOZZLE (PAIR)
▲ – PITCH NOZZLE
● – YAW NOZZLE

+ ROLL

YAW AXIS

SIDE VIEW

VIEW LOOKING
FORWARD AT
STA. 216
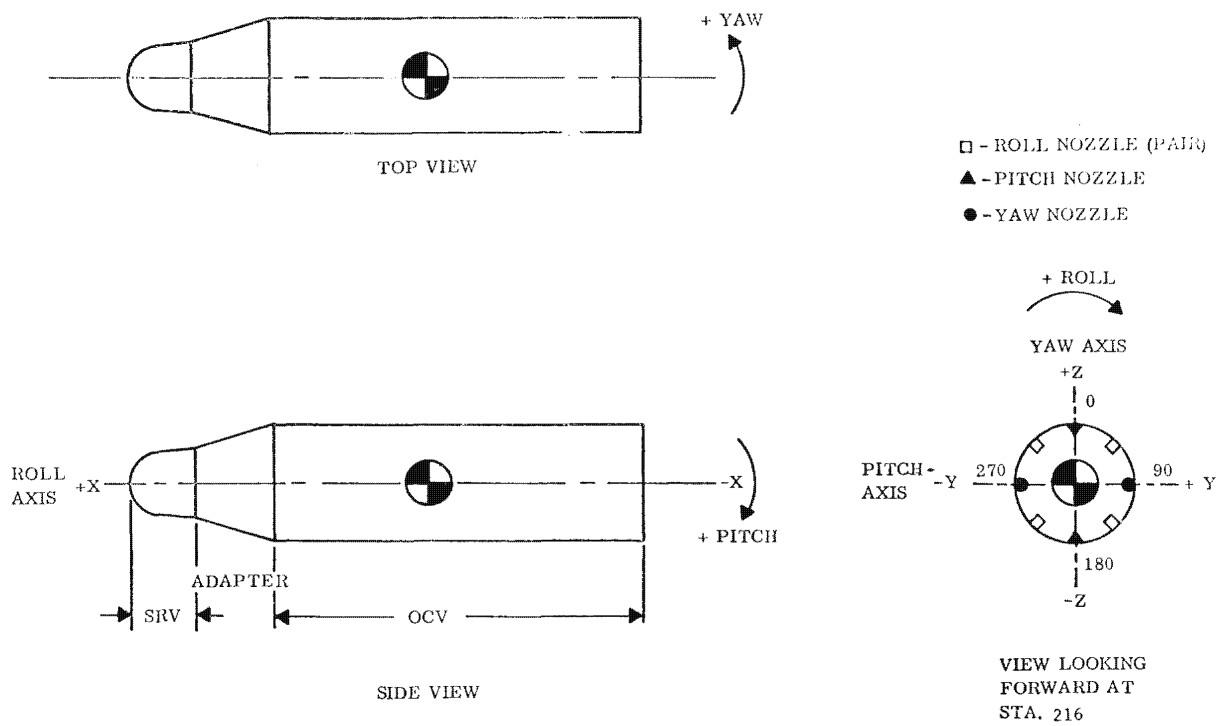
Figure 1-3 Axis Definitions

1-12

Table 1-2. Summary of Mass Properties, SV 951 to 960 (Sheet 1 of 5)

SV 951 Vehicle & Phase of Flight	Weight (pounds)	Center of Gravity (inches)			Moments of Inertia (slug-ft²)			Products of Inertia (slug-ft²)		
		x	z	y	I_{xx}	I_{zz}	I_{yy}	I_{xz}	I_{xy}	I_{zy}
SV just prior to separation	3588.2	145.58	.042	.474	331	2670.9	2658.7	38.5	0	1.1
SV following SRV separation	3243.7	157.04	.046	.525	324.9	1739.8	1727.7	39.9	-4.13	-1.25
SRV at separation	344.6	37.73	.0125	-.009	6.26	12.59	12.82	-.02	-.013	-.104
a. After spin	343.9	37.70	.0125	.010	6.25	12.56	12.78	-.02	.004	-.104
b. After retro	303.9	35.58	.0142	.011	6.08	9.89	10.11	-.019	.006	-.104
c. After despin	303.2	35.55	.0142	-.010	6.06	9.85	10.05	-.019	-.015	-.104
d. SRV at re-entry	248.8	32.17	.0086	.001	5.15	6.16	6.03	.002	-.017	-.09
e. Capsule	150.8	30.16	.0194	.001	2.45	2.88	2.78	.005	-.017	-.09
OCV-Adapter following separation from Agena	3201.0	156.22	.041	.532	316.7	1698.2	1686.5	39.7	-3.90	-1.25
OCV-Adapter at end of mission	3031.0	152.80	-.731	.561	303.3	1547.5	1538.3	7.3	-3.9	-1.25

SV 952 Vehicle & Phase of Flight	Weight (pounds)	Center of Gravity (inches)			Moments of Inertia (slug-ft²)			Products of Inertia (slug-ft²)		
		x	z	y	I_{xx}	I_{zz}	I_{yy}	I_{xz}	I_{xy}	I_{zy}
SV just prior to SRV separation	3648	147	.24	.60	330	2800	2800	58	-.8	--
SRV at separation	363.6	37.7	.04	--	6.7	13.5	13.0	--	--	.19
After spin up	362.8	37.7	.04	.02	6.7	13.5	13.0	--	.02	.19
After retro-fire	323.2	35.7	.04	.02	6.5	10.9	10.3	.01	.02	.19
After despin	322.6	35.7	.04	.01	6.5	10.8	10.3	.01	--	.19
SRV at re-entry	262.7	32.0	--	--	5.3	6.0	5.6	--	--	.03
Capsule	160.9	30.1	--	--	2.6	3.2	3.1	--	--	.03
OCV-A after separation from Agena	3216	157.8	.27	.69	314	1730	1710	56	-6.2	-.2
OCV-A end of mission	2998	153.5	-.71	.74	308	1540	1530	16	-4.1	.3

64SD4760

Table 1-2. Summary of Mass Properties, SV 951 to 960 (Sheet 2 of 5)

SV 953 Vehicle & Phase of Flight	Weight (pounds)	Center of Gravity (inches)			Moments of Inertia (slug-ft^2)			Products of Inertia (slug-ft^2)		
		x	y	z	I_{xx}	I_{yy}	I_{zz}	I_{xz}	I_{xy}	I_{zy}
SV just prior to SRV separation	3996.0	148.0	+.42	+.91	377	2835	2884	66	-7.0	-3.0
SRV at separation	364.17	37.697	-.008	-.003	6.6	13.54	13.45	+.025	-.038	+.079
SRV after spin-up	363.45	37.672	-.008	.016	6.59	13.51	13.43	+.025	-.020	.079
SRV after retro	323.65	35.699	-.009	.018	6.29	10.80	10.72	.024	-.018	.079
SRV after despin	323.05	35.67	-.009	.004	6.28	10.76	10.69	.024	.011	.079
SRV at re-entry	261.64	31.86	.003	-.003	5.11	6.08	5.75	.057	-.056	-.009
SRV capsule	161.37	-	-	-	-	-	-	-	-	-
OCV after separation from Agena	3566	158.0	0.46	1.02	360	1717	1767	60	-9	-3
OCV at start of deboost	3326	155.4	.56	0.4	338	1655	1612	35	-	-
OCV at end of deboost	3044	152.6	.87	-.65	301	1500	1520	12	-5	-2

SV 954 Vehicle/Phase of Flight	Weight (lb)	Center of Gravity (inches)			Moments of Inertia (slug-ft^2)			Products of Inertia (slug-ft^2)		
		x	y	z	I_{xx}	I_{yy}	I_{zz}	I_{xz}	I_{xy}	I_{zy}
SV at launch	4178.1	151.1	0.08	0.92	398.5	3048.9	3092.4	63.0	-14.0	-8.0
SV at start of mission	4070.9	150.1	0.15	0.99	379.9	2965.1	3010.8	63.7	-12.8	-6.2
SRV at separation	380.6	37.9	0.0	0.0	7.1	16.1	16.0	0.03	0.0	0.08
SRV after spin-up	379.88	37.9	0.02	0.0	7.0	16.0	15.9	0.03	0.02	0.08
SRV after retro fire	340.09	36.0	0.02	0.0	6.7	13.4	13.3	0.03	0.02	0.08
SRV after despin	339.49	36.0	0.003	0.0	6.7	13.3	13.6	0.03	0.0	0.08
SRV at re-entry	273.10	31.8	-0.003	-0.002	5.2	5.9	5.9	0.03	-0.01	0.02
Capsule	170.44									

64SD4760

Table 1-2. Summary of Mass Properties, SV 951 to 960 (Sheet 3 of 5)

SV 955 Vehicle & Phase of Flight	Weight (pounds)	Center of Gravity (inches)			Moments of Inertia (slug-ft^2)			Products of Inertia (slug-ft^2)		
		x	y	z	I_{xx}	I_{yy}	I_{zz}	I_{xz}	I_{xy}	I_{zy}
SV launch	4162	151.16	-0.07	0.90	403	3106	3101	65.0	-10.0	-7.0
SV orbit injection	4057	150.03	0.00	0.98	384	3015	3012	64.0	-9.0	-5.0
SV prior to SRV separation	3967	148.18	0.00	0.69	377	3049	3046	57.0	-11.0	-5.0
OCV after SRV separation	3616	159.93	0.00	0.76	370	1911	1908	51.0	-11.0	-5.0
SRV after separation	381.22	37.62	0.00	0.00	7.4	15.3	15.2	0.01	-0.03	0.06
SRV after spin-up	380.51	37.59	0.02	0.00	7.3	15.3	15.1	0.01	-0.01	0.06
SRV after retro-fire	340.68	35.71	0.02	0.00	7.0	12.5	12.4	0.01	-0.01	0.06
SRV after despin	340.09	35.69	0.00	0.00	7.0	12.5	12.3	0.01	-0.02	0.06
SRV re-entry	274.30	31.77	0.00	0.00	5.1	5.7	5.7	0.01	0.03	0.00
Capsule retrieval	174.50									
OCV deboost	3161	156.02	0.36	-0.56	324	1743	1718	16.0	-6.0	-5.0

SV 956 Vehicle & Phase of Flight	Weight (pounds)	Center of Gravity (inches)			Moments of Inertia (slug-ft^2)			Products of Inertia (slug-ft^2)		
		x	y	z	I_{xx}	I_{yy}	I_{zz}	I_{xz}	I_{xy}	I_{zy}
SV @ launch	4219	149.93	-0.07	0.70	405.7	3121.0	3163.8	75.4	-9.4	-11.3
SV @ orbit injection	4113	148.79	0.00	0.77	387.4	3026.4	3071.4	74.6	-10.4	-9.3
SV prior to SRV separation	4010	147.08	0.00	0.50	380.8	3036.3	3080.4	66.7	-10.4	-9.3
OCV after SRV separation	3622	158.70	-0.01	0.56	374.2	1904.7	1949.1	60.8	-9.2	-9.4
SRV after separation	387.90	37.26	0.009	-0.031	6.63	14.37	14.08	0.027	0.033	0.047
SRV after spin-up	387.70	37.23	0.026	-0.031	6.59	14.34	14.01	0.027	0.057	0.047
SRV after retro-fire	347.44	35.34	0.029	-0.035	6.29	11.52	11.19	0.023	0.055	0.047
SRV after despin	346.86	35.31	0.013	-0.035	6.26	11.47	11.13	0.023	0.039	0.047
SRV @ re-entry	287.20	31.81	0.016	-0.011	5.04	6.14	5.97	-0.014	0.008	-0.002
Capsule @ retrieval	186.59									
OCV @ deboost	3167	154.67	0.36	-0.79	322.7	1729.6	1746.0	26.	-5.7	-7.0

64SD4760

1-15

Table 1-2. Summary of Mass Properties, SV 951 to 960 (Sheet 4 of 5)

SV 957 Vehicle & Phase of Flight	Weight (pounds)	Center of Gravity (inches)			Moments of Inertia (slug-ft^2)			Products of Inertia (slug-ft^2)		
		x	y	z	I_{xx}	I_{yy}	I_{zz}	I_{xz}	I_{xy}	I_{zy}
SV at launch	4240	149.710	0.075	0.840	417.42	3135.50	3178.00	-4.200	76.500	-8.500
SV at orbit injection	4134	148.560	0.145	0.914	398.96	3041.10	3085.90	-4.200	75.600	-6.600
SV prior to SRV separation	3955	144.850	0.307	0.160	369.80	2998.10	3028.40	-0.400	53.500	-5.400
OCV after SRV separation	3552	159.720	0.161	0.886	391.30	1966.40	2012.40	-5.750	72.910	-6.600
SRV after separation	402.70	154.610	0.553	-0.640	6.76	14.86	14.54	0.064	0.017	0.018
SRV after spin-up	401.97	37.047	-0.001	-0.014	6.72	14.83	14.46	0.013	0.017	0.018
SRV after retro-fire	362.36	37.023	0.016	-0.014	6.42	11.96	11.59	0.086	0.014	0.018
SRV after despin	361.75	35.189	0.018	-0.015	6.38	11.93	11.57	0.067	0.014	0.018
SRV at re-entry	299.40	35.164	0.002	-0.015	5.10	6.22	6.01	0.046	-0.002	-0.045
Capsule at retrieval	199.02	31.598	0.007	0.003	-	-	-	-	-	-
OCV at deboost	3215	154.610	0.553	-0.64	339.90	1732.60	1748.70	-0.900	27.500	-4.000

SV 958* Vehicle & Phase of Flight	Weight (pounds)	Center of Gravity (inches)			Moments of Inertia (slug-ft^2)			Products of Inertia (slug-ft^2)		
		x	y	z	I_{xx}	I_{yy}	I_{zz}	I_{xz}	I_{xy}	I_{zy}
SV at launch	4241	149.8	0.0	0.70	411.0	3144.0	3185.0	75.00	-12.0	-12.00
SV at orbit injection	4141	148.7	0.1	0.80	392.0	3040.0	3092.0	75.00	-13.0	-11.00
SV prior to SRV separation	3950	147.0	0.1	0.50	387.0	3036.0	3090.0	70.00	-13.0	-11.00
OCV after SRV separation	3542	159.0	0.1	0.60	381.0	1926.0	1972.0	64.00	-13.0	-11.00
SRV after separation	407.52	37.3	0.0	-0.02	6.6	14.8	14.6	0.01	0.0	0.11
SRV after despin	366.19	35.4	0.0	-0.02	5.4	11.1	11.1	0.02	0.0	0.11
SRV at re-entry	304.29	31.7	0.0	-0.03	4.8	6.2	6.2	0.0	0.0	0.0
Capsule at retrieval	199.68	-	-	-	-	-	-	-	-	-

*Based on calculated weight and balance information

64SD4760

Table 1-2. Summary of Mass Properties, SV 951 to 960 (Sheet 5 of 5)

SV 959* Vehicle & Phase of Flight	Weight (pounds)	Center of Gravity (inches)			Moments of Inertia (slug-ft^2)			Products of Inertia (slug-ft^2)		
		x	y	z	I_{xx}	I_{yy}	I_{zz}	I_{xz}	I_{xy}	I_{zy}
SV @ launch	4282	149.8	0.61	0.03	419.0	3210.2	3165.8	76.7	-5.5	-11.2
SV @ orbit injection	4176	148.7	0.67	0.10	400.6	3118.3	3071.8	75.6	-5.6	- 9.3
SV prior to SRV separation	4025	145.0	-0.09	0.26	371.2	3058.9	3026.5	52.7	-2.0	- 8.1
OCV after SRV separation	3620	157.5	-0.10	0.29	364.5	1907.7	1875.0	53.4	-4.7	- 8.0
SRV after separation	394.8	37.103	-0.011	-0.001	6.83	14.57	14.89	0.024	0.013	-0.028
SRV after spin-up	394.1	37.080	-0.011	0.015	6.79	14.50	14.87	0.024	0.032	-0.028
SRV after retro firing	354.1	35.240	-0.012	0.017	6.49	11.62	11.98	0.022	0.034	-0.028
SRV after despin	353.5	35.216	-0.012	0.002	6.46	11.56	11.95	0.022	0.016	-0.028
SRV @ re-entry	291.0	31.712	-0.001	0.0	5.18	6.10	6.32	0.0	0.0	-0.068
Capsule @ retrieval	189.7									

*Based on calculated weight and balance information

SV 960* Vehicle & Phase of Flight	Weight (pounds)	Center of Gravity (inches)			Moments of Inertia (slug-ft^2)			Products of Inertia (slug-ft^2)		
		x	y	z	I_{xx}	I_{yy}	I_{zz}	I_{xz}	I_{xy}	I_{zy}
SV @ launch	4295.7	149.7	0.0	0.0	420	3164	3210	76	-17	-8
SV @ orbit injection	4189.7	148.5	-0.1	0.7	402	3067	3115	74	-16	-7
SV prior to SRV separation	3925.7	144.7	0.2	-0.1	373	3026	3063	51	-14	-6
OCV after SRV separation	3556.7	157.2	0.2	-0.1	366	1882	1920	51	-16	-6
SRV after separation	369.5	37.1	0.0	0.0	6.9	14.8	14.7	--	--	--
SRV @ re-entry	266.3	31.8	0.0	0.0	5.2	6.5	6.5	--	--	--
Capsule @ re-entry	164.8	--	--	--	--	--	--	--	--	--

*Based on calculated weight and balance information

64SD4760
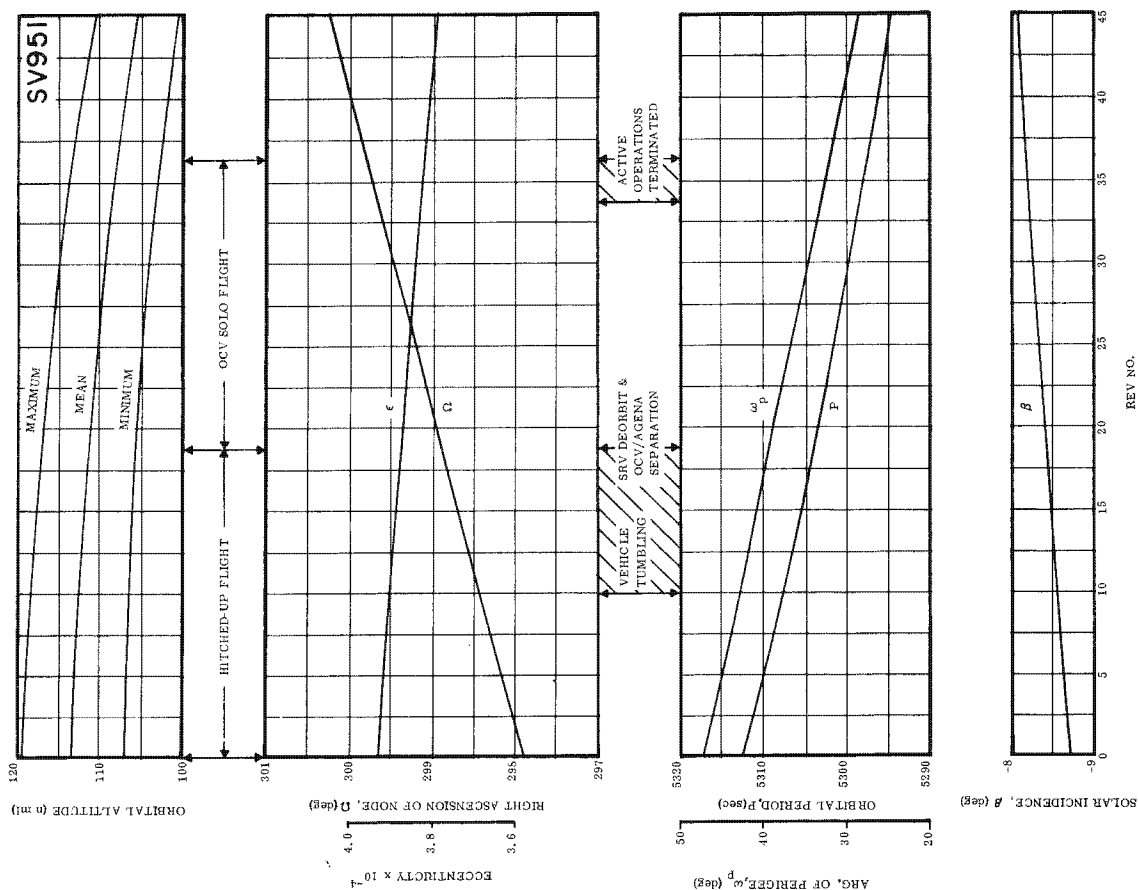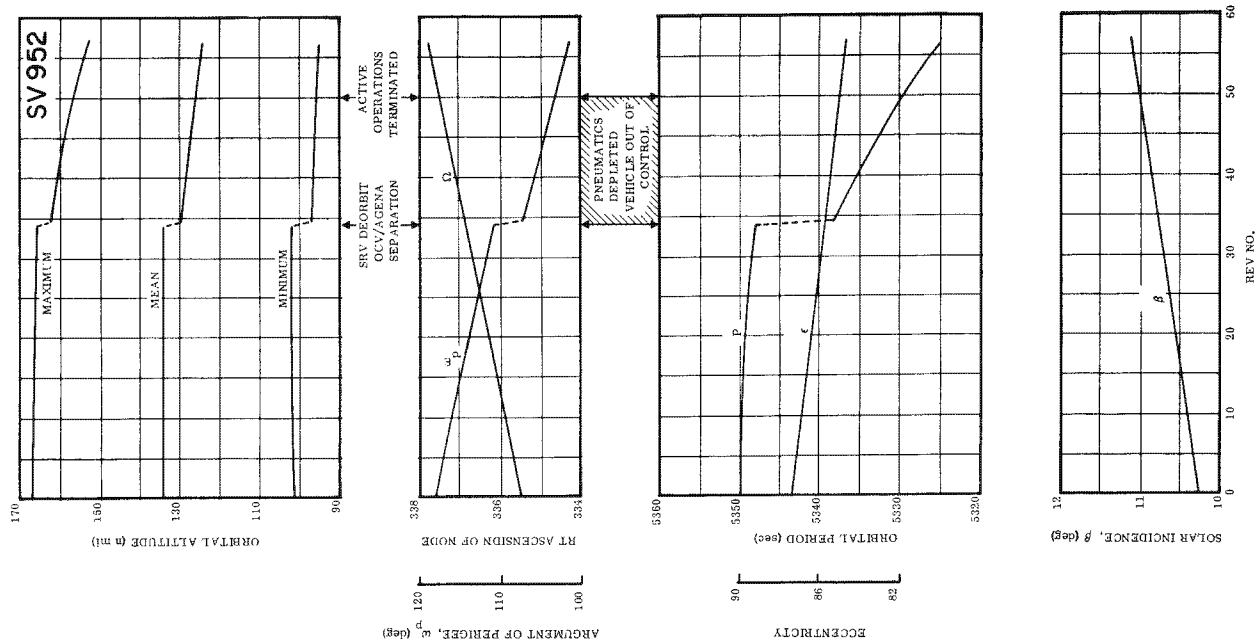
Figure 1-4. Time Histories of Significant Orbital Parameters (Sheet 1 of 5)
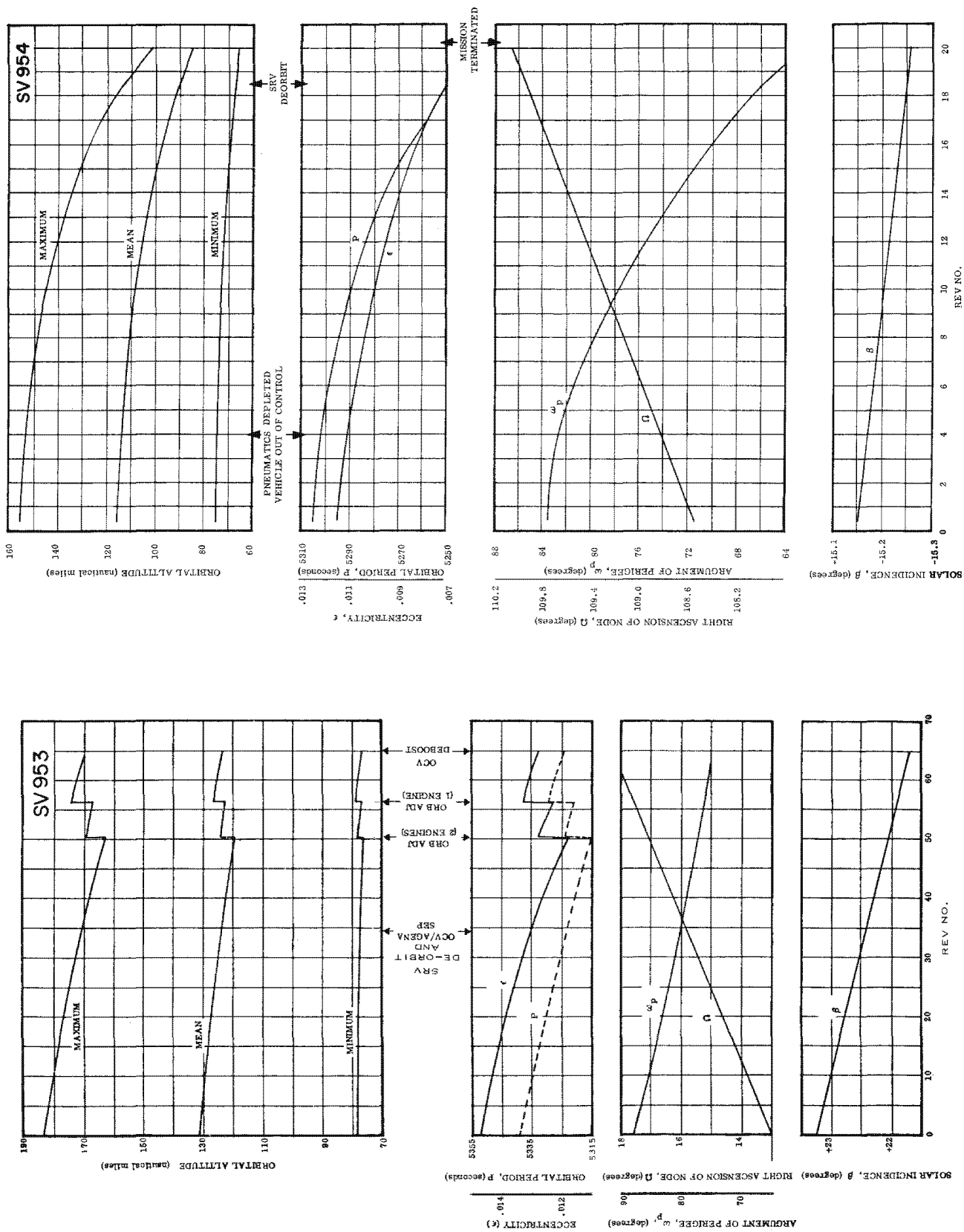
Figure 1-4. Time Histories of Significant Orbital Parameters (Sheet 2 of 5)

64SD4760

1-19
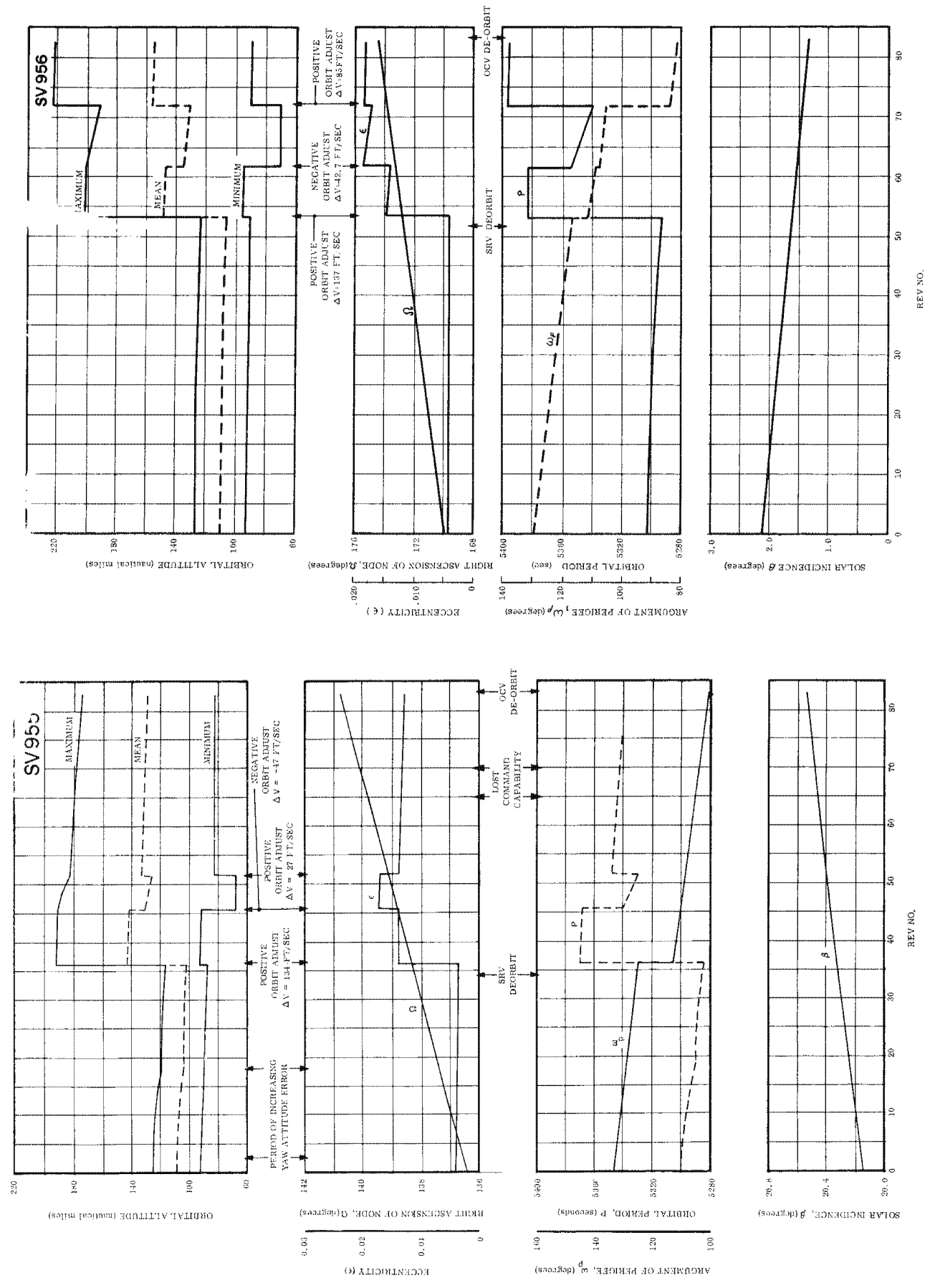
Figure 1-4. Time Histories of Significant Orbital Parameters (Sheet 3 of 5)
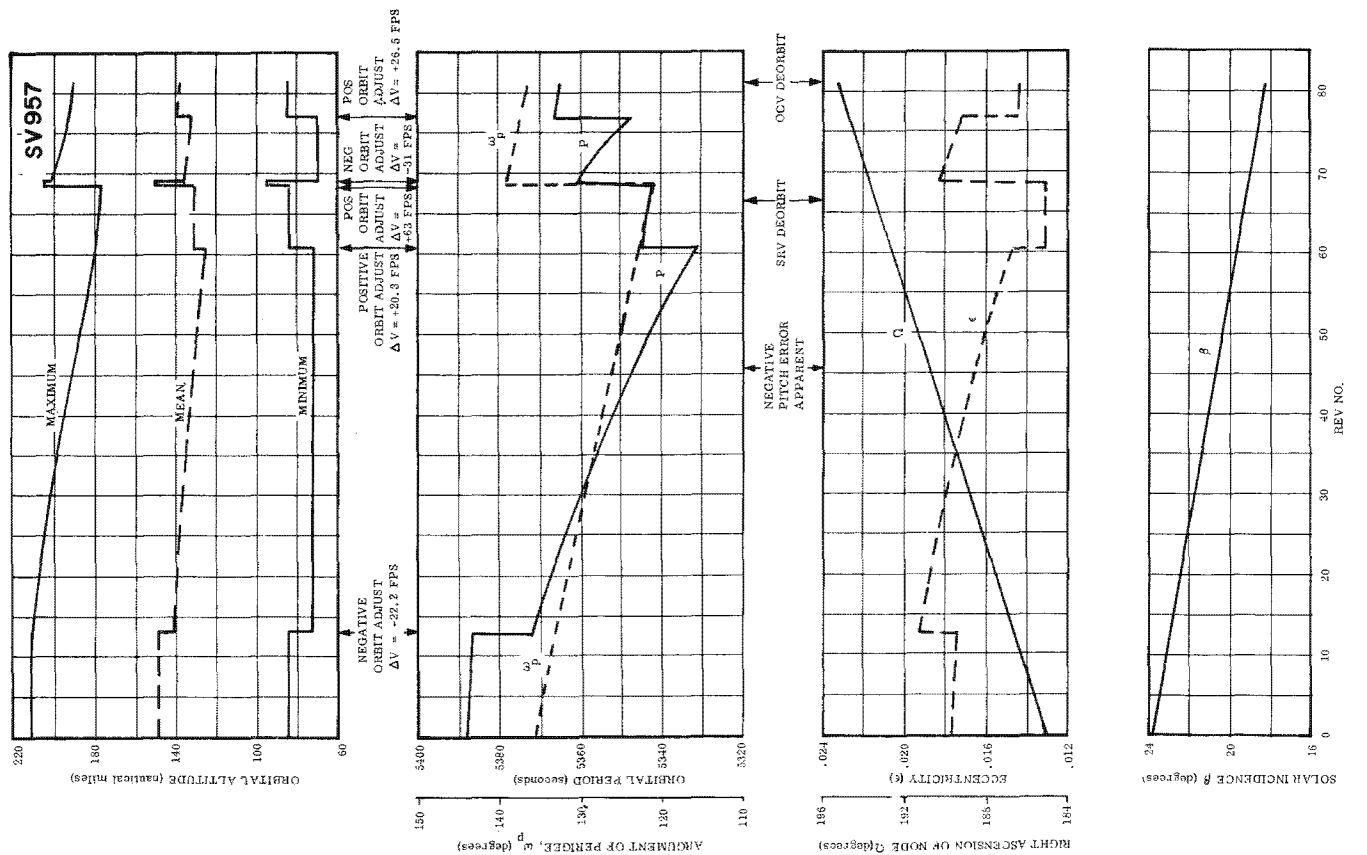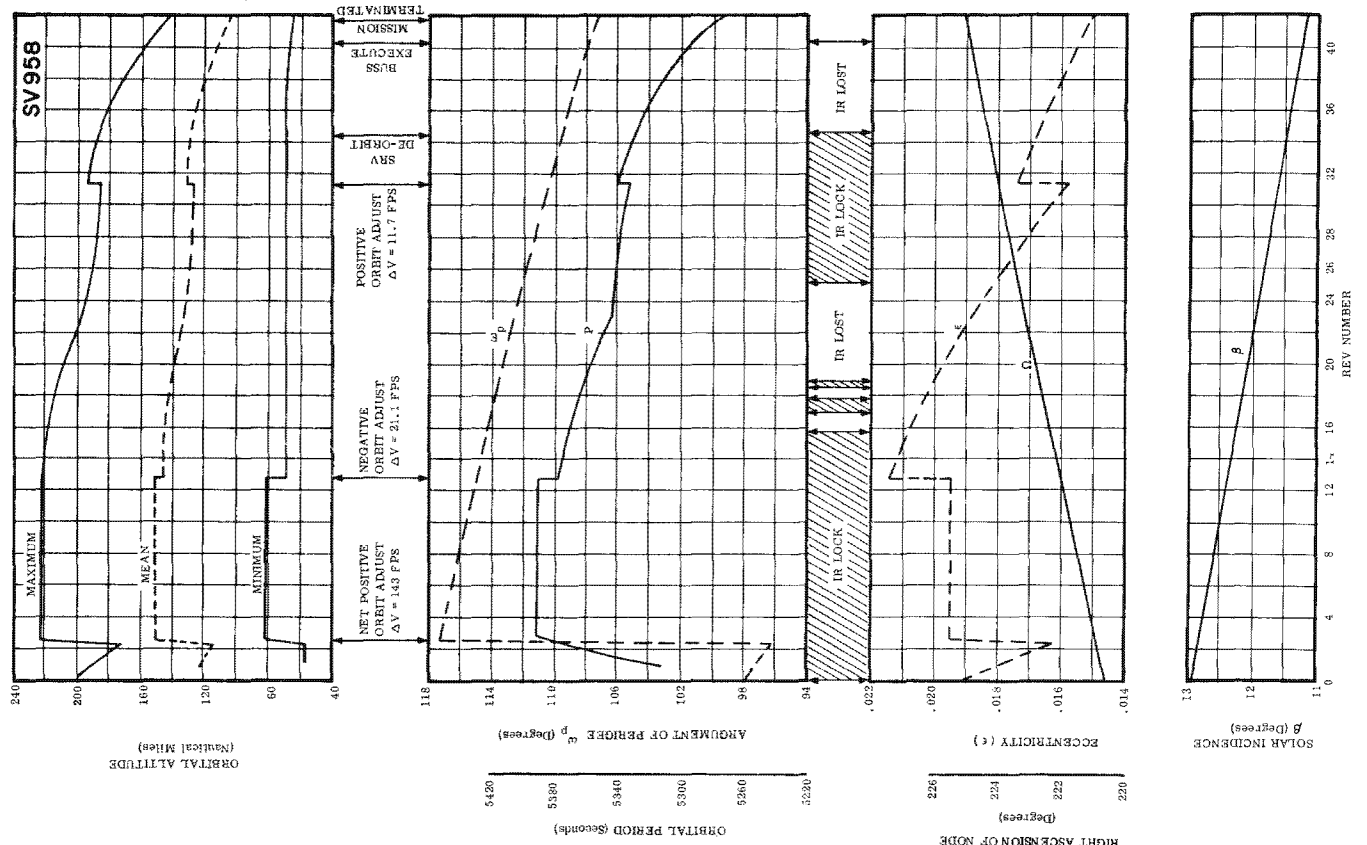
Figure 1-4. Time Histories of Significant Orbital Parameters (Sheet 4 of 5)
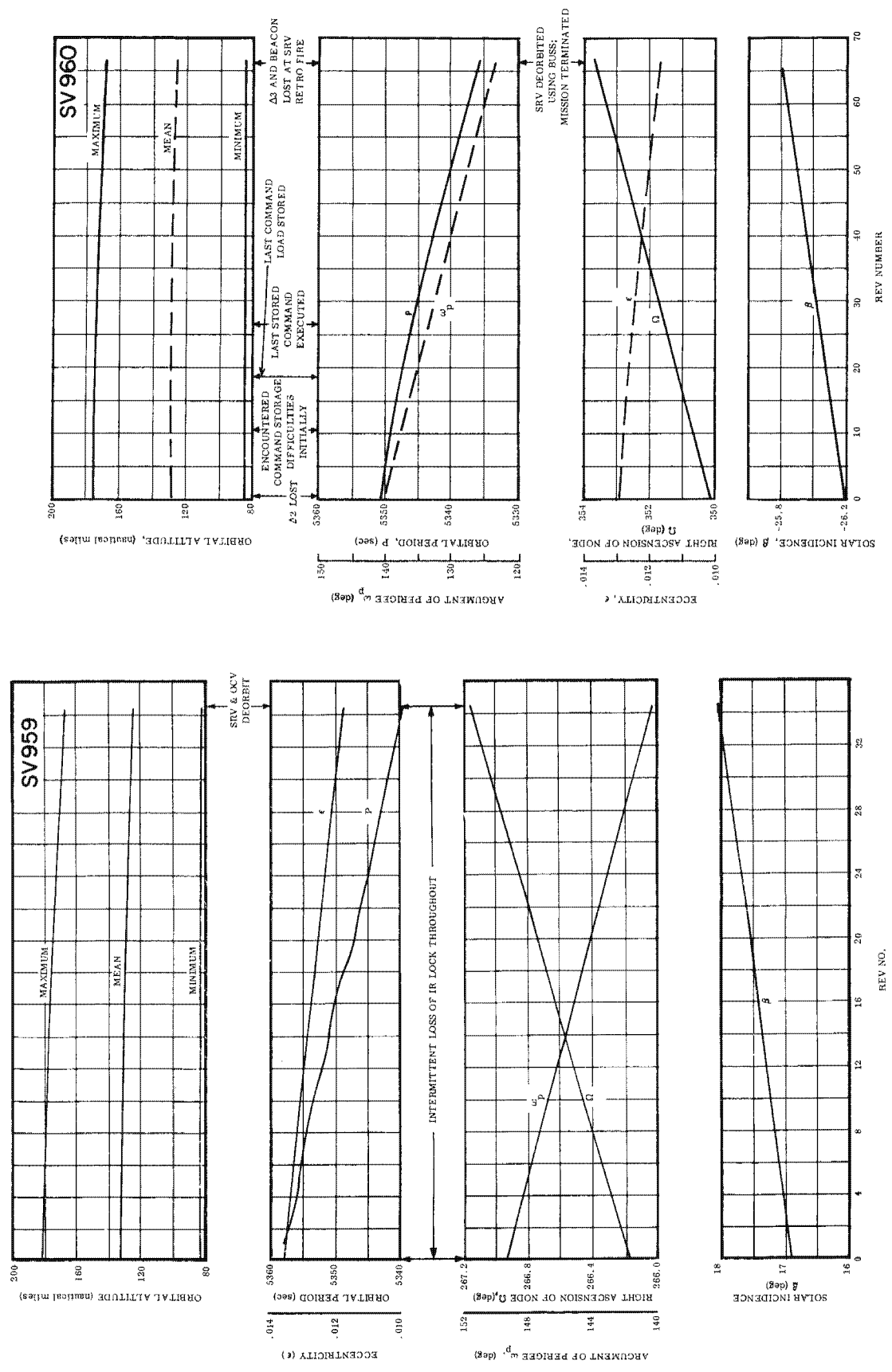
Figure 1-4. Time Histories of Significant Orbital Parameters (Sheet 5 of 5)

Table 1-3. Initial Orbital Parameters (SV 951-960)

Vehicle	Apogee (n mi)	Perigee (n mi)	Inclination (deg)	Eccentricity	Period (min)
951	119	107	95.35	0.0004	88.50
952	165	102	94.36	0.0089	89.17
953	183	78	99.13	0.0147	88.98
954	156	75	97.90	0.0150	88.42
955	121	96	95.60	0.0038	88.30
956	124	96	95.69	0.0040	88.37
957	210	85	103.55	0.0176	89.80
958	194	57	101.10	0.0192	88.58
959	180	84	93.06	0.0130	89.30
960	176	85	95.50	0.0130	89.17

64SD4760
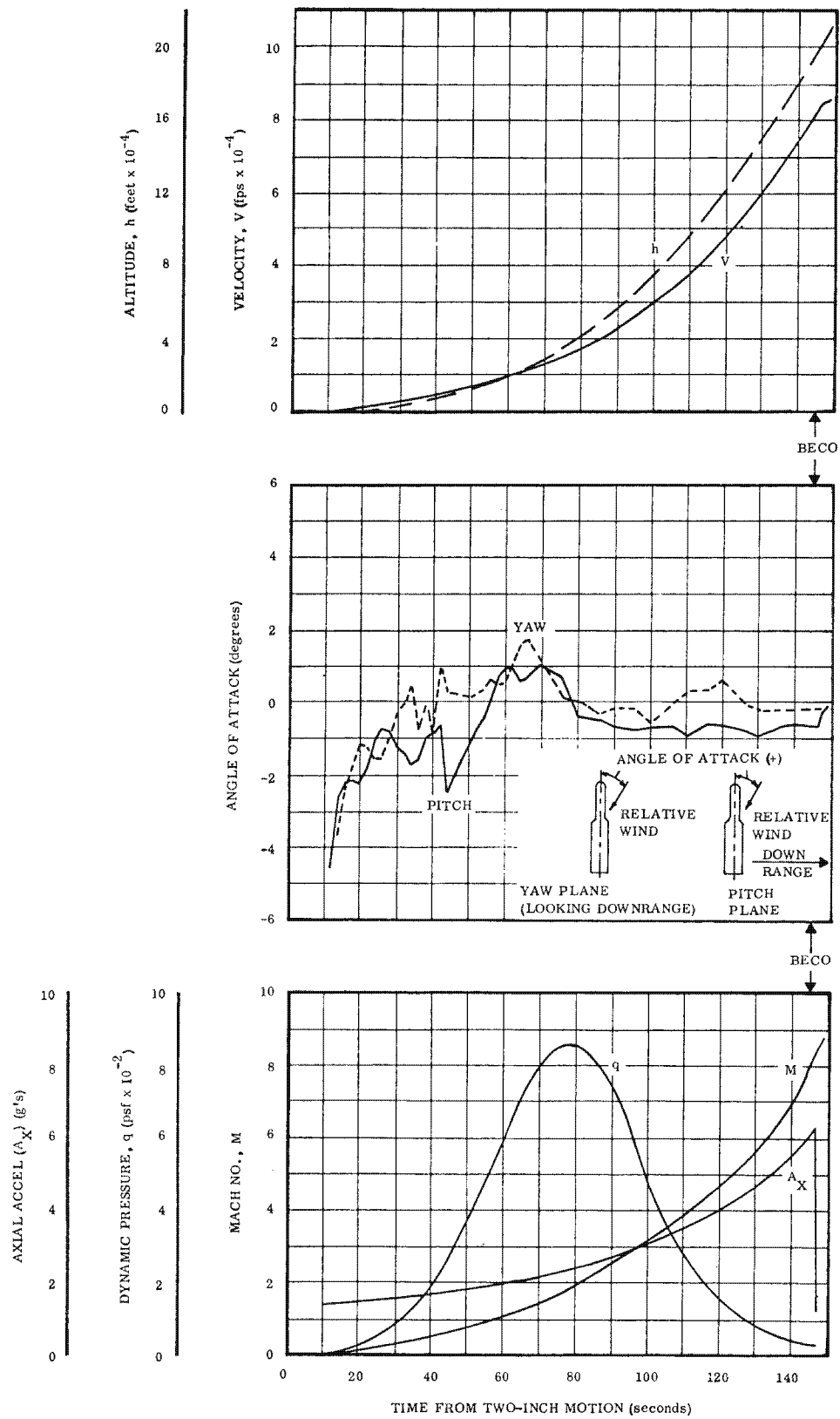
Figure 1-5. Typical Time Histories of Ascent Trajectory Parameters

64SD4760

SECTION 2

OPERATIONAL ASSURANCE ANALYSIS SUMMARY

This section summarizes the flight problems encountered through SV 960, along with their associated corrective actions. Other pertinent factors that either degraded or could have degraded or otherwise affected system capability or performance are also included.

This information is provided in this manner for the express purpose of minimizing the learning curve and its effects early in the conceptual phase on any subsequent program.

2.1 TELEMETRY, TRACKING, AND COMMAND SUBSYSTEM

The purpose of the Telemetry, Tracking, and Command (TT&C) Subsystem is threefold:

a. To provide high quality real-time and recorded telemetry data for vehicle evaluation and status determination

b. To provide tracking data for ephemeris generation and predictions

c. To provide a capability to change the mission plan by updating the existing stored commands with revised commands.

The TT&C Subsystem components had all been flight-tested on previous programs before being utilized in the Program 206 subsystem. Small modifications were made to the existing design of the command portion of the subsystem (such as addition of double stored word capability, revision of an inadequate command decoder, etc.), but basically no new components were added that had not previously demonstrated flight reliability. Therefore, with the advent of SV 951, the confidence level of a successful flight was quite high, and although some flight anomalies have since occurred, the adequacy of the TT&C Subsystem design has been firmly established.

2.1.1 TELEMETRY

2.1.1.1 Airborne Tape Recorder

The operation of the tape recorder was satisfactorily demonstrated throughout the ten Program 206 flights with minor exceptions. The first flight substantiated a need for a more optimum pre-emphasis schedule, a noise-free oscillator for tape-speed compensation, and a counter that would indicate new recorded segments. A new pre-emphasis schedule was assigned to the recorded spectrum, and test procedures were strictly

64SD4760

followed. The crystal oscillator (14.5 kc) was replaced by a fixed input voltage-controlled oscillator to improve compensation. The combination of these two items greatly improved the quality of playback data.

A recorder counter was designed and added to the vehicle beginning with SV 954; however, SV 952 and SV 953 utilized the first degree stages of the secure word counter to indicate new recorder segments. Time annotation of recorded segments was appreciably simplified.

Only one major failure (SV 955) occurred during all the flights that curtailed recorder operations. The low speed motor belt broke, preventing the magnetic tape from moving during the record sequences. A similar malfunction occurred during ground tests on a different recorder. The analysis proved that the tension roller used on this belt was deficient in face width. The roller was replaced with a wider roller in SV 956 and all vehicles after SV 960.

2.1.1.2 RF Link

There are two telemetry links ($\Delta 2$ and $\Delta 3$) within the satellite vehicle. Each one consists of a serial arrangement of a transmitter, power amplifier, high voltage power supply, cables, and switching elements. There are several instances during the history of Program 206 flights when the $\Delta 2$ link became degraded. On SV 951 severe degradation was apparent from liftoff throughout the operation; SV 956 had a ten db reduction of power during rev 48 to the end of the flight; and, SV 960 had a complete loss of the link sometime during rev 1 but before entrance at Thule on rev 1. It was hypothesized that the links of satellite vehicles 951 and 956 were reduced in power because of a degradation of the power amplifier. However, this could neither be substantiated nor refuted through telemetry data analysis. Because of the failure of the $\Delta 2$ link on SV 960, and the inability to definitely determine which of the components failed, an engineering investigation is to be performed. This investigation will pay particular attention to the duty cycle of both links prior to launch and to possible thermal differences that may exist between the $\Delta 3$ and the $\Delta 2$ links.

64SD4760

2.1.1.3 Failure of the 30 x 2.5 Multiplexer

The 30 x 2.5 Multiplexer is a dual channel multiplexer in which one channel modulates the 10.5 kc VCO in both real-time and playback transmission, and the other channel modulates the 30.0 kc VCO in real time transmission only. During the SV 960 real-time transmission to Thule on rev 13, it was observed that no reference pulse was present in the received wave train. Investigation revealed that only the first fourteen pulses of the wave train were being transmitted. Data recorded sometime during rev 10 and played back at Thule on rev 21 showed that the wave train shifted from a 30-pulse frame to a 14-pulse frame with no discontinuities.

In the circuit diagram (figure 2-1), it can be seen that for 30 x 2.5 operation, eight stages of a nine-stage counter are used to count-down the master oscillator. The fifth and sixth stage of the counter are decoded by the "Y" matrix and the seventh, eighth, and ninth stages are decoded by the "X" matrix. A logical AND operation is performed on the various outputs of these matrices by each of the output gates and the output of the respective gates is fed to the limiter amplifier.

In order for the multiplexer to limit its scanning to the first fourteen pulses there would have to have been a failure of flip-flop No. 5. This deduction can be reviewed by referring to the Truth Tables in figure 2-1. In the Truth Table "XY" it can be seen that pulses 1 through 14 require a logical AND operation with all of the outputs of decoding matrix "Y" and the $X_{5, 6, 7, 8}$ outputs of decoding matrix "X". In the Truth Table "X", it can be seen that these "X" outputs have in common the "set" state of flip-flop No. 5. It is therefore concluded that flip-flop No. 5 failed in the "set" condition.

An analysis of flip-flop No. 5 revealed that failure of the flip-flop would only result from a failure of diodes CR1 or CR2, or transistors Q1 or Q2. A short in CR1 would prevent the flip-flop from accepting a reset signal, while an open circuit of CR2 would prevent the flip-flop from changing its state. An open circuit in Q1 or a short circuit in Q2 would maintain the flip-flop in the set condition.

64SD4760

2-3

C05099047

64SD4760

2-4
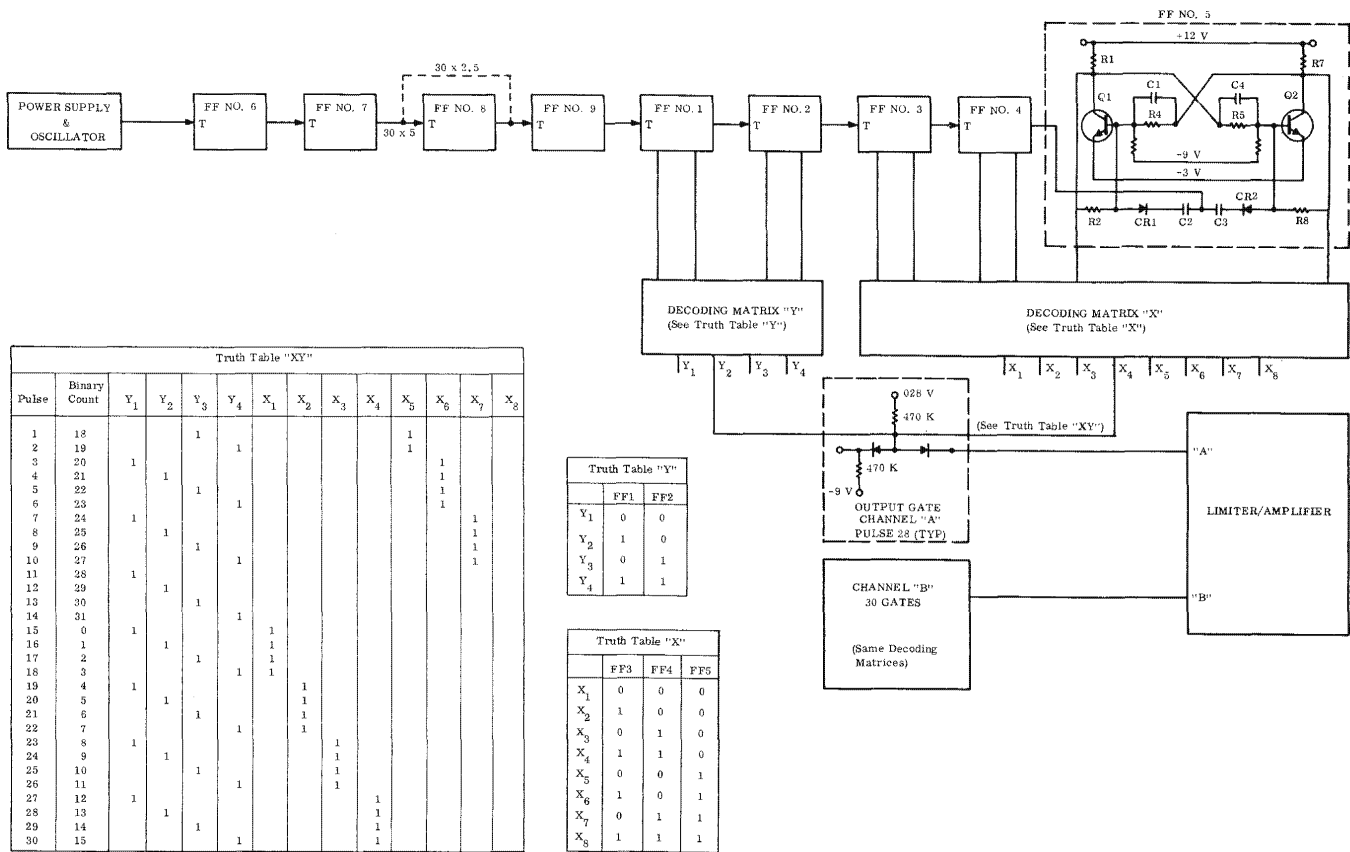
Figure 2-1.   30 x 2.5 Multiplexer Logic Diagram

Truth Table "XY"

Pulse	Binary Count	Y_1	Y_2	Y_3	Y_4	X_1	X_2	X_3	X_4	X_5	X_6	X_7	X_8
1	18			1						1			
2	19				1					1			
3	20	1									1		
4	21		1								1		
5	22			1							1		
6	23				1						1		
7	24	1										1	
8	25		1									1	
9	26			1								1	
10	27				1							1	
11	28	1											1
12	29		1										1
13	30			1									1
14	31				1								1
15	0	1				1							
16	1		1			1							
17	2			1		1							
18	3				1	1							
19	4	1					1						
20	5		1				1						
21	6			1			1						
22	7				1		1						
23	8	1						1					
24	9		1					1					
25	10			1				1					
26	11				1			1					
27	12	1							1				
28	13		1						1				
29	14			1					1				
30	15				1				1				

Truth Table "Y"

	FF1	FF2
Y_1	0	0
Y_2	1	0
Y_3	0	1
Y_4	1	1

Truth Table "X"

	FF3	FF4	FF5
X_1	0	0	0
X_2	1	0	0
X_3	0	1	0
X_4	1	1	0
X_5	0	0	1
X_6	1	0	1
X_7	0	1	1
X_8	1	1	1

A design review of the multiplexer revealed the following:

a. Transistors operate at:

50% of the maximum breakdown voltage (base to emitter)

75% of the maximum breakdown voltage (collector to emitter)

10% of the maximum breakdown voltage (collector to base)

56% of minimum current gain

b. Diodes operate at:

12% of maximum breakdown voltage

33% of maximum forward current

c. Resistors operate at:

1% of rated power

Corrective Action. No corrective action is anticipated since the failure is without precedent and since all the affected parts are operated well within their ratings.

2.1.1.4 Failure of the 10.5 kc VCO

During the SV 960 Thule pass on rev 33, it was observed that the 10.5 kc VCO had failed. With the loss of Delta 2, there was only one telemetry link and therefore limited opportunity to transmit playback data. Consequently, it could not be determined exactly where the failure of the 10.5 kc channel occurred, nor if additional diagnostic data could indicate the mode of failure.

Corrective Action: No corrective action can be taken since the failure mode could not be ascertained and there is no previous history, in flight or in test, of a similar failure.

64SD4760

2-5

2.1.1.5 Failure of Delta 3 and S-band Beacon

During the SV 960 Kodi pass on rev 66, immediately subsequent to SRV retro-rocket fire, there was an instantaneous loss of the Delta 3 telemetry link and the S-band beacon. No specific cause for the simultaneous failure of these components of two different systems can be found. However, the power controller and its associated cabling is common to both components. The power controller is mounted in the adapter section immediately behind the rocket but separated from it by the molecular heat shield. On SV 960 additional cutouts were made in the shield. It is thus possible that sufficient clearance existed between the cutouts and the associated structure to permit exhaust particles from the rockets to damage the power controller or its harnessing with resultant instantaneous failure in both the Delta 3 link and the beacon.

Corrective Action: This vehicle was the last vehicle to use a molecular heat shield. Subsequent vehicles will have no protection at all from the rocket exhaust and the flights of such vehicles will provide additional data on the effectiveness of the shield and the susceptibility of the components of the adapter section to the rocket exhaust.

2.1.2 TRACKING

2.1.2.1 Irregular Tracking Pulses

There exists an inherent deficiency in the S-band beacon transmitting circuit which causes the transponder pulse output to be triangular in shape and reduced in power during the first two revs of each vehicle's flight. Although this irregularity was only reported during the flights of satellite vehicles 953, 954, 957, and 960, the possibility exists that the pulses were also deficient during the other flights as well. During these early revs, beacon lock could not be attained until the vehicle had reached a 5 degree rise point, and loss of lock occurred approximately at the 5 degree set point. Thus, specification limits were not compromised by this irregularity. (See Section 3.3.2, S-band Beacon Capability.)

64SD4760

Corrective Action: Several tests will be run to try to duplicate this phenomenon. The RF cables, antenna, and antenna window will be tested at peak power levels of 3 kw until break-down occurs at pressure variations from ambient to 50 microns of mercury and temperature variations from room ambient to $300^{\circ}F$. No tests are planned of the beacon itself since previous tests yielded negative results in a vacuum of at least 150 microns of mercury. It has been concluded that the beacon seal is not being broken because the beacon would not then recover as evidenced on later revs.

2.1.3 COMMAND

2.1.3.1 Command Loading

During the SV 951 flight some difficulties were experienced when attempting to load commands. The accept/reject monitor (channel 17, 52.5 kc) output signal is fed directly into the AGE 125 console at the tracking station to verify the acceptance of a transmitted command. It was found that the ambient level of this monitor was too high, causing some noise pulses to be interpreted as accept pulses thereby "spoofing" the ground equipment. A modification to the telemetry monitor to lower the ambient level was incorporated on SV 952 and subsequent vehicles. The "spoofing" problems have not been experienced since.

2.1.3.2 Power Sequencer Failure

During the flight of SV 951, inadvertent disabling of the command decoder was experienced because EMI adversely affected the operation of the power sequencer. While executing commands, spurious power transients were generated. These transients, when they were of sufficient amplitude, caused the relay supplying +6 volts to the command decoder to de-energize, thereby disabling the command decoder and causing improper command executions. SV 952 and subsequent vehicles were modified to include additional logic circuitry in the power sequencer which has prevented the recurrence of this problem. In addition, more stringent ground testing of the Command Subsystem was initiated to assure that transients on the 28 volt bus were ineffective in each case.

64SD4760

2.1.3.3 Command Decoder Busy Condition

As a result of the power sequencer problem in SV 951, the command decoder was left on in a "busy" condition on numerous occasions. A "busy" condition occurs whenever the command decoder is in the process of executing a command, thus effectively inhibiting readout of the programmer. The inhibiting of the readout prevents any attempt to execute two commands at the same time. Because of the busy condition of the decoder in SV 951 many additional commands were precluded from their expected execution. It was recommended at that time to incorporate a telemetry "busy" monitor to aid the post flight analysis effort in determing when the commands in the programmer would be blocked. The command decoders were modified to provide this telemetry indication but higher priority items were using all available telemetry space. Therefore, the monitor could not be allocated to a telemetry channel until later vehicles.

2.1.3.4 Code 4 Interference

Whenever Agena tracking and/or commanding was performed during the "hitched-up" flight of SV 952, the SV command decoder would sporadically respond with reject pulses. On four occasions accept pulses were received, all at the Boss tracking stations; no other tracking station received accept pulses. It has been noticed during the ten Program 206 flights that a high density noise environment exists over the New Boston tracking station. This noise environment plus a possible gate failure within the PPD could have caused the sporadic acceptance of Agena commands. In addition, the gate failure would have definitely caused reject pulses to be generated by the command decoder whenever Agena commanding was attempted.

To prevent this problem from recurring, in-house and field testing of the PPD became more stringent. Pulse positions of the S-band interrogation were varied to ensure against inadvertent commanding by an alien source. SV 953, the last vehicle to fly in the "hitched-up" mode, experienced no command interference problems with the Agena.

64SD4760

2-8

2.1.3.5 RMA Disable

One of the early problems associated with the Command Subsystem's interface with the Attitude Control Subsystem was displayed by SV 953. The RMA disable commands were not consistently executed causing an excessive use of control gas while performing maneuvers. It was determined from an intensive analysis that a possibly marginal input signal voltage to the RMA could have caused intermittent RMA disabling upon command. To increase the input signal voltage at the RMA, a diode, which was in series with the signal, was replaced by relay contacts thereby increasing the signal by approximately .7 volts. No further difficulties were encountered with this interface in any of the subsequent vehicles.

2.1.3.6 Airborne Clock

The airborne vehicle clock had proven itself as a highly reliable timing device, both on past programs and also on the first few Program 206 flights. However, on SV 955 the clock either advanced to a high count or reset to zero during a dormant period between tracking stations. At the same time the four sonic delay lines within the command programmer were either erased or garbled. A transient resulting from a piece part failure within the programmer could have caused this condition.

The piece part which was assumed to have failed was one of 40 bypass capacitors on the +28 volt input line to the programmer. These capacitors are utilized to filter any a-c ripple or transients off the 28 volt bus before entering the module. Any one of these capacitors could momentarily short to ground thus removing 28 volt power from the programmer. This would allow the clock and word storage lines to assume a random bit configuration when power was eventually restored when the capacitor burned open.

For the next three revs following the loss of command capability, the vehicle telemetry had to be energized by use of the unsecure BUSS command link. On the fourth rev, a

64SD4760

secure BUSS command was sent energizing the PPD. The command subsystem was properly loaded with new commands at this time and total command capability was recovered.

There were no modifications made to the command subsystem as a result of this problem. The cause of the failure was assumed to be random in nature and additional changes were deemed not necessary.

During a later flight, SV 957, the vehicle clock lagged the ground system time by an increasing linear amount (220 milliseconds per day). This increasing deviation between the two time systems was attributable to an offset of the crystal oscillator frequency within the command programmer. Although this frequency offset was within component spec tolerances, the desirability of rewording the system specification to reflect the component spec became apparent. Also, in-house and field tests became more stringent with regard to clock drift and/or offset. SV 958 was found (during ground tests) to have had an out-of-spec vehicle clock which was replaced using a spare programmer. The problem of clock drift and/or offset has not been experienced again on any Program 206 flight; however, a capability analysis of vehicle clock versus system time correlation was performed for flight SV 960. The results of this analysis are discussed in Section 3.3.6.

2.1.3.7 Command Programmer

Further difficulties encompassing the command programmer resulted during the flight of SV 958. First the 10 pps timing signal failed on rev 16; then, complete programmer power supply failure occurred during rev 36. These two failures were a direct result of over-heating. The temperature cycling experienced during this flight is suspected to have caused the component mounting board material (Photoseran) used in the programmer to have flexed enough to break a weld on the board resulting in the catastrophic failure. Similar experiences were noted during ground thermal tests of programmers. Beginning with programmer number six, the component board material was changed to epoxy glass, a nonthermal-sensitive material. Prior to SV 958, two of the original five programmers were flown

64SD4760

2-10

successfully (no temperature cycling occurred during these flights). The remaining two units were returned to the vendor for modification and all nonredundant circuitry was mounted on epoxy glass.

Another anomaly peculiar to SV 958 was the failure to execute a stored command (DSPC 3) during rev 20. Speculation as to the various failure modes was made but no logical conclusion could be drawn. This problem was never evidenced in any of the other nine satellite vehicles flown in Program 206 and, therefore, the problem remains unresolved.

2.1.3.8 Delay Line Readout

A difficulty was encountered involving the command programmer and command decoder during in-house testing of SV 958. The command decoder input threshold on the gated megacycle pulse width was not within specification. The minimum pulse width acceptable to the decoder was 240 nanoseconds; whereas, the lower specification limit for the command programmer readout is 200 nanoseconds. The command decoder was modified to accept a pulse width of 160 nanoseconds thereby making it more compatible to command programmer readout. Effectivity of this modification was SV 958; however, there was no evidence in Program 206 history that indicates incompatibility between programmer and decoder before SV 958.

2.1.3.9 Loss of Stored Command Capability

Between revs 10 and 18 during the SV 960 flight increasing difficulty was experienced in accepting stored time commands although no real-time commands were rejected. From rev 19 on no stored commands were accepted; by rev 28 the last successfully stored command, loaded on rev 18, was successfully executed. In order to determine the nature of the malfunction several on-orbit tests were conducted. In addition, several post flight tests were conducted on identical vehicles. Based on these tests, it has been concluded that a portion of the bit-read circuitry of the information pulse circuitry of the Command Subsystem was the probable cause of failure.

64SD4760

To facilitate the deductions pertaining to the command decoder refer to figure 2-2 and the following description of circuit operation. In the diagram the circuits pertaining to the processing of the real-time commands and the circuits common to both real-time and stored-time commands are shown in a horizontal progression. The circuits for the stored-time commands only are shown in a vertical progression.

Since the real-time commands were successfully executed, it can be seen in the diagram that the "information flip-flop" was functioning, and that shift pulses were being produced by NAND 21 by the bit-read pulses via the "one-shot" circuit. Therefore, a failure in the information channel of stored commands would result from the failure of NAND 32 or an open line from the "information flip-flop" to NAND 32. If NAND 32 short-circuited, the information passed through the "select line" gates would all be logical "ones" and the command thus simulated would be rejected for having an improper parity indication. An open line effect to NAND 32 would also result if the input diode to NAND 32 failed as an open circuit. A failure in the bit-read channel to the programmer would have resulted from a failure of NAND 34, the failure of the resistor which furnishes the drive current to the programmer, or the failure of the gate within the one-shot circuit between the logical "one" output and the logical "zero" output. Within the command programmer the bit-read signal initiates a "one-shot" circuit which is common to all storage lines. It is possible that this circuit failed. However, during the prelaunch operations similar difficulties were experienced between real-time commands and stored-time commands. The programmer was replaced but the difficulties persisted. It is therefore concluded that the cause of the difficulty was not in either programmer and consequently improbable that this "one-shot" circuit failed during flight.

On orbit, since some stored-time commands were accepted between revs 10 and 18, it was postulated that reception might be a function of warm-up time per pass for the command decoder. Consequently, an attempt was made to store "twelve-minute resettable" commands for execution prior to station entrance. It was anticipated that by midstation pass the decoder would have warmed up sufficiently to accept stored commands. The results were not only inconsistent but were partially responsible for the loss of two critical command
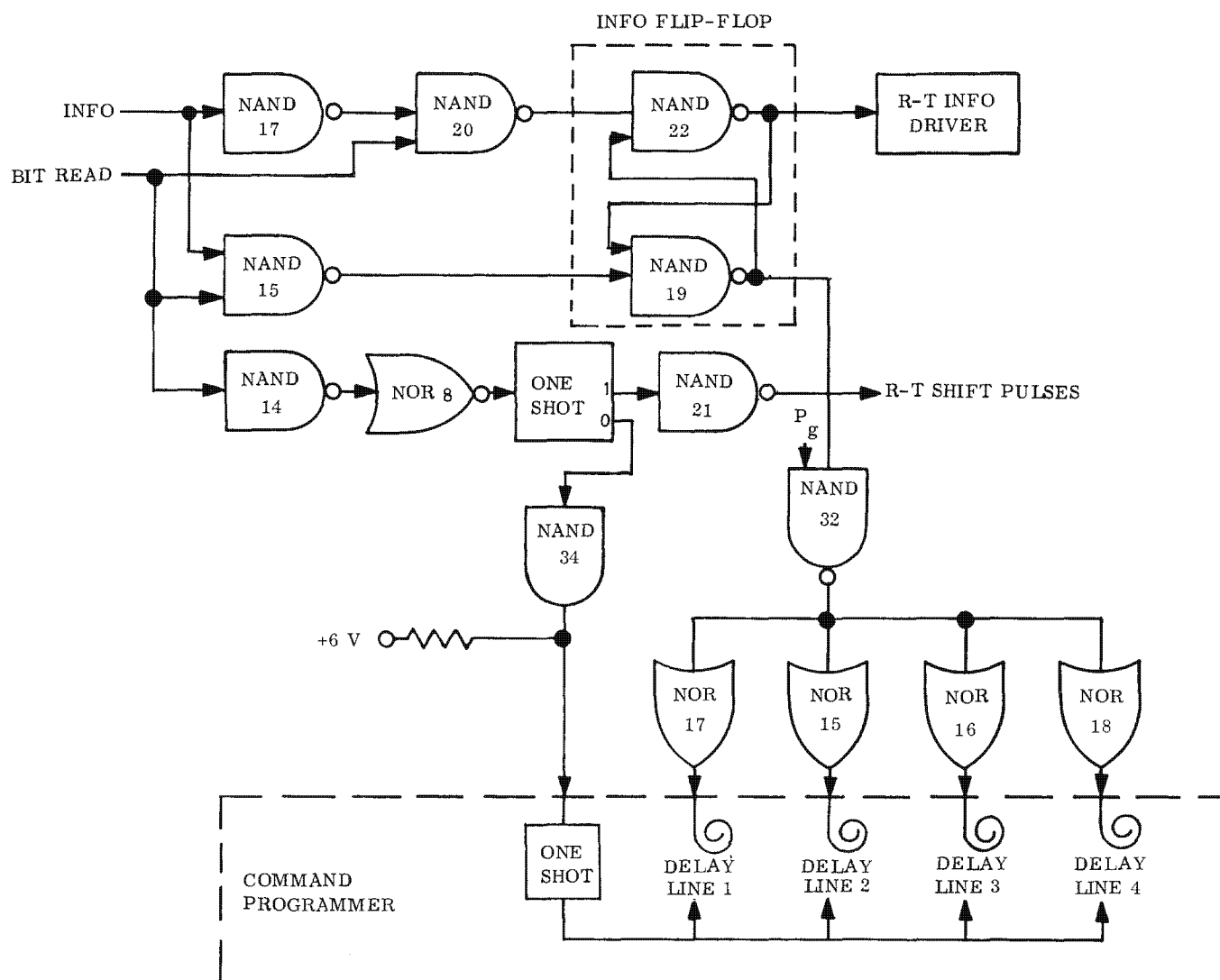
Figure 2-2. Command Decoder Input Circuit and Programmer Interface Diagram

64SD4760

2-13

sequences. Since the command system was in the stored mode, and since stored (37-bit) commands were not being accepted, the real-time enable command also could not be accepted. Thus the system would remain in the stored mode until the six-minute timer (in its twelve-minute resettable mode) expired. The timer did not expire before additional commands were read out from the programmer. These additional commands were blocked by the stored mode of the command decoder and reset the timer for an additional twelve minutes. This cycle of events was repeated until after the critical sequences had been blocked and until at least twelve minutes expired before successive readouts.

Although real-time commands were being executed, and therefore correctly processed by the PPD, it was additionally postulated that the pulse-position discrimination of the PPD might be marginal. The position of the pulses within each group was therefore varied. The results were negative.

Although the parity of stored commands is checked in the respective delay line in which a word is about to be stored, and although the simultaneous failure of all four delay lines was considered improbable, the parity of transmitted stored commands was nevertheless varied. All such command transmissions were rejected. The bit count of the transmitted stored words was varied from 30 to 50 bits per word. These transmissions also were rejected.

Under the assumption that the eleventh harmonic of the Delta 3 telemetry transmitter was simulating S-band transmission, the S-pulses were omitted from each pulse group of the transmitted stored words. No "reject" signals were received and the interrogate monitor remained at the appropriate level thereby indicating that no spurious signals were present. Under the assumption that either the S-band beacon was off frequency, or that the beacon or PPD was being overdriven, the transmission frequency, power, and pulse repetition rate were varied. Again, no positive results were obtained.

In order to verify that all real-time commands were being accepted, a series of approximately 130 RTC 11 commands and approximately 130 RTC 12 commands were transmitted.

64SD4760

2-14

None of these commands were rejected. Since there are eight bits per real-time command, at least two thousand bits were received with no spurious interference. The lack of interference within the duration represented by two thousand bits implies that spurious interference was not a factor in the rejection of stored commands.

Two specific types of post-flight laboratory tests were conducted on command subsystem components and on the entire subsystem in two identical vehicles. Bit-read tests were conducted at the command decoder/programmer interface and the effect of the eleventh harmonic of the Delta 3 link was evaluated on SV 961 and SV 965. Additional capacitance was added in parallel with the coaxial cable that conducts the bit-read pulse from the command decoder to the programmer. It was found that 8700 picafarads had to be used to effect a malfunction. This capacitance is equivalent to adding an additional 310 feet of coaxial cable between the two components. Since there is only 5 feet of cable between the components in the vehicle it is concluded that more than ample drive exists at the interface.

During the field tests of SV 961 it was indicated that the eleventh harmonic of the Delta 3 link was interfering with the S-band beacon. Replacement of the power amplifier eliminated the interference. Before this power amplifier was substituted in SV 965 during in-house tests, the susceptibility of the S-band beacon to the eleventh harmonic was measured. It was found that malfunction of the beacon occurs between 35 and 55 microvolts. It was also found that the power amplifier of SV 965 produced only 3.5 microvolts, a safety margin of 20 db. However, when the SV 961 power amplifier was substituted in SV 965, it produced an 80 microvolt eleventh harmonic at the beacon input. This level resulted in beacon malfunction. The nature of the malfunction was such that both real-time commands and stored-time commands were randomly rejected. By varying the coupling between the S-band antenna and the Delta 3 antenna a different proportion of real-time to stored-time commands would be accepted. However, no variation could achieve complete rejection of stored-time commands with simultaneous complete acceptance of real-time commands.

64SD4760

2-15

The conclusions drawn from these tests are that:

a. The eleventh harmonic can cause beacon malfunction in both RTC and STC if the eleventh harmonic present at the beacon input is greater than 35 microvolts.

b. The SV 961 power amplifier had an excessive eleventh harmonic.

c. The performance of SV 960 was not the same as that of SV 961 and SV 965, since all RTC were accepted and all STC were rejected.

Corrective Action: Although the eleventh harmonic did not cause the malfunction of SV 960, the magnitude of the eleventh harmonic of the Delta 3 power amplifier of any subsequent vehicle shall be compared against the susceptibility of the beacon of that same vehicle to such harmonic.

No corrective action can be taken in the command decoder bit-read or information circuits because the specific failure could not be identified. However, field handling and test procedures are being reviewed to assure that coax cabling and harnessing are not degraded by changing components that fail in test.

64SD4760

2-16

2.2 STABILIZATION SUBSYSTEM

The function of the Stabilization Subsystem is to maintain the SV at specified attitudes within prescribed position and rate tolerances, relative to the earth. The subsystem also provides the capability to maneuver the vehicle to the various required attitudes at selected rates upon command.

In general, the Stabilization Subsystem has performed satisfactorily during most of the flights to date. A chronological summary of subsystem performance is presented in the Flight Summary Table in Section 1.

The basic components comprising the Stabilization Subsystem and their association to each other are shown in figure 2-3. The function of each component and the subsystem flight problems associated with each, along with the corrective action taken to assure subsequent satisfactory performance, are summarized in the following paragraphs.

2.2.1 IR HORIZON SCANNING SYSTEM (IRHSS)

The purpose of the IRHSS is to provide an attitude reference relative to the local vertical by performing the following: scanning the earth horizon with the two IR scanners mounted on the TARS platform and processing the resultant electrical signal to provide pitch and roll error measurements. These error measurements, in the form of a dc voltage, are supplied to the TARS platform via the compensator to provide a continuous correction of the pitch and roll attitude errors of the platform.

In general, IRHSS performance has been satisfactory. The only hardware failure encountered to date resulted in a pitched-down attitude error of the platform (and therefore the satellite vehicle) of 5 degrees after approximately 42 satisfactory revs on the SV 957 flight. This failure involved the the shorting of a relay in one of the scanner inhibit circuits, and did not degrade vehicle stability.

64SD4760

2-17

64SD4760
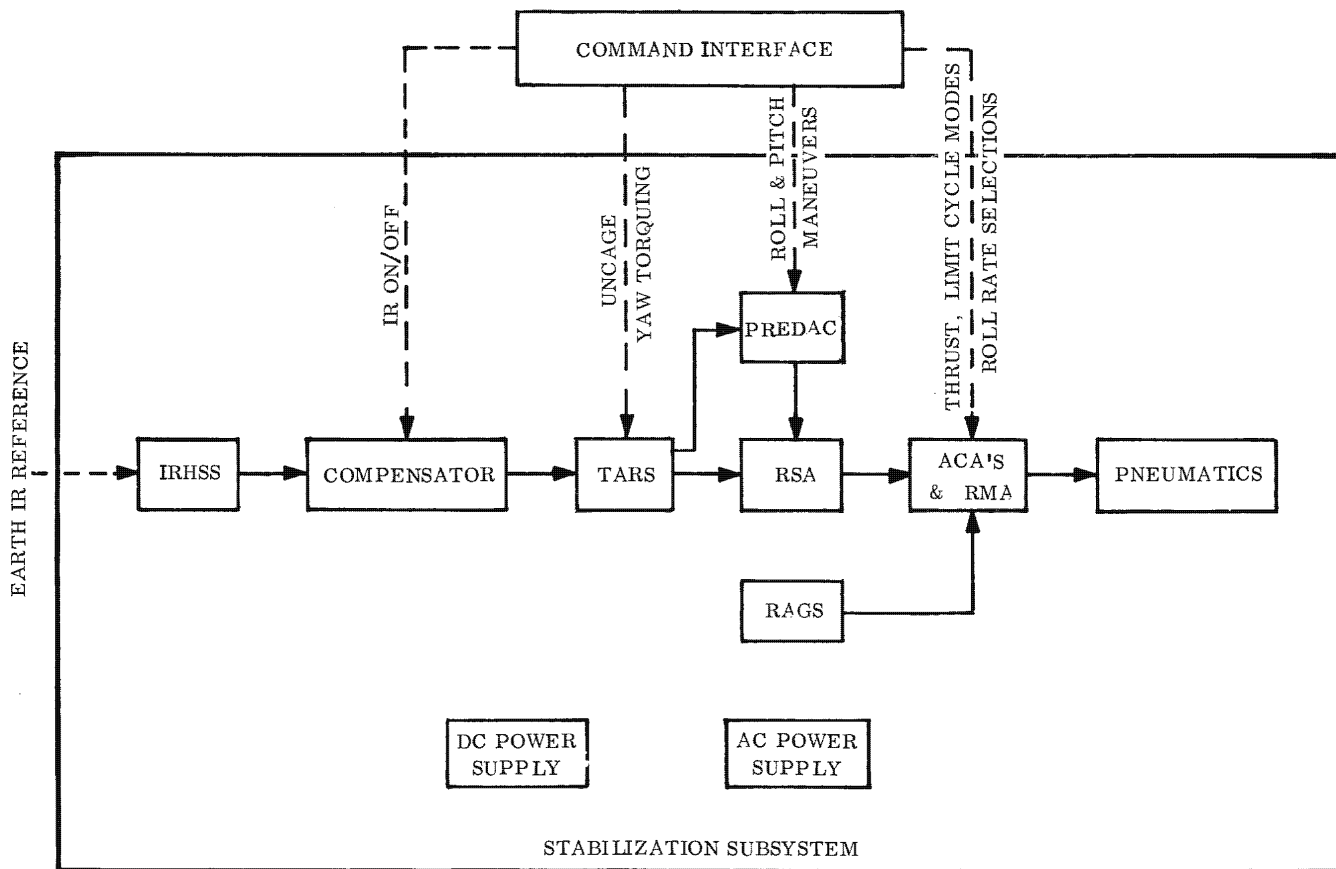
Figure 2-3. Stabilization Subsystem Simplified Block Diagram

2-18

Corrective action included review of the relay vendor's quality control techniques throughout the production cycle, including the x-ray inspection of existing relays and the teardown of stocked relays. Incorporation of more reliable relays in the scanner inhibit circuits has been and is being accomplished on subsequent vehicles. This approach of corrective action has been successful in that this anomaly has not recurred.

Loss of lock to the horizon reference was experienced four times during the SV 958 flight. This problem was not attributed to any subsystem failure, but rather to interference with the scanner fields of view by portions of the aft bulkhead thermal blanket, believed to have been ripped and dislodged during separation of the SV from the Agena. Because loss of lock was observed during two of the four occasions in the vicinity of the South Pole (and probably occurred in the same region on the other two occasions), it is believed that the lower earth IR radiation in this region, in conjunction with high altitude, contributed to the losing of the horizon reference by providing marginal IR stimuli. Therefore, the observed interference within the scanners' fields of view had a much more significant effect on losing the reference in this geographical region.

During the SV 959 flight, frequent loss of the IR horizon reference was again experienced. Separation conditions were nominal and there was no evidence of significant interference within the scanners' fields of view. Analysis revealed that on two occasions, lock was definitely lost in the South Polar region, and probably occurred over this same area on all other occasions. It was concluded that earth IR stimuli available to the scanner in the South Polar region was less than that necessary for IRHSS computation of attitude errors and caused automatic inhibit of the system outputs. Substantiating evidence showed that large seasonal variations of IR radiation also exists in the North Polar region. Amplitudes of the scanner preamplifier voltages from certain flights were very near the inhibit level as the vehicles passed over this region during the winter months in the northern hemisphere. Experimental data acquired over the South Polar region during the SV 960 flight (mid August) revealed even lower temperatures than observed during the North Polar passes of SV 955. The resultant voltage amplitudes of SV 960, although not low enough to inhibit the IRHSS, would have resulted in the inhibit of some systems previously flown, based on ground test measurements.

64SD4760

2-19

Several safeguards have been instituted to prevent loss of the IR horizon reference during future flights. The IR can be programmed "off" (Compensator command) during the period of South Polar passage, at least during the southern hemispheric winter months. In this mode, the vehicle will be inertially stable (fixed rate bias) and will not be susceptible to the high torquing rates previously experienced in the IRHSS inhibit mode. The inertially stable drift rates have been reduced to a minimum (approximately 2.5 deg/hr) to insure the capability of horizon re-acquisition with the "IR on" command following the "off" period. As a backup, automatic "IR off" commanding has been provided by utilization of the IRHSS inhibit signals for this purpose; "IR on" will occur automatically when the system becomes uninhibited. A search mode, upon command, has also been incorporated to allow gyro torquing at much higher rates (approximately 250 deg/hr) than in the "IR off" mode. This mode will thus cause horizon re-acquisition to occur more quickly in the event that lock has been lost.

In order to recognize more quickly the status of the IR system, samples of various scanner preamp-telemetered outputs have been made available for reference during on-orbit operations. (See figure 2-4.)

2.2.2 COMPENSATOR

The compensator receives the pitch and roll error signals provided by the IRHSS and converts these signals to a signal of lower response at a different voltage level. This, in effect, damps out short-period fluctuations of signal from the IRHSS, thus providing smooth corrections to the TARS platform gyroscopes. The properly scaled voltages correspond to the desired gyro torquing rate for the magnitude of error measured.

The compensator provides for the "IR on" and "IR off" commands by commanding of a relay which passes or blocks the processed IR signals enroute to the TARS platform. Although this component has performed nominally to date, a modification was introduced on the SV 960 vehicle to provide for the automatic "IR off" and "IR on" feature governed by the IRHSS inhibit circuit as discussed in Section 2.2.1.

64SD4760

64SD4760

(A)   NORMAL EARTH-SKY WAVEFORMS - DUTY CYCLE ≈ 50%

| A | B | C | D | E | F |
| Hot Earth | Cold Earth | Leading and Trailing Edge Clouds | Misc Cold Clouds | Large Cloud-Center Earth Pulse | Total Cold Cloud Cover |

(B)   ABNORMAL EARTH-SKY WAVEFORMS

| G | H | I |
| All Earth - Few Clouds | All Earth - Moderate Clouds | All Earth - Many Cold Clouds |

| J | K | L | M | N |
| Earth Pulse with Sun Spike | Sun Spike - Low (< 10% Earth dc) | Sun Spike - Medium (No Earth dc) | Sun Spike - Tlm Sat. (No Earth dc) | Sun Spike - Tlm Sat. and Mixer Sat. (No Earth dc) |

| O | P | Q |
| All Sky | Earth Pulse - 18% Duty Cycle | Earth Pulse - 75% Duty Cycle |

Figure 2-4.   Sample Earth-Sky Waveforms for Barnes 13-127 HSS

2-21

2.2.3 THREE AXIS REFERENCE SYSTEM (TARS)

The purpose of the TARS is to provide a stable rotating reference, aligned to the local vertical, about which attitude of the SV may be measured and controlled. The TARS consists of a gimbal assembly (TARS platform) and an electronics package (TARS EP). The TARS platform contains the three integrating gyroscopes which provide position reference. These gyros are maintained at the proper reference by the IRHSS inputs received via the compensator and by a gyrocompassing network designed for yaw error reference. The gyro outputs drive torquing motors to maintain the desired platform roll and pitch attitudes relative to the computed reference regardless of vehicle motion. The TARS EP contains all amplifiers and other electronic equipment which support the functional requirements of the platform. Five resolvers are contained within TARS which are used to measure angles between the platform and SV and to provide the result as an input to the resolver summing amplifier. These signals are then combined with commanded roll and pitch angles and converted to vehicle attitude error signals.

The TARS has performed extremely well on all flights to date, with no evidence of failure. As a result of other component failures in the subsystem, TARS has become involved as a probable contributor toward failure of the dc power supply on two occasions. During the SV 952 and SV 954 flights, where loss of control gas resulted in prolonged vehicle tumbling, the platform was "picked up" on its gimbal stops and caused high current drain through saturation of the torque motors. This overload probably created overheating of one of the motors which shorted and caused burnout of the power supply on each of these flights.

During the SV 955 flight, a roll-pitch gyro uncage command was executed and not followed by a fly reverse or fly forward command. This caused the yaw gyro compassing circuitry to be disconnected from the roll gyro loop, which resulted in an increasing yaw angle during a period of about 16 revs due to free gyro circuit torquing. The error was corrected on rev 18 when its cause was discovered; the system performed normally thereafter. (Refer to Section 2.9.2 for corrective action.)

During the SV 958 and SV 959 flights, higher than nominal torque motor voltages were evident throughout, but in no way affected vehicle performance.

64SD4760

Although it is known that higher voltage levels are the result of small torques opposing the gimbal motion, the source of opposing torque was not positively identified. However, action has been taken on subsequent vehicles to correct all possible sources of opposing torque. These are as follows:

a. Increasing clearance between the thermal shroud and the platform-mounted thermal band, where contact was possible due to close tolerances.

b. Increasing restraint and venting of aft bulkhead thermal blanket to prevent possible contact with the platform through pressure-differential "ballooning" during powered flight.

c. Measuring of internal bearing friction during the test cycle.

Normal pitch torque motor voltages were observed on the SV 960 flight.

2.2.4 RESOLVER SUMMING AMPLIFIER (RSA)

The purpose of the RSA is to convert resolver outputs (indicating gimbal to vehicle angles) into vehicle attitude error signals. These error signals are then factored into the commanded vehicle pitch and roll angles received via PREDAC to enable accomplishment of the desired maneuvers. The RSA has performed properly throughout all flights to date.

2.2.5 PITCH-ROLL ELECTRONIC DIGITAL TO ANALOG CONVERTER (PREDAC)

The function of PREDAC is to utilize the pitch and roll maneuver commands from the Command Subsystem in the form of binary bits to modify the electrical signals from the resolvers, thus inserting the desired vehicle attitude information for processing by the RSA.

The PREDAC has functioned normally on all flights to date in response to each programmed command. However, during flight SV 951 and SV 958, a single occurrence of a spurious

64SD4760

roll angle was evident and indicated that spooking within either PREDAC or within the digital processing circuits had caused the change of state. When these changes of state occurred, the vehicles were in a slow tumble as a result of lost IR lock. Re-commanding during the SV 951 flight enabled return to the proper state. During the SV 958 flight however, reinitiation commands could not be executed to correct the improper PREDAC state.

Commencing with SV 952, the input circuits were somewhat desensitized. Because this spooking has been rare and has never taken place under normal flight conditions, and because the situation is normally correctable by commanding, no action has been taken to further desensitize the PREDAC input circuitry.

2.2.6 RATE GYRO SYSTEM (RAGS)

The RAGS consists of one rate gyro for each vehicle axis to provide references for rate limiting of vehicle motion by the Attitude Control Amplifiers (ACS's) and Roll Maneuver Amplifier (RMA).

Except for one failure of the rate gyros due to an over-temperature condition (SV 954) the RAGS has performed normally. During other flights (SV 951, 952, 955), prescribed gyro temperature control was the only problem encountered. This problem was principally caused by improper passive temperature control design (package internal and external coatings and insulating materials), and did not result in any RAGS problems during these flights. (Refer to Section 2.7.2.)

The SV 954 failure resulted from an over-temperature condition which was caused by the continuous application of full heater power (the exact cause of which is unknown). The corrective action consisted of incorporating a redundant thermostatic high temperature cutoff control on SV 955 and subsequent vehicles, which removes all heater power at $172 \pm 5^{\circ}$F. This action, together with the use of proper passive thermal control devices and improved heater control circuitry electrical insulating materials, has resulted in satisfactory temperature control on all flights commencing with SV 956.

64SD4760

2-24

2.2.7 ATTITUDE CONTROL AND ROLL MANEUVER AMPLIFIERS (ACA's and RMA)

Through the use of logic circuits and threshold detectors, these amplifiers provide control of the vehicle's pneumatic thrust nozzles to maintain vehicle attitude and rates within desired limits. One ACA is provided for each vehicle axis. The logic circuits are constructed to provide either the fine limit cycle (with or without rate roofs) or coarse limit cycle mode, with high or low thrust nozzle control, as required by command. The RMA works in conjunction with the roll ACA and, when enabled, allows roll maneuvers to be completed at either medium or high rates. (Low rate maneuvers require only the roll ACS.)

No failures of any ACA or RMA have occurred on any flight to date, although some difficulty in maintaining the desired enable or disable states was experienced during two early flights.

During the SV 951 flight, the ACA's were disabled several times, and at another time, an inadvertent RMA enabled-ACA disabled (medium rate) state was also induced, thus causing rapid depletion of control gas. Both conditions were apparently caused by sensitivity to EMI noise generated within the command interface circuitry. Commencing with SV 952, the input circuitry of the ACA's and RMA's were desensitized to prevent recurrence of this difficulty, which resulted in an apparent satisfactory solution to the spooking problem.

During the SV 953 flight, the RMA, once enabled, could not be consistently disabled. This resulted in all commanded low-rate roll maneuvers to be performed at the medium rate, dictated by the enabled RMA, although the selected vehicle roll angles were in all cases attained satisfactorily. In addition, excessive gas usage resulted when the roll ACA was commanded to coarse limit cycle with the RMA enabled (prohibitive flight mode). This anomaly, its cause and corrective action, is discussed further in Section 2.1.3.5.

2.2.8 POWER SUPPLIES

The functions of the power supplies are self-evident. Failure of the dc power supply occurred on the SV 952 and SV 954 flights. On both occasions, the failure followed periods

64SD4760

of prolonged vehicle tumbling at high rates which had caused continuous voltage saturation of the gimbal torque motors. While this condition does not create an overload greater than the capacity of the power supply at the supply temperatures observed, it is felt that the torque motors overheated from the prolonged saturation and eventually shorted. This caused instantaneous power supply failure to occur during periods of time where telemetry data was not available for verification in each instance. Because these failures were secondary effects, no corrective action was necessary.

2.2.9 PNEUMATICS

The pneumatics system consists of the stored Freon gas, the various control nozzles, and the solenoids and activation valves which control the flow of gas. All the pneumatics components have operated well throughout the program, with no evidence of failure. Commencing with SV 953, storage tank heaters were incorporated to improve previously unsatisfactory temperature maintenance which allowed significant loss of available impulse during hitch-up flight. (Refer to Section 2.7.1.)

Upon Stabilization Subsystem activation during the SV 952 flight, following SV/Agena separation, a large disturbance torque was experienced simultaneously with a rapid loss of gas pressure. All control gas was expended within half a rev, with an associated loss of attitude control capability.

The suspected cause of this gas loss was an open secondary fill valve. A laboratory test, designed to duplicate this condition, reproduced nearly identical results. Revised field test procedures and safeguards were implemented to prevent recurrence of this problem, and have proven successful.

Progressive increase in vehicle weight (and therefore moments of inertia) resulted in a lower than optimum high thrust control torque-to-moment ratio during the early OCV and SV (OCV plus SRV) flights. This lower ratio became critical on the SV 956 flight. It

64SD4760

resulted in high-rate roll maneuver settling times and maneuver durations of approximately 6 seconds higher than nominal because the associated low decelerations caused switching line overshoot on completion of the maneuvers.

A temporary 11.4% increase in nozzle thrust was expedited for use on the SV 957 vehicle. This reduced the settling times to a satisfactory level. The thrust levels were optimized on SV 958 and subsequent vehicles with a further thrust increase of 18.6% which resulted in nearly zero-settling times and nominal maneuver performance.

It became evident during early flights that the impingement of high-thrust roll nozzles on the vehicle's aft bulkhead produced the following two effects:

a. Thrust was applied to the vehicle which added energy to the orbit (which decreased apparent B-factor), thereby producing changes in the calculated orbit parameters which were difficult to predict.

b. Disturbances were produced about the pitch and yaw axes during medium and high rate roll maneuvers. These disturbances are of little concern because the resultant attitude excursions are insignificant, and rates and attitude errors are quickly reduced to within limits as the associated maneuver is completed.

In an attempt to reduce the apparent drag effects, the high-thrust roll nozzles were moved aft from the bulkhead 3 more inches on SV 959. Because of other problems with attitude control on this flight, the effectiveness of this action could not be ascertained. The nozzles were moved back to their SV 958 locations for the SV 960 flight when it was determined that, in the SV 959 configuration, they were within the IRHSS scanners' field of view for certain combinations of roll and pitch angles. Although no evidence of IRHSS performance degradation due to this condition alone could be found, the action was taken to prevent the possibility of sun reflection off the nozzles into the scanners at various sun/vehicle aspect angles.

64SD4760

Small seat leakage of the high pressure regulator was apparent from the higher than normal lockup pressures in the regulated high pressure manifold during the flight of SV 960. In spite of this apparent leak, the regulator otherwise functioned normally and over-pressurization of the system was not indicated at any time. High and medium roll maneuver performance appeared normal. Possible effects of the leak on steady-state performance are discussed in Sections 3.2.5 and 3.4.3.

The regulator leakage is considered random in nature and to have been caused by scratching of the seat by foreign objects. Therefore, no corrective action is planned.

64SD4760

2.3 BACK-UP STABILIZATION SUBSYSTEM (BUSS)

The function of BUSS is to orient the vehicle into the desired attitude for deorbit of the SRV in the event the primary Stabilization Subsystem is unable to perform this function. The subsystem operates by utilizing magnetometers to measure the angles between vehicle axes and the earth's magnetic field. The resultant voltage outputs are used to actuate control gas nozzles which cause the vehicle to be rotated about its axes until the outputs are within desired error limits. For the geographical area over which BUSS is required to be energized, the resultant vehicle attitude (parallel to the magnetic field) coincides with the desired attitude relative to the earth for SRV deorbit.

BUSS was first flown and first utilized on the SV 954 flight for SRV deorbit by necessity due to loss of primary attitude control capability. The system was also used for SRV deorbit during the SV 959 flight, when maintenance of IR lock was uncertain, and again during the SV 960 flight when lack of command capability precluded use of the primary subsystem.

During the SV 955 and 956 flights the system was activated experimentally following OCV deboost engine cutoff which was completed under control of the primary subsystem. A large yaw angle was induced prior to activation of BUSS to offer an initial condition outside the BUSS switching lines. BUSS performance during each of these experiments was unsatisfactory due to a single, but different component failure. A similar experiment was conducted during the SV 957 flight with altogether satisfactory results.

Due to loss of primary command capability, deorbit of the OCV following SRV separation could not be initiated during the SV 958 flight. BUSS was initiated in this case in order to deactivate the primary system and create a large vehicle angle of attack as a means of inducing deorbit through increased drag. BUSS performance was nominal, although the stabilization and command portions of the subsystem experienced apparent problems early in the flight.

64SD4760

2-29

2.3.1 COMMAND

During the SV 955 flight, failure of either the K3 or K9 relay within the J-box prevented the command sequence from activating the BUSS pneumatics or control electronics and subsequent functions, although the primary system was deactivated. Because no history of failure of this type relay existed before this flight, it was considered random in nature. No difficulty with either of these relays has since been experienced.

Apparent spurious command tones were received by the SV 955 and 958 subsystems, indicated by the existence of unintentional command mode changes. The spurious commands did not result in unsatisfactory subsystem performance, however, and the desired modes were re-commanded without difficulty. Because this problem is inherent in a single tone system no corrective action was taken. Similar problems will be eliminated with the dual tone command system to be flown starting with SV 964.

2.3.2 TELEMETRY

Prior to the launch of SV 954 electrical power to the BUSS telemetry was intentionally severed as a precaution due to problems experienced with the SV primary command system. This action, coupled with loss of the primary Stabilization Subsystem DC power supply in flight, resulted in virtually no telemetry data for use in analyzing BUSS performance. However, use of the SV continuous current monitor and telemetry signal strength records allowed enough basis to offer evidence of proper operation (refer to Section 2.3.3). The prelaunch anomaly could not be reproduced in the laboratory; no corrective action was taken.

Telemetry channel calibration techniques resulted in a 10% low Q-magnetometer telemetered output compared with the G-BUSS computer printout utilized on orbit for SV 955. Improved calibrations corrected this problem on all subsequent flights thru SV 959. However, SV 960 results revealed differences of similar magnitude to that of SV 955 in the pitch and roll axes, either due to the same type calibration errors or to SCO drift. Since this occurrence is considered random in nature, no further corrective action will be taken.

64SD4760

2.3.3 STABILIZATION

The SV 954 BUSS is believed to have operated nominally, based on the minimal data available (ref Section 2.3.2). The continuous current monitor revealed solenoid valve operation, while signal strength data indicated a change in vehicle attitude following activation. Because of the high vehicle tumbling rates at time of activation, it is believed that all control gas was consumed before rates could be damped and proper attitude achieved. Impulse required to overcome the initial conditions presented was beyond the design of the system. Attitude at time of SRV separation allowed successful recovery.

SV 956 performance analysis revealed that the No. 4 pneumatics solenoid was inoperative. Examination of prelaunch test records revealed that the failure could have been induced by burn-out of the solenoid due to an improper test procedure or that a broken wire or improper connector mate existed at time of launch. Modifications to the field test procedures were made to preclude recurrence of either possibility.

An increase of Q-magnetometer scale factor was experienced during the SV 958 flight. The cause is unknown, although very high vehicle temperatures early in the flight could have been contributory. The deadband and hence the limit cycle period were decreased, but performance was not degraded.

64SD4760

2-31

2.4 ELECTRICAL POWER AND SIGNAL DISTRIBUTION SUBSYSTEM

The Electrical Power and Signal Distribution (EP&SD) Subsystem consists basically of a primary power source, a back up power source for the command programmer, and the wiring and hardware required to deliver the power to the various vehicle subsystems. The primary source consists of five silver oxide-zinc batteries in parallel which provide a nominal 28.0 volt unregulated d-c supply voltage.

This subsystem has demonstrated its ability to adequately support a five-day primary mission; it has not been mission-limiting on any of the flights to date.

2.4.1 CELL SHORTS

During the battery activation period or in-flight, the first three flight vehicles experienced battery failures that were attributed to cell shorts resulting from: 1) extended battery storage with its associated material decomposition and deposits; 2) weak plate separator systems; and 3) separators damaged during reworking. These battery deficiencies have been eliminated by closely coordinating battery procurement with flight schedules, rejecting reworked cells, and by tightening the battery vendor's inspection and quality control procedures.

2.4.2 OVER-TEMPERATURE FLIGHT CONDITIONS

The battery temperature sensors, normally mounted on the battery cases, were improperly mounted in the battery wells on the first two flights precluding accurate determination of the battery temperatures. However, the performance of the batteries on these flights was characteristic of battery over-temperature conditions.

Two ground thermal vacuum tests of the batteries were performed to resolve the flight observed phenomena. As a result, the batteries' passive thermal control was modified by removing the low emissivity taping on all battery surfaces except for the inside surface

64SD4760

2-32

(mounting side) and the removal of the super-insulation caps placed over each battery. In addition, the battery heater thermostats were changed from a set point of $72^{\circ}F$ to $34^{\circ}F$. These modifications, made initially on SV 953, proved to be effective.

2.4.3 OVER-TEMPERATURE STORAGE

Two programmer back-up batteries were activated for potential use on SV 952. Each of these batteries had individual cell, open-circuit voltages of 1.60 volts instead of 1.80 volts. Two non-activated batteries from the same lot were subsequently analyzed by the battery vendor and were found to be very dry (an indication of over-temperature storage).

The corrective action taken was the use of temperature warning tags on the battery shipping and storage containers and shipment of new batteries directly to the field to minimize storage time. The ability to fly newly manufactured batteries on each vehicle will be attained in the near future.

2.4.4 INCOMPATIBLE VOLTAGE INDICATIONS

It was noted on SV 958 and SV 959 that the command decoder and back-up battery voltage indications were higher than the operational bus voltage measurement. Since the command decoder and back-up battery voltage monitoring points are downstream of the operational bus, it is physically impossible for those voltages to be higher than the operational bus. The incompatibility was attributed to faulty telemetry calibration. An improved calibration procedure has been implemented and proven satisfactory.

2.4.5 PREDISCHARGE

Schedule difficulties for the first three flights made it desirable to omit the vehicles' step-down voltage regulation hardware and instead, reduce bus voltages to acceptable system levels by a predischarge procedure. This procedure substantially reduced the capacity of the batteries to the point where a five-day primary mission could not have been flown with these vehicles.

64SD4760

2-33

Predischarge caused the batteries to be in a comparatively drier state when installed in the vehicles, this condition increased the probability of chemical deposits and cell shorts on these flights. In addition, predischarge masked the best method (activated wet stand) for detecting shorted cells. It increased the electrolytic action in the batteries, driving some of the cells off their peroxide peak (higher initial voltage) toward the 1.6 open-circuit voltage plateau, making it difficult to detect shorted cells. For this reason, a monitored five-day wet stand, prior to predischarge, was instituted with SV 952.

The incorporation of the necessary voltage step-down hardware, starting with SV 954, eliminated the need for predischarge.

64SD4760

2.5 SRV SUBSYSTEM

The Satellite Re-entry Vehicle (SRV) Subsystem has the purpose of withstanding the powered flight and orbital environments as a portion of the SV, and of becoming a self-contained vehicle for re-entry and recovery after separation from the OCV. Throughout the Program, this objective has been met, climaxed by successful aerial recovery of the capsule. All functions associated with the de-orbit and recovery sequences have been nominal, except for the minor items discussed below.

2.5.1 SPIN AND DESPIN PERFORMANCE

During the developmental phases of Program 206, it was thought that the minimum spin rate of the SRV should be 70 rpm if dispersion requirements were to be met. Actual spin rates, however, have been significantly below that figure, averaging 57.3 rpm, with no apparent effect on dispersion; this indicates that the original criterion was somewhat conservative. The maximum residual spin was to be a maximum of 10 rpm, restricted by lateral loading conditions thought possible during re-entry. Flight data has always been below that limit, averaging 7.6 rpm. Other aspects of the spin/despin performance are discussed in 3.7.4.

2.5.2 OVERFLOW OF TELEMETRY BATTERY ELECTROLYTE

Post flight examination of the first two capsules showed that the telemetry battery had, in each case, vented electrolyte to the interior of the capsule during descent. Examination of these and similar batteries revealed that on some batteries delivered by the vendor vent valves had been incorporated which did not meet Program 206 specifications. Both batteries mentioned above were from this group. The batteries with inadequate vent valves were replaced with the proper type initially on SV 953.

Although no leakage occurred on SV 953, it was evident again in the SV 954 capsule. At this point it was determined that the internal electrolyte absorbtion chamber capacity

was insufficient, necessitating installation of an external tube packed with cotton as an overflow chamber. This tube was first installed on SV 955, and no electrolyte overflow has been experienced since.

2.5.3 DISCONNECT 1 TELEMETRY AMBIGUITY

On the second and third flight vehicles, telemetry indicated that the Disconnect 1 function had not occurred properly. In both instances the telemetry indication was found to have been incorrect during the post flight capsule examination; the anomalous indication was the result of a breakwire being shorted to capsule ground. An insulation sleeving had been designed to protect against this condition after the first occurrence, but it was improperly installed on SV 953. Emphasis was placed on proper installation for SV 954, and no problems have been experienced since.

2.5.4 HIGH TELEMETRY EVENT LEVELS

Throughout the flight phase, the voltage levels telemetered to signify occurrence of de-orbit events have been significantly higher than those in the Calibration Book. The levels have returned to near nominal following the switch to the recovery battery reference at the time of thrust cone separation. Calibration Book levels are taken from prelaunch test data, where the voltage supply is 30 volts, the nominal thrust cone battery voltage. However, actual thrust cone thermal battery voltage is generally higher (between 32 and 35 volts), causing the greater deviation. The maximum battery voltages as inferred from the telemetry event levels have not exceeded the upper specification limit of 36 volts; therefore, the telemetry levels must be considered to have been within the expected possible range.

2.5.5 PREMATURE TELEMETRY MODE TRANSFER

Ejection of the thrust cone assembly normally activates series-redundant switches to change SRV telemetry from de-orbit to recovery mode. On SV 958, SRV telemetry was in the recovery mode when first acquired, and remained in that configuration throughout

64SD4760

the de-orbit and recovery sequences. It was suspected that the high temperatures experienced during the first two revs were sufficient to cause a switch malfunction leading to the premature mode change. Post flight thermal-vacuum testing verified the possibility of switch failure under the initial orbital conditions. No corrective action was required.

2.5.6 TOOL IN CAPSULE

A torque wrench handle was found inside the SV 959 capsule following recovery. Although its presence did not degrade SRV performance, such incidents have been and will be averted subsequently by a tool check and count at appropriate times in the processing cycle.

2.5.7 INOPERATIVE FLASHING LIGHT

The flashing light was not operating when the SV 960 capsule was recovered. It was found during post flight analysis that the flashing light controller was not supplying power to the light. This resulted from a diode failure within the controller. Since no controller failures are known to have occurred before, and the failure is considered random, no corrective action is felt necessary.

64SD4760

2.6 SEPARATION SUBSYSTEM

When properly commanded, the Separation Subsystem performs electrical, mechanical, or pyrotechnic functions necessary to effect vehicle separation sequences. Maximization of reliability and safety have been stressed through the design and flight phases. The discussion below deals with problems which have arisen during the flight phase, and the necessary changes to the subsystem, as well as any items which might contribute to improved design.

2.6.1 SHAPED CHARGE REPLACED BY V-CLAMP

The original design of the Separation Subsystem relied on a shaped charge to cut the vehicle skin and allow separation of the SV from the Agena. However, consideration of possible shocks from the charge detonation led to the substitution of a V-clamp for the shaped charge. Time limitations precluded the implementation of this change on the first flight, therefore SV 951 was separated by the shaped charge, with no apparent deleterious effects. The second flight vehicle was equipped with the V-clamp. During analysis of that flight, it was noticed that the explosive bolts used to break the clamp had imparted roll rates of 1deg/sec. to the SV. These rates were at the specification limit, and it was decided to reverse two of the four bolts, so that the individual thrusts would be offsetting. This was to be done on a noninterference basis. The first applicable vehicle was SV 959, when no roll rate was observed following separation. All other aspects of the V-clamp separation have been normal throughout the period of its use.

2.6.2 SEPARATION SPRING MONITORS

The four separation spring monitors were intended to provide a measure of SRV separation velocity and tip-off rates. This was to be accomplished by measuring absolute and relative duration of contact of a fully-accelerated sliding bar and a stationary brush. Velocity could be computed by knowing the length of the bar, and tip-off rates by correlating relative duration with location on the vehicle periphery. On the early vehicles, it was found to be

64SD4760

very difficult to perform the necessary calibration of the four units in the installed configuration. In addition, the cotter pin used to restrain the bar until readied for flight was located such that the bar could easily be damaged during pin insertion. The units have remained in the vehicle, but little useful information has been obtained. After SV 966, no spring monitors will be installed.

2.6.3 SAFE & ARM DEVICES

Four safe and arm devices, designed to lock out spurious "fire" signals, are used within the Separation Subsystem as safety precautions during ground checkout and powered flight. During field testing of the first vehicle, a test unit failed to arm. It was thought that the many testing operations had worn the mechanism to the point where internal friction was causing fluctuations in the current being drawn. When the negative portions of these current fluctuations reached zero, the SCR in the separation controller shut off and removed power from the mechanism. Although this particular failure was in a test unit, a shunt resistor was added to the circuitry in the separation controller to keep the SCR's in conduction if similar conditions should occur in a flight unit.

2.6.4 IFD CATCH BOX REPLACED BY BUNGEE CORD

The In-Flight Disconnect (IFD) between the SRV and the adapter separates with considerable force. To keep this piece of hardware from damaging other adapter parts, a "catch box" was conceived. The installation of this item, however, made preflight mating of the IFD a difficult task. Therefore, the catch box was replaced by a restraining bungee cord with the same purpose. This change was made effective on the first vehicle, and has been used successfully throughout the program.

2.6.5 POST-FIRE SQUIB CIRCUIT SHORTS

In various instances during the flight phase, the continuous TLM channel monitoring battery current indicated high current usage immediately following firing of squibs. This is

64SD4760

evidence of shorting of the squib leads, a condition which had been expected to occur occasionally. Protection against post-firing squib circuit shorts has been designed into the system, and proved adequate in all cases.

2.7 ENVIRONMENTAL CONTROL SUBSYSTEM

The Environmental Control Subsystem was designed to provide the proper working environment for the various sections and components of the SV. Gross temperature control has been maintained primarily through the use of vehicle and component coatings. Heaters have been employed only where necessary to maintain more precise control. The feasibility of this concept has been verified by the generally successful control of vehicle internal temperatures.

Particular problem areas which have become evident during the Program 206 flight phase, and which required changes to the subsystem, are discussed below along with any items which might contribute to improved design.

2.7.1 PNEUMATIC STORAGE TANK HEAT LOSS

The original concept for thermal control of the pneumatic storage tanks was that prelaunch heating would raise gas temperature to a point where superinsulation blankets covering the tanks could maintain stored thermal energy at necessary levels. However, on the first flight, gas temperature decayed approximately 100 F^o during the first 18 revs, compared to the 10 to 20 F^o predicted. The excessive heat loss was felt to be a result of blanket compaction over the tank area, a condition which would have reduced the insulation effectiveness of the blankets.

Two fixes were incorporated prior to the second flight: 1) a patch was attached to the existing blankets over the tanks to help correct for the compacted condition of the insulation, and 2) a low emittance coating was specified for the forward portion of the tanks to decrease the rate of radiant heat transfer directly from the tanks to the adjacent station 209 bulkhead.

Again, heat loss was much greater than expected on SV 952. It was later found that the tank blankets had been very tight before launch, and that the patch had not covered all the

64SD4760

compacted area. It was thus suspected that major heat loss was again through the blankets. In addition, some heat was lost by radiation due to the partial omission of the low emissivity tank covering, and by conduction due to the omission of the small blanket behind the TARS electronics package.

At this point, it was of prime importance to insure proper energy maintenance for the third flight (SV 953). Hence, one of the three tank AGE heater segments was connected to vehicle power for flight, so that up to 40 watts of heat could be applied to the tanks in orbit. These heaters were controlled with 110°F thermostats. In addition, the proper emissivity coatings were applied to tanks and bulkhead, and the blankets were modified to stand off from the tanks slightly. Finally, the temperature sensors previously on the tank mounts were moved to the tank surface to give a more accurate indication of tank temperatures. Since the incorporation of these measures, no further problems have been encountered in maintaining tank temperatures.

2.7.2 RAGS TEMPERATURE MAINTENANCE

The thermal design of the RAGS package was based upon maintaining the gyro fluid temperature at $165 \pm 2.5^{\circ}$F. To maintain these temperatures, internal heaters were provided for the package. SV 951 and SV 952 had no direct telemetry measurement of RAGS gyro fluid temperatures, resulting in some uncertainty as to the in-flight temperature levels. It was evident, however, that the SV 952 RAGS package ran too hot with a component cover emissivity of 0.05. SV 951 and SV 953 and subsequent vehicles have had a RAGS cover emissivity of 0.90. Telemetry changes were instituted for the third vehicle to provide a more direct measurement of RAGS internal temperature. These consisted of locating a sensor on the outer surface of the pitch gyro inside the RAGS cover, and adding a resistor to the gyro block sensor circuit to widen its temperature range.

No problems were experienced with RAGS temperature maintenance on the third flight. It was determined from prelaunch data that a $+17.0^{\circ}$F bias existed between the gyro fluid

64SD4760

and the pitch gyro case temperatures. On this basis, orbital data indicated fluid temperature was being controlled by the internal heaters at 168 to 169°F.

Failure of the internal temperature controller which governs gyro heater power, on SV 954 led to the installation of a series-protective thermostat on SV 955 and subsequent vehicles. Nevertheless, the RAGS package temperature on SV 955 was abnormally high at 175 to 185°F; this was above the control range of the protective thermostat. Inspection of vehicles then in the prelaunch cycle showed that proper precautions were not being taken in the RAGS installation and alignment to insure consistent and adequate heater conduction path in the thermal mounting. Therefore, the overheating on SV 955 was felt to have resulted from insufficient means to dissipate internally generated heat, rather than faulty control of the heaters. Major emphasis was placed on proper thermal installation procedures for subsequent vehicles, and this has since proved effective in maintaining RAGS temperatures at the desired levels.

2.7.3 LOW PROPELLANT LINE TEMPERATURE

During the later portion of the fifth flight, the oxidizer line temperature sensor reading was approaching the oxidizer freezing point. The sun angle, however, was such that the fuel line should have been the colder, indicating that the two sensors may have been switched. Orbit Adjust Subsystem performance was not affected, as line temperature increased at the time of engine firing. Physical examination of the propellant line installation revealed that low emissivity taping, necessary to maintain line temperature in the cold BUSS section, had been inadvertently omitted from the Block II vehicles. Proper taping was initiated on SV 957. (It was too late in the cycle to correct the condition on SV 956.) During the flight of SV 956, line temperatures were not severely low, and were about equal corresponding to the high sun angle. Taping of the lines on subsequent vehicles has maintained temperatures within the desired range.

2-44

2.7.4 HITCH-UP FLIGHT THERMAL CONTROL RAMIFICATIONS

The Hitch-Up mode of flight was that configuration in which the SV remained attached to the Agena for one or two days following launch. The only thermal change presented by Hitch-Up was the interposition of the Section 7 skin between the aft bulkhead and its normal sink condition of cold space. In order to reduce the apparent heat sink for the aft bulkhead, a low α/ϵ external coating was used on the Section 7 skin. This was found to maintain aft bay temperatures within the desired range. The rapid loss of heat from the cold gas tanks (Section 2.7.1) which occurred during the Hitch-Up portion of the mission was attributable to excessive thermal losses through the superinsulation blanket and was not a function of the Hitch-Up flight mode.

64SD4760

2-44

2.8 ORBIT ADJUST SUBSYSTEM

The Orbit Adjust capability is provided by a pair of separately operated ablative thrust chambers. A low thrust-to-weight ratio and controlled firing duration provide the precise changes in vehicle orbital velocity which result in perturbations in the orbit. The subsystem was not loaded on the first two flights and was used only for deorbiting the OCV on SV 954 and 959; the subsystem was never activated on SV 960. Performance has been excellent for each orbit adjust maneuver for which it has been given the opportunity to perform. Some problems have occurred which, because of timing or other anomalies, have not affected mission success, but could have had serious consequences under other circumstances. These problems are discussed below.

2.8.1 REGULATOR ICING

During engine operation, propellant tank pressures are maintained by a regulated flow of gaseous nitrogen (GN_2) from a high pressure tank to the volume around the propellant bladders in the low pressure tanks. About half-way through the deorbit firing of SV 954, propellant pressures (and flow rate) began to decay steadily, causing a corresponding decrease in engine thrust. Following cutoff, pressures gradually returned to normal. (Actual deorbit was not attained at this time because of vehicle tumbling during the engine firing.)

The cause of this malfunction was diagnosed to be regulator icing. It is thought that the continued flow of GN_2 through the regulator lowered the gas temperature below the dew point, causing internal regulator icing. Deposits of ice building up resulted in the gradual decay in pressures. When the flow stopped and the regulator was warmed by its environment, the ice melted, allowing pressure to return to normal.

Nitrogen, as supplied by the vendor, is guaranteed to have a dew point below $-60^{\circ}F$. However, the loading of the tanks is accomplished through underground lines which are subject to condensation of water; the nitrogen pumped through these lines evidently picked up

64SD4760

enough additional moisture to raise the dew point. Subsequent expansion of the gas through the regulator lowered local temperature enough to freeze the moisture present in the gas. Following this flight malfunction, procedures were instituted to properly purge the loading lines before charging to insure a dew point of -65°F into the pressurant tank. No trouble has been experienced since.

2.8.2 THROAT EROSION

Ground testing of the thrust chambers revealed that occurrence of throat erosion after approximately 7 minutes of cumulative firing time was not uncommon. This has occurred only once in the five flights that firing time has exceeded 7 minutes. (SV 956, when the symptoms of throat erosion, i.e., increased GN_2 usage, increased propellant usage, and increased thrust, were all evident.)

The occurrence of throat erosion in ground testing prompted the initiation of studies to determine what corrective action, if any, should be taken prior to SV 956. Investigations to date indicate that the injector is the primary cause of throat erosion. This appears to be the result of poor fabricating techniques. Spray pattern analyses, new welding techniques, and closer control of the injector assembly were inaugurated as part of the action planned by the vendor to eliminate the problem. In addition, starting with SV 966, the oxidizer injector size will be made smaller to alleviate erosion. This change involves a corresponding 2% reduction in performance.

2.8.3 PRESSURANT LEAK

On SV 959, GN_2 pressure was normal from launch to the time of subsystem activation. Following activation, pressure dropped steadily by 83.4 psi/hr. This rate is sufficient to preclude subsystem operation after about 54 hours from activation. During the deorbit firing, gas usage returned to near normal, indicating that the leak had begun to deminish.

64SD4760

It appears as though the pressure loss was through one of the two relief valves in the subsystem. The relief valve can chatter under vibration, and is subject to self-contamination. It is suspected that during powered flight, a small piece of dirt or metal was caught between the valve poppet and the seal. No indication of this would have been evident prior to activation, since any pressure in the propellant tanks was confined to the liquid side of the system by the bladders. As soon as activation occurred, leakage would have been evident. Reseating would occur gradually, as the contaminating material became imbedded in the soft poppet seal. Any vibration during engine firing would accelerate the gradual reseating.

Starting with SV 973, a new valve, with a slightly slower response time will be used. This relief valve is at present being used on another space program and has been qualified at the component level.

64SD4760

2-47

2.9 OPERATIONAL SYSTEM

2.9.1 COMPUTER PROGRAM, MODULE PERFORMANCE

2.9.1.1 GCOMMAND

GCOMMAND assembles and generates a command tape to control certain vehicle functions and produces a Command Block List and Chronological Command List which format the commands prior to their transmission to the vehicle. The majority of the GCOMMAND module changes have been made to provide software changes to compensate for hardware functional characteristics or redefinition of desirable program logic.

Following the SV 952 flight, the logic was modified to assure that the PPD is on any time that the recorder is programmed ON in the playback mode (C+ commanded with R2+). This modification provides the capability to turn the recorder off by real-time commanding. A subsequent logic change was designed to prohibit turning telemetry off for less than 30 second durations. This change, dictated by hardware limitations, causes telemetry to be left on continuously for station contacts less than 30 seconds apart since these contacts appear as overlaps to the GCOMMAND module.

During the flight of SV 960, all of the commands stored in the vehicle from a given command load were executed for the first time; this revealed the need for further refinement in program logic. Timer resets are not inserted in the final station pass for a given load since this pass sequence is not normally executed because of command updating. A logic change to correct this situation will be implemented with SV 968 in conjunction with TD 35.

A programming error in the "hand spec" ALTER mode was discovered during the SV 953 flight. An erroneous TT&C command was generated in this mode which was subsequently deleted by rerunning the module. The program has been corrected to preclude recurrence of this problem. The redundancy option used for SV 960 failed to provide the desired

64SD4760

redundancy in generating a message. The initializing sequence logic, the cause of this failure, will be corrected for use with SV 963.

2.9.1.2 GTERMIN

The GTERMIN module determines times for initiating the SRV de-orbit sequence when given a specified latitude and rev number at impact, or determines the latitude and longitude of impact when given de-orbit sequence start time.

Certain factors were neglected in the initial formulation of the tables for this module. For use with SV 951 and SV 952, these inaccuracies produced an SRV uprange intrack impact prediction error of 66 n mi. Thus, the following factors, initially disregarded, were incorporated for use with SV 953: 1) effects of outgassing on de-orbit weight; 2) variation of drag with angle of attack changes; 3) separation spring force contribution to total effective retro impulse; and 4) effective retro I_{sp} was 2.6% low.

Further improvements were made to the module following the flight of SV 960. The re-entry trajectory x, y, z, $\dot{x}$, $\dot{y}$, and $\dot{z}$ parameters will no longer be listed on the binary output tape after the 1.1 g point in the trajectory is reached. The presence of this additional data caused inaccuracies to be provided in the Hula acquisition messages.

2.9.1.3 GCOMPAT

The GCOMPAT subroutine checks each command load for the presence of "taboo" or otherwise undesirable command combinations. This subroutine, originated and used for SV 951 and 952, was found to be inadequate. It was not capable of handling all of the data presented and the resulting overflow created erroneous error printouts. Because of these problems, it was recommended that this subroutine not be used with SV 953.

As a result of the SV 955 yaw around anomaly, an additional "taboo" mode was identified and added to GCOMPAT. This new GCOMPAT check, added for use with SV 957, assures

that a fly forward/reverse command follows an RPGU command within 600 seconds. Subsequent updating of the subroutine was performed for use with SV 960. One of the added checks was to preclude enabling of the RMA while in roll coarse deadband. This taboo mode was stored but corrected before being executed on SV 959.

2.9.1.4 GTELIM

The GTELIM module is composed of two subroutines, CIMAGE and VEST. CIMAGE produces an updated Chronological Command List and an updated Delay Line Image. At any given time CIMAGE contains all commands in the vehicle, loaded from preceding command messages. VEST forms the vehicle status tables and produces a listing of the predicted vehicle status as a function of system time.

All of the GTELIM problems occurred, and were corrected, prior to the flight of SV 955. For the flight of SV 952, the CIMAGE subroutine failed to update the current image with real-time 666 hybrid messages. Octal correctors were used to correct this problem and the subroutine functioned normally for SV 953. However, during this flight, the GTELIM updated command list indicated that the roll channel was in coarse deadband when fine deadband was the actual commanded state. This problem was created by a programming error that was alleviated with octal correctors during the mission.

A VEST subroutine interface problem became apparent when the secure count required updating in the MPES*for SV 954. The subroutine was modified to take the secure count directly from CIMAGE which is automatically updated with the current MPES secure count. The MPES secure count is corrected with MPESCHN cards.

2.9.1.5 GBURN 2

The GBURN 2 subroutine determines the secondary orbital elements which are applicable for orbit prediction following an orbit adjust.

*Mission Parameters and Event Storage

64SD4760

2-50

An error printout occurred while running GCHAP for SV 953 indicating that the minimum allowable semimajor axis had been exceeded. This printout was caused by a value for the semimajor axis in the GBURN 2 subroutine which proved to be unrealistic. This parameter was therefore decreased to the allowable minimum.

2.9.1.6 GPRESENT

The GPRESENT module provides formatted outputs of the sequences stored in MPES and has a limitation of 40 sequences in the SEQTAB. This limitation was exceeded during the SV 953 mission and GPRESENT was unable to list all of the sequences. No modification was made to the module since the number of sequences generated during that flight were considered excessive.

2.9.1.7 GMPESCHN

The GMPESCHN module provides a means for changing the MPES by card input. This allows formulating on-orbit command and sequence definitions and changing of vehicle and environment parameters. With this feature new commands can be created or old commands redefined in the event that hardware difficulties are encountered on-orbit.

An error on an input card to this module was indicated on-line without an associated error stop during the SV 953 operation. As a result, this portion of the module logic was modified to produce a recoverable error stop beginning with SV 954.

2.9.1.8 GECALL

The GECALL module is called by COP whenever a GE module function card is read. GECALL reads the MPES into memory, establishes co-contractor/GE interfaces, forms the ORBEL and CHAP Tables from the OAJ Table, and updates the MPES TORBEL Table with the Reference Pool TORBEL Table. These new tables are then used to update the ORBEL and CHAP Tables in MPES.

GECALL could not handle all of the factors provided by OAJ Table for SV 957. The module can only operate on two orbit adjusts at a time although three were present in the OAJ Table. Also, the module only had the capability to recompute the burn for one of the adjusts. Octal correctors were used to ignore the third adjust and to allow recomputation of all of the adjusts presented to the module. This procedure was to be followed on subsequent flights as required.

2.9.1.9 GCOMINT

The GCOMINT module checks the command paper tape and validates such things as control bits, command bit structure, and parity prior to transmission to the vehicle. Through the flight of SV 959 the module was designed to perform the parity check against the entire second word instead of each half of the second word. As a result, during the flight of SV 959, a newly-defined command had two parity errors in word 2 that canceled each other. The parity problem was noted at one of the tracking stations and the command message was regenerated. Starting with SV 960, the parity check was to be made against each part of the second word.

2.9.2 ON-ORBIT OPERATIONS

2.9.2.1 Delay Line "Telltales"

During the flight of SV 952, a telemetry blink to verify proper delay line operation caused the loss of valuable OCV/AGENA separation and initial OCV stabilization data. On subsequent flights telemetry blinks were not to be commanded during revs in which de-orbit of the SRV or OCV are to be performed.

2.9.2.2 Initialization Sequence

During the SV 953 "Hitch-Up" flight phase, OCV-"Solo" Stabilization Subsystem initialization sequences were inadvertently generated because PARAM +88 and +89 (system time

64SD4760

of Solo begin) in MPES were incorrect. These parameters were changed on orbit to the correct values and were to be checked more closely prior to each subsequent flight.

2.9.2.3 Loss of Telemetry Contact

During a rev 4 station pass with SV 954 a command message based on early rev tracking data with the required widening factors was loaded. For the actual orbit achieved, this station contact was relatively short; and, because no timer reset commands were provided by this newly-loaded message, early power controller turn-off of the TT&C Subsystem resulted with an associated loss of 125 seconds of data. This problem was created by the command loading which erased a required timer reset command. This problem can only be avoided by closer checking of the command list at the selected loading stations.

2.9.2.4 Vehicle Clock Deviation

A vehicle clock linear deviation of approximately 218 milliseconds per day, relative to system time, occurred during the flight of SV 957. The maximum error noted prior to a software correction was 290 milliseconds. Step corrections of 200 milliseconds each were accomplished through GMPESCHN three times throughout the flight.

A software clock calibration slope correction was available but not used because such a correction had not been checked out in advance. However, during the on-orbit rehearsal for SV 958, a slope correction was successfully exercised and was available for use should significant linear clock deviations be encountered on subsequent flights.

2.9.3 OPERATIONAL TELEMETRY

The operational telemetry allocations and readout groupings mostly proved satisfactory. The exceptions were as follows:

64SD4760

2-53

2.9.3.1 Freon Tank Temperatures

During the first two flights the Freon tank temperatures decayed rapidly during the "hitched-up" flight phase. As a result, the tank temperature sensors gained prominence and were found to have insufficient range. The sensors were of little other on-orbit use since they were allocated to the 90 x 1/18 multiplexer. In addition, the in-line temperature sensor was of little value as a backup monitor because gas was not flowing during these flight periods. The tank sensors' ranges were broadened and they were relocated from the tanks' support structure directly to the tank surfaces on SV 953. On SV 954, the sensors' outputs were also allocated to Band 16 and given an operational B priority to permit real time monitoring.

2.9.3.2 Battery Temperatures

For the first two flights the operational battery case temperature monitors were installed in the battery wells instead of on the cases. Thus, the battery temperatures were not available for on-orbit use. The proper procedure of bonding the sensors to their respective battery case was instituted with SV 953.

2.9.3.3 Reallocation of Stabilization Subsystem Functions

Because of the recurrent loss of IR lock to the horizon reference in the South Polar region with SV 958 and SV 959, steps were taken to monitor this phenomena on orbit. These steps included the addition and/or reallocation of pertinent stabilization telemetry functions beginning with SV 960. These were:

a.   Reallocating the IR pitch and roll computer outputs to a playback multiplexer.

b.   Adding the preamp signals to recorder channels.

c.   Telemetering the IRHSS inhibit event function.

64SD4760

SECTION 3

SYSTEM CAPABILITY ANALYSIS

The information provided in this section, resulting from the analysis of those system functions which best describe the various aspects of the total system's capability, is intended to enhance the operational utilization of the vehicle system. Statistical methods and techniques have been used to a large extent in analyzing these system critical parameters.

Raw data, generated externally, as well as internally to the flight vehicles, have been used in this analysis. In some instances, this information system has been lacking, thus precluding the analysis of certain critical parameters, notably orbit adjust engine performance, and vehicle thermal deformation.

3.1 RELIABILITY SUMMARY

This section summarizes the performance of the ten Program 206 Vehicles launched to date in light of flight reliability requirements, where flight reliability relates to that portion of the program involving the actual launch, orbital flight, re-entry, and recovery of the SV or portions thereof.

The outcomes of the flights are determined by reviewing the summary of performance in two categories:

- Primary mission performance is the SV flight performance for which required and demonstrated values are to be compared.

- Total mission performance which provides an over-all picture of the flights and their reliability achievement.

64SD4760

Where the SV performance, during the planned primary mission defined in the System Test Objectives, is such that GE-ASPD is potentially eligible to receive 90% or more of the maximum incentive fee, the primary mission will be defined as a success (presuming any failures during the operation are GE/ASPD responsibilities). This criterion shall be applied to the assessment of system flight reliability where the hardware is provided the opportunity to perform successfully.

Table 3-1 represents a reliability summary for the primary missions for which five successes were achieved in nine opportunities to perform. The cumulative flight performance has also been quoted in terms of reliability numbers associated with a 90% one-sided confidence level, binomial distribution.

The reliability summary presented in table 3-1 and figure 3-1 is for the total mission performance where success signifies system performance without failure. Even though partial success was achieved during portions of some flights, for purposes of total mission reliability classification they appear as failures, since the vehicles did not provide full capability for the entire duration of the planned mission (both primary and solo portions where divided as such).

Figure 3-2 is a plot of the hardware failure rate trend, as evidenced by the flight experience of SV 951 through SV 960. The hardware failures represented are of both a critical and non-critical nature. Critical failures are defined as those which affect vehicle system performance to the degree that the successful outcome of any given flight (total mission) is jeopardized. Each point plotted reflects the failure rate from the previous flights. The solid line shows the apparent trend of decrease (improvement) in the hardware failure rate with the number of flights flown.

The apparent flat trend of system reliability shown in figure 3-1 appears to be incompatible with the system reliability improvement that might be inferred from the decreasing hardware failure rate shown in figure 3-2. Closer examination (see sketch that follows) shows that both critical and non-critical hardware failure rates of the first ten flights were decreasing, but were relatively high compared to the goal of .024 failures/day.

64SD4760

3-2

Table 3-1. Reliability Summary-Primary Mission Performance

Satellite Vehicle	Scheduled Duration (days)	Predicted Probability of Success	Outcome	Cumulative Demonstrated Reliability
951	1	0.84	Success	0.90
952	2	0.85	Success	0.95
953	2	0.88	Success	0.965
954	2	0.71	Failure	0.86
955	2	0.79	Failure[1]	0.75
956	3	0.68	Success	0.80
957	3	0.68	Success	0.83
958	4	0.61	N/A[2]	0.83
959	4	0.61	Failure	0.76
960	5	0.57	Failure	0.70

Table 3-2. Reliability Summary-Total Mission

Satellite Vehicle	Scheduled Duration (days)	Predicted Probability of Success	Outcome	Cumulative Demonstrated Reliability
951	3	0.62	Failure	0.10
952	3	0.55	Failure	0.05
953	4	0.58	Success	0.54
954	5	0.48	Failure	0.44
955	5	0.53	Failure[1]	0.37
956	5	0.53	Success	0.51
957	5	0.53	Failure	0.45
958	5	0.56	N/A[2]	0.45
959	5	0.56	Failure	0.41
960	5	0.57	Failure	0.37

Notes:

(1) SV 955 had previously been defined as a success, but further detailed data analyses revealed a component failure which reversed the outcome definition.

(2) SV 958 was defined as N/A because it was not given the opportunity to perform because of poor separation and orbit injection conditions.

64SD4760

3-3

3-4
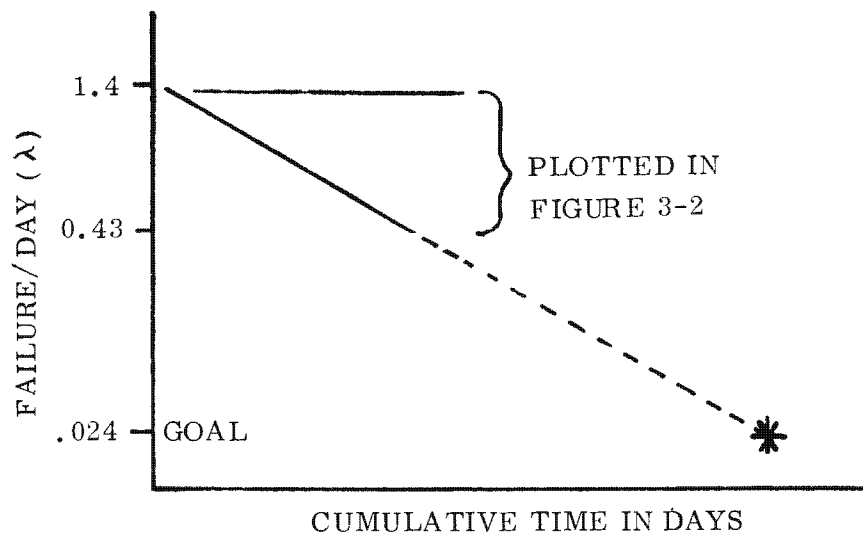
Therefore, the incidence of critical hardware failures (total mission-limiting) has not yet reached a level where a large number of missions can be flown without expecting a failure of this type sometime in the operation. Thus, the information presented in figures 3-1 and 3-2 is compatible, since a single failure (substantiating the decreasing hardware failure rate trend) could be mission-limiting and be reflected as a failure in the system reliability.

64SD4760

3-4

NOTE:
CUMULATIVE RELIABILITY ACHIEVEMENT
BASED ON 90% ONE-SIDED BINOMIAL
CONFIDENCE LIMITS.
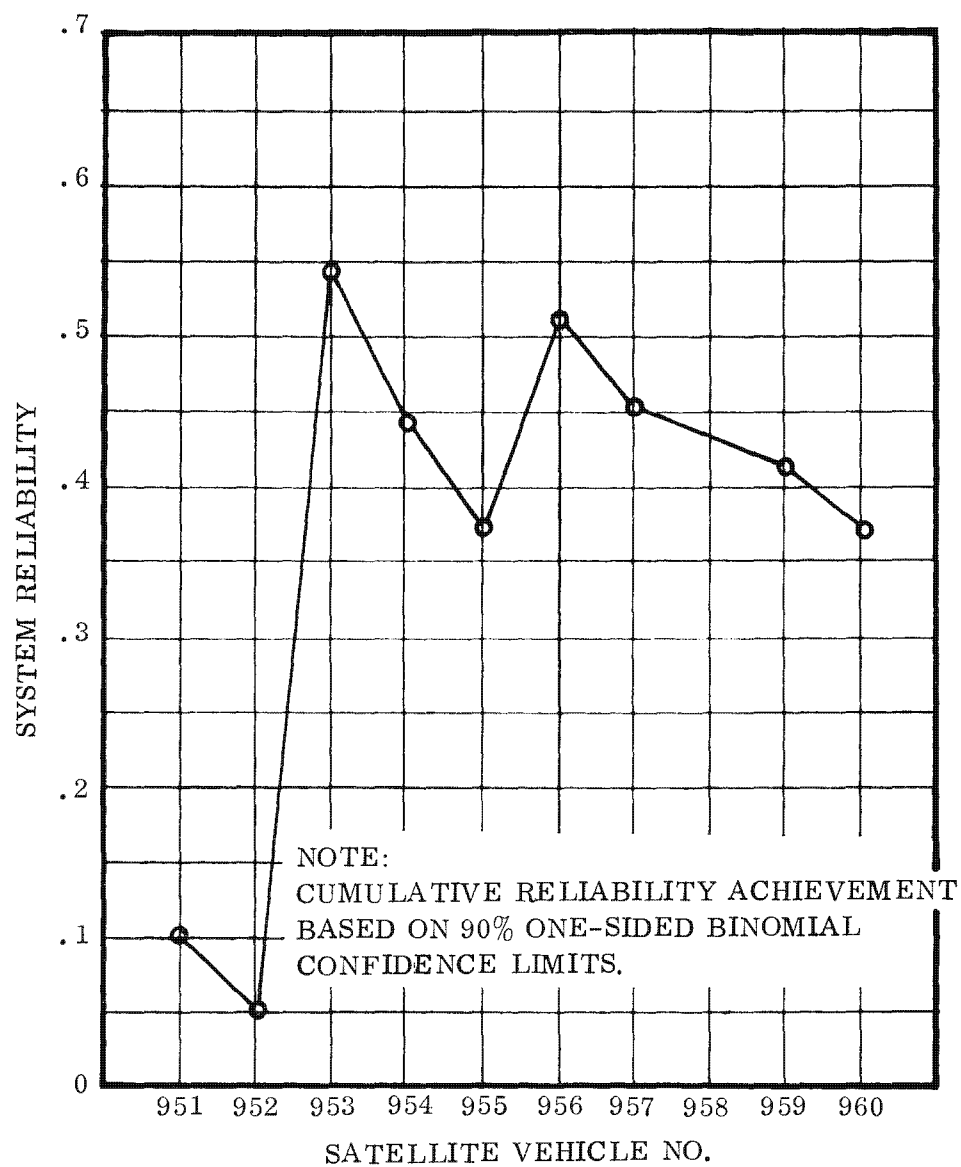
Figure 3-1.   Demonstrated System Reliability - Total Mission

64SD4760

3-5
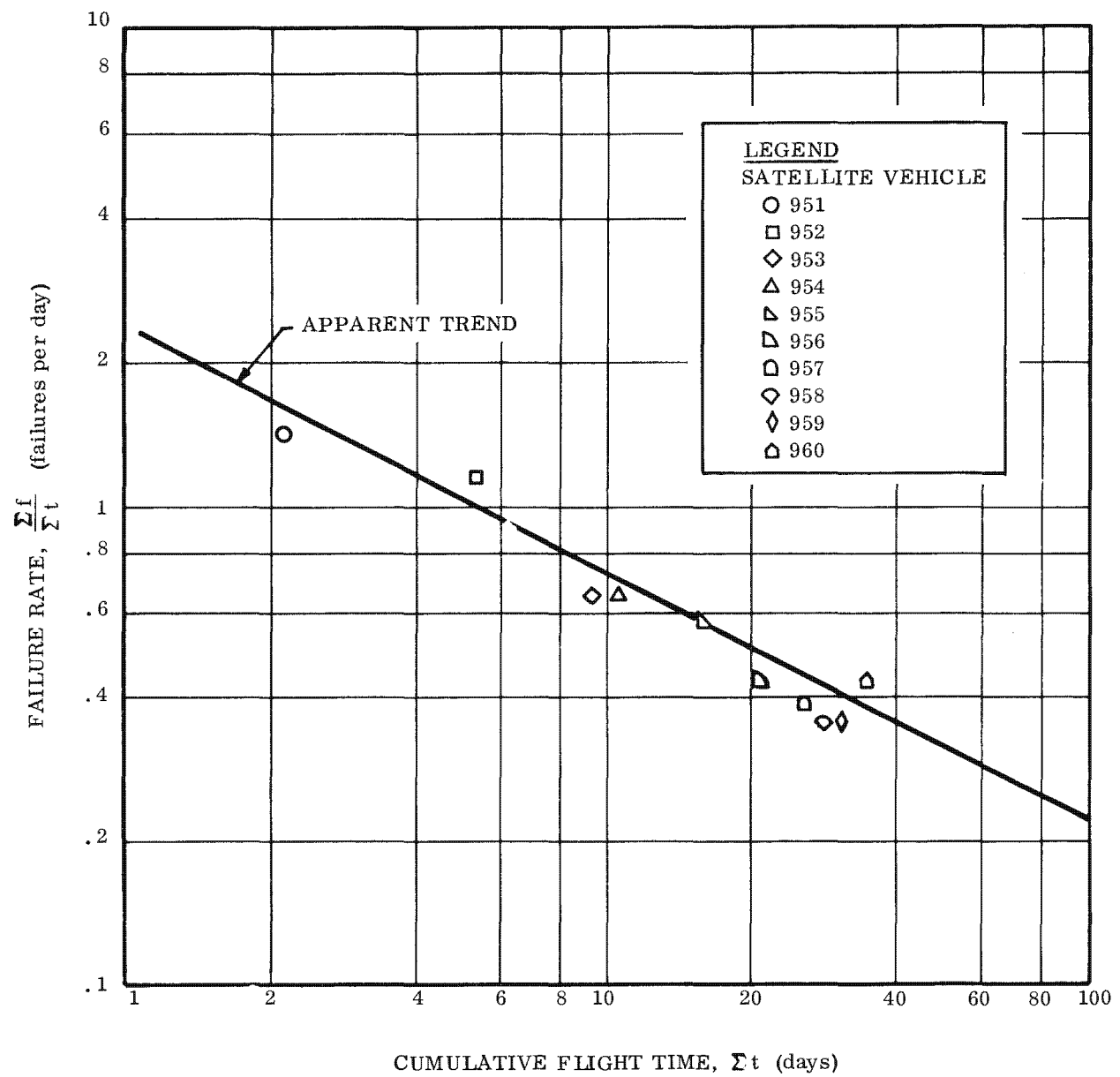
Figure 3-2.   Flight Hardware Failure Rate Trend

64SD4760

3-6

3.2 SYSTEM TECHNOLOGIES

The parameters describing vehicle external environment and those parameters which significantly affect system capability and/or design are discussed in this section. Also included are phenomena useful for operational utilization of the vehicle. The suitability of employing temperature sensors as attitude error detection devices is also discussed.

3.2.1 ATMOSPHERIC DENSITY MODEL-COEFFICIENT CORRELATION

To obtain meaningful results from the orbit mechanics, attitude control, and thermodynamic analyses, it is necessary to have correlation with, and understanding of the actual atmospheric parameters. Because atmospheric parameters throughout the range of orbital attitudes encountered on Program 206 flights have not been precisely known, and because of expected variations with season, several model atmospheres were made available for ephemeris studies and flight data analyses. As a result, early attempts to account for vehicle thermal and aerodynamic characteristics were difficult since precise correlation with a known atmosphere was impossible. Subsequent correlation studies succeeded in detecting changes in apparent vehicle drag attributed to high vehicle maneuvering activity. (Refer to Section 3.2.5.) In addition, comparisons of aerodynamic moment and drag measurements, during periods of relatively little vehicle activity, with the various model atmospheres, has resulted in the following conclusions:

    a.   Good correlation of flight data with U.S. Standard Atmosphere, 1962, exists for altitudes less than 95 nautical miles.

    b.   Sparse data available above 100 nautical miles indicates closer correlation with L-DENSITY than with the 1962 Standard Atmosphere.

    c.   Certain predictable effects on vehicle attitude control performance can be concluded from aerodynamic moment data.

64SD4760

3-7

3.2.1.1 Aerodynamic Moment Correlation

Attempts to correlate observed flight aerodynamic pitch and yaw moments with theoretical data commenced during analysis of the SV 955 flight. Slopes of vehicle pitch and yaw rates (fine-rate telemetry) were measured at selected altitudes, and plotted against the coincident deadband error in comparison with derived theoretical curves. Although some rough correlation was accomplished, results were not adequate for close atmospheric model correlation. The same technique was used in analyzing the SV 956 flight, with similar results. Although these early attempts did not include correction factors, later determined to be important, the major contributing factor to the lack of correlation is now believed to have been rate slope measurement resolution. Accelerations induced by aerodynamic forces at altitudes above 70 nautical miles are of magnitudes similar to those produced by system electrical biases, drift, etc.

SV 958 flew at extremely low altitudes (as low as 57 nautical miles) during the first two revs. The data derived from this period has proven to be the most valuable in evaluation of vehicle moment characteristics and atmospheric density model. Rate slopes at these altitudes ($<$ 62 n mi) were considerably larger than those previously observed at the higher altitudes and thereby offer good measurement resolution and minimize effects of other contributions to the slopes.

Contributions to the over-all atmospheric density correlation with measured aerodynamic moments were also provided by the pitch-down maneuver performed on the SV 956 flight spanning altitudes between 70.5 and 71.9 nautical miles, and by the inadvertent development of a large yaw angle during the SV 955 flight due to improper commanding.

3.2.1.1.1 Results of Low Altitude Data Analysis.

In order to offer a concentration of useful solutions obtained from the small amount of flight data available, the data were normalized into units of torque-per-degree angle of attack versus altitude. This procedure allowed subsequent confirmation of the assumed moment coefficient slope with angle of attack for the small angles involved. Results are plotted in figure 3-3.

64SD4760
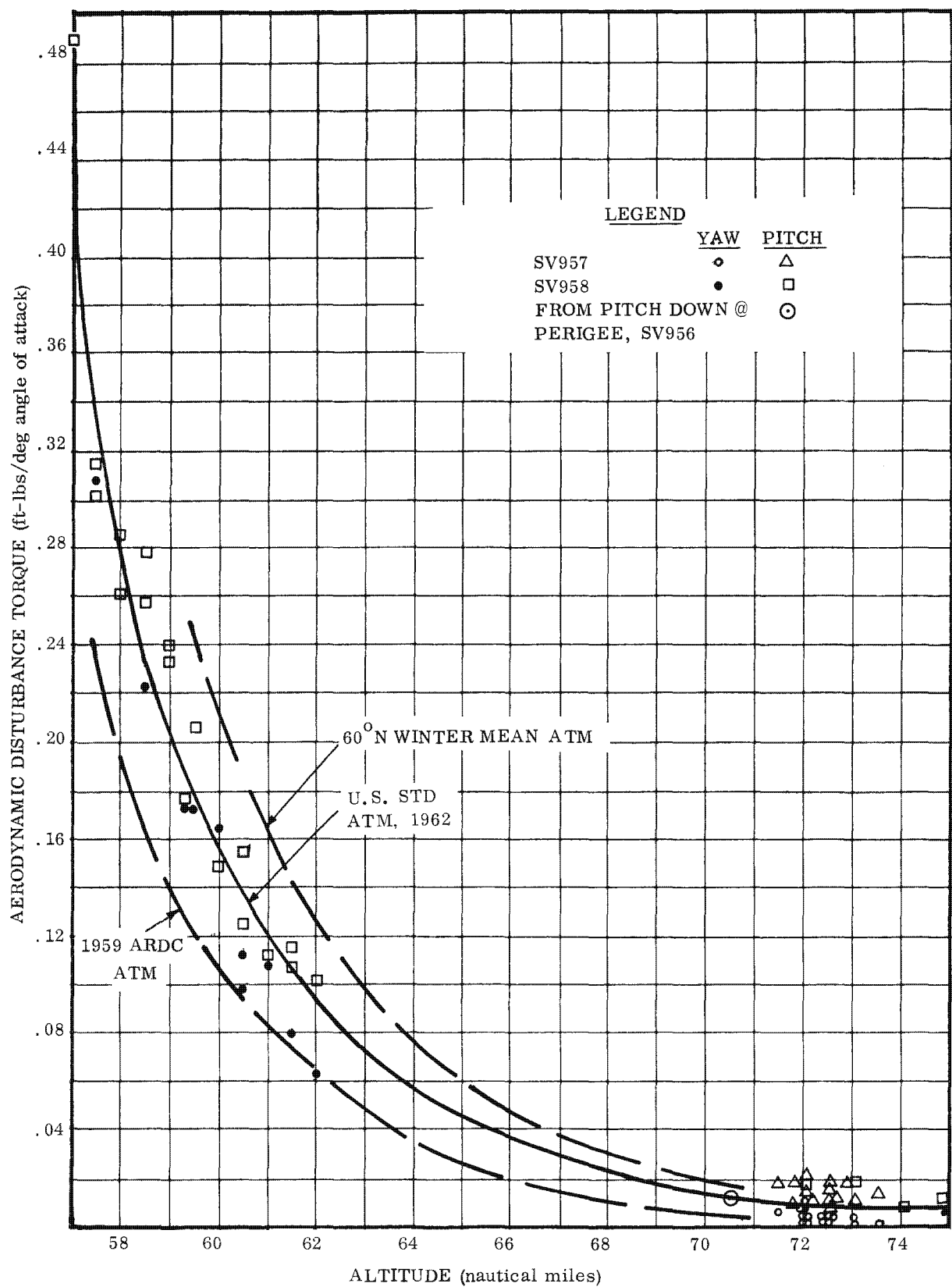
Figure 3-3. Comparison of Corrected Flight Aerodynamic Moment Data with
Model Atmospheres, 57 to 75 Nautical Miles

64SD4760

3-9

3.2.1.1.2 Theoretical Data. The three theoretical curves presented in figure 3-3 are based on the following equation:

$$T' \text{ (torque per degree)} = qA \, C_{m_\alpha} \, d$$

where:

$q = 1/2 \, \rho \, V^2$ (where ρ is obtained from the applicable model atmospheric density curve)

C_{m_α} (theoretical moment coefficient slope with angle of attack) = 0.030 per degree for small angles, with $\alpha_{TH} \cong 0.6$ (flight temperature data)

A (vehicle frontal area) = 19.62 ft^2

d (vehicle diameter) = 5.0 ft

V = average velocity for given altitude (based on ephemeris)

3.2.1.1.3 Measured Data. Emperical data was measured and converted to similar units as follows:

$$T' \text{ (disturbance torque per degree angle of attack)} = \frac{\ddot{\theta}' \, I}{57.3}$$

where:

I = Vehicle moment of inertia about pitch or yaw axis (slug/ft^2)

$\ddot{\theta}'$ = rate slope, measured and normalized to units of acceleration per degree angle of attack (deg/sec^2/deg)

Rate slopes and deadband errors were very accurately measured at system times corresponding to various preselected altitudes. Because rate data is about individual (pitch and yaw) vehicle axes, it was necessary to measure the component of the total angle of attack about each of these axes. Pitch and yaw data were therefore considered separately while ignoring the geometric intereffects (i.e. pitch angle assumed zero when calculating yaw angle).

3.2.1.1.4 Pitch Measurement and Correction Factors. The pitch angle of attack is comprised of ψ_{DB} (deadband angle), PA (path angle, from ephemeris), ψ_E (gyro error due to electrical biases and/or IR horizon scanner errors), and ψ_A (alignment errors within the system).

3.2.1.1.5 Yaw Measurement and Correction Factors. The yaw angle of attack is comprised of θ_{DB}, θ_E, θ_A, and θ_W (the angle of relative wind, or angle of molecular flux) relative to the flight path. θ_W was determined to be very significant in the results, but because very little knowledge of the actual parameter exists, a purely theoretical value was selected as follows:

$$\theta_W = \text{arc tan } \frac{1515 \cos (\text{latitude} + \text{inclination} - 90 \text{ deg}}{26,000}$$

where:

1515 ft/sec is the earth tangential velocity at the equator; 26,000 ft/sec is an arbitrarily selected value used to represent the average vehicle flight path velocity vector.

θ_W is positive (from the West) for a north-south pass and negative for the south-north pass. Although it is certain that the earth's equatorial tangential velocity is not truly representative of the wind velocity at the vehicle position and altitudes considered, sparse information from various technical publications indicates that winds at these altitudes do vary between 0.8 to 1.4 of the local tangential velocity vector, variable with season and geographical location. It would be expected that the true theoretical values would be represented by a gradual decay of velocity with altitude, approaching zero at infinity. The value of 1515 fps is therefore considered to be representative for purposes of correlation.

64SD4760

3-11

3.2.1.1.6 <u>Angle Measurement Limitations</u>. There is no way possible to measure the gyro error components of the angle of attack. These are assumed to be small, however, because of the inherent Stabilization Subsystem accuracy in this regard. Alignment error tolerances within the system are at least an order of magnitude smaller than the measured deadband errors and are therefore ignored for purposes of simplification. Similarly, effects due to center of gravity offset are ignored because of the low magnitude of the effect and complexity in calculation. Any effort to achieve a more accurate correlation must include both of these factors, along with any electrical bias measurements or calibrations available from ground test. The equation for producing normalized values of $\ddot{\theta}$ was therefore reduced to:

$$\ddot{\theta} \left(\frac{\text{deg/sec}^2}{\text{deg}} \right) = \frac{\text{rate slope}}{\text{measured deadband + corrections}}$$

For pitch,

$$\ddot{\theta} = \frac{\text{rate slope}}{\psi_{DB} + PA}$$

For yaw,

$$\ddot{\theta} = \frac{\text{rate slope}}{\theta_{DB} + \theta_W}$$

3.2.1.1.7 <u>Selection of Data Points.</u> In order to minimize effects of the unknown or deleted angle of attack contributors, data points were measured only where the deadband angles exceeded one degree (pitch and yaw in coarse limit cycle mode). The data collected during Thule and Kodi station passes for the first two revs of SV 958 provided the low altitude points. Yaw data from Thule, rev 2 was deleted due to evidence of yaw gyro compassing, indicating existence of an undetermined but small yaw angle. This data did not show significant disagreement with the other results, however.

64SD4760

3-12

3.2.1.1.8 <u>Summary of Low Altitude.</u> As shown in figure 3-3, the data correlates extremely well with the curve based on the U.S. Standard Atmosphere 1962 model, particularly the one pitch data point obtained at the lowest altitude (57 n mi) from the Thule station pass on rev 2.

3.2.1.1.9 <u>Altitudes Above 70 Nautical Miles.</u> Using the same techniques applied for the very low altitude calculations, a similar correlation was attempted for higher altitudes ($>$70 n mi), using SV 957 and SV 958 data. In figure 3-3, the apparent mean value shows fairly good correlation with the 1962 Standard. Deviations of individual points are of the same order of magnitude as for the lower altitudes when presented on the same scale. However, when the scale is expanded as presented in figure 3-4, the range of absolute error is more pronounced even though the mean value of the data still shows fairly good average correlation with the curve based on the 1962 Standard Atmosphere. As previously mentioned early in this section, this spread is believed to be due to the increased significance of angle and rate contributing factors which are either unattainable or omitted from the calculations. The favoring of pitch data to the high side of the average, and yaw data to the low side, tends to support this belief.

3.2.1.1.10 <u>Pitch-Down at Perigee, SV 956.</u> Data obtained from the experimental pitch down at perigee during the SV 956 flight tends to confirm the earlier results. (See figures 3-3 and 3-4.) This single point was obtained from measurements of the rate slopes (between rate limits) from the pitch-down maneuver. These were plotted against the changing pitch angle as shown in figure 3-5. As shown in figure 3-5, the initial slope of the curve is 0.00025 deg/sec^2/deg. Conversion yields a disturbance torque (moment) of:

$$T' = \frac{\ddot{\theta} I}{57.3} = \frac{.00025 \ (3031)}{57.3} = .0132 \ \text{ft-lbs/deg}$$

3.2.1.1.11 <u>Yaw Moment Correlation with L-DENSITY, SV 955.</u> During the early revs of the SV 955 flight, improper commanding of the vehicle resulted in decoupling of the yaw gyro compassing loop for a period of about 16 revs. This caused a large ($\approx$ 55 degrees) yaw angle to be developed gradually over the period of time at a fairly constant rate. The

64SD4760

3-13
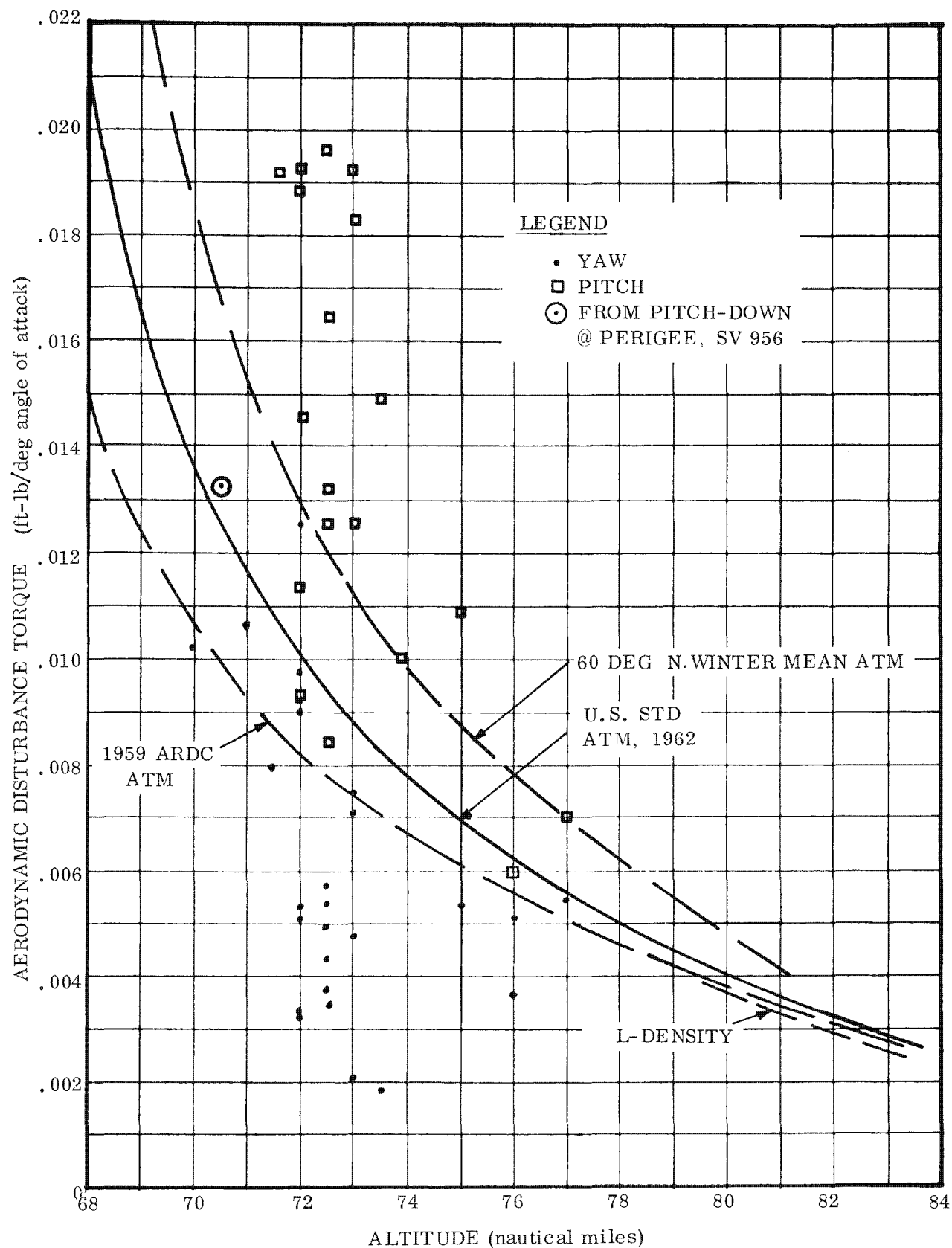
Figure 3-4. Comparison of Corrected Flight Aerodynamic Moment Data with
Model Atmospheres, 68 to 82 Nautical Miles

64SD4760

3-14
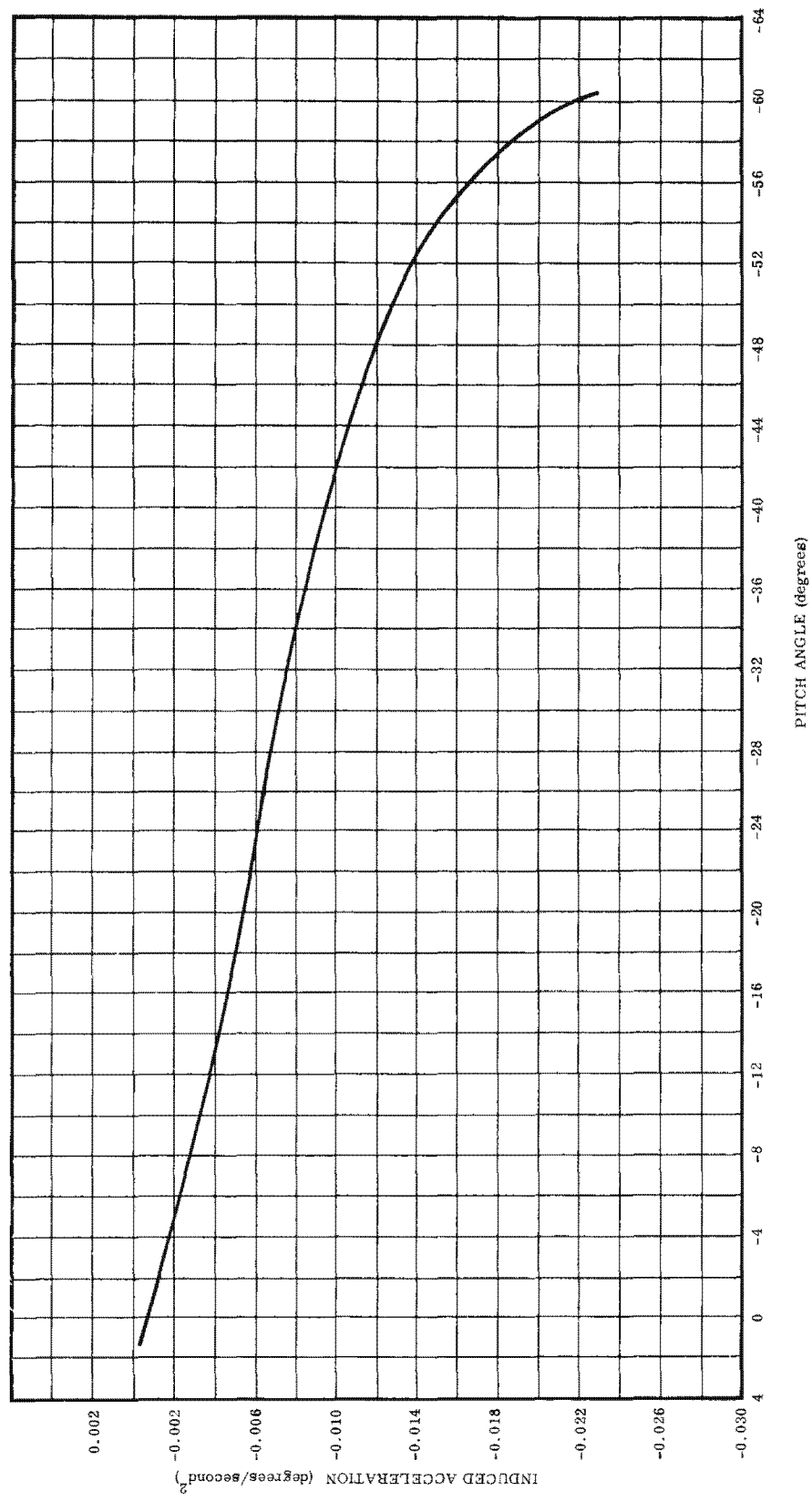
Figure 3-5. SV 952 Aerodynamic Pitch Accelerations During Pitch-Down Maneuver, Altitude Range of 70.5 to 71.9 Nautical Miles

64SD4760

3-15

yaw angle history during this period was computed by several means and the combined result, shown in figure 3-6, is considered to be fairly accurate. This provided a means of examining disturbance torques at high angles of attack at high altitudes.

Conversion of data into torque-per-degree angle of attack is not practical because of rapid change of C_m versus α slope at the large angles of attack considered. Therefore, a different means of presenting data for atmospheric density correlation is necessary. Rate slopes at the various corrected yaw angles were again measured and altitudes were obtained from ephemeris data. The rates were then converted into moment coefficients using both the U. S. Standard Atmosphere, 1962 model and L-DENSITY, by the following equation:

$$C_m = \frac{2\ddot{\theta}I}{57.3\,\rho V^2 Ad} = \frac{1.07\,\ddot{\theta}}{\rho V^2}$$

where:

$\ddot{\theta}$ = measured angular acceleration.

$\ddot{\rho}$ = density based on each model atmosphere.

The results, plotted versus angle of attack, are presented in figure 3-7 and are compared with the theoretical moment coefficient curve.

Because of the apparent closer agreement of measured data* to the theoretical C_{m_α} curve, it is concluded that L-DENSITY is more valid than the 1962 Std Atmosphere at the higher altitudes (at least in the region between 97 to 109 n mi covered by the data).

The drop-off of measured moment coefficient at high angles of attack (>30 deg) relative to the theoretical, is possibly explained by the simplification of the computer program used to

---

*based on calculations using L-DENSITY

64SD4760

3-16

LEGEND

● ANALYTICAL CORRELATION WITH EPHEMERIS DATA ON ORBIT

○ COMPUTED FROM $\dot\Phi = 0.068 \sin\theta$,

    WHERE $\dot\Phi$ = AVERAGE ROLL RATE

□ COMPUTED FROM $\dot\psi = 0.068 (1 - \cos\theta)$,

    WHERE $\dot\psi$ = AVERAGE PITCH RATE

▲ COMPUTED FROM BUSS MAGNETOMETER OUTPUTS

FLY-FORWARD COMMANDED

BEST ESTIMATE

ESTIMATED GYRO COMPASSING HISTORY

ROLL PITCH GYRO UNCAGED (RPGU) COMMANDED

YAW ANGLE, θ (degrees)

REV NO.
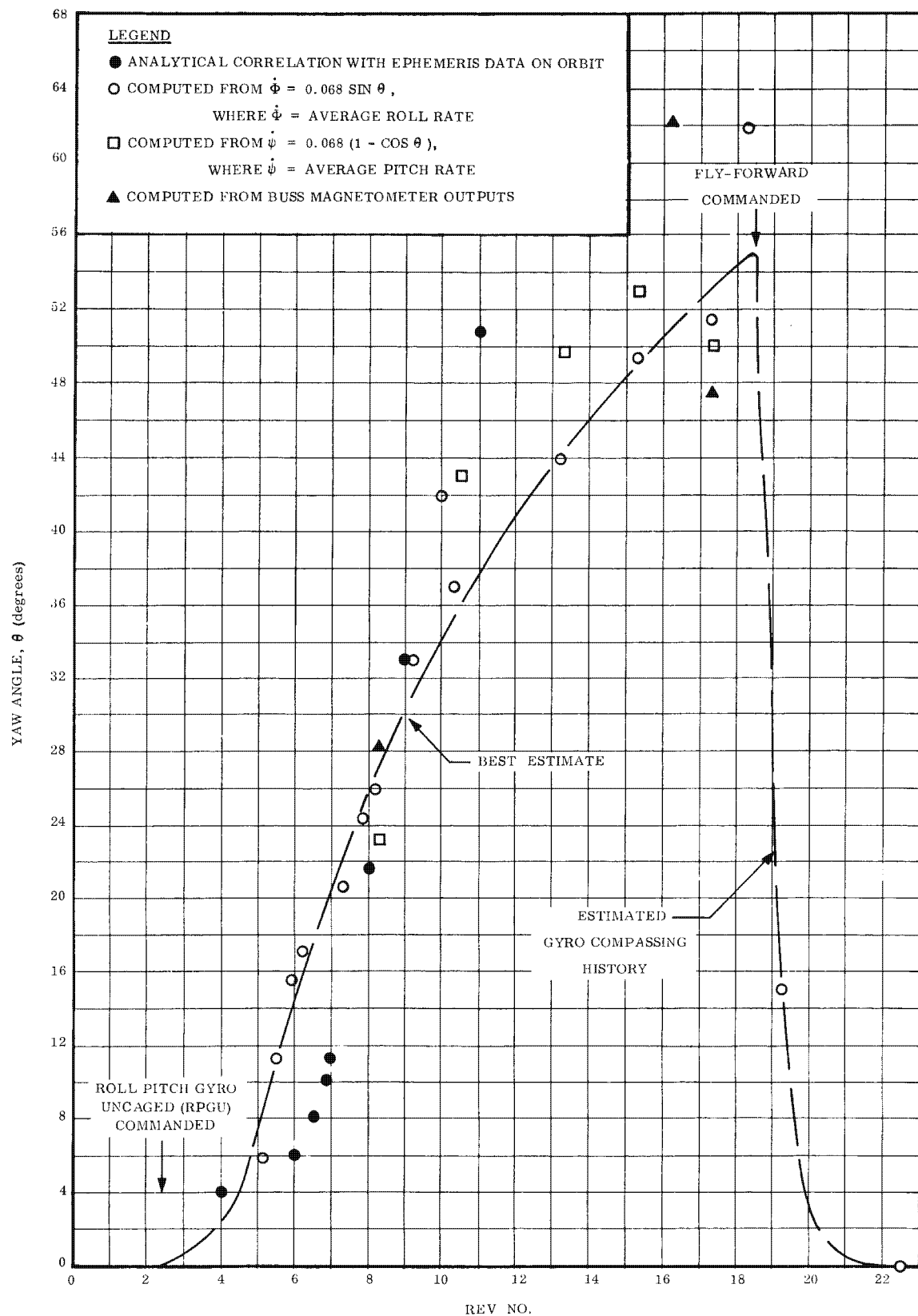
Figure 3-6. Yaw Angle Versus Rev Number, SV 955
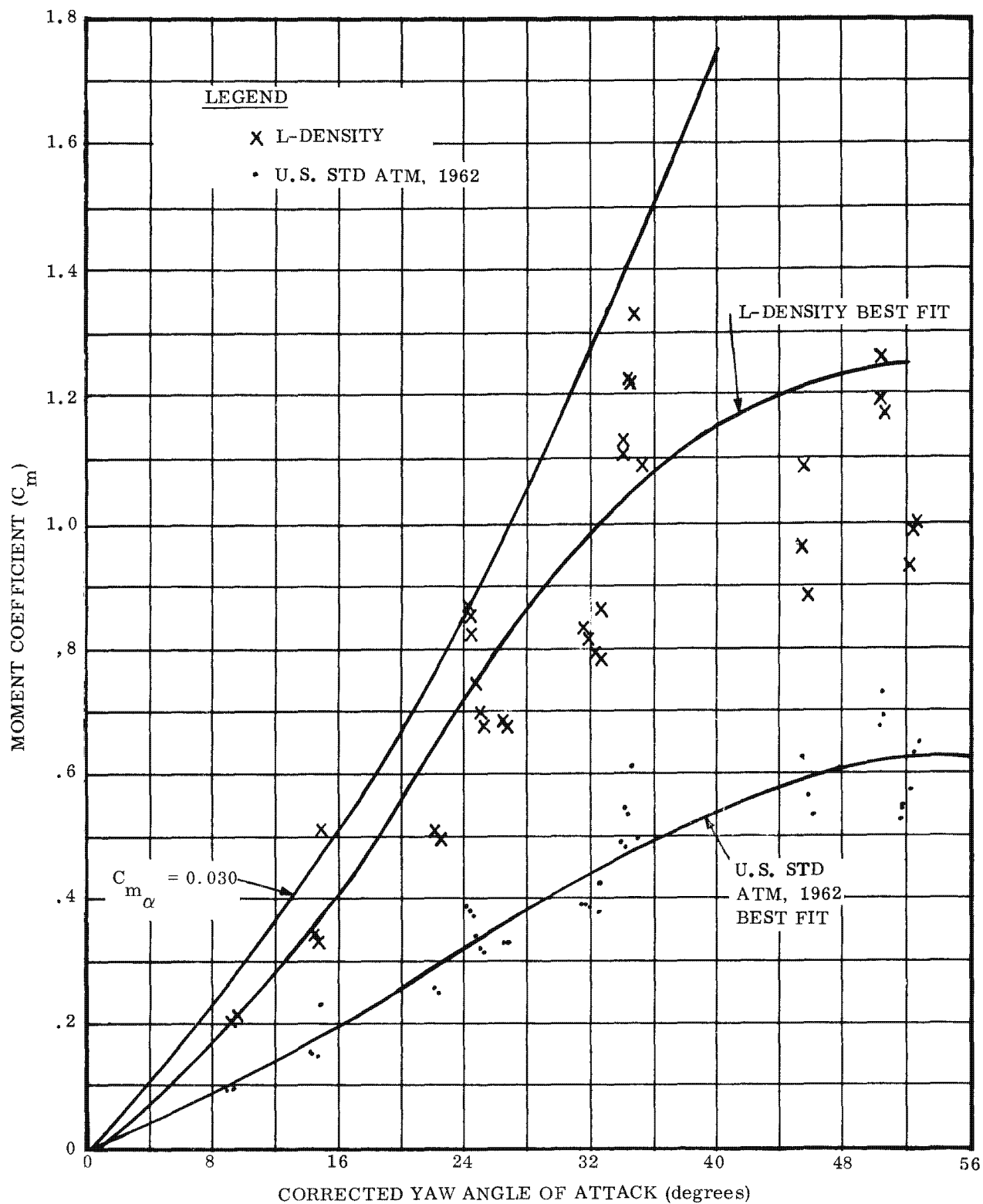
Figure 3-7. Yaw Moment Coefficient Determination Based on SV 955 Flight Data, 97 to 109 Nautical Miles

64SD4760

3-18

derive the theoretical values. The program results assume a flat vehicle aft bulkhead while the actual configuration most likely offers much more aerodynamic drag at high angles of attack. Therefore, the moment coefficient slope decay indicated by the measured data appears realistic. Stability characteristics while flying reverse tend to confirm this likelihood. Results of disturbance torques encountered during yaw-arounds have not yet been analyzed sufficiently to enable plots of calculated coefficients for angles of attack through $\pm$ 180 degrees.

3.2.1.2 Aerodynamic Drag Correlation

The atmospheric drag force per unit mass on the vehicle is expressed by:

$$F_D = -\frac{C_D A}{2m} \rho V^2 = B_0 \rho V^2$$

The 0-subscript designates the B -value which applies to the quiescent vehicle, uninfluenced by roll maneuver activity. For the Program 206 flights, $\rho = \rho_{L\text{-DENSITY}}$ and the drag coefficient calculated by the expression $C_D = \frac{2m}{A} B_0$ is inseparable from the L-DENSITY atmospheric model. For any other atmospheric model characterized by $\rho = \rho'$,

$$C_D' \rho' = \frac{2m}{A} B_0 \rho_{L\text{-DENSITY}}$$

If the maximum expected drag coefficient value (2.7) is assigned to C_D', ρ' becomes a nominal expected density which can be solved for by

$$\rho' = \frac{2m}{2.7A} B_0 \rho_{L\text{-DENSITY}} = R \rho_{L\text{-DENSITY}}$$

Here R is the ratio $\frac{C_D}{2.7}$ in the first table of Section 3.2.5.

Assuming that the drag at perigee is the dominant effect (contributes highest percent of total drag per rev) the computation of R was performed and the associated density values were

64SD4760

determined and plotted at the perigee altitudes (altitudes of 92 n mi and lower) in figure 3-8. Figure 3-9 shows the complete range of theoretical values of C_D for various reflection coefficient values. The value of 2.7 used in the above equation is based on this figure. Based on L-DESNITY values, a C_D of 3.5 is required. This value is outside of the theoretical limits.

Over-all results therefore support the validity of the U.S. Standard Atmosphere, 1962 as yielding a better match to observed performance than does the L-DENSITY model for the range of altitudes represented by the data.

3.2.1.3 Accommodation Coefficient Correlation

Accommodation coefficient measurements, based on flight data obtained at low altitudes, are discussed in Section 3.8.1. A coefficient (α_{TH}) of 0.6 ± 0.2 was computed as nominal using the 1962 Std Atmosphere. This value indirectly supports the correlations of flight data with this model atmosphere using the expected drag and moment coefficients. Figures 3-10 and 3-11 show the theoretical moment coefficient versus angle of attack for various values of reflection coefficient (σ'), and accommodation coefficient (α_{TH}). The slope corresponding to the high (≈ 0.8 to 0.9) value of σ' expected coincides with a C_m slope of 0.030 and α_{TH} of about 0.6 for small angles of attack. The common correlation of all values as well as C_D (sect 3.2.1.2) with the U.S. Standard Atmosphere, 1962 lends mutual support to all data obtained for the altitudes involved in these analyses.

3.2.1.4 Effects on Attitude Control Capability

The results of flights to date indicate capability of the Stabilization Subsystem to maintain the desired attitude at all altitudes flown thus far in the program. If the 1962 Atmosphere is utilized, altitude limits, below which vehicle control will be unable to overcome aerodynamic moments for each mode or maneuver, can be predicted fairly accurately. The control torque available (high or low thrust) divided by a safety factor (> 1) dictates the maximum disturbance torque permissible; this, in turn, dictates the minimum altitude for the attitude (angle of attack, hence C_m) selected by solution of the moment equations for ρ.

64SD4760

3-20
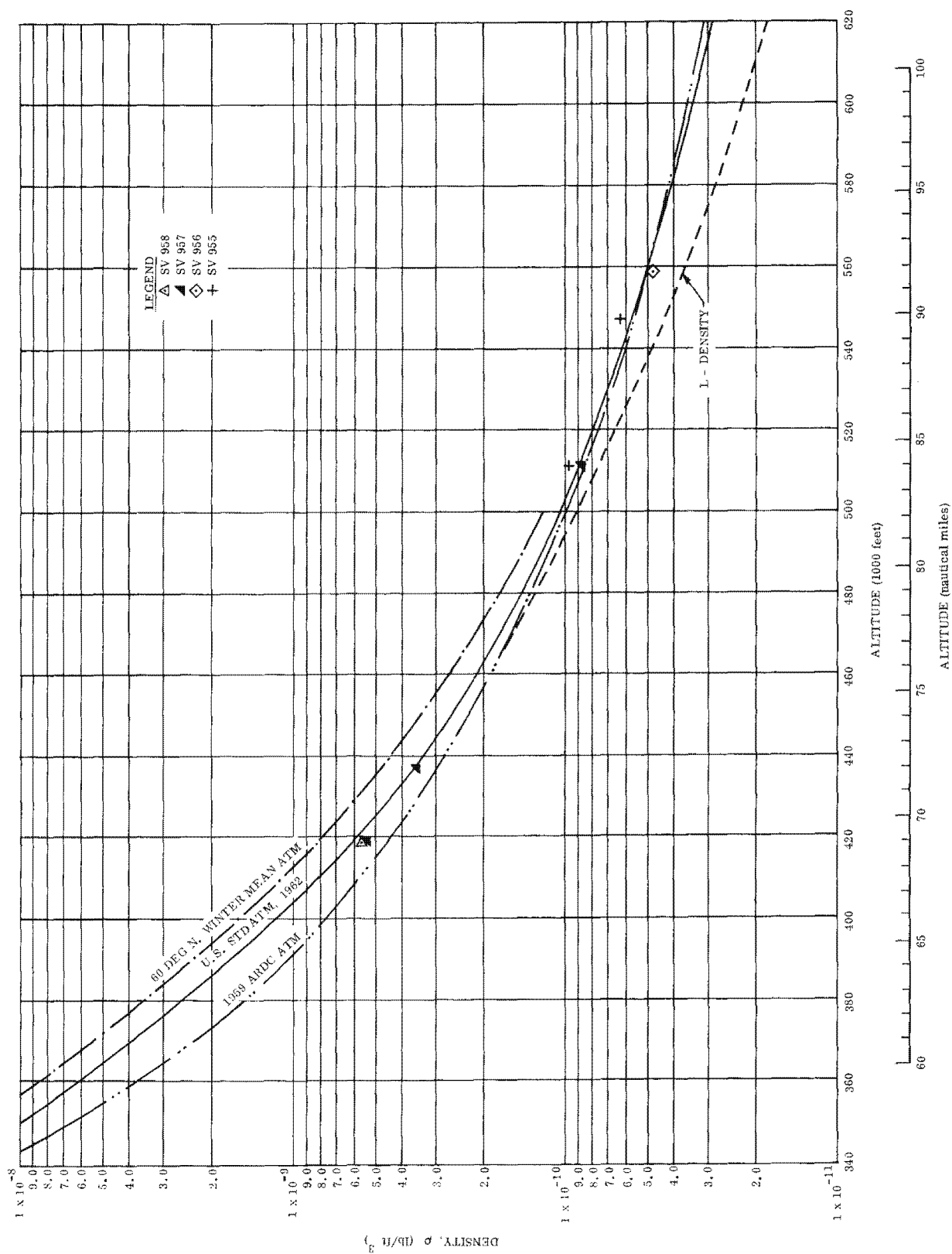
Figure 3-8. Comparison of Flight Aerodynamic Drag Data with Model Atmospheres, $\leq$ 92 Nautical Miles

64SD4760

3-21
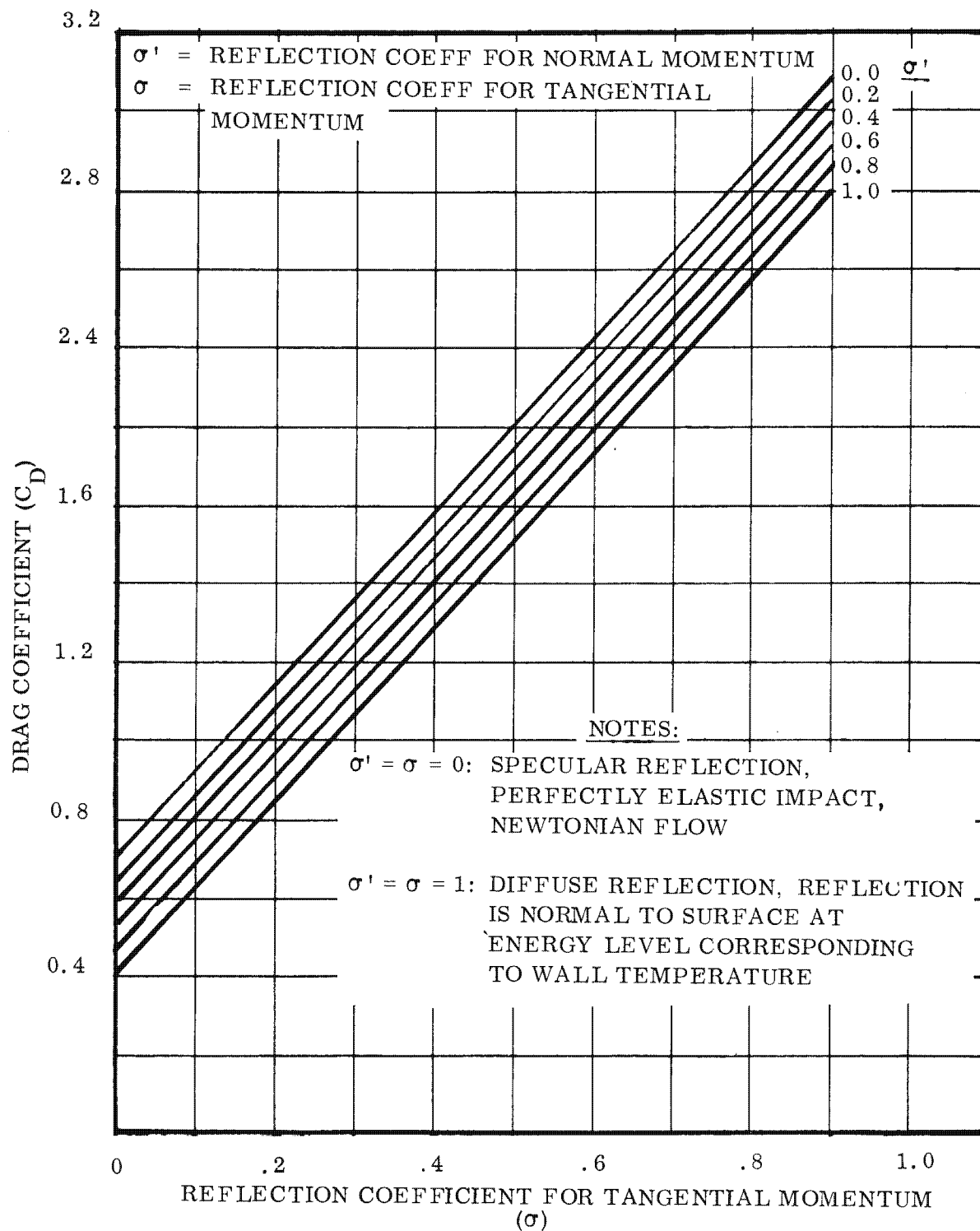
Figure 3-9. Theoretical Drag Coefficients Versus Reflection Coefficients

64SD4760

3-22
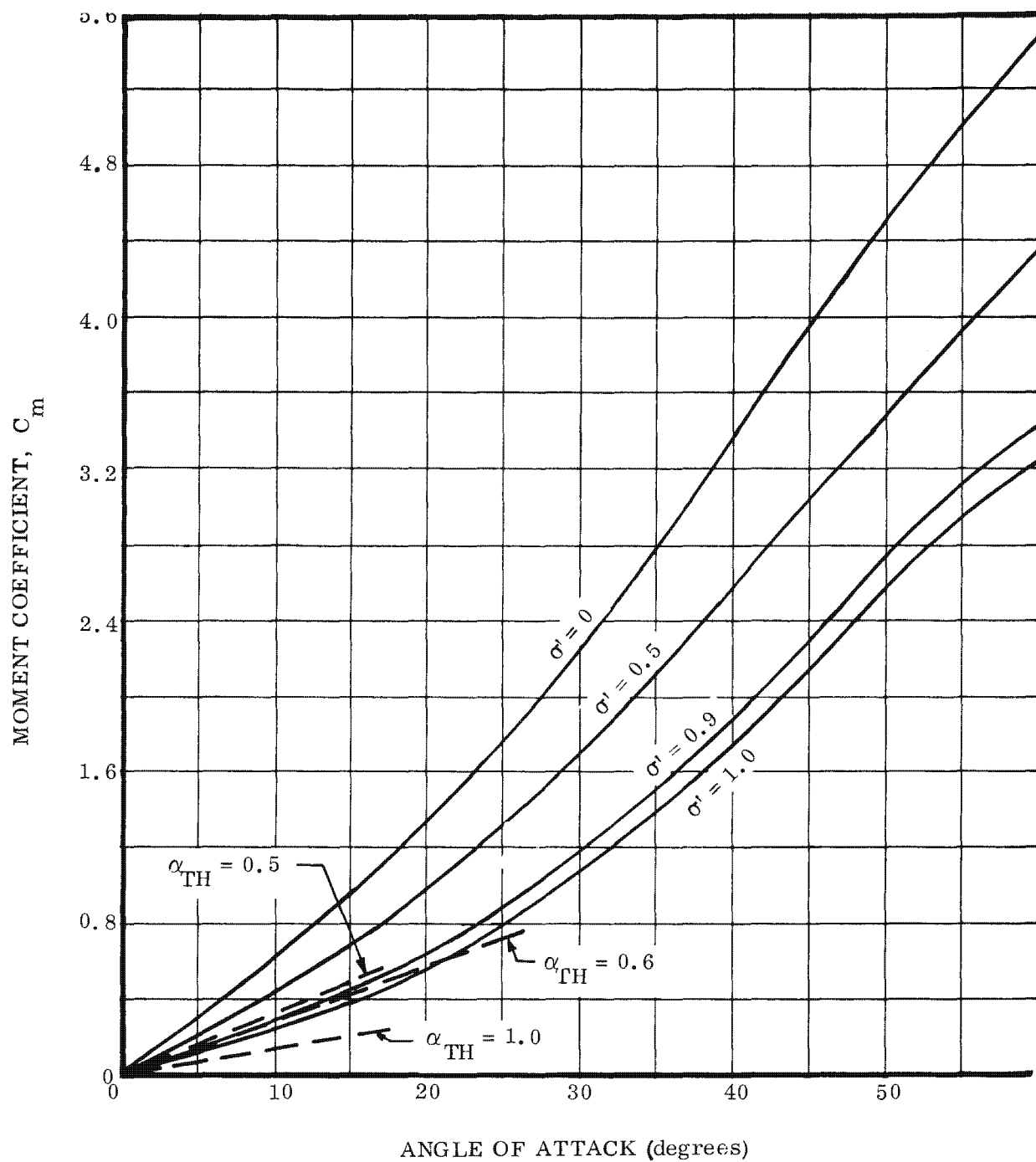
Figure 3-10. Theoretical Moment Coefficient – Accommodation Coefficient Correlation
for $\sigma \cong 1.0$

64SD4760

C05099047
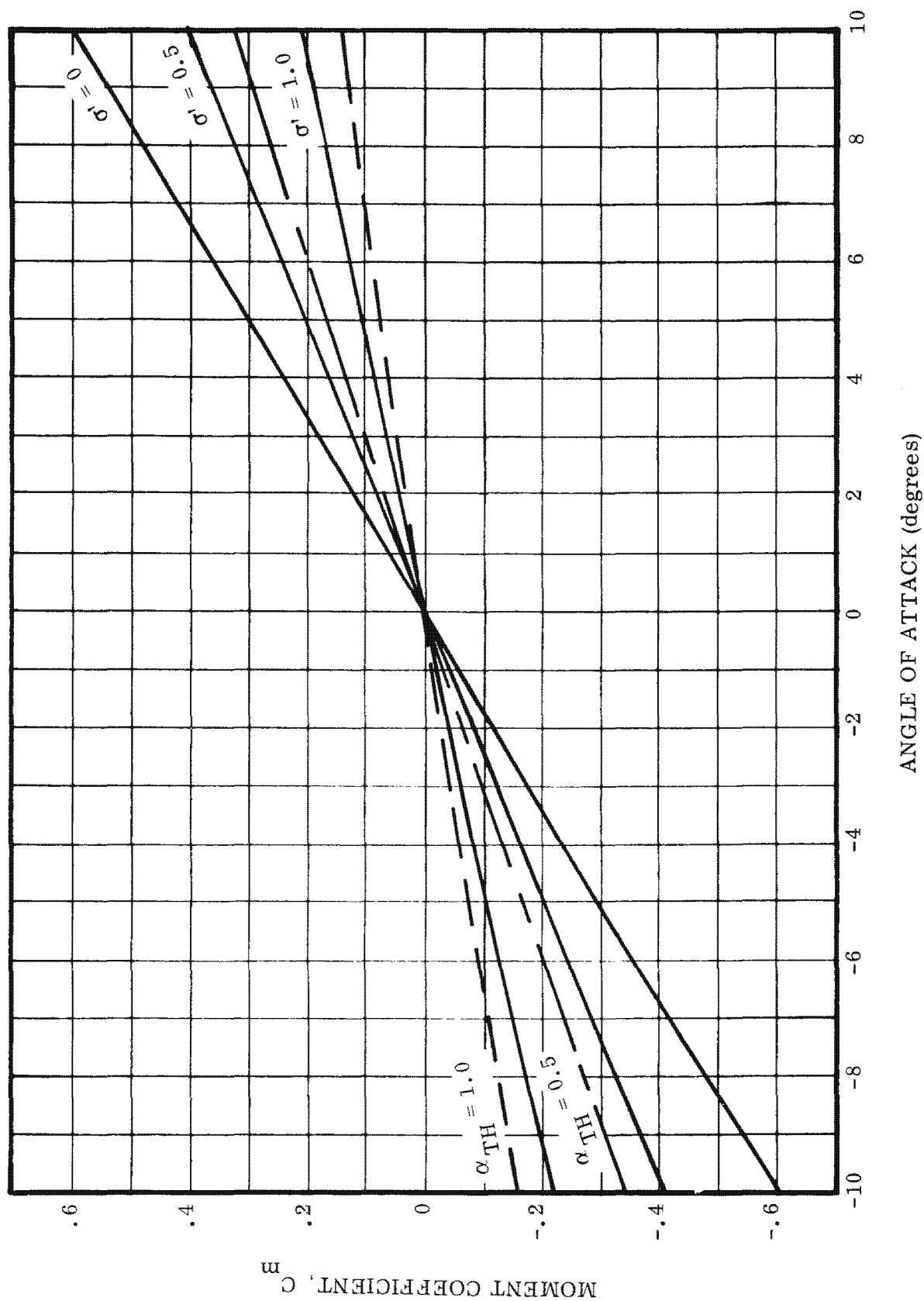
Figure 3-11. Theoretical Moment Coefficient – Accommodation Coefficient Correlation, Small Angles of Attack

64SD4760

3-24

At low altitudes (less than 70 nautical miles), resolution of telemetry data may be adequate for use as an aid in determining vehicle attitude relative to the flight path. Above 70 nautical miles, data resolution is not adequate for this purpose unless accurate calibrations of various system parameters and center-of-gravity travel are used to correct results.

The favoring of one switching line at low altitudes can be predicted fairly accurately as a function of orbit parameters (relative wind based on latitude, and path angle) enabling a refinement in vehicle attitude predictions. By refinement of the calculations using calibrated vehicle parameters, upper wind profile measurements are possible (estimated practical up to 65 miles). More flight data at the required altitudes are necessary if continued study is desirable.

It is significant that for small angles of attack (figure 3-11) data points deviate very little from the plot. This indicates that platform pitch and yaw attitude errors were very close to zero relative to the rotating reference.

3.2.2 EARTH IR RADIATION STUDY

Data obtained from flights prior to SV 960 have indicated that severe seasonal variations in earth infrared (IR) radiation may occur in the band pass of the infrared horizon sensing system (IRHSS) used on this vehicle. In order to implement a study of this phenomenon, the IRHSS was calibrated to be used as a radiometer. Using the calibration curves obtained, peak-to-peak earth-sky voltage was converted to equivalent black-body earth temperatures at various geographical points. Major emphasis was placed on the South Pole vicinity, the coldest area at the time of the SV 960 flight.

Figure 3-12 shows the equivalent black-body temperatures measured in the vicinity of the South Pole. Temperatures measured at the same geographic points, viewed on a number of different revs, were within five degrees of each other even though opposite heads may have made the measurements. A reasonable estimate of the accuracy of all readings is then ±10 degrees Kelvin.

64SD4760
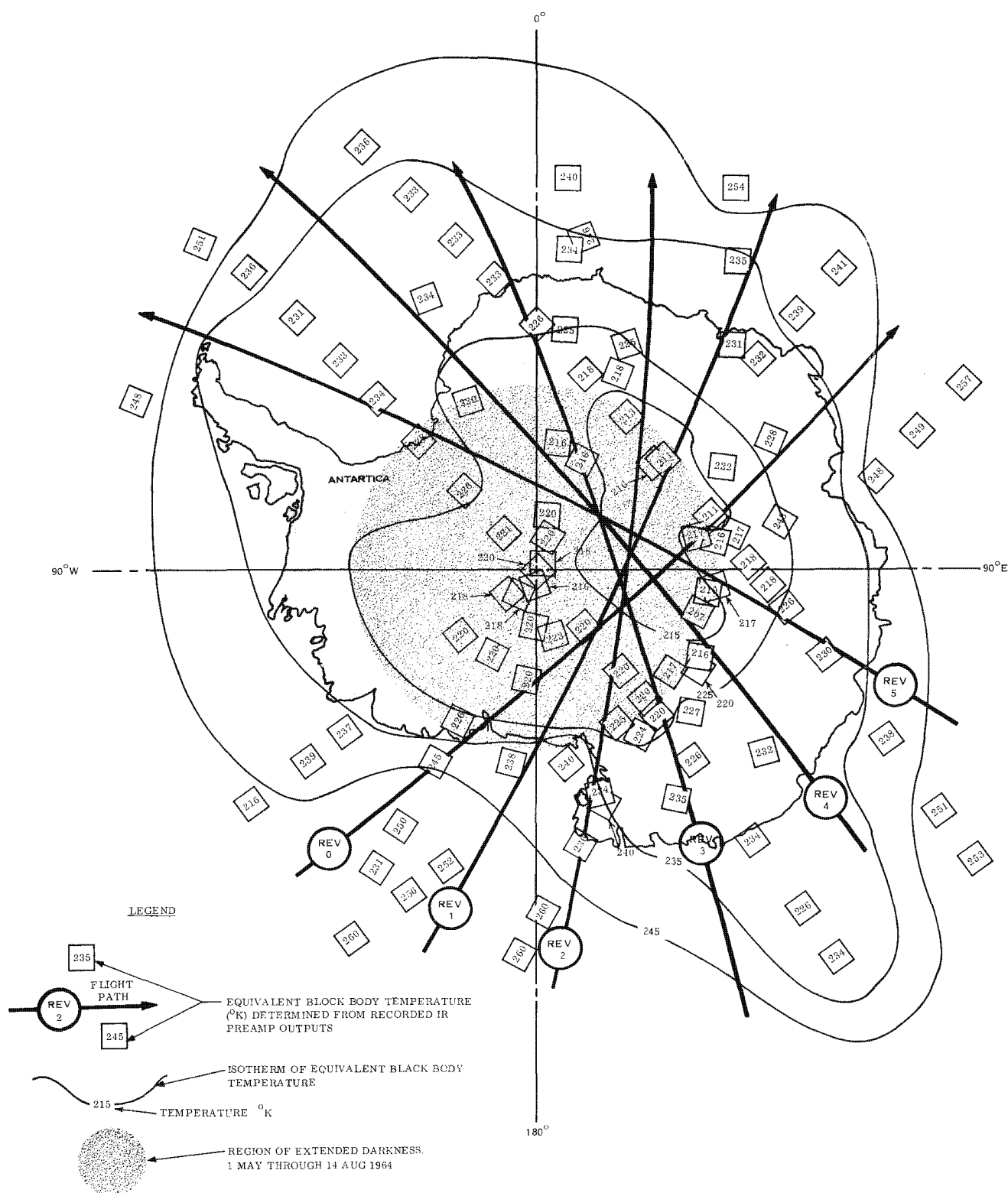
Figure 3-12. Equivalent Black-Body Temperature
Mapping of South Polar Region, SV 960

64SD4760

3-26

The temperatures given as "equivalent black-body earth temperatures" are not to be misconstrued as meaning that the earth radiates energy as a true black body. These temperatures are the black-body temperatures which would radiate the same total amount of energy as that radiated by the earth when the black-body spectrum and earth radiation spectrum are modified by the optical efficiency of the scanner used to make the measurements. The word "earth" should be interpreted as including the atmosphere above the earth. Two different scanner systems, viewing the same horizon at the same time, would give two different "equivalent black-body temperatures" unless both scanner systems had identical optical efficiency curves, or unless the earth were truly emitting energy as a black body.

Because of the late launch of SV 960, the β angle was -26 degrees, causing the left-hand scanner temperatures to be between 110 to 115°F, while the right-hand scanner was between $130\text{-}135^{\circ}$ F in the vicinity of the South Pole. With these temperatures, the temperature threshold for inhibit was 204° K (LH) and 199° K (RH). Although this particular system was not observed to inhibit, the earth-sky signal near the South Pole was marginal, and another system possibly could have inhibited. In fact, inhibit would have occurred if the left and right heads were interchanged. Inhibit levels: 217° K (LH) and 192° K (RH).

Calibration of individual scanners (voltage output vs. apparent black-body radiation) was not accomplished on SV 951 through SV 959; therefore, earth temperature mapping, using these flight data, cannot be accomplished with as much accuracy as with the SV 960 data. However, because of the importance of determining variation of the earth's equivalent black-body temperature with season and geographical location, available data from all flights to date have been analyzed to the extent possible. In order to standardize results, the SV 960 right-hand scanner calibration curve was used to convert all data to the equivalent black-body temperatures.

Results of plotting mean temperatures versus latitude for each flight are presented in figure 3-13. Deviation of data points from the mean curve for each vehicle were no larger than $\pm 20^{\circ}$ K, with approximately 80% of the data within $\pm 10^{\circ}$ K. Because of deviations in scanner temperatures with Beta angle, and because of the individual scanner characteristics on the different vehicles, the variation of actual temperatures from the data plotted (using

64SD4760
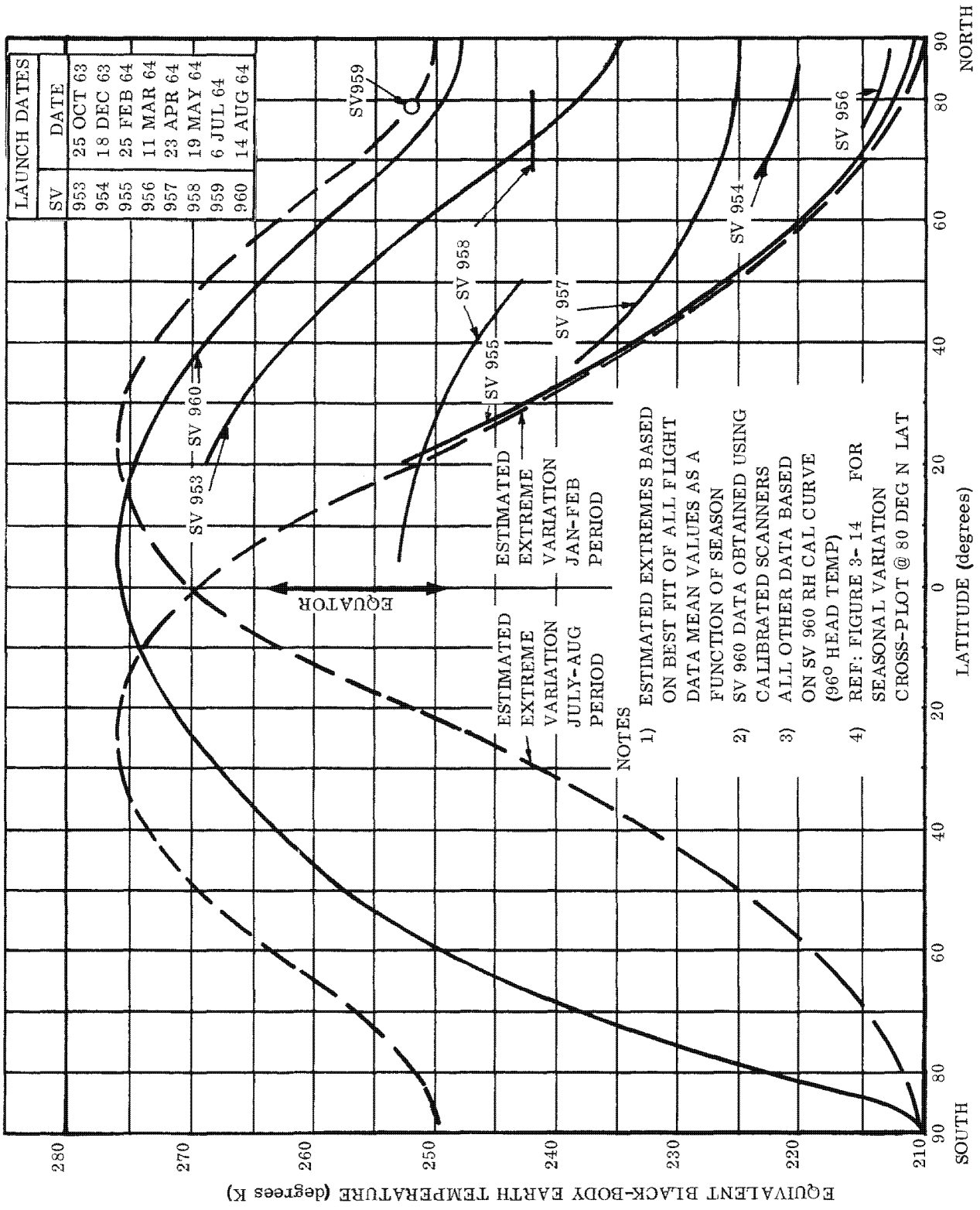
Figure 3-13. Apparent Variation of Earth Temperature with Latitude

the single SV 960 RH calibration curve) may be as much as 20° K (constant) from that which would be obtained using calibration curves for each individual scanner. No playback IR preamplifier data was available for flights prior to SV 960; therefore only northern hemisphere data points were available.

Based on the resulting curves, an estimate of the average extreme seasonal temperature limits, assumed to be symmetrical about the equator, was plotted in the figure. Maximum seasonal variation would be expected in the polar regions. Also, temperatures in these regions would be least influenced by cold cloud cover. A cross-plot of figure 3-13 at 80 degrees North latitude is presented in figure 3-14. As expected, the best-fit plot is nearly sinusoidal with extremes during July and February. Cooling appears to occur at a slightly slower rate than warming. The lower than expected temperatures observed from the SV 958 preamplifier outputs in the temperate latitude region can possibly be explained by either:

a. an abundance of cold clouds in the region, or

b. a lower preamplifier gain of both scanners, or

c. a large variation in SV 958 scanner head temperature when compared with other vehicles, and variation as a function of latitude.

Although data points were eliminated where cold clouds obviously affected the measurements, cloud cover within the entire field of view is difficult to detect and, therefore, possibly is reflected in the analysis results. Thus cold cloud cover offers a reasonable explanation for the lower apparent temperatures. A lower gain in the preamplifiers is disputed by the data points obtained over the Thule tracking station, which were at a level expected for the particular time of year. Large variation in scanner temperatures when compared with other flights could have resulted from the initial very low altitude perigee of the flight; however, little variation of temperature with latitude is expected to have occurred. The latter is substantiated by the temperature surveys taken with SV 960.

Because of the better accuracy of temperature determination accomplished with calibration of individual scanners, continued analyses of future flights could result in seasonal variation plots in which more confidence can be placed.

64SD4760
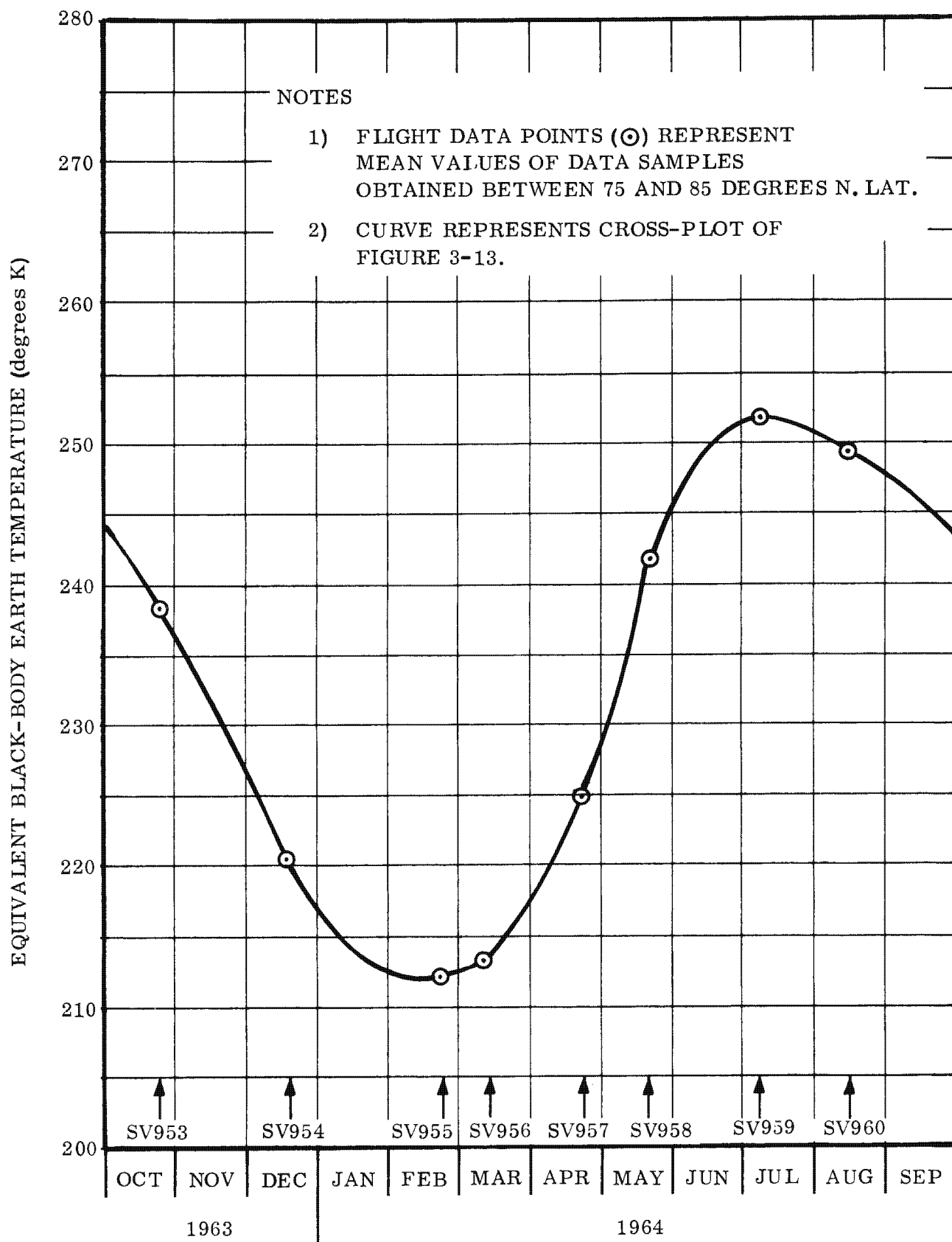
Figure 3-14. Apparent Variation of Earth Temperature
at 80 Degrees North Latitude with Time of Year

64SD4760

3-30

C05099047

3.2.3 SOLAR, ALBEDO AND EARTH RADIANT FLUX STUDY

An analytical study was undertaken to evaluate the orbital thermal space parameters encountered from SV telemetered skin temperature data. The parameters of interest were specifically the solar, earth albedo, earth radiant, and free molecular heating fluxes encountered by the vehicle. An objective of this study was to develop an automatic digital or analog computer technique to determine these basic radiation parameters from flight temperature data.

The general expression for the heat balance of a near-earth orbiting space vehicle can be written as follows:

$$S \alpha \bar{A} \cos \theta + A \, S \alpha \, \bar{A} \, F_e \cos \phi + E \, \epsilon \, \bar{A} \, F_e + Q_m = \epsilon \, \sigma \, \bar{A} T^4 - Q_I + C \frac{dT}{dt} \quad , \qquad (1)$$

where:

ϵ	= hemispherical infrared emissivity of vehicle surface.
α	= solar absorptivity of vehicle surface
$\bar{A}$	= vehicle surface area upon which flux impinges
T	= vehicle surface absolute temperature
Q_I	= internal heat dissipated
θ	= angle between incident solar ray and the normal to the vehicle surface
ϕ	= angle between solar ray and the vehicle's radius vector from the center of the earth
C	= capacitance of vehicle
F_e	= view factor from the vehicle to the earth
t	= time
$S \alpha \bar{A} \cos \theta$	= solar flux
$A \, S \alpha \, \bar{A} \, F_e \cos \phi$	= earth albedo flux
$E \, \epsilon \, \bar{A} \, F_e$	= earth radiant flux

64SD4760

3-31

Q_m = free molecular flux

$\epsilon \sigma \bar{A} T^4$ = vehicle radiant flux

$C \dfrac{dT}{dt}$ = stored energy

α_{TH} = thermal accommodation coefficient

S = solar flux constant

A = earth albedo flux constant

E = earth radiant flux constant

Once a vehicle is designed and the mission parameters (firing time, inclination, altitude, etc.) defined, vehicle temperatures are then a function of the radiation parameters (S, A and E) and the free molecular heat flux. The radiation parameters are primarily affected by season, atmospheric characteristics, and earth topography. Based on the data of many investigators, a design range was statistically determined for each parameter. For the Program 206 vehicle, the range selected is presented below:

Table 3-3 . Parametric Design Range

Parameter	Nominal	1σ Deviation
Solar (BTU/hr-ft^2)	440	4.4
Earth Albedo, dimensionless	0.38 of Solar	0.06 of Solar
Earth Radiant (BTU/hr-ft^2)	68.2	6.67

Orbital temperatures falling within the corresponding plus and minus 3σ extremities of the fluxes listed in table 3-3 represent the probable range of sink conditions.

The thermal sinks are defined as:

$$T_{x\sigma} = T_{nom} \pm \sqrt{(\Delta T_{x\sigma_S})^2 + (\Delta T_{x\sigma_A})^2 + (\Delta T_{x\sigma_E})^2 + (\Delta T_{x\sigma_{\alpha/\epsilon}})^2} \qquad (2)$$

where:

$T_{x\sigma}$ = sink temperature

T_{nom} = nominal sink temperature

$\Delta T_{x\sigma_S}$ = sink temperature difference due to $x\sigma$ deviation of the solar constant only with other parameters nominal

$\Delta T_{x\sigma_A}$ = sink temperature difference due to $x\sigma$ deviation of earth albedo only with other parameters nominal

$\Delta T_{x\sigma_E}$ = sink temperature difference due to $x\sigma$ deviation of earth flux only with other parameters nominal

$\Delta T_{x\sigma_{\alpha/\epsilon}}$ = sink temperature difference due to $x\sigma$ deviation of α/ϵ coating only with other parameters nominal

For $+3\sigma$ thermal sinks, $x = 3$.

When temperature surveys are performed during flight, a temperature history of the vehicle skin may be plotted. Knowing the temperature history and the orbital parameters for the given flight, a thermal balance (Equation 1) is used to calculate the heat flux (left-hand side of Equation 1), and in particular the values of S, A, E and Q_m which produced the observed temperature response.

SV telemetered skin temperature data is obtained from six circumferential positions on both the Adapter and OCV. The analysis to date has considered only SV 955-rev 24 Adapter temperature data with the temperatures tabulated as a function of percent revolution. The data was also plotted and integrated to determine the average temperature at each vehicle circumferential location during the revolution. The Orbit Heat Flux and Free Molecule

64SD4760

Heat Flux Digital Computer Programs (using the U. S. Standard Atmosphere, 1962) were run using the exact orbit parameters encountered on this rev, for the various adapter temperature-sensor positions. A time history of each type of flux in the left-hand side of Equation 1 was obtained, along with the orbital average flux for each sensor location. Two analytical techniques were then used in calculating the values of α_{TH}, S, A, and E which were implied by the flight data.

3.2.3.1 Steady-State Heat Balance

The first method considered was to establish a steady-state orbital average heat balance (Equation 1 minus the heat storage term) for each temperature sensor with use of the orbital average fluxes obtained from the digital computer programs and the average temperature for each flight sensor. The six resulting simultaneous equations were solved for α_{TH}, S, A, and E using the control coating values of α/ϵ which were measured prior to launch. Solutions for the four unknowns were obtained by using different combinations of four of the six skin sensor equations.

3.2.3.2 Transient Heat Balance

The second method considered utilized Equation 1 for a given sensor location. At each of nine orbital geographical locations (latitude and longitude) where temperature data was taken during rev 24, the rate of change of temperature and the corresponding orbit time fluxes were calculated. The corresponding heat balance equations were solved for α_{TH}, S, A, and E. Again, different combinations of four of the nine data interval equations were used.

3.2.3.3 Results

The results obtained by the two methods were totally unrealistic. Typical values of S, A, and E obtained are presented in table 3-4 and are compared to the nominal value expected.

64SD4760

Table 3-4. Typical Values of Calculated S, A, and E

Parameter	Nominal	Average Heat Balance	Transient Heat Balance
Solar BTU/hr-ft^2	440	382	331
Earth Albedo	0.38	-30.2	499
Earth Radiant BTU/hr-ft^2	68.2	2,472	-23,050

The values varied from plus to minus over 2 orders of magnitude depending upon the simultaneous equation grouping used. At this point in the study, the effort to obtain S, A, and E using a simplified analytical technique was concluded.

The study to define a simplified analytical technique using flight data to obtain the solar, earth albedo, earth radiant fluxes, and the accommodation coefficient encountered during each vehicle flight was not successful. However, several significant conclusions were reached as a result of the study:

1. Each flight sensor is not providing a simultaneous independent response. This is attributed to the local sensor installation.

2. The present sensor system readout accuracy is probably inadequate for this task. Analytical studies have shown that a difference as small as ± 10 F$^\circ$ in average vehicle temperature can imply as much as $\pm 1\sigma$ deviation in thermal sink temperature as defined in Equation 2.

3. A direct flux measuring instrument, such as a radiometer, would provide a better means of obtaining the values of these constants.

4. Internal dissipations may be affecting the local heat balances.

64SD4760

3-35

5. The analysis assumed constant values of S, A, and E throughout a revolution. Since local values of A and E can vary significantly, this assumption may cause large errors in the results for a local skin temperature while not significantly affecting internal components.

6. OCV skin temperature data should be used in future analysis since, for the OCV, the free molecular heat flux effects are not so pronounced as they are for the Adapter.

7. A more refined back-out analysis should be used if future study efforts are to be considered.

3.2.4 ATTITUDE ERROR DETECTION USING TEMPERATURE SENSORS

Post-flight analysis has shown that thermal instrumentation can be used to indicate attitude errors. Figure 3-15 shows a temperature history for the SV 957 Adapter skin at the 60-degree circumferential position, both before and after a five-degree pitch-down error occurred. Examination of the curve shows that the peak temperature increased about 20 F^{o} because of free molecular heating, and a corresponding phase shift occurred since the sun illuminated this skin area earlier during each orbit. This plot was obtained as a result of post-flight analysis using a total of 88 data points from many complete orbit temperature surveys. Examination of the data using only 24 data points was insufficient to confirm the attitude error. It should also be realized that, of the 12 vehicle skin sensors available, this sensor was the most severely affected (largest temperature change) by the attitude error.

To determine the feasibility of detecting small attitude errors in real time, a study was conducted to evaluate the magnitude of flux and the corresponding temperatures encountered with incremental attitude errors. The flux absorbed and the corresponding temperature response of four sensors, located on the OCV skin in the pitch and yaw planes, were calculated, using nominal space fluxes plus the free molecular heating associated with attitude errors up to 10 degrees. The assumed orbital conditions were a 70-nautical mile
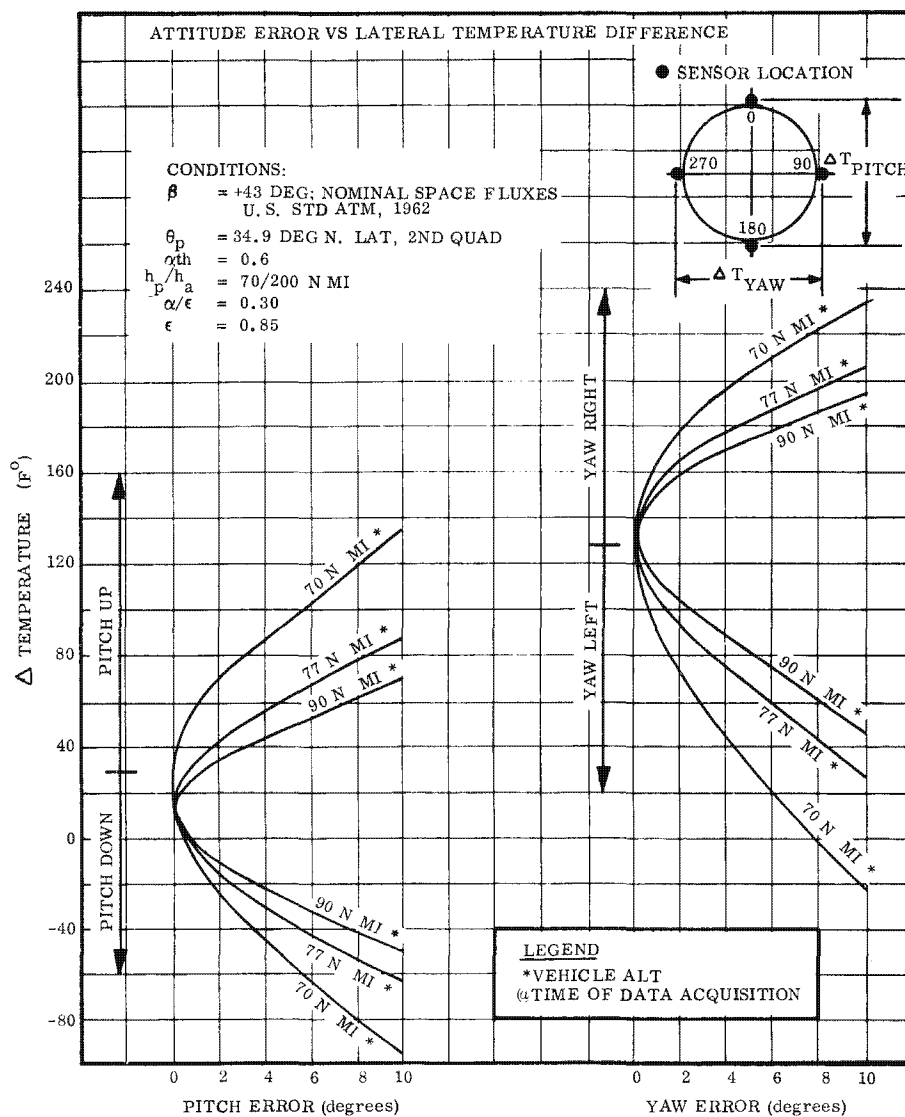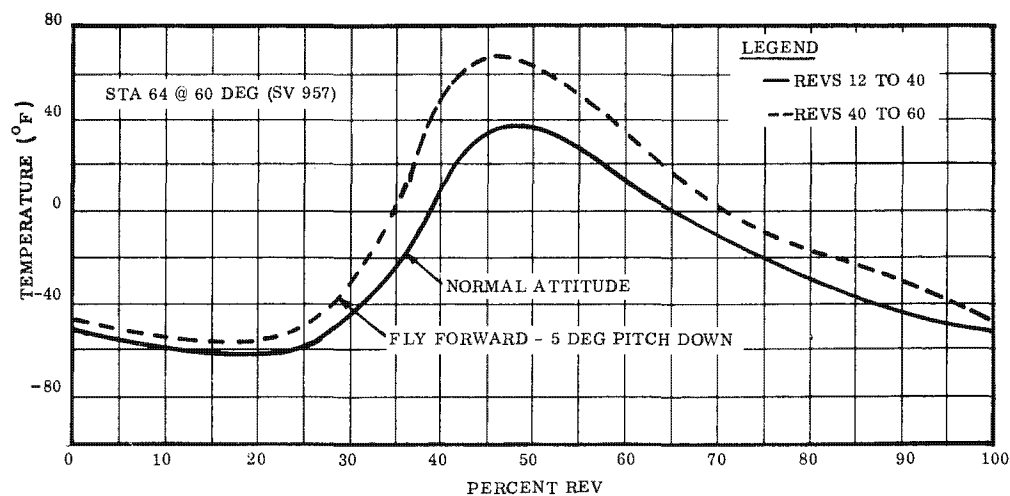
Figure 3-15.   Use of Temperature Sensors in Determining Attitude Errors, Demonstrated
(SV 957) and Theoretical

perigee located at 34.9 degrees North latitude, a 200 nautical mile apogee, a solar incidence angle of +43 degrees, the U.S. Standard Atmosphere, 1962 and an α_{TH} of 0.6. The results indicate that attitude errors can be sensed significantly only below 80 nautical miles, requiring that data be taken near perigee.

The difference and level of the radiation equilibrium temperatures corresponding to the absorbed fluxes are directly affected by the coating system selected. The difference and level both increase with decreasing emissivity. The low ϵ system is desirable because of high amplification factors, but is not practical from a manufacturing standpoint because of close-tolerance coating control problems. Results with the orbital conditions stated above for a high ϵ white-paint system (as is now used on the vehicle) are also presented in figure 3-15. Since the sensor range required to measure the temperature difference due to a 10-degree attitude error is equal to that required to measure absolute temperatures, absolute measurements using the proven white coating system seem most feasible at this time.

3.2.5 EVALUATION OF ROLL NOZZLE PLUME IMPINGEMENT (B-FACTORY STUDY)

Flight experience with the first six Satellite Vehicles on the Program indicated that roll maneuver activity imparted a forward thrust to the vehicle. It was assumed that this was caused by Freon impingement on the aft bulkhead; that is, the high-thrust roll nozzles were so mounted that the exhaust plume did not clear the physical boundaries presented by the aft bulkhead, insulation blankets, brackets, etc. The DDI computer program, used for ephemeris generation, accounts for all non-conservative effects by manipulation of the so-called B-factor $\left(B = \dfrac{C_D A}{2\,m} \right)$. Thus, changes in vehicle drag, or the addition of small thrust forces, are reflected by changes in B-factor. An analysis was made to establish the level of the velocity increment imparted to the vehicles by roll nozzle plume impingement.

3.2.5.1 Theory

A Satellite Vehicle, in a given near-earth orbit, experiences an energy loss caused by aerodynamic drag, $\Delta E/\text{rev}$. The lower the average orbital altitude, the higher will be ΔE.

64SD4760

If the vehicle experiences some impulsive thrusting, the ΔE/rev will be reduced in proportion to the number of thrust impulses imparted per rev. The thrust impulses to the vehicle are assumed to be the result of high-thrust roll nozzle plume impingement, and therefore the impulses per rev are considered to be proportional to the roll maneuver activity per rev. This has been expressed quantitatively in terms of the equivalent number of one-degree-per-second roll maneuvers performed per revolution and designated $\overline{M}$/rev.

Since vehicle geometry suggests that only the high-thrust roll nozzles can cause a serious impingement effect, only high rate (3 deg/sec) and medium rate (1 1/2 deg/sec) roll maneuvers are considered in the calculation of $\overline{M}$.

The effect of roll maneuver activity can be described as shown in the following diagram. For M = 0, the ΔE values are those due solely to the vehicle drag. As thrust impulses are imparted, ΔE/rev is reduced proportionately. The three curves shown are for three
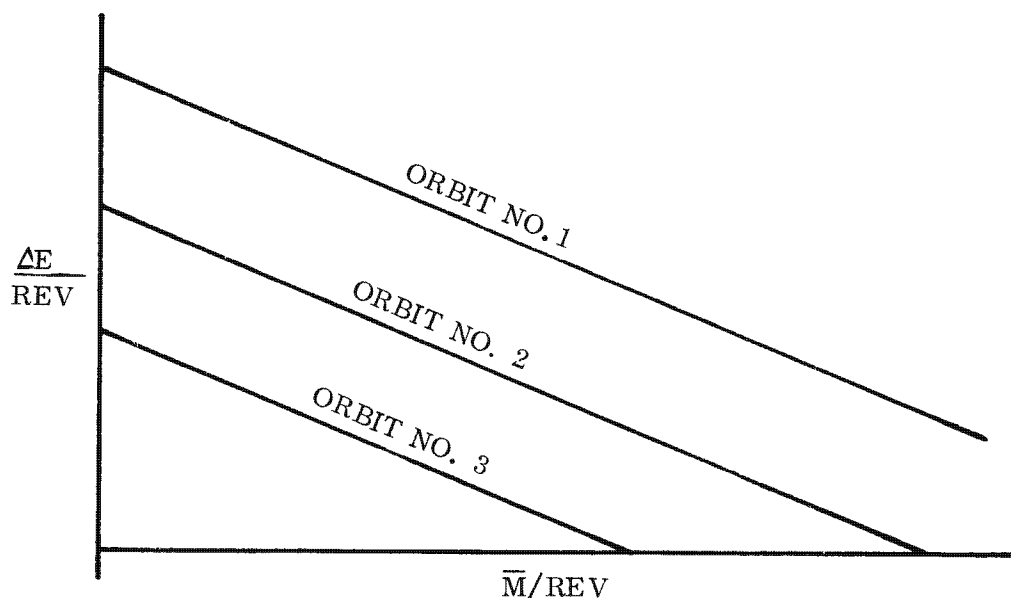
different altitude orbits; the average altitude of orbit no. 1 is lower than that of orbit no. 2, which, in turn, is lower than orbit no. 3. If the impingement thrusting effect does not vary, these curves must have identical slopes.

A change in energy results in a change in the orbital period, and for a relatively small number of revolutions they are directly proportional; that is, ΔE/rev $= K \overline{\Delta P}$, where K is a proportionality constant and $\overline{\Delta P}$ is the average period change per rev which is further defined below.

64SD4760

3-39

The mathematical model used in the DDI ephemeris generation program for SV 951-SV959 includes the $J_2^{(2)}$ (tesseral) harmonic term which perturbs orbital period as a function of longitude. This results in a sinusoidal fluctuation of ΔP (change in orbital period) with a cyclic period of twelve hours as shown in the following sketch. This may be expressed as $\Delta P = \overline{\Delta P} + A \sin \omega t$. It is the mean value $\overline{\Delta P}$ which is of interest in this study, for the change in $\overline{\Delta P}$ with time can be used as a measure of energy decay of the orbit.
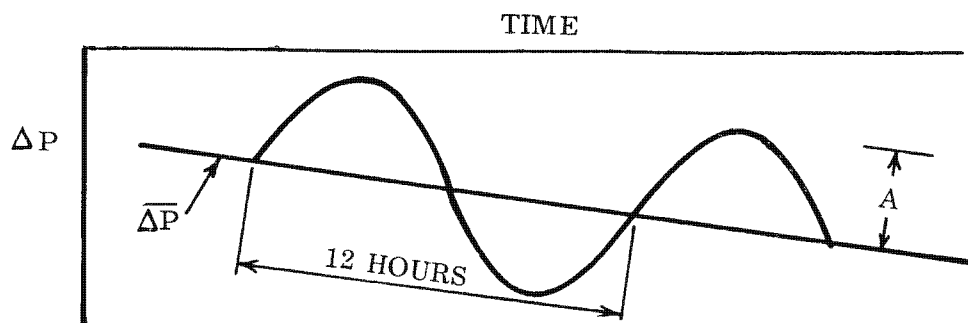
3.2.5.2 Evaluation of $\overline{\Delta P}$

Data were used from the best fit ephemerides (BFE) of SV 955 to 958 and SV 960. These ephemerides were constructed as series of segments, each initiated at a reference epoch with a specified value of B. For the BFE's, in general, a six-parameter fit was used with a B-factor specified to match tracking over the span of the segment. From the computed time of ascending node crossings, Δ-periods were determined for each ephemeris segment, and plotted as a function of rev no. as sketched below.

64SD4760

3-40
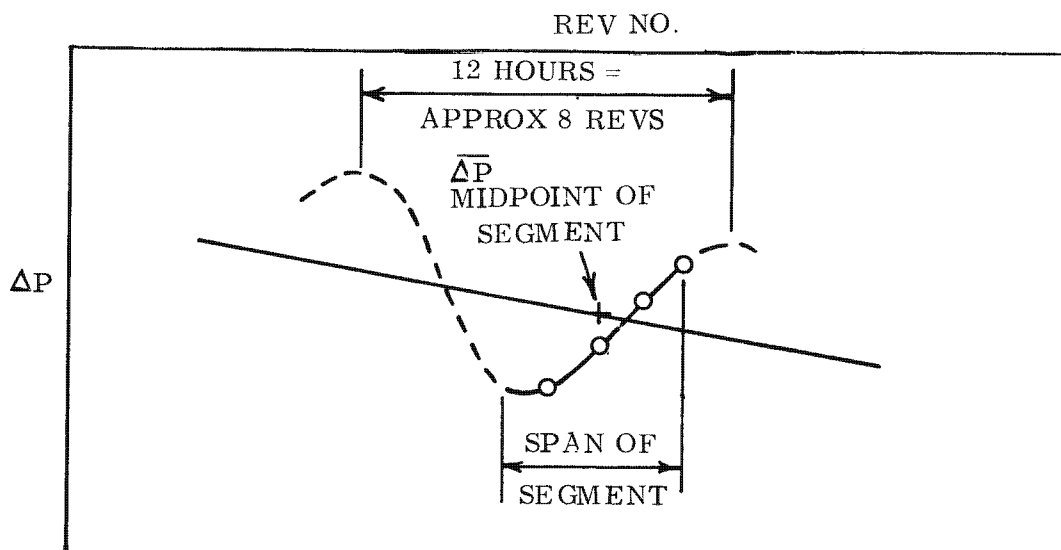
Construction of the complete sine curve representing a full twelve-hour span (or approximately eight revolutions for the applicable orbit) had been facilitated by running a number of epochs of the SV 956 ephemeris out for the full 12-hour cycle. With these data as a general guide to shape, and a correlation of the location of maxima and minima in terms of ascending node longitude, it was relatively simple to complete the construction of the full sine curve as shown by the dashed portion of the preceding diagram. The mean line of the constructed sine wave was determined graphically, and the average value of $\overline{\Delta P}$ for each segment was then read from the mean line at the mid point (in time) of the applicable data span. For SV 960 a more sophisticated gravity potential model was incorporated in the ephemeris generation program. This required no essential change in the method of evaluating $\overline{\Delta P}$, but introduced a slight variation in technique . The result was that the cyclic variation in period was no longer the simple sine wave with a twelve-hour period resulting from the $J_2^{(2)}$ term. The variation became, rather, a complex wave with a twenty-four hour period as shown in figure 3-16, part A. Those responsible for orbit generation have indicated that the more complex model does not significantly affect the vectors derived from the tracking data (including B-factors on seven parameter fits), but does result in an appreciable reduction in the residuals (ref 15).

Part B of figure 3-16 shows the $\overline{\Delta P}$ vs B characteristic for SV 960 derived from the various data spans. Values of $\overline{\Delta P}$ read from this characteristic are plotted vs $\overline{M}$ (part C of the illustration) to show more detail than can be seen in figure 3-17.

3.2.5.3 Determination of $\overline{M}$

Roll maneuver activity was expressed quantitatively in terms of the equivalent number of one-degree-per-second roll maneuvers performed per rev: $M = 3 \times$ No. of high rate rolls $+ 1.5 \times$ No. of medium rate rolls. In determining the average roll maneuver activity over a span of N revolutions, $\overline{M} = \Sigma M/N$, several weighting schemes were tried. These included triangular and rectangular weighting where M_1 and M_N for the first and last revs were excluded from the ΣM of the numerator. The best correlation was found when M_1 for the first rev only was excluded, and it is this definition of average $\overline{M}/$rev which was uniformly followed.

64SD4760

3-41
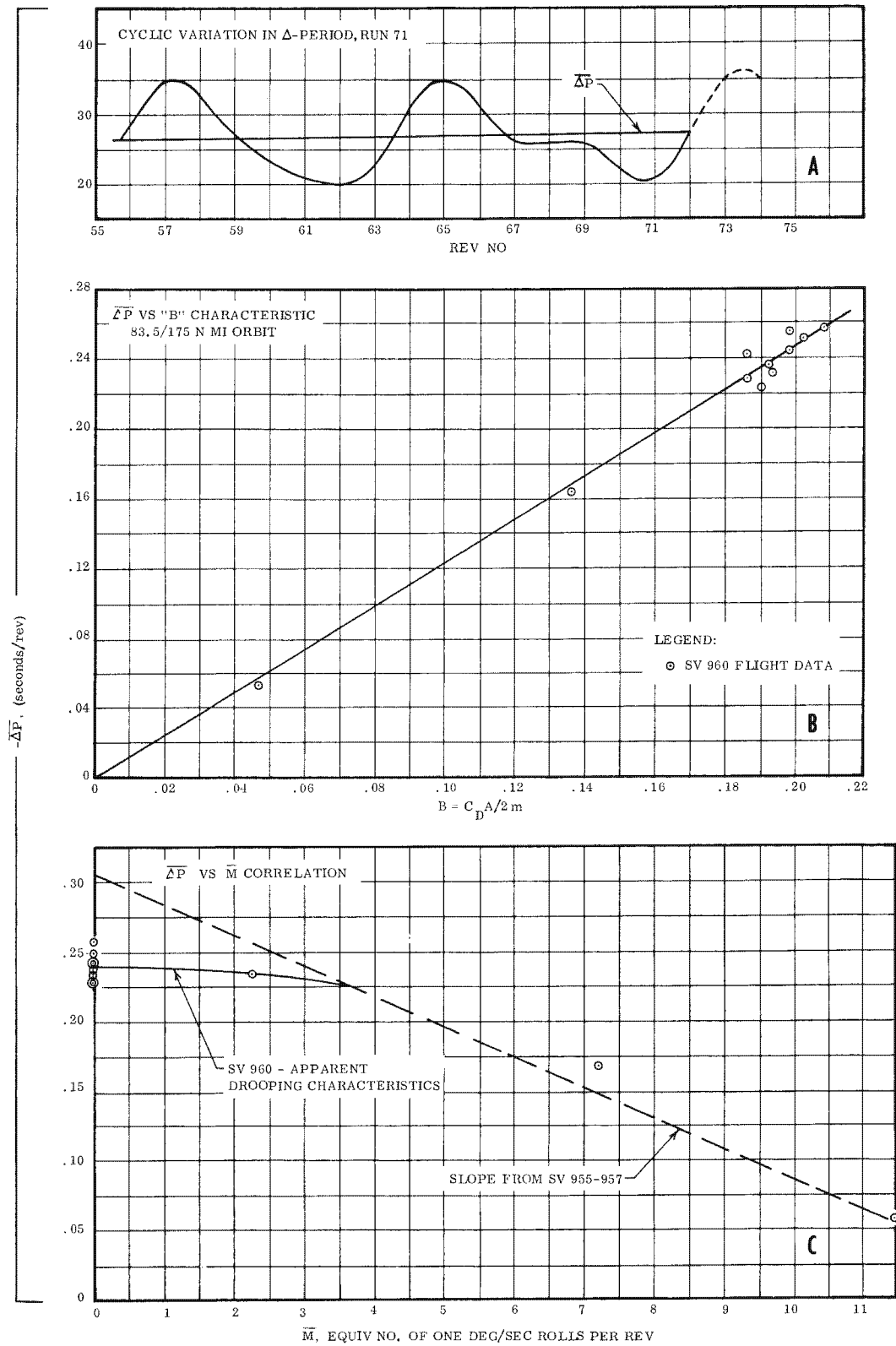
Figure 3-16.   SV 960 B-Factor Effects
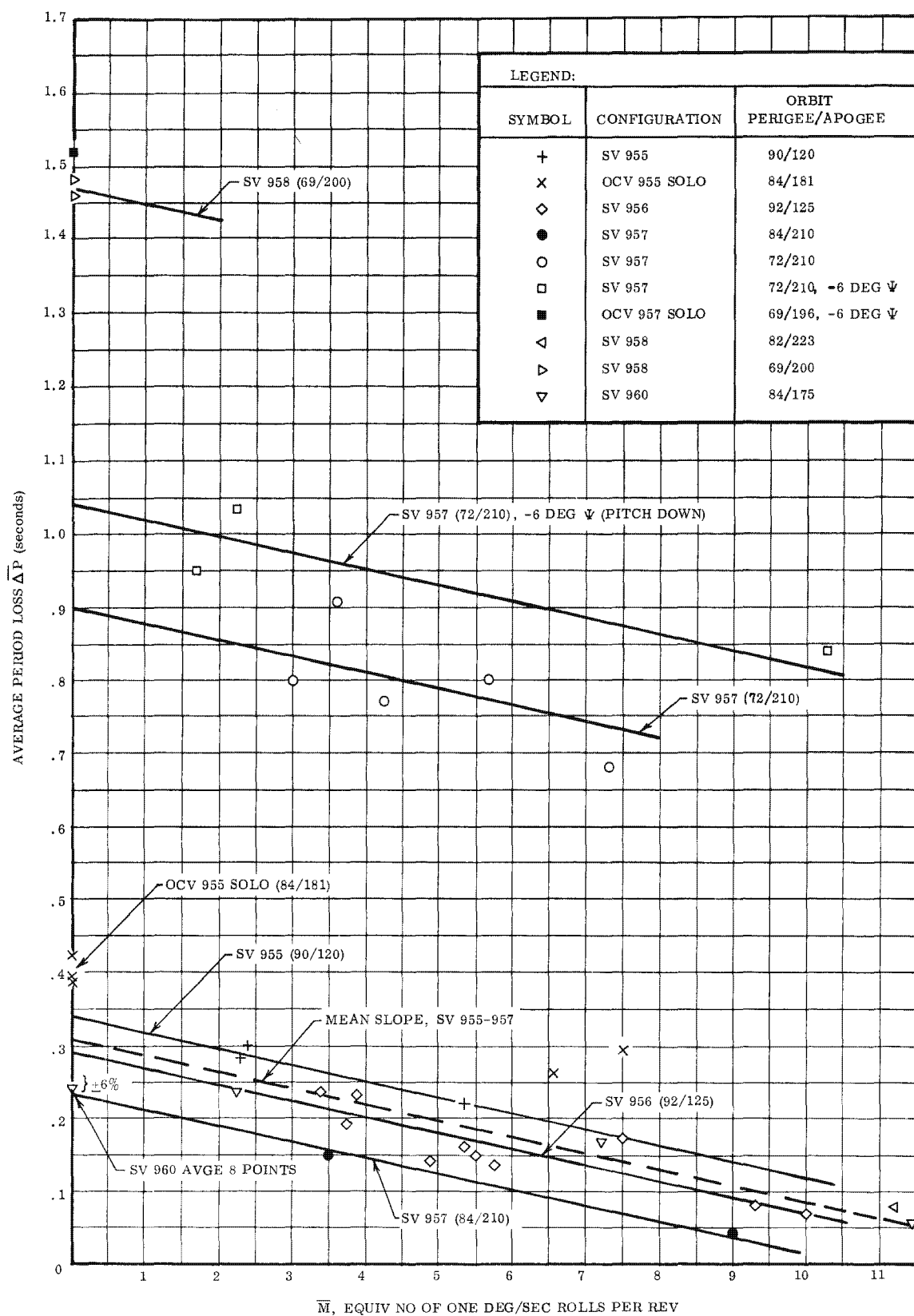
Figure 3-17. Results of Roll-Plume Impingement Δ V Study

3.2.5.4 $\overline{\Delta P}$ Versus B-Characteristic

For a given orbit, $\overline{\Delta P}$ is uniquely determined when the value of B is specified. However, minor random differences in perigee altitude, resulting from variations in fits to the track-ing data from span to span, produced considerable scatter in the $\overline{\Delta P}$ data. Decay in apogee altitude also introduced a small downward trend. It was necessary, therefore, before plotting against $\overline{M}$, to smooth the $\overline{\Delta P}$ data for all segments on a "given" orbit (relatively constant h_a/h_p relationship) to a single mean orbit. This was accomplished by plotting the $\overline{\Delta P}$ vs B-characteristic for the group of segments, and reading $\overline{\Delta P}$ for each from the mean line at the applicable value of B as diagrammed below. It is these smoothed values of $\overline{\Delta P}$ which have been used in the final plots vs $\overline{M}$.
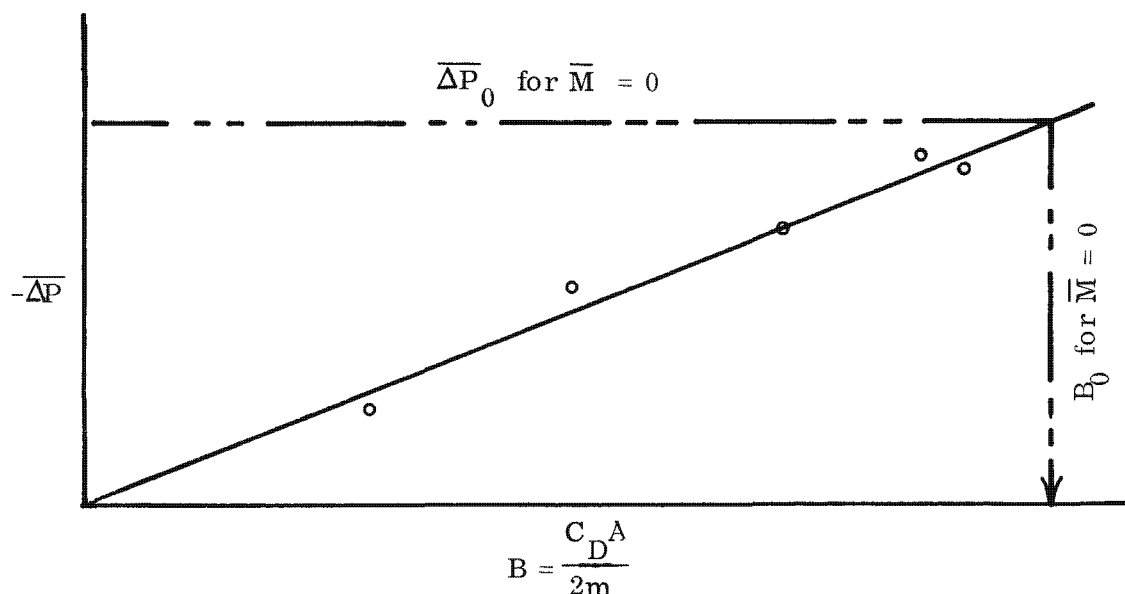
3.2.5.5 Results

From working curves as have been described, a series of final plots of $\overline{\Delta P}$ vs $\overline{M}$ was generated (figure 3-17). Although there is still considerable scatter in the data, a single representative slope $\overline{\Delta P}/\overline{M}$ for all Satellite Vehicles on all orbits plotted appears not unreasonable, with a value of 0.0223 second/roll. This slope can be converted to a velocity

64SD4760

increment by the relationship $\Delta V = \dfrac{\Delta P}{3P}$ V. The resultant mean velocity increment, $\dfrac{\Delta V}{M} = 0.035$ foot/second per one-degree-per-second roll, is equivalent to 0.05 foot/second per medium rate roll, or 0.10 foot/second per high rate roll maneuver.

The extrapolated intercept values, $\overline{\Delta P}_0$ at $\overline{M} = 0$, were converted to "quiescent" B-factor values by referring back to the mean $\overline{\Delta P}$ vs B characteristics. (Refer to Section 3.2.5.2 above.) Results for SV 956 – SV 958 indicated a mean $B_0 = 0.255$.

3.2.5.6 SV 960 Results

On the flight of SV 960 much data was obtained on a quiescent vehicle for the first time. The average B_0 for eight data spans totaling 48 revs at $\overline{M} = 0$ was 0.195. This is 24% less than the value expected on the basis of the earlier correlation. There are three points on figure 3-17 for SV 960 data spans with a range of roll activity values $2.25 < \overline{M} < 11.5$. The slope determined from the earlier correlation is not unreasonable for these three points. Extrapolated to $\overline{M} = 0$, the dash line yields $\Delta P_0 = 0.308$, corresponding to $B_0 = 0.250$. This is in excellent agreement with the earlier correlation.

In an effort to determine if the earlier data validate a linear interpolation to $\overline{M} = 0$, or substantiate the reduced B_0 values of SV 960, all values of B_0 were converted to a dimensionless drag coefficient by $C_D = \dfrac{2m}{A} B_0$.

The results were normalized by taking the ratio of the calculated C_D to a nominal expected value of 2.7. In an effort to broaden the data sample, the study was extended to include some data for OCV solo operation where quiescent data were available. In the following table, B_0 values which are underlined are for quiescent operation; all others are by linear extrapolation of the active data to $\overline{M} = 0$.

64SD4760

3-45

Table 3-5.   Calculation of Relative Drag, R

Configuration	Orbit	Weight[1]	$\overline{\Delta P}$[2]	B_0	C_D	R
SV 955	90/120	4000	0.340	0.315	3.98	1.47
OCV 955	84/181	3457	0.400	0.310	3.38	1.25
SV 956	92/125	4060	0.290	0.280	3.59	1.33
SV 957	84/210	4110	0.235	0.236	3.07	1.14
SV 957	72/210	4050	0.900	0.260	3.32	1.23
SV 957, -6 deg ψ [3]	72/210	3980	1.040	0.300	3.77	1.23
OCV 957	69/196	3300	1.521	0.348	3.62	1.19
SV 958	69/200	4010	1.470	0.266	3.37	1.25
SV 960	84/175	4125	0.241	0.195	2.54	0.94
SV 960	84/175	4125	0.308	0.250	3.25	1.21

Notes:

(1)   Weights estimated, assuming Δ W/rev to be constant over the span of operation.

(2)   Underlined values are for quiescent revs; other by extrapolation to $\overline{M} = 0$

(3)   For -6 degree pitch-down (ψ) condition, expected $C_D = 2.7 \times 1.13$.

It is apparent from inspection of the last column of this table that the SV 960 quiescent data alone represent a drag coefficient less than the expected value. The value corresponding to the extrapolated intercept at $\overline{M} = 0$ is in excellent agreement with the other three points based on quiescent data. There is also good general agreement between the extrpolated and quiescent points for other Satellite Vehicles.

3.2.5.7 SV 960 Conclusions

It is concluded that the apparent low drag for the quiescent vehicle, indicated by the SV 960 data, resulted from forward thrust introduced by a non-apparent condition peculiar to SV 960. The thrust in question is equivalent to that introduced by one high-rate roll per rev of normal operation ($\overline{M} = 3$).

The possibility exists that the small thrust necessary for this effect was provided by either a small pneumatics leak or normal venting from the high pressure regulator resulting from higher than normal manifold pressure caused by a known internal regulator leak. Fine rate telemetry indicated consistent, small external disturbance torque components in pitch and roll. The pitch torque component was an order of magnitude larger than the aerodynamic torques expected for the relatively high altitude orbit flown, while none is normally expected about the roll axis. These torques were not evident immediately following roll maneuvering activity, indicating the presence of an external leak which was pressure-sensitive and may have been related to the slight internal regulator leak observed. No evidence of an external pneumatics leak could be found from telemetry data, and steady-state impulse consumption was lower than expected throughout the flight. (Refer to Section 3.4.3.)

64SD4760

3-47

3.3 TELEMETRY, TRACKING AND COMMAND SUBSYSTEM

As operational assurance analyses continued with each flight, it became increasingly obvious that an analysis must be performed to determine the complete capability of the TT&C Subsystem, and to what degree this capability is being utilized in order to compare and determine the performance of this vehicle and future vehicles. Several critical parameters from each vehicle were chosen and thoroughly analyzed. The results were then combined to show that the calculated specification limits, previously set forth for acquisition and fade ranges of telemetry and beacon, have not only been adhered to, but they have been exceeded.

3.3.1 AIRBORNE TAPE RECORDER MANAGEMENT

The airborne tape recorder has a 933-second, continuous loop magnetic tape. During the record mode, the recorder also erases; therefore, if a record sequence is longer than 933 seconds, or if a group of sequences exceed this amount before any of the data is reproduced, the beginning of the sequence will be erased.

As shown in table 3-6, approximately 20% of the unique data was erased before it could be reproduced. This amounted to an average of 8,900 seconds of recorded data that was unobtainable per flight. In some instances this loss of recorded data caused a hardship on operational assurance analysis, but in all instances it displays a waste of power and recorder life.

Acquisition losses were also investigated but the average percentage of available data retrieved shows that less than five percent of unique data were lost because reproduction of data began before, or continued after, station contact.

64SD4760

Table 3-6. Tape Recorder Management

% Data Erased			% Total Recorded Data Retrieved			% Available Data Retrieved		
Max	Min	Avg	Max	Min	Avg	Max	Min	Avg
23.82	15.37	19.59	78.71	73.85	76.28	96.94	94.35	95.64

3.3.2 COMMAND CAPABILITY

The duration that the Verlort antenna can automatically track the space vehicle has been established as the command capability time. Information from four flights have been compiled to form a program total; the results are tabulated in table 3-7.

The subsystem design specification (reference 14) states that solid radar lock (autotrack) shall be achieved at 600 nautical miles. The results of this analysis prove that the Program 206 vehicle is functioning well within specification limits.

Table 3-7. S-Band Beacon Autotrack Capability Summary

Start of Autotrack					Loss of Autotrack				
Sample Size (n)	Range (n mi)		Elev Angle (deg)		Sample Size (n)	Range (n mi)		Elev Angle (deg)	
	Mean	Std Dev	Mean	Std Dev		Mean	Std Dev	Mean	Std Dev
65	704	69	2.89	1.01	70	689	90	3.04	1.19

Probability distribution curves (figure 3-18) were prepared for both achievement and loss of radar autotrack. These curves indicate that about 95% of the time, the ground antennas will be tracking when the vehicle reaches an elevation angle of 4.5 degrees. Loss of autotrack will occur at the same angle approximately 10% of the time, which means that for about 90% of the station passes, the elevation angle at loss of lock will be less than 4.5 degrees.

64SD4760

3-49

START AUTOTRACK

MEAN ($\bar{x}$) = 2.89 deg
STD DEV (S_x) = 1.01 deg
SAMPLE SIZE (n) = 65

AUTOTRACK ACHIEVED
~95% OF THE TIME

HORIZON

f (x)

ELEVATION ANGLE (deg)

LOSE AUTOTRACK

MEAN ($\bar{X}$) = 3.04 DEG
STD DEV (S_x) = 1.19 DEG
SAMPLE SIZE (n) = 70

AUTOTRACK LOST
~10% OF THE TIME

HORIZON

f (x)

ELEVATION ANGLE (deg)
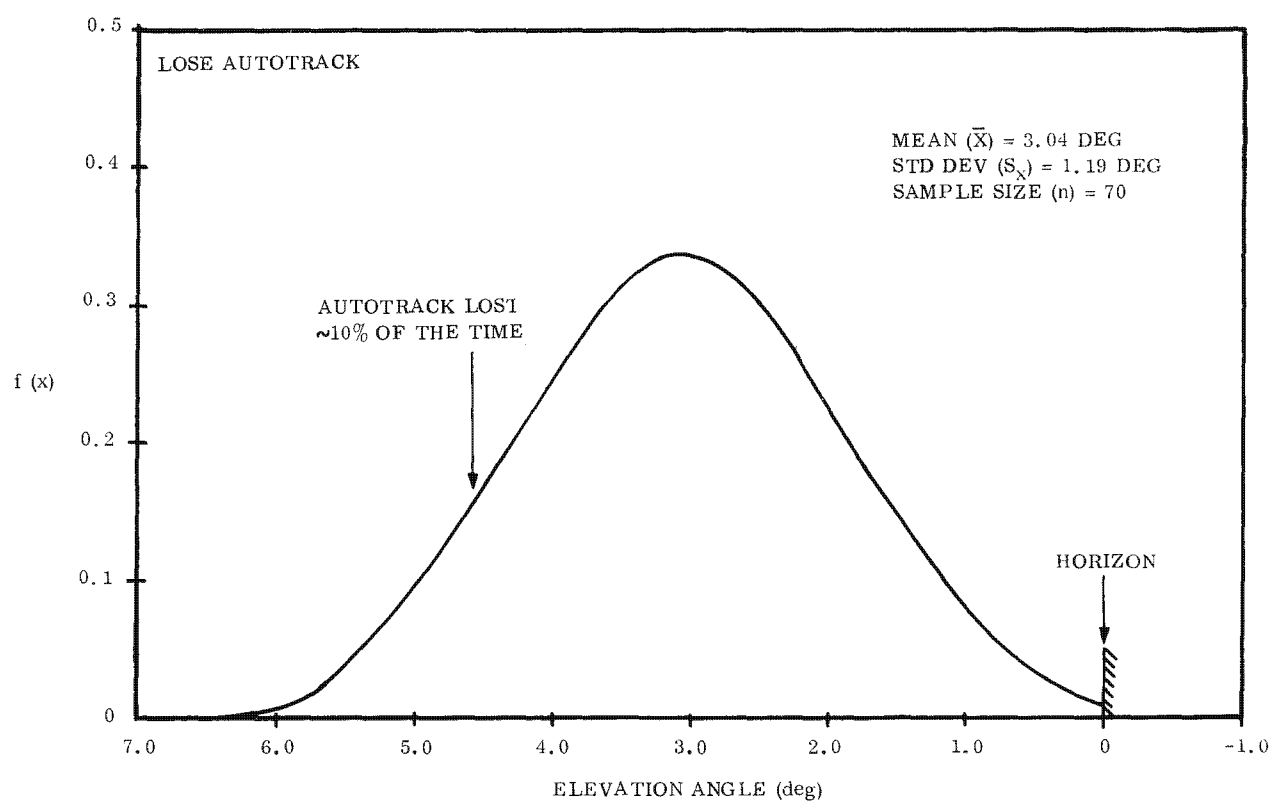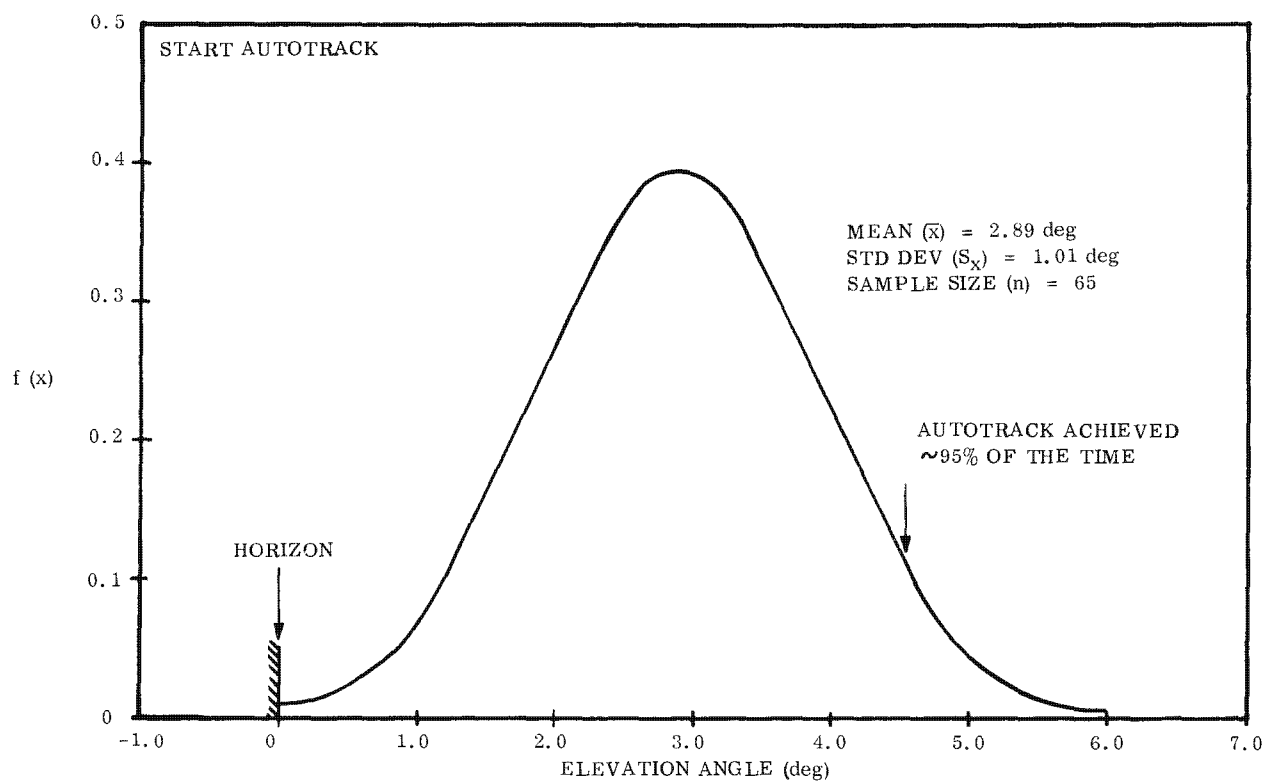
Figure 3-18. Beacon Autotrack Characteristics

64SD4760

3-50

The outcome of this analysis demonstrates the usefulness of the beacon beyond the specified five-degree set angle. When command loading at a station contact has been completed, the PPD can be deactivated by a real-time command. The command link will then be secure against alien interrogation, but the tracking link is still valid. Therefore, if the S-band beacon is kept energized until the zero-degree set point, much additional tracking data will be accumulated.

3.3.3 TELEMETRY ACQUISITION

An analysis of the telemetry rf link was performed in much the same manner as the beacon. Mean acquisition and fade ranges, which complement the analysis results given in ref 11, are tabulated in table 3-8. These summarized data represent the combined flight history of four vehicles, and therefore it is felt that these parameters represent program performance.

Table 3-8. Telemetry Contact Capability Summary

Acquisition					Fade				
Sample Size (n)	Range (n mi)		Elev Angle (deg)		Sample Size (n)	Range (n mi)		Elev Angle (deg)	
	Mean	Std Dev	Mean	Std Dev		Mean	Std Dev	Mean	Std Dev
76	814	84	0.59	0.93	58	765	109	0.93	1.30

Probability curves for acquisition and fade are presented in figure 3-19. The telemetry system is normally turned on and off at the zero-degree elevation angle, thus both curves lack a "tail." This is because the vehicle was well within acquisition range when the system was energized or deenergized. The practice of turning telemetry on and off at the zero-degree cone precludes early acquisition of the vehicle approximately 30% of the time and later fade about 25% of the time. If telemetry were energized at the minus one-degree cone on those station passes where negative masking is present, longer station contacts could be achieved.

TELEMETRY ACQUISITION

HORIZON (SIGNAL ACQUIRED
~ 30% OF THE TIME)

MEAN ($\overline{X}$) = 0.59 DEG
STD DEV (S_X) = 0.93 DEG
SAMPLE SIZE (n) = 76

SIGNAL ACQUIRED
~ 95% OF THE TIME

$f_{(x)}$

ELEVATION ANGLE (degrees)

TELEMETRY FADE

MEAN ($\overline{X}$) = 0.93 DEG
STD DEV (S_X) = 1.30 DEG
SAMPLE SIZE (n) = 58

HORIZON
(SIGNAL STILL ACQUIRED
~ 25% OF THE TIME)

SIGNAL LOST
~ 5% OF THE TIME

$f_{(x)}$

ELEVATION ANGLE (degrees)
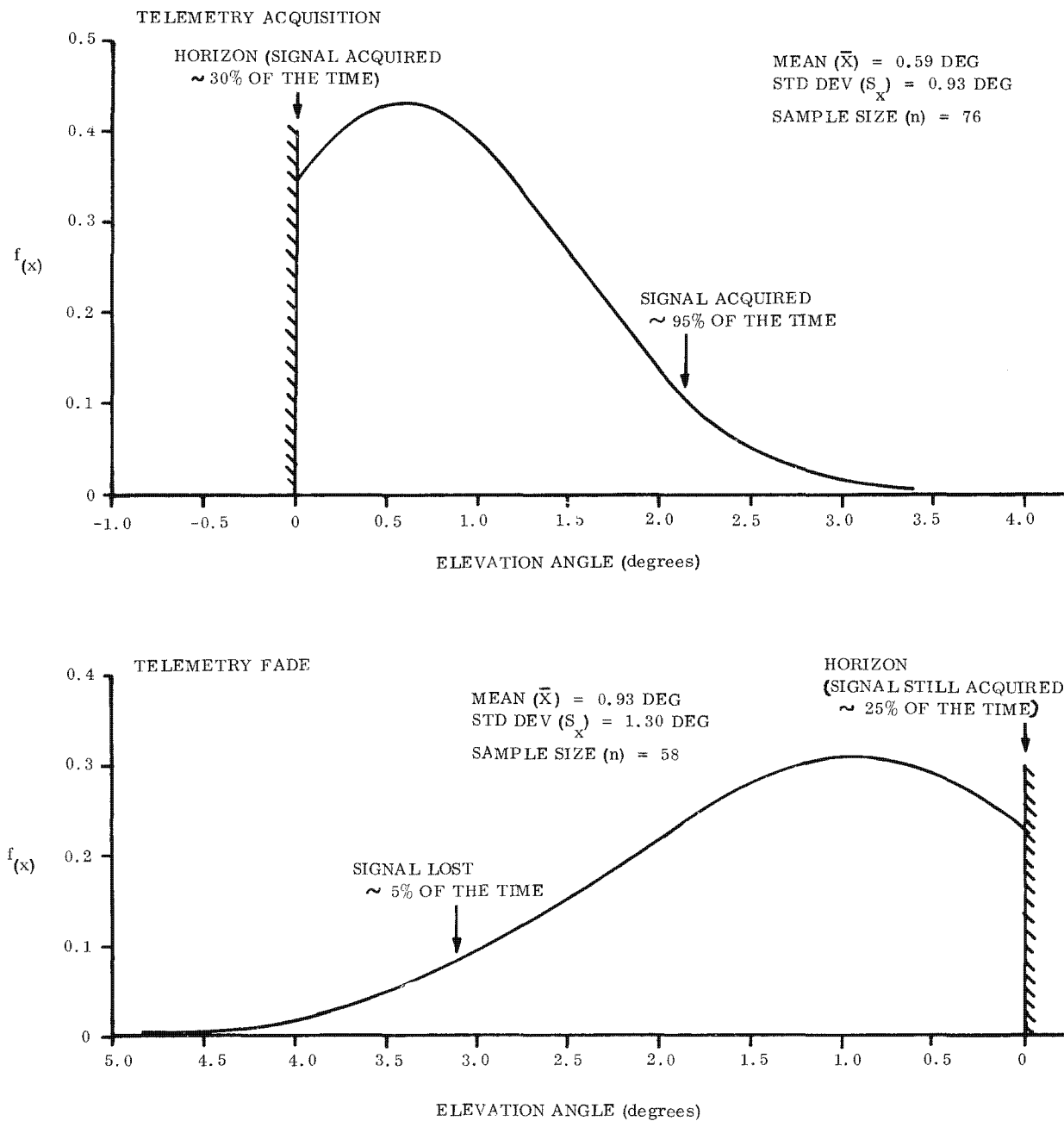
Figure 3-19. Telemetry Signal Acquisition and Fade Characteristics

64SD4760

3-52

It is quite apparent that masking has a significant effect upon station pass durations since the vehicle is at the lower elevation angles for the majority of the time for any pass. Figure 3-20 is a qualitative representation of this phenomenon. It can be seen that for masked station passes (either fade or acquisition), little benefit is derived with mid-pass elevation angles greater than 15 degrees.

The results of this analysis illustrates the usefulness of station contacts with extremely low mid-pass elevation angles.

3.3.4 DELAY LINE MANAGEMENT

The Command Subsystem has the capability of storing 396 words each time a command load is performed. This capability is rarely utilized, and to what extent it has been utilized is determined for SV 956 and SV 957. A tabulation of the capability used is presented in table 3-9, along with the percent of stored commands that were actually executed (before a new command load erased the existing command message).

Table 3-9. Delay Line Management

% Storage Capability Utilized/Flight		% Stored Words Executed/Flight	
Maximum	Minimum	Maximum	Minimum
80.7 (956)	61.0 (957)	59.2 (957)	55.0 (956)

3.3.5 VEHICLE CLOCK

In order to determine the accuracy of the vehicle clock, an extensive analysis was made on SV 960. Just prior to lift-off, the vehicle clock and system time were read from a telemetry record and tabulated. From these numbers, the delays produced by the data processing ground station in discriminating these signals was subtracted from each of the parameters. Next, the difference between the two times was calculated, and the remainder was used as the reference. At each subsequent Cook station contact, these same parameters
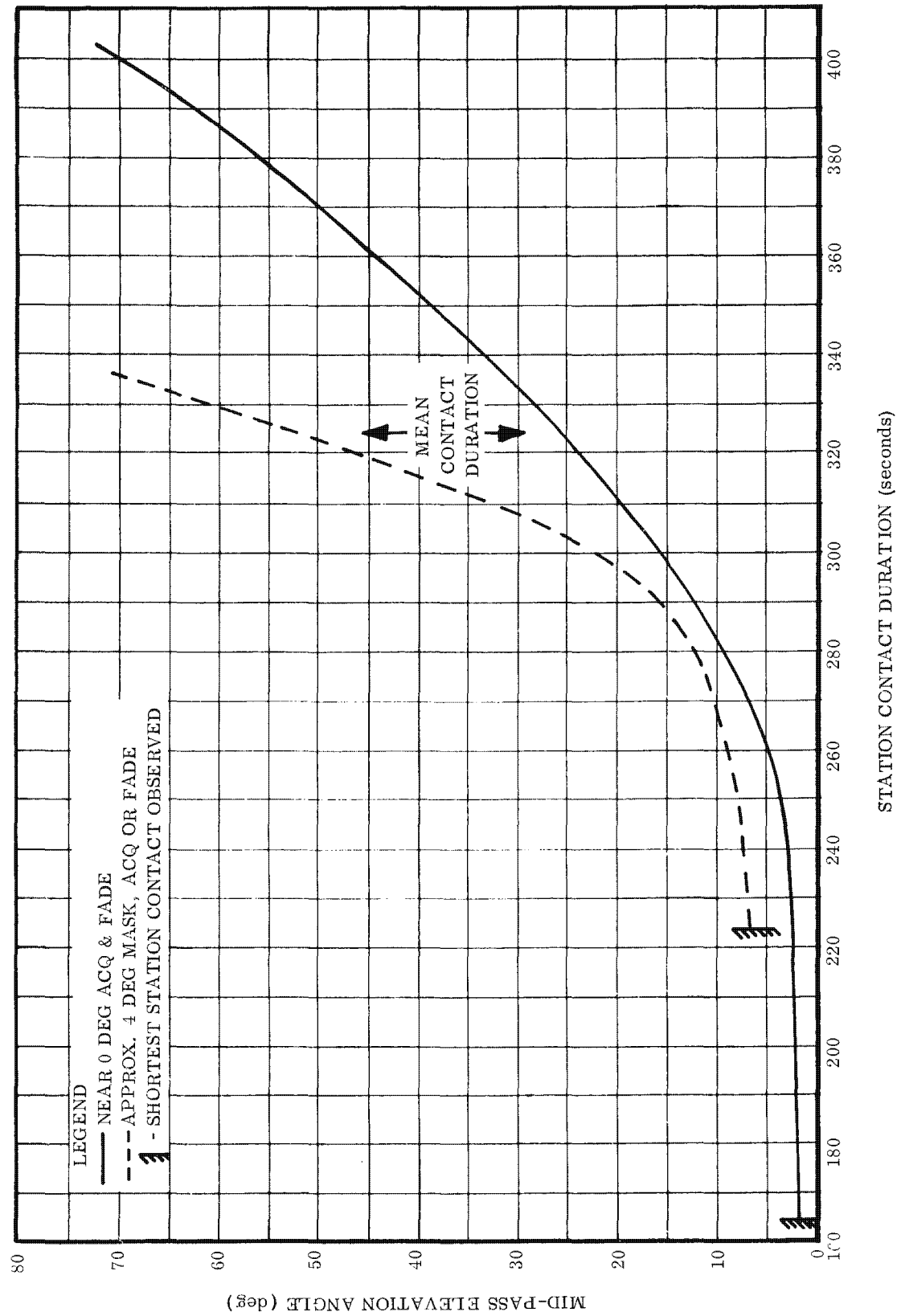
Figure 3-20. Station Contact Duration Versus Maximum Elevation Angle

64SD4760

3-54

were again read, and the same telemetry corrections made. In addition, orbital station pass delay of the vehicle clock telemetry as a result of vehicle slant range from the tracking station was taken into account.

Again, the difference between the system time and the vehicle clock was taken. The remainder should be equal to the reference established from prelaunch. If a difference exists, then either vehicle clock errors or tracking station system time errors are apparent. System time at Cook was used as the true reference in order to determine the accuracy of the reference. The Thule and Cook tracking stations are 3000 miles from WWV in Washington, D.C. (the calibrated source of system time); Hula, however, is within a few feet of WWVH-Hawaii. Therefore, by overlaying the vehicle clock - system time correlation performed using Hula stations with the correlation performed using Thule and Cook stations, any deviation between the system time at these stations would have been apparent. The best fit curve of points measured from all stations indicated a vehicle clock center frequency offset producing a linear delay of approximately 20 ms/day and a worst-case error of only one millisecond (See figure 3-21.). The one MS error could easily be attributed to a slight drift in the ground system clock over a 24-hour period. Hence, the use of system time as a calibrated reference is firmly established, and vehicle clock offset and/or drift can be determined to within one millisecond.

64SD4760
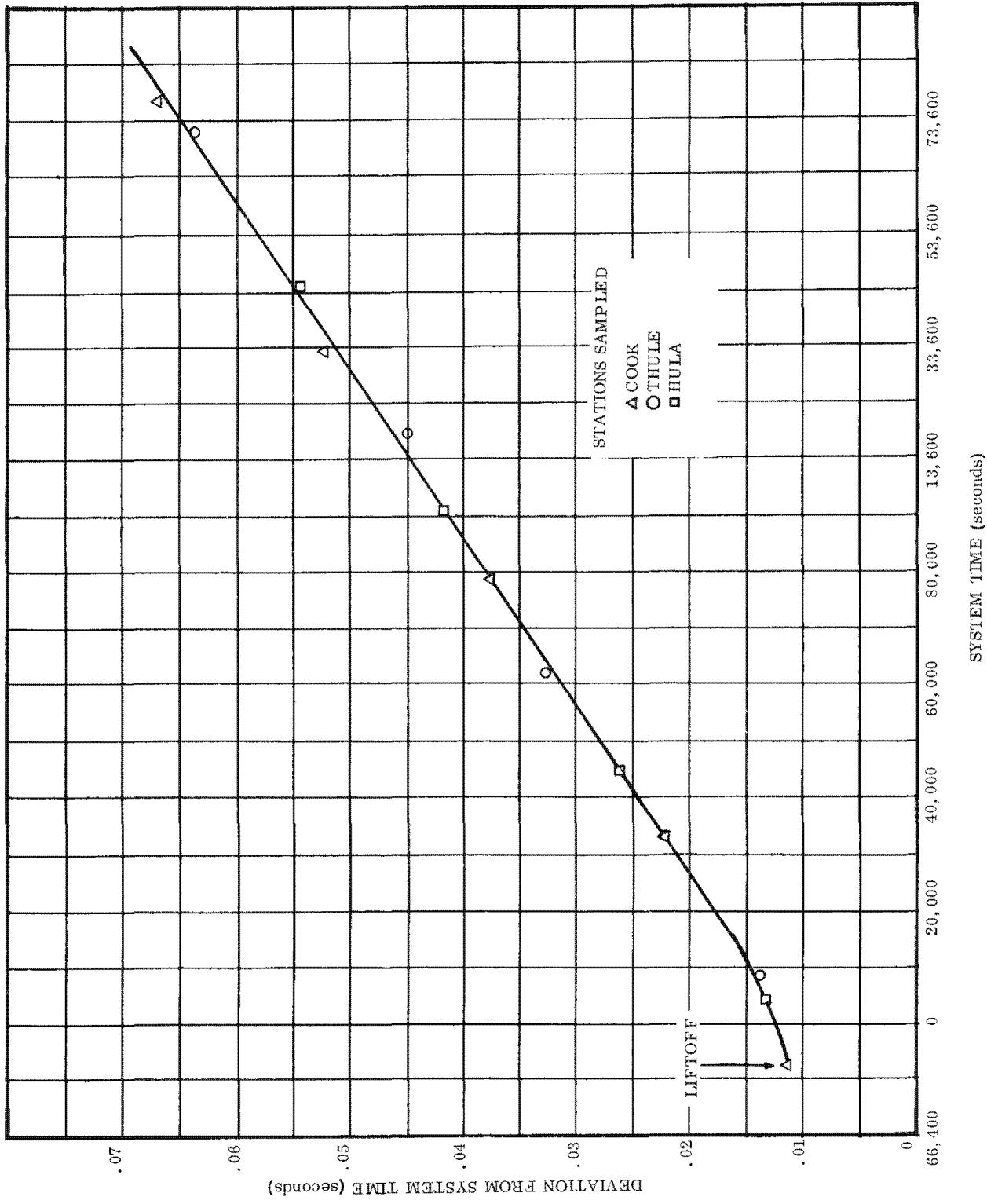
Figure 3-21. Vehicle Clock-System Time Correlation, SV 960

3.4 STABILIZATION SUBSYSTEM

Even though many of the functional characteristics of the Stabilization Subsystem are suitable for the type of capability analyses delineated throughout Section 3, they could not be so analyzed because of limitations imposed by the type and resolution of the telemetry provided. In addition, the lack of opportunity to perform appropriate experimental exercises also limited this type of analysis.

Those subsystem parameters, with which a reasonable capability analysis could be performed, are discussed below.

3.4.1 IR ACCURACY

Previous flight reports (ref 10, 11) have shown pitch and roll position reference error distributions. The errors presented in these distribution plots have been caused by IR disturbances, probably cold clouds, and were computed by subtracting attitude error from the integrated vehicle body rates using an analog computer. In figures 3-22 and 3-23 the composite error distributions, constructed using these data along with that obtained from SVs 958 and 960, are shown. These plots represent approximately 10 hours of cumulative flight data. The "per cent occurrence" represents the per cent of the sampled flight time that the various reference error magnitudes were observed. It is seen that the pitch position reference error was less than 1 degree 99.05% of the time, while the roll (and yaw) position reference error was less than 0.4 degree 98.87% of the time.

Comparison of the distributions for each flight, to that of the composite distribution for the four flights, showed nearly identical correlation attesting to the adequacy of the sample size and the random characteristics of the IR disturbances. Because of these random disturbance characteristics, these results are considered representative of system performance for any time of the year.

64SD4760

3-57

ERROR MAGNITUDE (deg)	PERCENT OCCURRENCE
< 0.2	74.23
< 0.4	91.50
< 0.6	96.80
< 0.8	98.82
< 1.0	99.05
< 2.0	99.6

NOTE:

MAX ERROR OBSERVED = 4.1 DEG

FLIGHT DATA

COMBINED FROM SV 956, 957, 958, 960

TOTAL NUMBER OF SAMPLES = 6222

CUMULATIVE TIME = 10.2 HOURS

PERCENT OCCURRENCE

PITCH POSITION REFERENCE ERROR (degrees)
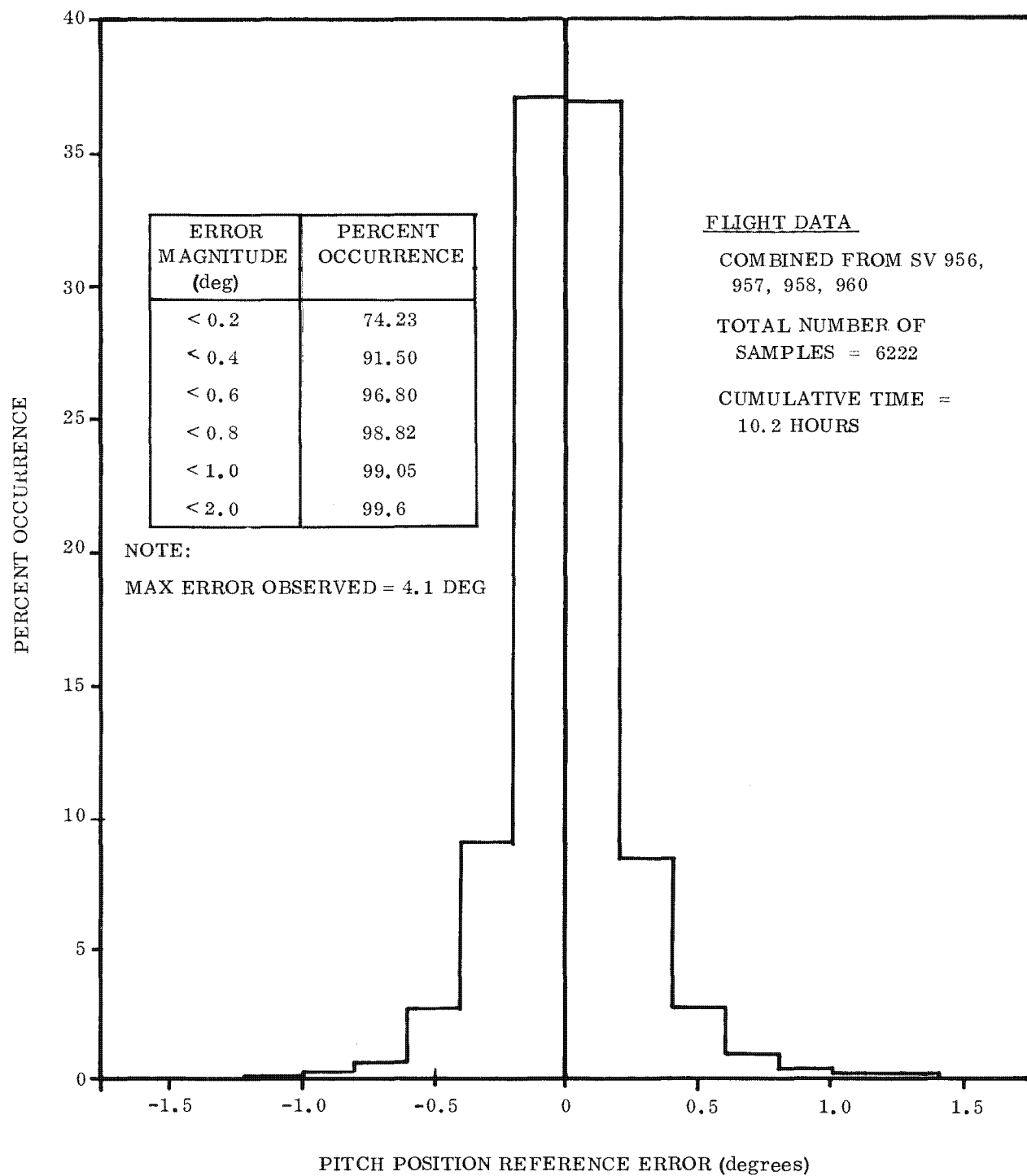
Figure 3-22. Distribution of Pitch Position Reference Errors Induced by IR Disturbances

64SD4760

3-58

ERROR MAGNITUDE (deg)	PERCENT OCCURRENCE
< 0.2	92.03
< 0.4	98.87
< 0.6	99.73
< 0.8	99.85
< 1.0	99.92
< 1.2	100.00

FLIGHT DATA

COMBINED FROM SV 957, 958, 960.

TOTAL NUMBER OF SAMPLES = 4045

CUMULATIVE TIME = 6.37 HOURS

PERCENT OCCURRENCE

ROLL AND YAW POSITION REFERENCE ERRORS (degrees)
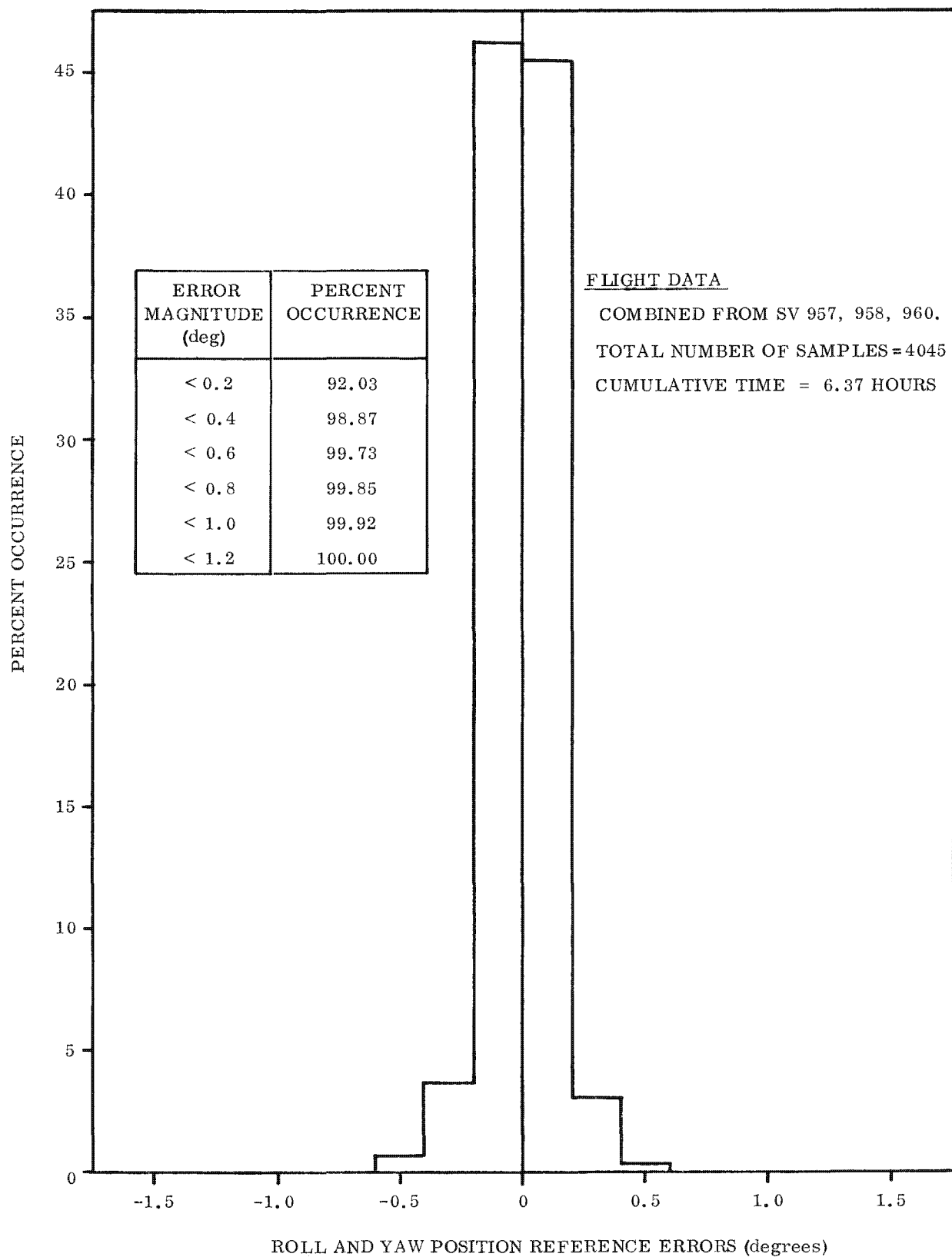
Figure 3-23.   Distribution of Roll and Yaw Position Reference Errors
Induced by IR Disturbances

64SD4760

3-59

3.4.2 ROLL MANEUVER PERFORMANCE

The information presented in this paragraph is applicable to vehicles similar to SV 958, i.e., having the same roll high thrust nozzle thrust levels and similar roll moments of inertia.

The roll maneuver accelerations/decelerations, rates and settling times, as determined from vehicles satisfying the above criteria, are summarized in table 3-10. The mean values shown are those which can most likely be expected from subsequent vehicles of the SV 958 configuration. The associated standard deviations reflect measurement accuracy as well as system repeatability.

As a note of explanation, settling time is defined as the interval between the time that the decelerating high thrust jet is turned off and the time when position and rate errors are reduced to within the rate roof boundaries ($\pm$0.3 degree attitude error, $\pm$0.015 deg/sec rate). Settling times are applicable only to high and medium rate roll maneuvers.

Figure 3-24 illustrates the time required to attain desired roll increments at the three roll maneuver rates possible. Here again, this information applies only to vehicles satisfying the criteria delineated above. The mean lines on the curve were determined from the times between command execution and the reduction of attitude errors to within rate roof boundaries, which are precisely measured. In addition, the $\pm 2\sigma$ limits were established, assuming that rate variability (table 3-10) is solely attributed to system repeatability, and are also shown in figure 3-24. Credibility of these limits has been provided by the fact that all of the measured data did not lie on the mean line, but did fall within these limits. This also lends credance to the assumption that rate variability is mainly a function of system repeatability.

The information presented in figure 3-24 and table 3-10 should be considered in the operational utilization of the vehicle.

64SD4760

3-60

Table 3-10. Roll Maneuver Performance Summary*

Rate Maneuvering	Acceleration (deg/sec^2)		Rate (deg/sec)		Settling Time (sec)	
	Mean	Std Dev	Mean	Std Dev	Mean	Std Dev
Low	0.09	0.04	0.26	0.01	--	--
Medium	Combined with high rates		1.76	0.07	0.76	0.15
High	3.10	0.34	3.37	0.09	0.75	0.15

*These performance data apply to vehicles having the SV 958 high thrust roll nozzle configuration, thrust levels, and similar roll moments of inertia.
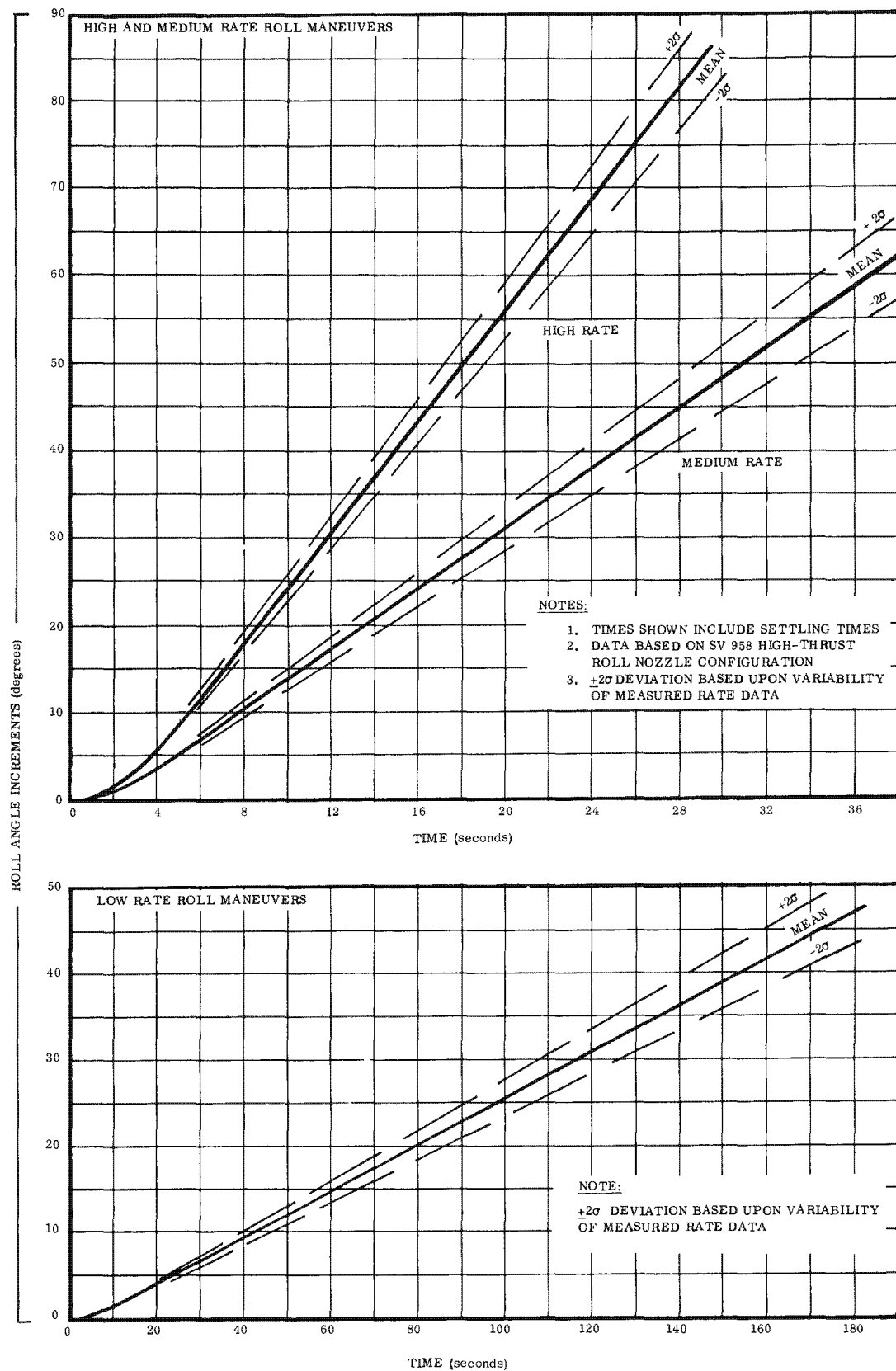
Figure 3-24. Program Mean Time for Completion of Roll Maneuvers

3.4.3 PNEUMATICS MANAGEMENT

The primary stabilization subsystem cold gas maneuver usage rates are summarized in table 3-11. Good agreement exists between the predicted and actual rates.

The minimum coarse limit cycling usage rate of 6.0 lb-sec/rev was obtained from SV 960 flight data and is considered to be an absolute minimum. It was determined from the period between rev 26 and rev 66 when the vehicle could not be exercised, allowing continuous limit cycling in the absence of aerodynamic disturbance torques at the relatively high orbital attitudes flown. Therefore, for a normal primary mission with perigee altitudes down to 75 n mi, coarse limit cycling usage rates nearer the maximum 11.7 lb-sec/rev seem more reasonable.

The 115 lb-sec/minute usage rate for an orbit adjust engine firing is considered possible after approximately seven minutes of cumulative engine firing when throat erosion, if any, is likely to occur. This usage rate has been atrributed to thrust vector misalignment resulting from the erosion.

The information presented in table 3-11 is representative of the Program 206 flight vehicles and should therefore be considered in the flight test planning for these systems.

64SD4760

3-63

64SD4760

Table 3-11. Control Gas Usage Rate Summary

Maneuver	Usage Rate Units	Predicted Usage Rate	Observed Usage Rate	
			Minimum	Maximum
High Roll	Lb-sec/maneuver	20	22.2	25.0
Medium Roll	Lb-sec/maneuver	10	11.3	11.3
Coarse Limit Cycling	Lb-sec/rev	15	$6.0^{(1)}$	11.7
Fine Limit Cycling	Lb-sec/rev	75	$75^{(2)}$	$75^{(2)}$
Average of over-all limit cycling for low altitude revs[3]	Lb-sec/rev	50	37.5	37.8
Orbit Adjust	Lb-sec/minute of firing	80 to 120	35	$115^{(4)}$

NOTES:

(1) Based on approximately 40 revs of quiescent flight data (SV 960)

(2) Estimated based on over-all usage rates/rev

(3) Perigee altitudes < 75 n mi

(4) Reflects orbit adjust engine throat erosion

3.5 BACK-UP STABILIZATION SUBSYSTEM

The performance of the Back-Up Stabilization Subsystem (BUSS) is best illustrated by the repeatability of the command event sequence and its conformance to the specification, and by the ability to provide the proper attitude reference for de-orbit of the SRV.

3.5.1 COMMAND EVENT TIME STUDY

An analysis has been performed on the timing of events in the BUSS "Real Time" command mode and is summarized in table 3-12. The last column of the table provides an estimate of the system event means based on flight data. If the ranges shown do not include their associated specified mean values, there is less than 5.0% chance that the flight hardware came from the population represented by the specification. If the differences significantly affect SRV de-orbit planning, then changes should be made in the prediction programs to account for these differences. However, accumulated flight data shows no major deviations.

Of particular interest, from an operational standpoint, is the elapsed time to be expected between the initiation of the KIK Zeke 31 command transmission and the beginning of the SRV de-orbit sequence. The point estimate of the mean (the most likely) duration between these events is 104.80 seconds.

3.5.2 STABILIZATION PERFORMANCE

When given the opportunity to perform, BUSS has demonstrated the ability to properly orient the SV for SRV de-orbit well within the specified time of 90 seconds. With the exception of SV 954, BUSS has provided a stable, controlled reference for de-orbit of the SRV. In the case of SV 954, it is felt that operation was nominal, but in overcoming the high vehicle total angular momentum, BUSS gas was depleted precluding attainment of the correct attitude. Refer to table 3-13 for a summary of BUSS stabilization performance.

64SD4760

Table 3-12. BUSS Event Time Study

| Description | | SV 960 Performance (seconds) | | Program Performance (seconds) | | | | |
BUSS Real-Time Event/Function	Reference Command Event	System Time of Occurrence	Actual ΔT Between Events	Specification Mean	Specification Std Dev	Summary Flight Data Mean	Summary Flight Data Std Dev	Best Estimate of System Mean 95% Confidence Level
Initiate Transmit (KIK-Zeke 31)	--	86303.68	--	--	--	--	--	--
Disconnect No. 1 and BUSS Gas On (T_o)	KIK-Zeke 31	86308.13	4.45	--	--	4.66	0.47	$4.17 < \mu > 5.15$
Disconnect No. 2 (T_1)	T_o	86333.59	25.46	25.00	0.17	25.29	0.12	$25.16 < \mu > 25.42$
Arm and Transfer (T_2)	T_1	00008.16	74.57	75.00	0.17	74.78	0.13	$74.64 < \mu > 74.92$
SRV Separate (T_2)	T_2	00010.98	2.82	2.50	0.17	2.60	0.16	$2.43 < \mu > 2.77$
Arm and Transfer (T_2)	Initiate Transmit (KIK-Zeke 31)	--	104.48	--	--	104.80	0.46	$104.31 < \mu > 105.29$

Table 3-13. BUSS Stabilization Performance Summary

SV	Vehicle Control Status @ BUSS Activation	Total Time to Stabilize (1) (seconds)	Available Impulse (pound-seconds)	Impulse Used to Stabilize (2) (pound-seconds)	Impulse Usage Rate After Initial Stabilization (2) (pound-seconds/second)	Remarks
954	Tumbling with large rates in all axes.	40	Unknown	Unknown	Unknown	Did not have BUSS telemetry. Total vehicle angular momentum exceeded BUSS capacity, depleting gas supply. Tumbling rates reduced; SRV successfully de-orbited.
955	90 deg yaw angle; yaw @ 0.4 deg/sec	N/A	N/A	N/A	N/A	BUSS did not actuate because of J-box relay failure.
956	90 deg yaw angle; yaw @ 0.4 deg/sec	N/A	610	N/A	N/A	No. 4 solenoid valve failed to operate, inducing vehicle tumbling and causing rapid depletion of gas.
957	45 deg yaw angle; yaw @ 0.4 deg/sec	22	688	90	0.30	BUSS satisfactorily stabilized the vehicle following OCV deboost engine cutoff.
958	Unknown attitude, tumbling with very low rates.	25	645	Unknown	Unknown	Noisy telemetry precluded precise determination of BUSS performance although it was known to have properly stabilized the vehicle.
959	Flying reverse, pitched down and stable with small errors from normal attitude.	18	600	75	0.24	Satisfactory SRV de-orbit achieved.
960	Flying forward and stable.	59	600	260	Negligible	Satisfactory SRV de-orbit achieved.

Notes:

1) Specified time to stabilize is 90 seconds
2) Sufficient impulse is required, following initial stabilization, to be stabilized 105 seconds after BUSS activation.

64SD4760

3-67

3.6 ELECTRICAL POWER AND SIGNAL DISTRIBUTION SUBSYSTEM

This section provides information which is helpful in predicting the capacity of a vehicle's power source before each flight and serves as the criteria upon which to judge subsystem performance and ultimate on-orbit capability.

3.6.1 DEMONSTRATED PERFORMANCE

3.6.1.1 Mission Life Expectancy

The demonstrated mission life quoted for any flight has been based upon the normal primary power usage rate for the flight, and upon the predicted ampere-hour capacity of the power source available for flight. The flights of SV 955 through SV 957 had the capacity to support an expected average mission life of 92 revs. SV 958 had an exceptional power source and it was expected that, had a normal mission been performed, 99 revs could have been flown. The average mission life demonstrated is estimated to be between 89 and 99 revs based on the following criteria (at the 95% confidence level):

a. Minimum of 1900 ampere hours available for flight.

b. Primary power demand ($\pm 2\sigma$) between 19.0 and 21.8 ampere hours/rev.

c. A sun inclination angle (β) between +25 and 0 degrees.

The results of the flights of SV 959 and SV 960 are not included in this average mission life expectancy. These two flights did not permit a sufficiently accurate determination of primary mission power usage rates which is required to fix the mission life.

64SD4760

3-68

3.6.1.2 Voltage Regulation

The minimum observed plateau voltage of 27.6 volts was obtained on the flight of SV 956 where the β-angle was approximately zero degrees. The maximum plateau voltage of 28.0 volts was obtained during the flights of SV 957 and SV 960. These flights had β-angles of +21.0 and -26.0 degrees respectively.

Since the higher β-angles cause higher battery temperatures (batteries 2 and 3 for positive β-angles, and batteries 1, 4 and 5 for negative angles), which in turn cause higher output voltages, the levels observed were as expected and compatible with temperature-voltage test results.

The voltage levels observed during the SV 958 and SV 959 flights were not considered valid, because of miscalibration of the telemetry voltage sensors, and they were not included in performance determinations.

3.6.2 PREDICTED PERFORMANCE

3.6.2.1 Limiting Voltage Definition

The minimum voltage upon which the ensuing program and flight power source capacity predictions are based is 27.54 volts at the battery terminals (1.53 volts/cell). Factoring in the IR drop and voltage regulation as a function of temperature, the voltage at the power distribution center is then 27.0 volts at a nominal 20-ampere total load. A one-volt drop from the distribution center therefore results in the minimum specified input voltage of 26 volts at the operationally limiting six-volt power supplies.

3.6.2.2 Program Estimate of 15-Day Wet Stand Capacity

Figure 3-25 represents the normal distribution curve of the 15-day wet stand capacity expected to be available from any future flight battery. The curve is based on the
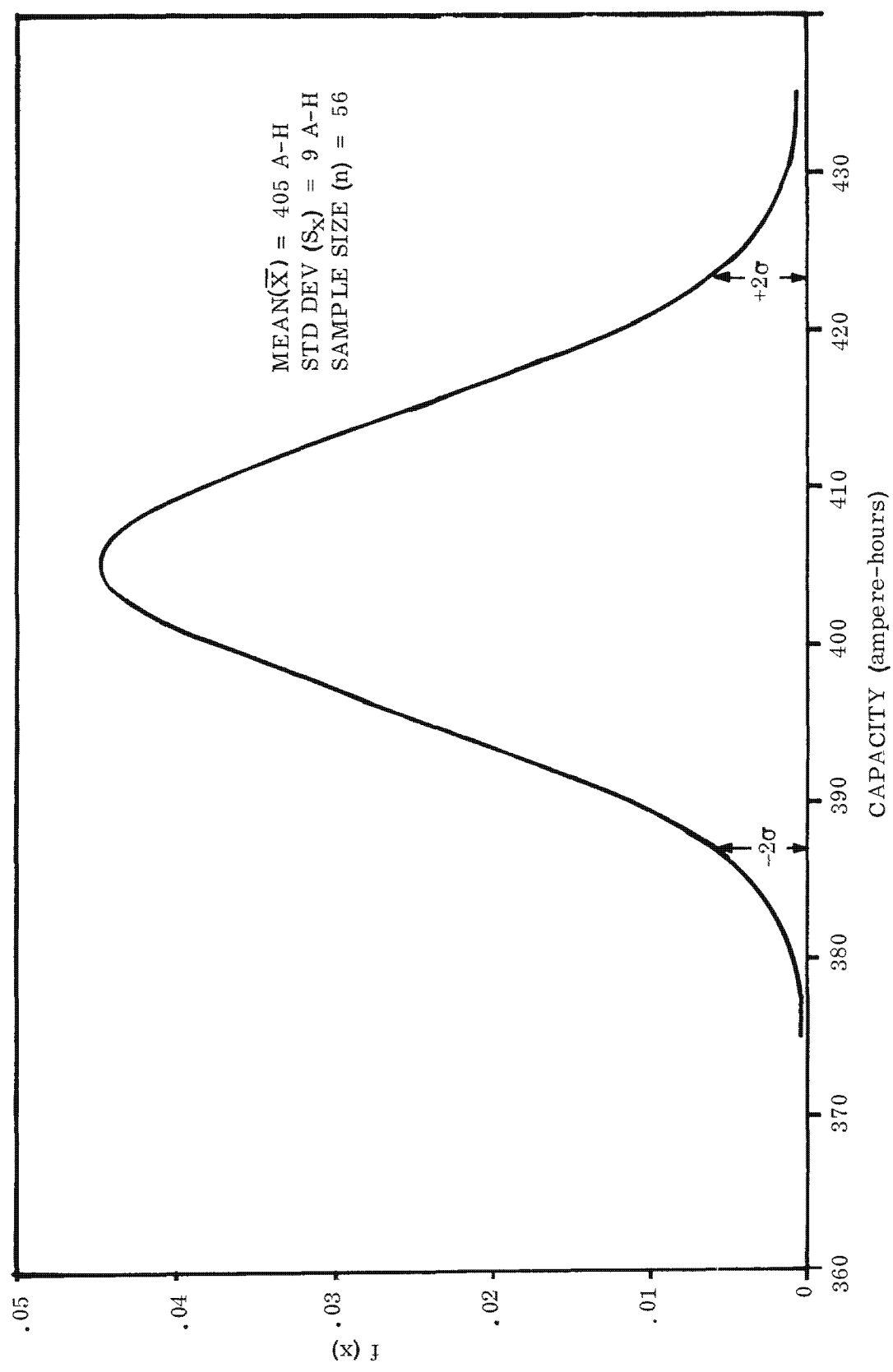
64SD4760

3-69

MEAN($\overline{X}$) = 405 A-H
STD DEV (S_X) = 9 A-H
SAMPLE SIZE (n) = 56

Figure 3-25. Operational Battery Predicted 15-Day Wet Stand Capacity

64SD4760

operational (OA) sample cells from battery No. 63 and subsequent. Most of the cells were tested after a 15-day wet stand while some were tested after a four-hour wet stand. In the cases where cells were tested after wet stands of other than 15 days, correction factors were applied to obtain the 15-day wet stand level. Dry stand losses, preflight pad usage, and additional derating/uprating for wet stands other than 15 days are not included. As such, the curve represents the capacity of a newly fabricated battery after a 15-day activated wet stand.

Not all batteries subsequent to No. 63 were used in this analysis. The SV 958 batteries exhibited exceptionally high ampere-hour capacities and uniformity, and a few others had unreasonably low capacity, thereby precluding meaningful statistical combination of the data.

As more OA sample cell data becomes available, the information presented in figure 3-25 will be updated and become more meaningful since subsequent testing will be accomplished after the 15-day wet stands.

The 405 ampere hours per battery represents 2025 ampere hours total, and is the nominal expected of a new battery which includes 15-day wet stand losses with a cutoff of 27.0 volts at the power distribution center. Using the -2σ ampere-hour/battery value of 387, and the $+2\sigma$ primary usage rate of 21.8 ampere hours/rev, which is calculated from flights one through eight, a full mission can be performed (83^+ revs) with essentially a zero margin assuming nominal prelaunch derating. The nominal capacity/demand, again with nominal prelaunch derating, results in a full mission with an eleven-rev margin or a total of 94^+ revs (see figure 3-26).

3.6.2.3 Individual Flight Capacity Predictions

The basic mechanism of predicting the performance of an individual flight is to statistically analyze the data from the OA sample cells (two cells/battery or total of ten); this results
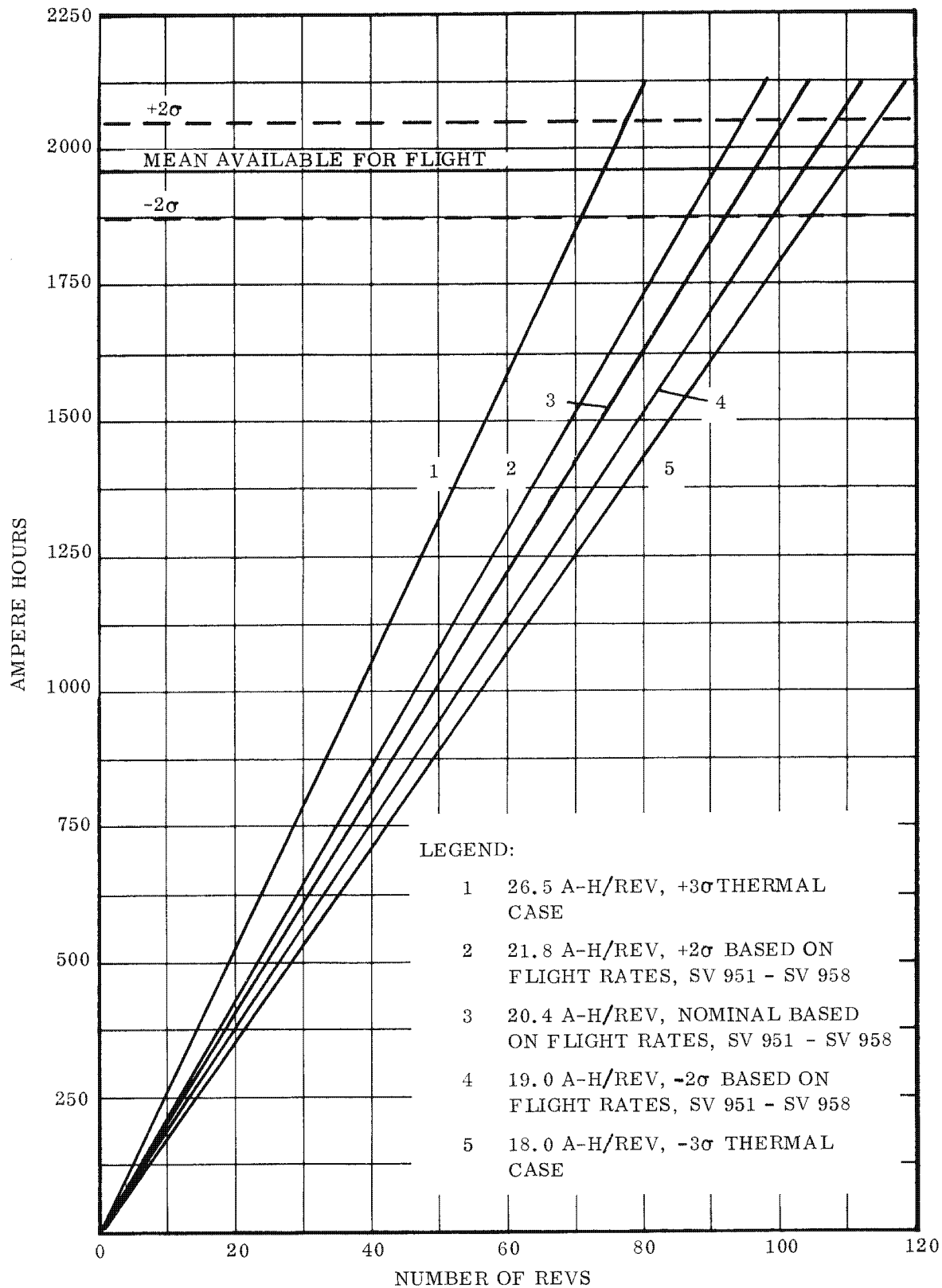
Figure 3-26, Expected Flight Capability, Program 206 Power Supply

64SD4760

3-72

in an "as manufactured" or new battery capacity after a 15-day wet stand. The new battery is then derated for inherent capacity losses due to dry stand and to pad usage, and then derated or uprated for actual or predicted activated wet stand. These derating factors are firmly established, but because of logistics and field operations margins, the actual derating on any given battery will vary from flight to flight. It should be noted that while the analysis is rigorously applied where possible, the basic nature of any electrochemical device is sufficiently variable that good engineering judgement is required as an adjunct to analysis.

Chemical interactions cause degradation in battery capacity. Dry stand losses have been determined as being 1/2% of rated capacity of an individual battery per month. On a 400-ampere hour basis, a one-month dry stand would result in a 400 x 1/2% or 2-ampere hour loss. The activated wet stand losses have been statistically determined using four-hour and 21-day wet stand data. A nominal loss of 31 ampere hours for 21 days was calculated, based on a cell cutoff voltage of 1.53 volts. From past experience, it is known that the initial five days of wet stand are most severe, and the rate of loss decreases for subsequent wet stand. A degradation rate of three ampere hours per day per battery for the first five days, and one ampere hour per day for the following 16 days has been determined. These rates are to be directly applied, i.e., for a ten-day activated wet stand, the derating in ampere hours would be 5 x 3 ampere hours/day plus 5 x 1 ampere hour /day for a 20-ampere hour loss in capacity.

Figure 3-27 typifies the operational battery capacity derating anticipated as a function of flight temperatures. This information was derived from limited thermal testing of OA sample cells. It therefore cannot be rigorously applied to EP&SD in-flight performance predictions. However, this information can be used to indicate potential subsystem problems in support of a five-day mission.
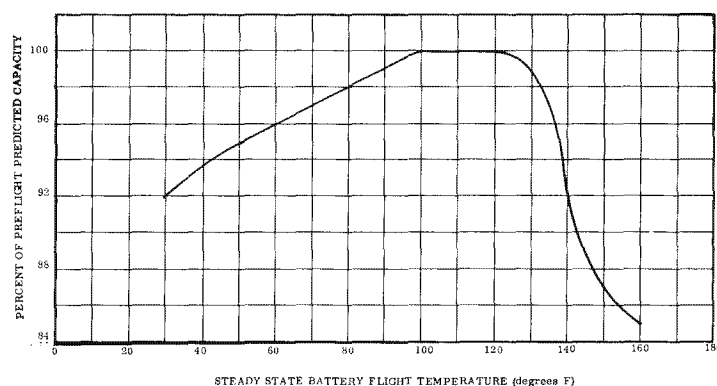
Figure 3-27. Temperature Derating Effects on Operational Battery Capacity
64SD4760

3-73

3.6.2.4 Program Prediction

The program flight prediction is based on OA-sample cell data of batteries No. 63 and subsequent for a total of 56 cells.

The step-by-step method used to predict the expected electrical power capability for a given flight is as follows:

a. Determine program system capacity based on 15-day wet stand (OA) sample cell data.

The mean capacity of the OA-sample cells was obtained by adding the capacity of the individual cells at a cutoff voltage of 1.53 volts under a 4-ampere load, and then dividing the total by the number of cells used (56).

Mean $(\bar{X})$ = 405 A-H

Standard Deviation (S_x) = 9.00 A-H

Sample Size (n) = 56

$+2\sigma$ = 423 A-H

-2σ = 387 A-H

Therefore, mean system capacity = 5 x 405 = 2025 A-H

$+2\sigma$ system capacity = 5 x 423 = 2115 A-H

-2σ system capacity = 5 x 387 = 1935 A-H

b. Determine losses due to dry stand. Dry stand losses are based on an assumed 3-month dry stand prior to battery activation.

Battery "A" -1/2%/month x 400 A-H x 3 months = -6 A-H

Battery "B" -1/2%/month x 400 A-H x 3 months = -6 A-H

Battery "C" -1/2%/month x 400 A-H x 3 months = -6 A-H

64SD4760

Battery "D" -1/2%/month x 400 A-H x 3 months = -6 A-H

Battery "E" -1/2%/month x 400 A-H x 3 months = -6 A-H

Total   -30 A-H

c. Estimate pad usage = -85 A-H (expected)

d. Determine expected wet stand (uprating or derating).

Assume five days from activation to flight = 15 - 5 = +10 days at 1 A-H/day/bat.

Uprating 10 x 1 x 5 = +50 A-H

Note: If wet stand exceeds 15 days, the derating factor would be computed in a similar manner.

e. Estimate nominal capacity available for flight.

Step a   +2025 A-H

Step b   -30 A-H

Step c   -85 A-H

Step d   +50 A-H

          1960 A-H

Note: This step is repeated for $\pm 2\sigma$ capacity

f. Determine flight duration based on $\pm 2\sigma$ demonstrated primary ampere-hour usage rates (neglecting temperature effects).

Nominal $= \dfrac{1960}{20.4 \text{ A-H/rev}}$ = 96.0 revs

Best Case $= \dfrac{2050}{19.0 \text{ A-H/rev}}$ = 107.7 revs

Worst Case $= \dfrac{1870}{21.8 \text{ A-H/rev}}$ = 85.8 revs

Figure 3-26 illustrates the range of performance expected during the program using the derated capacities calculated in steps a through e.

3.6.2.5 Expected Voltage Regulation with Beta Angle Effects

Figure 3-28 represents a preliminary effort to delineate the voltage regulation for the three expected battery temperature conditions resulting from different β angles. The five-battery equal-temperature condition, resulting from a zero or near zero β angle, exhibits approximately equal discharge of each battery. Therefore, the voltage regulation characteristics are the same as for a single battery. As determined from SV 956 flight data, the expected temperature is in a 45 to 55°F range.

The two-battery hot (90°F) and three-battery cold (30°F) condition was observed on the flights of SV 955 and SV 957 with β angles of approximately 20.0 degrees and 21.0 degrees respectively. The three-battery hot (110°F) and two-battery cold (30°F) case was observed on the flight of SV 960 with a β angle of -26 degrees. However, the flight duration was not sufficient to observe the hot batteries' break point. The voltage regulation effects are the same in both cases with the exception that the hot plateau voltage in the three-battery hot case has a longer duration, as expected. In either case, the initial plateau voltage is high because of the hot batteries having a higher output voltage. As the hot batteries begin to come off of the plateau, the operational bus voltage starts to drop with the hot batteries unloading and the cold batteries picking up the load. Because the cold batteries are assuming control of the bus voltage, the temperature voltage effect combined with the increased loading per battery result in the "bottoming" of the voltage.

It should be noted that the cold batteries are still on their plateau voltage while the hot batteries are practically expended at their break point. After "bottoming", the voltage will increase to a new plateau because the increased load on the cold batteries causes a greater internal loss with a subsequent increase in temperature to 85°F or greater. The cold batteries eventually break, or come off their plateau, as a three-(or two, as the case may be) battery voltage system.
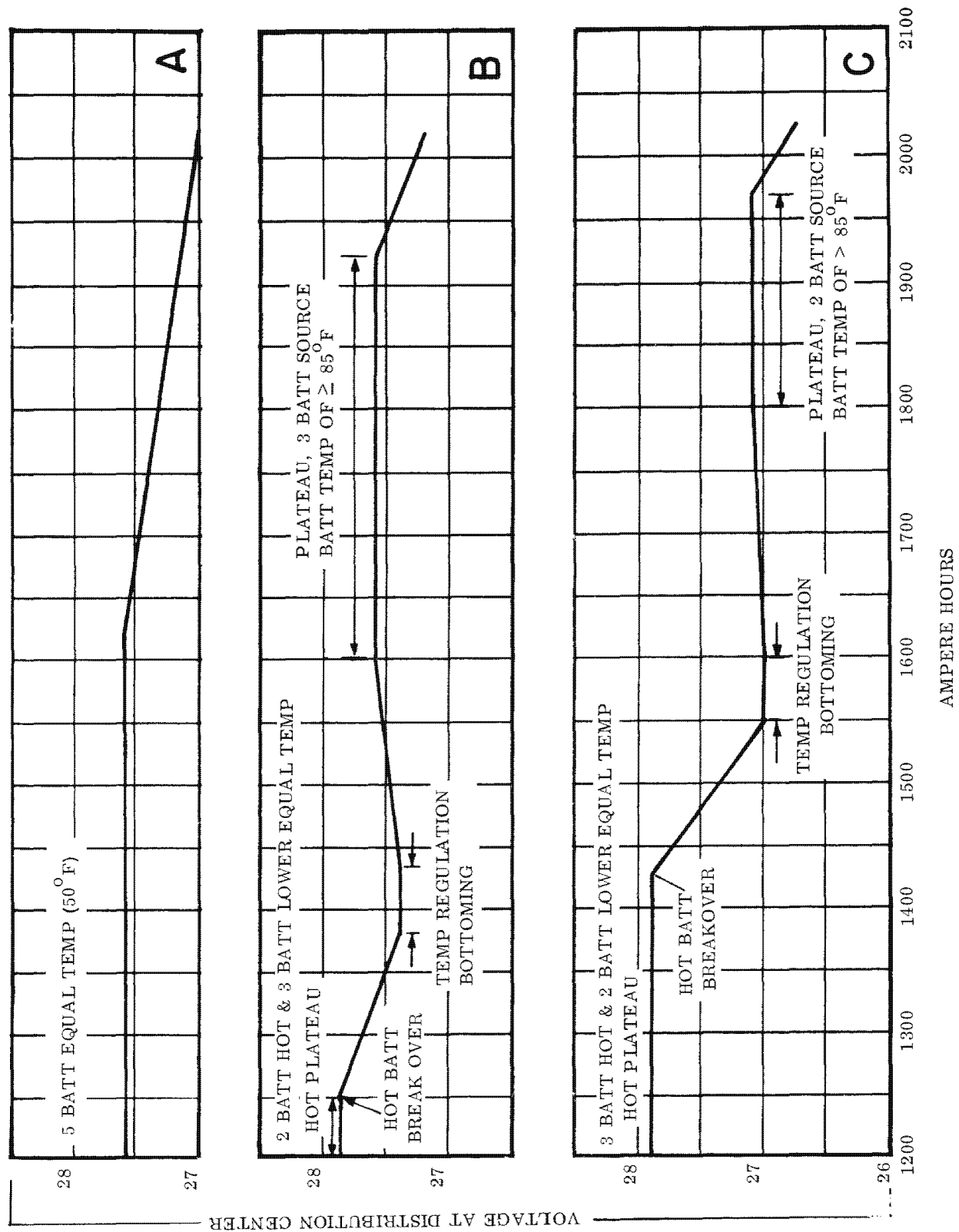
64SD4760

3-76

Figure 3-28. Expected Voltage Regulation Showing Temperature Effects

64SD4760

The voltage between the plateau and bottoming levels has been shown as a straight line at this time even though this is not the case. An "S" curve is the expected characteristic. Further effort is required to delineate this characteristic more precisely. The battery thermal time constant and the variation of radiated heat dissipation, due to the battery door emissivity, significantly affect the voltage bottoming characteristic. Nominal transfer conditions were assumed for the curve build up after bottoming in conjunction with a total steady-state load of 20 amperes.

Further effort is required to determine: (1) the battery thermal losses over its load spectrum; and (2) the effect of emissivity tolerance of the battery doors. These factors determine the temperature of the battery or batteries and as such, the voltage regulation and load division . Temperature-voltage regulation characteristics have been determined on a cell basis and correspond adequately with the previously predicted temperature-voltage regulation characteristics used to construct figure 3-29.

3.6.2.6 Temperature Effect on Voltage Regulation

Figure 3-29   illustrates the results of a temperature-voltage load test conducted on three operational cells using a fluid bath for temperature control. As shown in figure 3-29 ,   the voltage under load is dependent on the temperature, and increases with rising temperatures until the range of 130°F - 150°F is reached. At this point the voltage appears to level off and remain relatively constant under a given load. The voltage at any given termperature is a function of the load and decreases with increasing load. The voltage variation with load is dependent on the temperature, and the variation increases with decreasing temperature.

The voltage variation with load and temperature is also dependent on the state of discharge (capacity) of the cells, largest at the beginning and end of the discharge. The large variation at the beginning of discharge is expected since this is the region (20-60 ampere hours) of peroxide to oxide transition where the positive plate has the lowest conductivity. A voltage drop-off which occurred at the higher temperatures in the 320-370 ampere hour

64SD4760
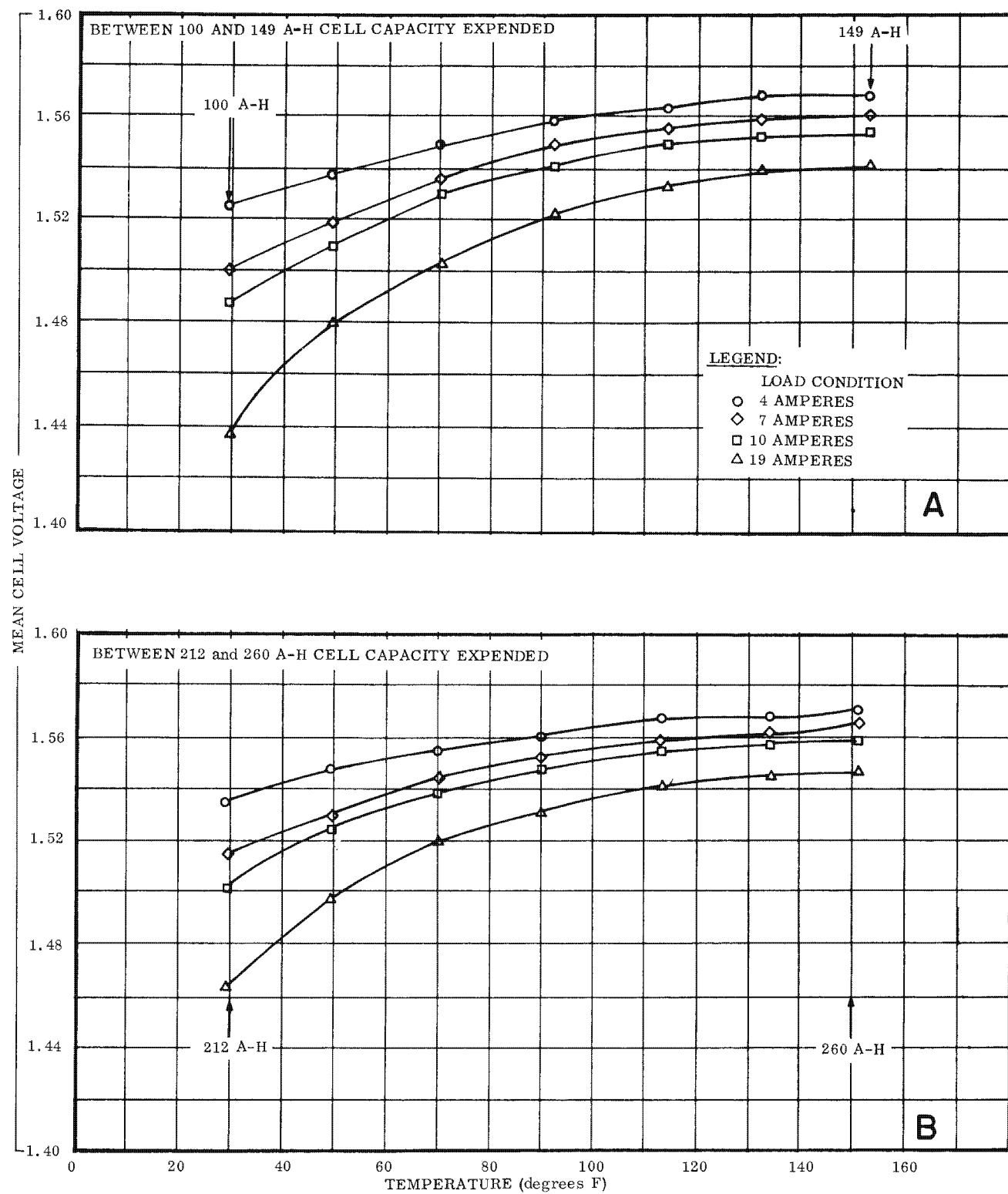
Figure 3-29.   Effects of Temperature on Cell Voltage

range was also expected since the discharge passes the knee of the voltage curve in this region, and the cell is not capable of supporting a high rate of discharge.

This test supports the flight test results which have shown that the battery load distribution is dependent on the battery temperature. It also supports the higher operational bus voltages obtained at the higher β angles as discussed in Section 3.6.1.2.

3.6.3 OPERATIONAL CONSIDERATIONS

BUSS is recommended for SRV recovery with a one or two battery system because of the lower voltage restraints of BUSS. The removal of all unnecessary electrical load is strongly recommended. Table 3-14 presents the regulation expected under pulse loadings, in preparation of SRV de-orbit, with the one and two battery system.

Table 3-14. One and Two Battery System Voltage Regulation
At Separation Using BUSS

Load (amps)	Regulation (volts @ Dist Center)		
	One Battery		Two Batteries
	> 20% Capacity Remaining*	< 20% Capacity Remaining	< 20% Capacity Remaining
20	.27.3	25.9	26.7
50	26.0	23.0	24.0

*Battery temperature at approximately $85^{\circ}F$

Either the primary stabilization subsystem or BUSS can be used for SRV de-orbit, using a three (or more) battery system because of the reduced pulse loading.

3.6.4 SUBSYSTEM POWER DEMANDS

A breakdown of the major subsystem power demands based on flight data, test data, and where necessary, engineering judgement, has been accomplished. A brief description of the methods used to obtain these power demands is included.

3.6.4.1 Telemetry, Tracking, and Command (TT&C) Subsystem

The power demand for the TT&C Subsystem was obtained by determining the total times for each mode of operation: telemetry on-off, record, and playback. The total current requirements with all components operating during each mode was multiplied by the time; the total demand was obtained by a summation of all the modes of operation.

3.6.4.2 Stabilization Subsystem

The power demand for the Stabilization Subsystem was obtained from test data and supported by limited flight data. The current measured during testing included current required to operate heaters, and regulated and unregulated power supply outputs to all stabilization components. The RAGS and TARS gyros were temperature stabilized, and several roll angles were commanded.

3.6.4.3 EP&SD, Separation, Orbit Adjust, SRV, and BUSS Subsystems

Since these subsystems demand very little power, no attempt was made to isolate each subsystem. The value was derived by engineering judgement based on knowledge of the subsystems and their associated components.

3.6.4.4 Environmental Control Subsystem

The mean power demand for environmental control, for a one-rev period, has not been determined at this time. This determination is, by the nature of the subsystem, very

64SD4760

difficult to obtain since any heater or groups of heaters may be on or off at any time during a rev. Therefore, the probable demand was obtained by totaling the "known" values and subtracting the result from the flight mean vehicle demand.

3.6.4.5 Power Demands

The mean vehicle power for demand (SV 951-SV 958) was 20.4 A-H/rev. The power demands for each subsystem is given in table 3-15.

Table 3-15. Subsystem Power Demands

Subsystem	Demand/Rev
TT&C	3.4 A-H
Stabilization	10.8 A-H
Environmental Control	5.5 A-H
All Others	0.7 A-H
Total	20.4 A-H

The accuracy of this prediction is considered to be approximately $\pm$ 5%. The primary variation in power demand expected between flights can most likely be attributed to the Environmental Control Subsystem. The contribution of the TT&C Subsystem is about $\pm$ 0.2 ampere hour.

3.6.5 CURRENT SIGNATURES

Figure 3-30 shows representative current signatures for various events which occur during a Program 206 flight. It is not anticipated that the signature for any event will be identical from flight to flight, but it is expected that the signature pattern will be identifiable. The signature plus the known time of scheduled event occurrence, therefore provides a positive identification of the event.

64SD4760

3-82
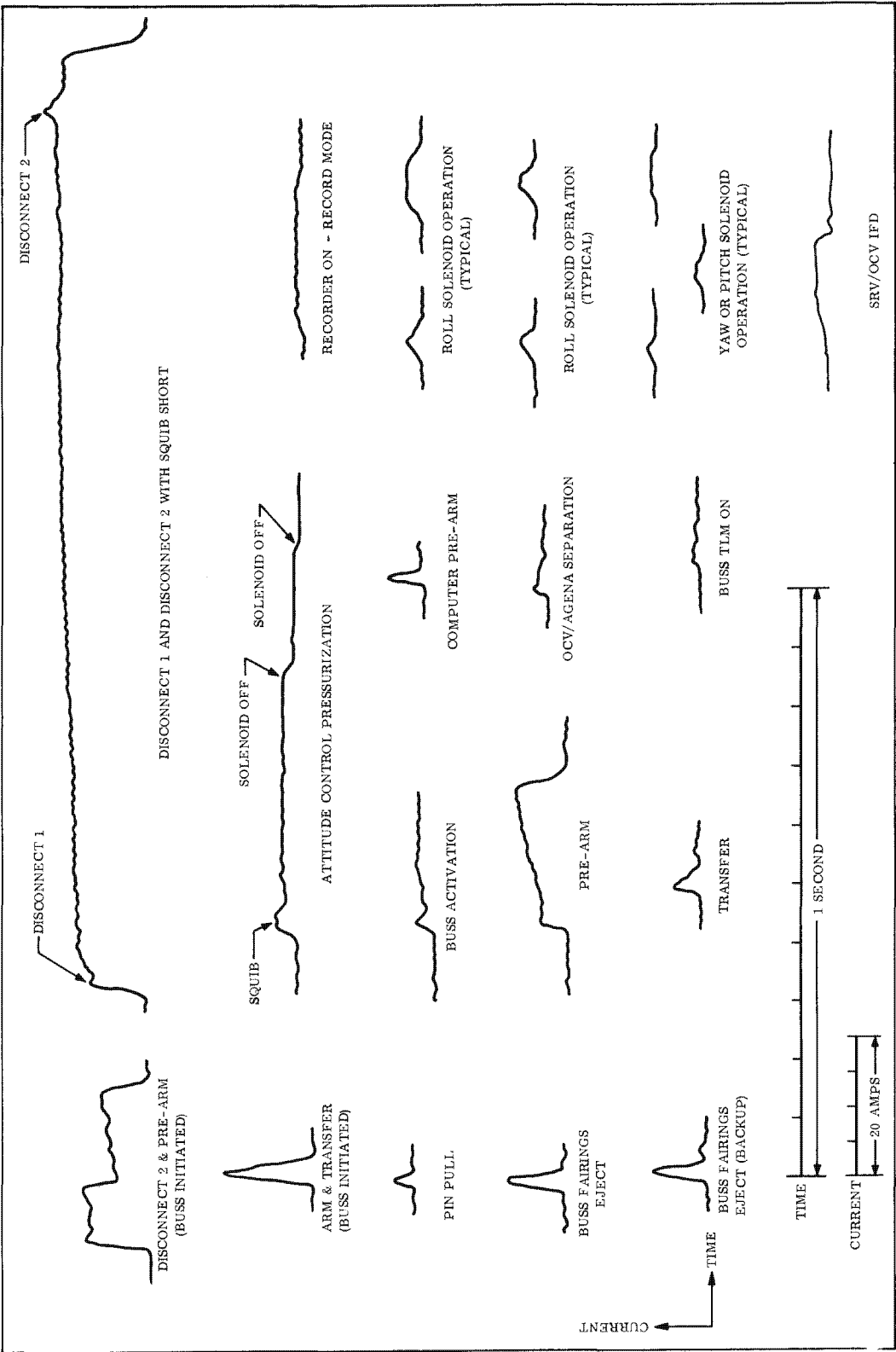
Figure 3-30. Representative Event Signatures from Continuous Current Monitor

64SD4760

3-83

3.7 SRV SUBSYSTEM

The capability of the SRV Subsystem is best described in terms of the parameters leading to its successful recovery. The major contributors to this objective are evaluated below.

3.7.1 IMPACT DISPERSION STUDY

The SRV impact dispersion history has been used to develop an estimate of the $+2\sigma$ ellipse of expected dispersion for the Program. This ellipse encloses the area about the planned impact point within which 97 out of 100 recoveries are expected to occur. In calculating the ellipse, it has been assumed that the distribution of the recovery points about the mean is normal, both in-track and cross-track.

Figure 3-31 shows the various impact points and two ellipses. The larger ellipse is based on the actual dispersion of the recovery point from the predicted point. (Vehicles 954 and 958 are omitted from this analysis because of lack of control and unknown attitude at the time of separation.) This ellipse, by definition, includes errors introduced from any source: vehicle attitude, thrust misalignments, tracking data, software inaccuracies, atmospheric conditions, etc. It should be noted that the SV 951 and SV 952 recovery points used in constructing the large ellipse have been corrected to reflect changes made in the basic GTERMIN program constants as a result of the in-track dispersions experienced on those flights. The large ellipse is, therefore, the range of expected actual dispersion for succeeding flights as determined from previous flight data.

The smaller ellipse reflects dispersion caused only by the SRV hardware and prediction software (i.e., compensation has been made for as many of the contributing variables as were known). The ellipse therefore represents the demonstrated accuracy and repeatability of the SRV hardware/software combination. Since both SV 959 and SV 960 were controlled by BUSS during separation, precise pitch and yaw angles are indeterminate and therefore cannot be compensated for sufficiently to include corrected impact points in the small ellipse.

64SD4760

3-84
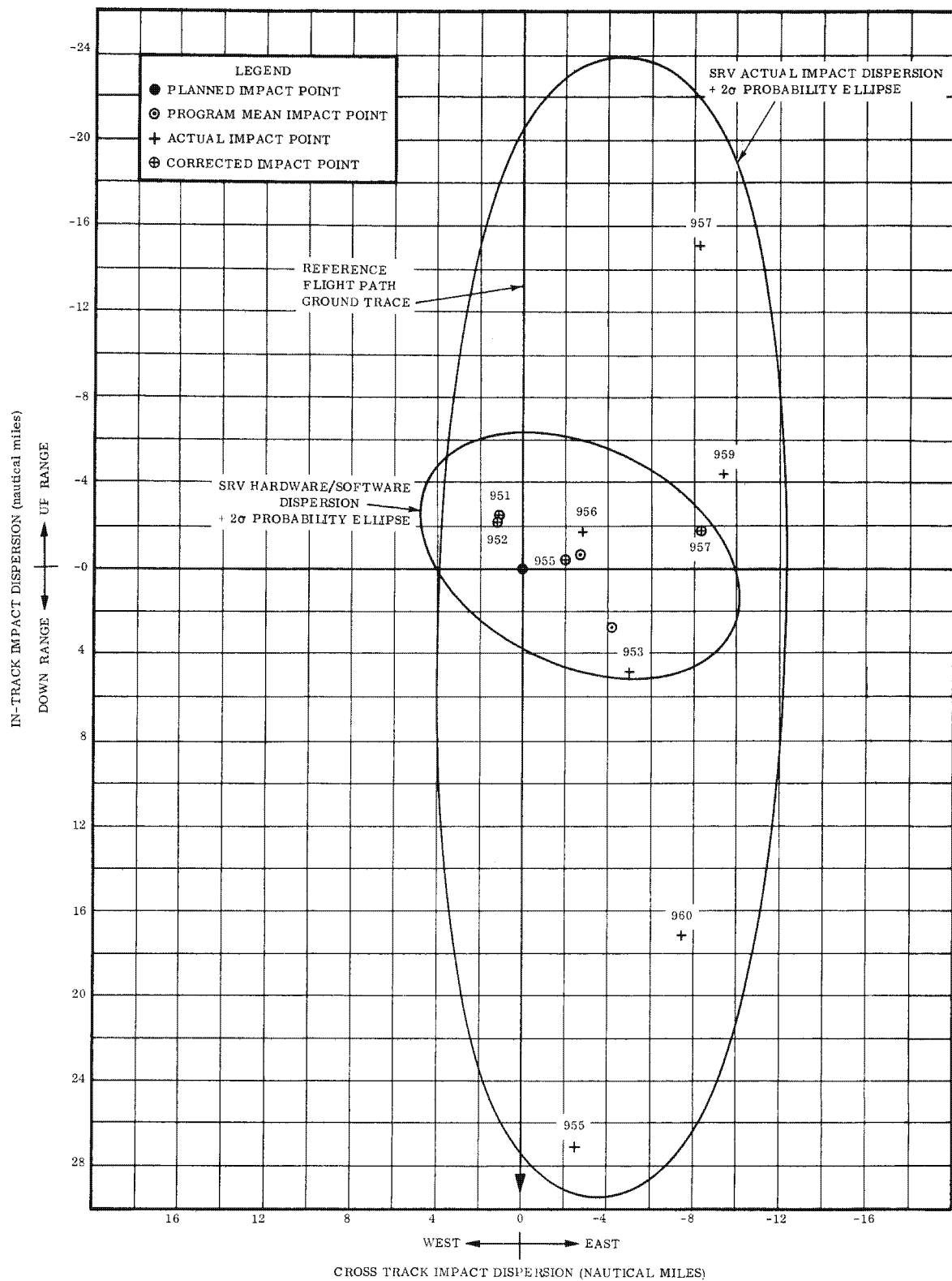
Figure 3-31. SRV Impact Dispersion

Certain conclusions may be drawn from the orientation, size, and overlap of the two ellipses. The center (mean) of both ellipses lies very close to the predicted impact point, both in-track and cross-track, indicating that no major biases exist in the system hardware/ software combination. The fact that both means are east of the prediction is probably a reflection of prevailing westerly winds from de-orbit to recovery. Cross-range dispersion is much less susceptible to external effects, as evidenced by the similarly narrow (15 n mi) widths of the two ellipses, and the fact that the major axis of the large ellipse is nearly parallel to the reference ground trace. Finally, and perhaps most important, since the first ellipse was drawn, succeeding vehicles have fallen within the boundaries of the preceding ellipse. This is evidence of the credibility of the large ellipse, and indicates that it could be considered in recovery force deployment for a normal SRV de-orbit (including de-orbit via BUSS).

3.7.2 SEQUENCE OF EVENTS

An analysis has been performed on the timing of events controlled by electronic or pyrotechnic time delays which could affect impact dispersion. The results of this analysis are summarized in table 3-16. The last column contains an estimate of the program mean based on flight data. If this range does not include the specified mean value, there is less than a 5.0% chance that the flight hardware came from the population represented by the specification. If the corresponding contribution to dispersion is significant, then changes should be made in the prediction programs to account for that error. However, accumulated flight data shows no major deviations.

3.7.3 PROBABILITY OF SUCCESSFUL RECOVERY

The record of recoveries of the SRV capsule provides a basis for calculating the probability of successful recovery for each succeeding vehicle. Based on a binomial distribution, and 10 successes in 10 opportunities, the probability of successfully recovering the 962 SRV capsule is included in the range of 69% to 100% at the 95% confidence level.

Table 3-16. SRV Event Time Study

Description		Specification (sec)		Program Performance, Event Timing				
				No. of Flights Observed	Fit Data Summary (sec)		Best-Estimate Program Mean, 95% Confidence Level	
Event or Function	Reference Command or Event	Mean	Std Dev		Mean	Std Dev	Lower Limit	Upper Limit
OCV/SRV inflight disconnect	Transfer command	0.9	0.13	10	0.99	0.04	0.96	1.02
Spin up	Inflight disconnect	3.4	0.10	10	3.43	0.30	3.22	3.64
Retro ignition	Spin-up signal	1.25	0.03	10	1.22	0.04	1.19	1.25
Despin	Retro signal	10.75	0.18	9	10.58	0.14	10.47	10.69
Thrust cone separation	Despin signal	1.5	0.15	9	1.53	0.13	1.43	1.63
Retro	Transfer	5.55	0.17	10	5.64	0.11	5.56	5.72
Recovery inhibit timer closed	Arm command	860.0	6.6	5	860.77	5.84	853.53	868.01
Recovery inhibit timer open	Inhibit close	50.0	3.3	4	54.3	2.13	50.9	57.7
Ejection of parachute thermal cover	Opening of ~3g switch	34.0	0.5	8	33.47	0.26	33.25	33.69
Deployment of pilot parachute	Ejection of thermal cover	N/A		8	0.77	0.09	0.70	0.84
Main parachute deployed in reefed configuration	Deployment of pilot parachute	N/A		7	10.75	0.17	10.59	10.91
Main parachute fully disreefed	Deployment of main parachute	N/A		7	4.36	0.30	4.08	4.64

3.7.4 SPIN AND DESPIN PERFORMANCE

The spin and despin tanks of the SRV are filled with a mixture of 10% Freon and 90% nitrogen. It was originally thought that this mixture would exhibit an I_{sp} of 52.7 pound-seconds per pound. Based on this estimate, the predictions for spin and despin rates have been made for the Program. Actual spin and despin rates have been about 10% higher indicating that the effective I_{sp} of this gas mixture is approximately 57.6 pound-seconds per pound.

3.7.5 RE-ENTRY AND COVER EJECTION CONDITIONS

Table 3-17 lists the re-entry conditions (velocity and flight path angle at 325,000 and 400,000 feet) and the cover ejection conditions (Mach number and dynamic pressure) for each vehicle. These numbers were taken from the computed trajectories determined to be the "best-fit" for each vehicle, and are presented to show the range of these parameters experienced on Program 206.

Table 3-17. Re-entry and Cover Ejection Conditions

SV	Re-entry Conditions, 400,000 ft		Re-entry Conditions, 325,000 ft		Cover Ejection Conditions	
	Velocity (ft/sec)	Flight Path Angle (degrees D.F.H.)	Velocity (ft/sec)	Flight Path Angle (degrees D.F.H.)	Mach Number (M)	Dynamic Pressure (lb/ft^2)
951	25505	-2.77	25590	-2.87	0.93	100
952	25574	-2.35	25660	-2.44	0.93	106
953	25654	-1.84	25735	-1.98	0.94	104
954	25091	-0.96	25170	-1.57	0.92	114
955	25521	-2.28	25619	-2.41	0.93	112
956	25544	-2.22	25642	-2.35	0.93	119
957	25842	-1.90	25938	-2.01	0.93	122
958	25489	-0.95	25563	-1.31	0.92	126
959	25705	-2.24	25791	-2.28	0.93	124
960	25701	-2.21	25797	-2.27	0.93	108

3.8 ENVIRONMENTAL CONTROL SUBSYSTEM

3.8.1 LOW ALTITUDE CAPABILITY

A primary consideration in determining the minimum altitude capability of the SV is the maximum amount of thermal energy which can be absorbed from aerodynamic heating of the external surfaces. Excessive heating of the external surfaces causes the structure and internal component temperatures to rise significantly, thus greatly increasing the chances for failure. The altitudes at which the heating becomes excessive are predictable, within tolerances, and should be used to avoid either failures or ultra-conservatism in design which inhibits system capability.

The results of the fly-low capability analysis are summarized in figure 3-32 which shows the conditions beyond which there is expected to be excessive heating. This analysis included interpretation of flight data, analytical determination of accommodation coefficient and thermal model, and analysis of critical point temperatures as a function of the variables.

Flight experience has been gained from the Program 206 flight vehicles at altitudes where aerodynamic heating is not negligible in the total energy balance (and, in fact, may be dominant in some cases). The results are probably the only practical data of its kind in this regime and are sufficiently accurate and reliable to draw several conclusions. This experience has resulted in the ability to predict aerodynamic heating analytically in a much more realistic manner than the original Program 206 low altitude studies; that is, it is no longer felt necessary to consider the maximum accommodation coefficient (1.0) combined with the worst case (highest density) atmosphere, and $+ 3\sigma$ S, A, and E fluxes. More specifically, the use of the U. S. Standard Atmosphere, 1962 profile at altitudes below 80 nautical miles, in conjunction with a thermal accommodation coefficient of approximately 0.6, has been shown to be the nominal condition with tolerances of ± 0.2 sufficient to handle the extremes.

A word of caution is necessary however; a thorough understanding of the phenomena occurring, and the predicted results in terms of absorbed thermal energy requires a
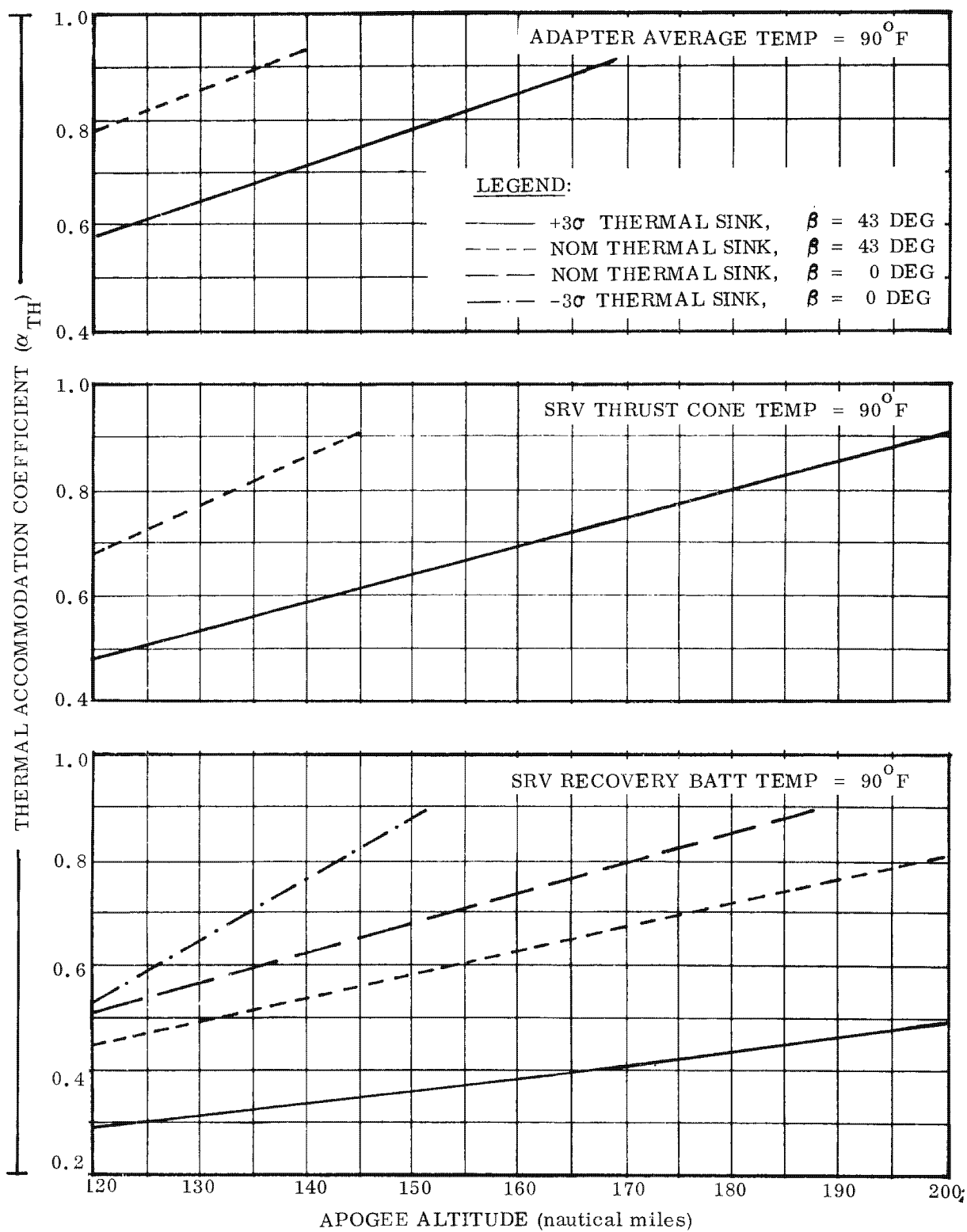
64SD4760

Figure 3-32. Limiting Altitude Conditions for Control of Critical Temperatures

considerably greater volume of good data than that obtained to date. It would be highly desirable to accumulate a sufficient store of information from the Program 206 flights to determine a statistical variation. This means that data should be obtained from future flights on a continuing basis. It should be pointed out that, in spite of the number of flights to date, there are only three vehicles which contribute significantly to the analysis (SV 955, SV 956 and SV 957); other flights were either outside the altitude range of interest (SV 951 to SV 954 and SV 960), too short in duration (SV 954 and SV 959), without telemetry as was SV 958, or without temperature surveys as in the case of SV 953. Data from the first two revs of SV 958 would have been of particular interest if the heating had not been so great as to cause saturation of temperature sensors.

3.8.1.1 Selection of Atmosphere

The density (ρ) itself is not obtainable with the current vehicle instrumentation; however, correlation of flight aerodynamic data with theoretical aerodynamic coefficients was obtained for altitudes under 92 nautical miles using the U. S. Standards Atmosphere, 1962 density model. Values of the accommodation coefficient, α_{TH}, together with this density model are then used to calculate vehicle free molecular heating and temperatures.

3.8.1.2 Accommodation Coefficient

Figure 3-33 shows families of curves calculated using specific SV 956 flight parameters. The flight temperatures on the illustration show that the Adapter temperatures correspond well with the thermal conditions of nominal external fluxes and $\alpha_{TH} = 0.7$. Data from SV 955 gave similar indications, though results were limited by the recorder failure. Figure 3-34 is a plot of SV 955 and SV 956 molecular shield data compared to a calculated curve. The flight temperatures are obviously lower and correspond to an α_{TH} of approximately 0.5. Figure 3-35 presents calculated and flight SRV forebody temperature data for SV 957. The data points generally indicate the α_{TH} to be approximately 0.4.
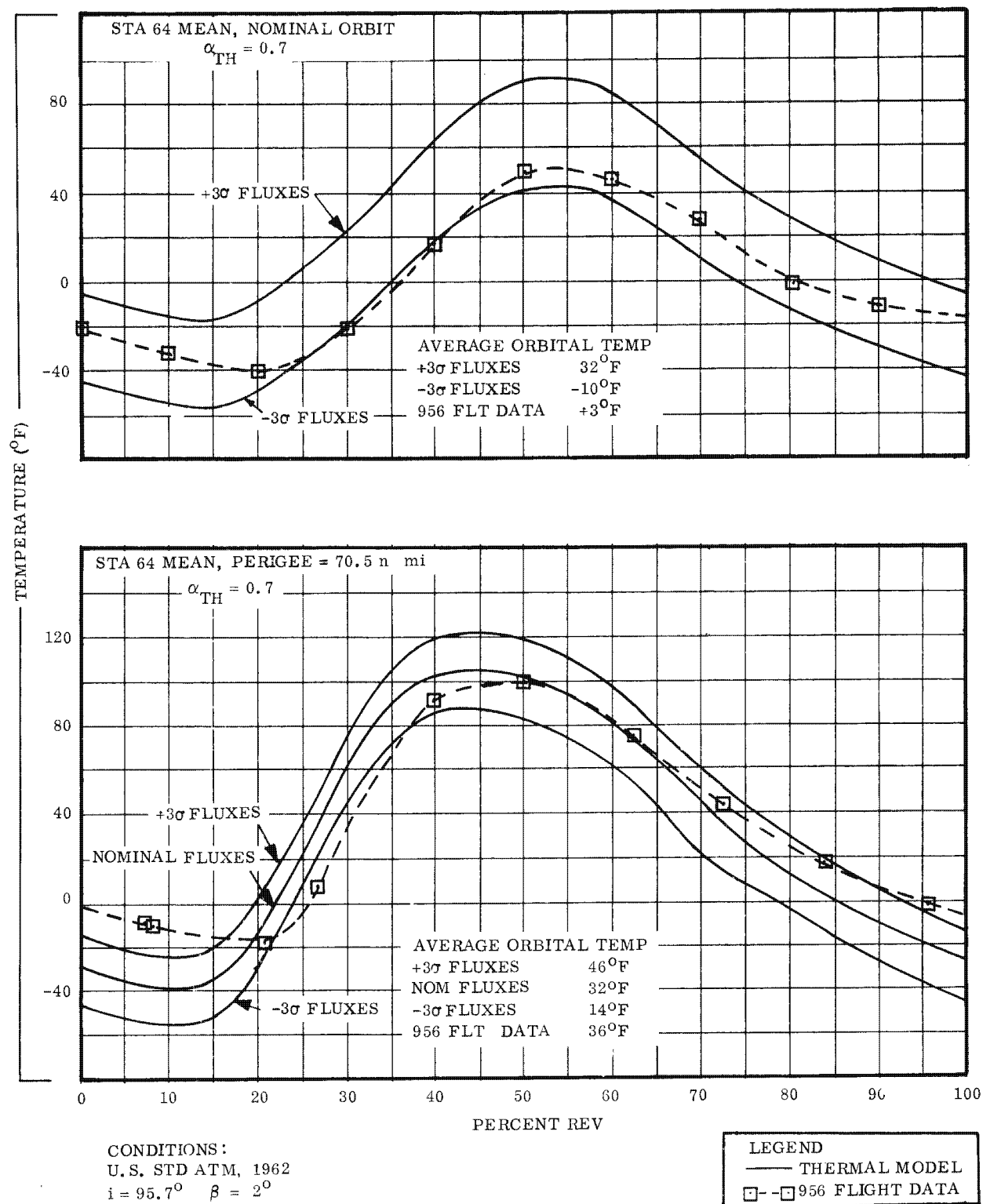
Figure 3-33. SV 956 Adapter Flight Temperatures Compared to Thermal Model
Using Actual SV 956 Orbit

64SD4760

LEGEND

FLIGHT DATA

—△— 956 FLY LOW, ALT ≅ 70.5 n. mi.
—□— 955 FLY LOW, ALT ≅ 69 n. mi.
—⊙— 956 REV 24, ALT ≅ 95 n. mi.
— — CALCULATED TEMPERATURE RESPONSE
(1959 STANDARD ATMOSPHERE, $\alpha_{TH} = 1.0$)

Figure 3-34. Comparison of Flight Temperatures to Predicted Temperatures
for Molecular Heat Shield

64SD4760
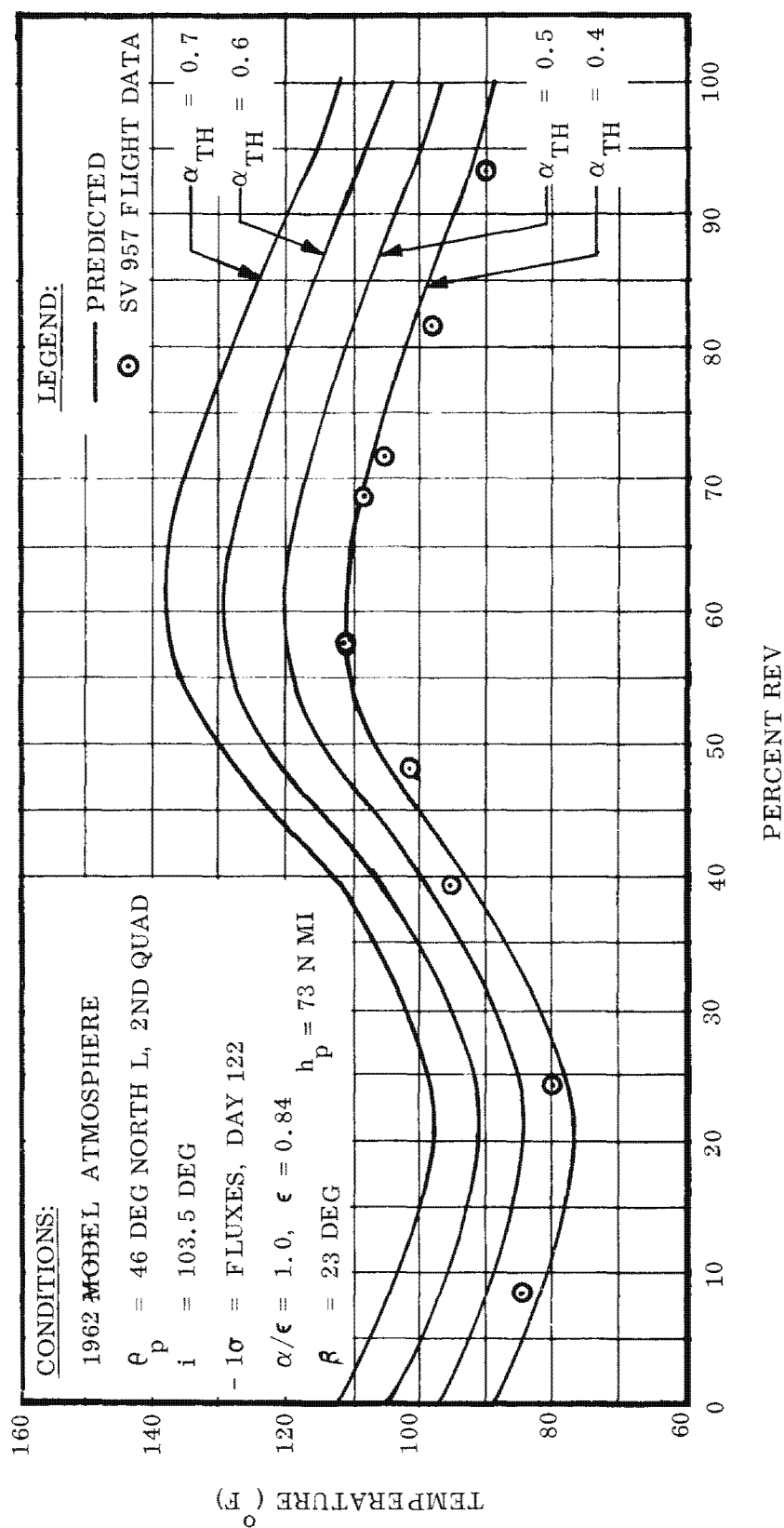
Figure 3-35. Predicted and Flight Temperatures for SV 957 SRV Forebody Stagnation Point Backface

64SD4760

3-94

On the basis of the U. S. Standard Atmosphere, 1962 density model and the comparisons above, there is considerable justification for stating the limits for the thermal accommodation coefficient as 0.6 ± 0.2. If it is desired, greater precision in predicting capability and/or orbital severity will require a considerably greater knowledge of the effect on accommodation coefficient of material, temperature, incidence angle, and atmospheric density, and thus will require a greater degree of accuracy and selectivity in instrumentation.

3.8.1.3 <u>Limiting Conditions for Low Altitude</u>

Fly-low capability is limited by the amount of free molecular heating which the more sensitive vehicle components or areas can receive without exceeding their specified temperature limits. The following are the most sensitive to molecular heating and therefore are the most limiting to low altitude operation. They are listed in the order of their sensitivity.

    a.   Recovery battery: 90° F maximum, a function of the average SRV temperature.

    b.   SRV stagnation point backface: 190° F maximum to protect shield bond.

    c.   SRV skirt: 230° F maximum to prevent thermal stresses.

    d.   Adapter average temperatures.

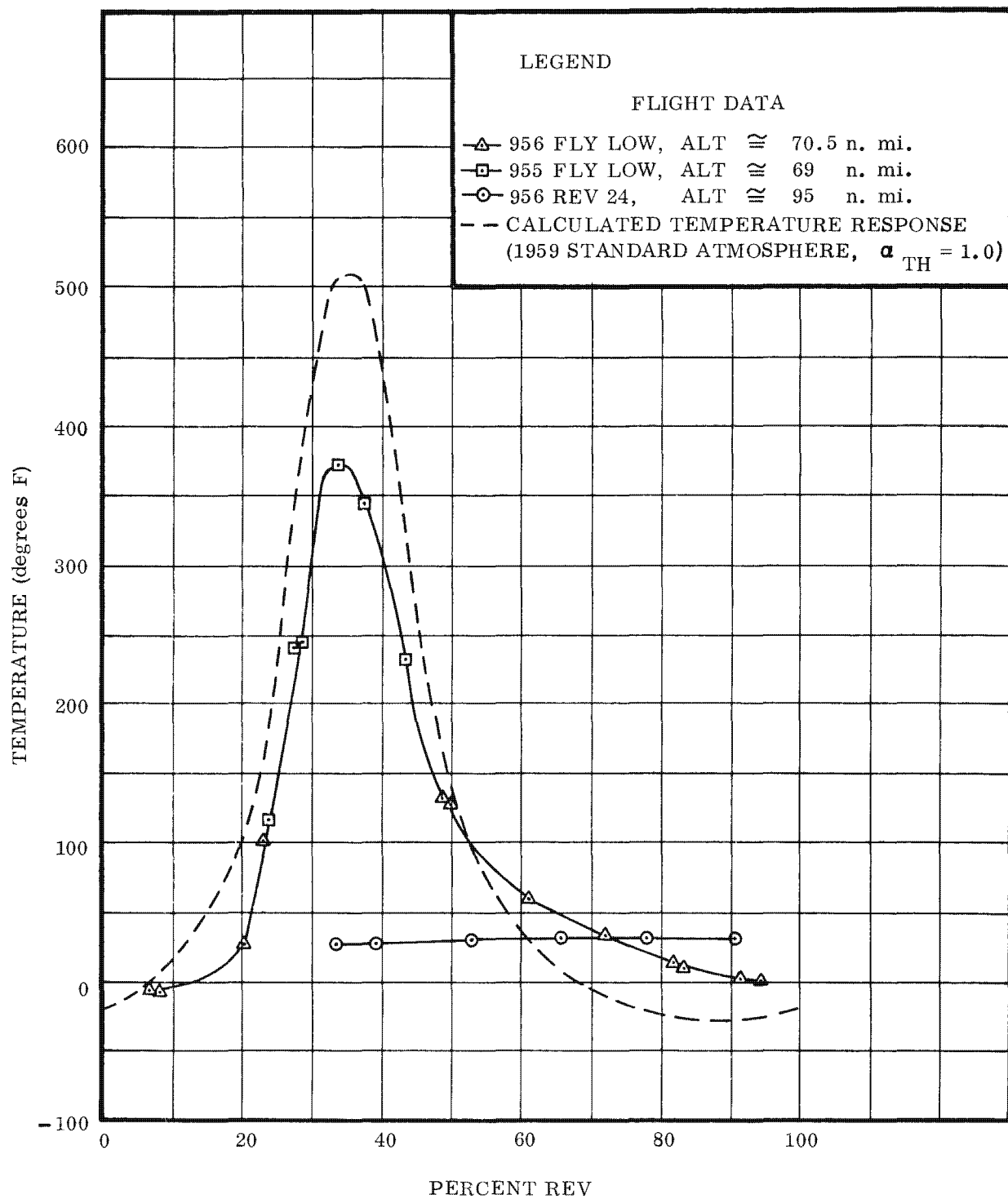The perigee is limited to a minimum altitude of 68 nautical miles (nominal fluxes, $\beta = 0$) regardless of apogee, because of the 190° F maximum for the forebody stagnation point backface temperature. This requirement is based only on the peak heat flux received by the heat shield, which is a function of the minimum orbit altitude.

The Aerospace System Specification, which is the GE compliance document, has been changed, effective with SV 969 and subsequent, to reflect a 70 nautical-mile minimum altitude with an apogee altitude to be determined by "flying by thermometer" using real-time data. The expected limiting apogee altitudes, were evaluated by calculating the resulting temperatures for the above components holding a constant perigee altitude and varying β angle, thermal sink conditions, accommodation coefficient, and apogee altitude.

The temperature of the recovery battery and thrust cone, and the average Adapter temperatures were first evaluated as a function of apogee altitude at various S, A, and E thermal sink conditions and for $\alpha_{TH} = 0.6$. The temperatures were calculated a second time, again as a function of apogee altitude, but varying α_{TH} so that its effect was known. Figure 3-32 cross-plots the results to show the conditions at which the maximum allowable temperatures are expected. It is obvious that the limiting conditions for the recovery battery are most stringent. For example, with $\alpha_{TH} = 0.6$, nominal thermal sinks, and with $\beta = 0$ degrees, the integrated heating effects associated with an apogee of 135 nautical miles will force the recovery battery temperature to the 90° F limit. In addition to the altitude limits indicated by the study of average molecular fluxes, figure 3-36 shows the limit imposed due to peak flux conditions at the stagnation point and in the skirt, and indicates that the minimum altitude at the given conditions ($\alpha_{TH} = 0.7$) is 163 nautical miles.

3.8.1.4 Fly-Reverse Effects at 70 Nautical-Miles

Prior to the flight of SV 958, a restriction had been placed upon the minimum perigee for SRV deboost. This was based upon the possibility of exceeding limiting component and insulation temperatures in the aft bay while flying reverse. The minimum perigee was specified as 75 nautical miles based upon an α_{TH} of 1. TARS electronics package component temperatures were analyzed for the 68.6 nautical-mile perigee fly-reverse conditions present during the SRV deboost sequence of SV 958 on rev 34. This analysis indicated that no overheating of the package should have occurred. Assuming an initial temperature of 100° F, the temperature rise flying reverse, during a 20-minute interval spanning perigee, was calculated to have been 24° F. The component temperature limit is 125° F. Unfortunately, the 90 x 1/ 18 multiplexer was disabled on rev 16; therefore, no flight data is available for concurrence.

The other temperature-sensitive aft bay area is the superinsulation covering the Freon tanks and plumbing. Current analysis has also indicated that this blanket configuration, consisting of six pairs of aluminum foil and tissue glass covering 28 layers of aluminized mylar, will not exceed limiting temperatures at this perigee altitude.
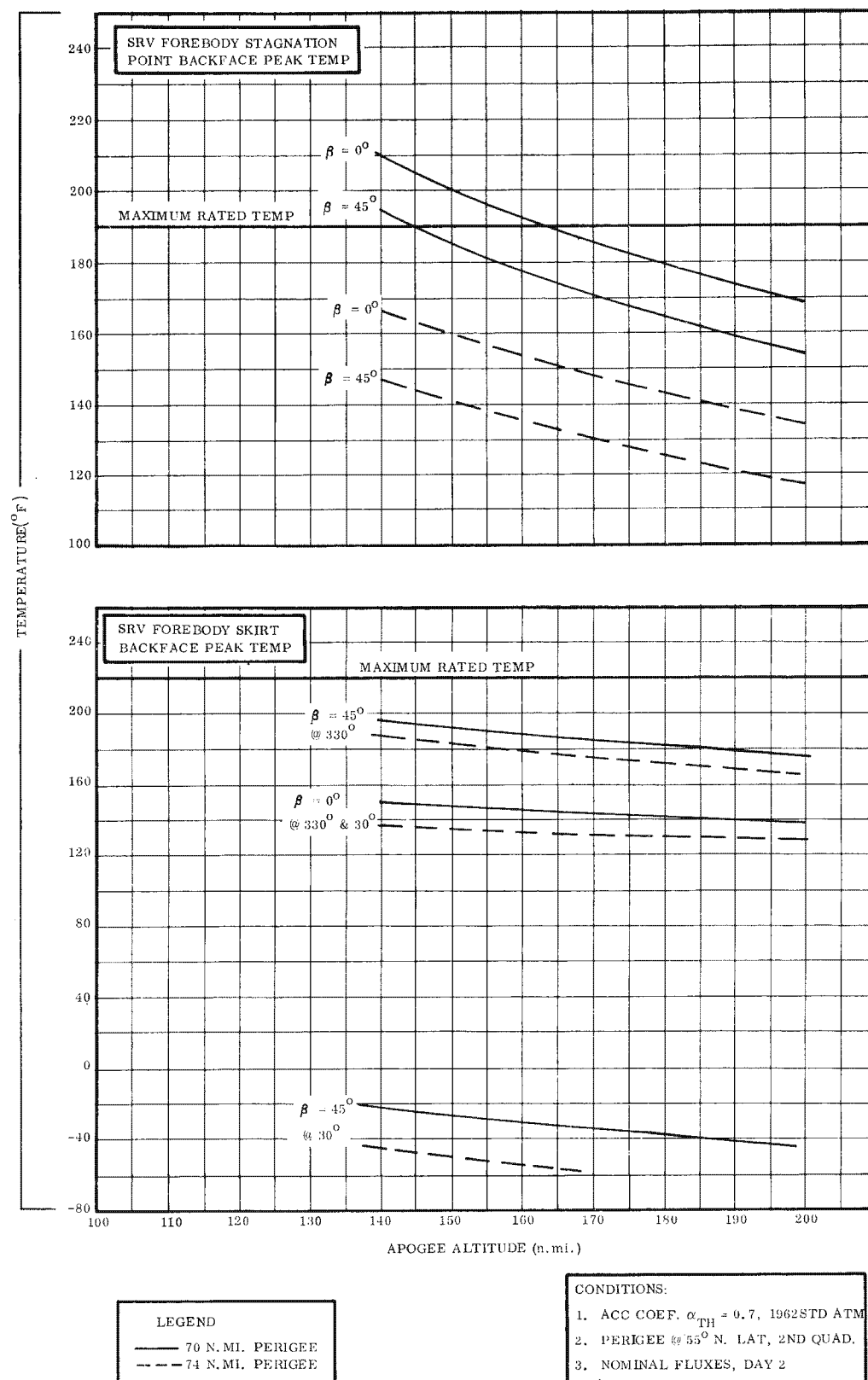
Figure 3-36.   Variation in SRV Forebody Backface Peak Temperature with Varying
Apogee Assuming Two Fixed Perigee Altitude Conditions

It is therefore concluded that fly-reverse at 70 nautical miles will not result in excessive aft bay component temperatures.

NOTE

The thermal restriction covering fly-reverse duration
with the SRV (for 70 n mi perigees and above) still
remains in effect; that is, for solar incidence angles
(β) in excess of ± 15 degrees, the SRV shield is
limited to 1-1/2 revs flying reverse; for β angles less
than $\pm$ 15 degrees, no time limitation is imposed.

3.8.2 THERMAL ORBITAL SEVERITY

A detailed study has been made to determine the effects of orbital environment upon vehicle environmental control power demands. The desired results of the study were twofold: to statistically evaluate those factors which produce the environment; and, based upon this statistical model, evaluate the particular environment and environmental control power demand of specific vehicles from the flight data.

3.8.2.1 Contributors to Satellite Vehicle Internal Temperatures

Those factors which affect the orbital temperatures of a satellite vehicle are listed below. Excluded are those items which are a function of the spacecraft geometry and structural materials.

64SD4760

3-99

Orbit Characteristics:

Launch site

Day of launch

Hour of launch

Inclination

Flight duration

Perigee altitude

Eccentricity

The combined thermal effect of these parameters is defined by the angle the sun makes with the orbit plane (β).

Heat Fluxes:

Solar radiant (S)

Earth radiant (E)

Earth albedo (A)

Free molecule (Q_m)

Internally generated

Thermal Control Coating Parameters:

Solar absorbtivity (α)

Infrared emissivity (ϵ)

Each of the foregoing parameters has an associated tolerance or range of values which will cause shifts in vehicle temperatures. The orbit plane solar incidence angle (β) is one of the prime parameters which very strongly influences the anticipated thermal environment. Since the orbit characteristics and their possible ranges are well defined for the Program 206 vehicle, launch times are limited by the beta angles in the range from -38 to 0 to +43 degrees. Perigee altitude and eccentricity affect the magnitude of free molecule heat flux impinging upon the vehicle and in addition define the vehicle proximity to the earth as a thermal radiation source.

The nominal values of solar, earth albedo and earth radiant fluxes and their associated tolerances used in the design of the Program 206 vehicle are given in table 3-18.

64SD4760

Table 3-18. Design Values of Space Fluxes

Flux	Nominal Value	3σ Tolerance
Solar radiant	440 BTU/hr-ft^2*	$\pm$ 13.2 BTU/hr-ft^2
Earth albedo	0.38 of solar	$\pm$ 0.18 of solar
Earth radiant	68.2 BTU/hr-ft^2	$\pm$ 20.0 BTU/hr-ft^2

*The nominal solar flux value also varies as a function of the day of the year.

Free molecular heat flux is a function of atmospheric density as given by an atmospheric model such as the U. S. Standard Atmosphere, 1962. Internally generated flux is that which is radiated by the vehicle skin due to local component dissipation. The thermal control coating parameters are selected by analysis to provide optimum local skin temperatures commensurate with allowable component temperatures. (When control of temperature extremes is beyond the capability of α/ϵ coatings, thermostatically controlled heaters become necessary.)

3.8.2.2 Concept of Orbital Severity

The variation in all the foregoing parameters made it a design necessity to determine the hot and cold extremes in environment. A selection of those parameter values which contributed to the mathematical extreme would have, however, resulted in an unnecessarily conservative design.

It was found that the vehicle temperatures, resulting from many different combinations of the possible values of the flux and the coating parameters, were normally distributed. The variability of this distribution about the mean, by its nature and derivation, is defined as the thermal orbital severity expected and/or possible for Program 206. The $\pm$ 3σ (99.87% probability) points of orbital severity were selected as design limits to insure that for all but the most extreme conditions the resulting flight temperatures would fall within the design range.

64SD4760

To evaluate the actual thermal orbital severity encountered in flight, this study utilized the various vehicle bay skin temperatures, since they are the areas thought to best reflect the thermal orbital severity, and in addition, have the best instrumentation for this type of study. The thermal design of these bays had been planned so that internal temperatures would be responsive only to the average skin temperature (a function of orbital severity) and not to the instantaneous skin temperature. Correspondingly, those components which require heater power are of sufficient thermal inertia to be generally immune to sink temperature variations within an orbit. Therefore, heater power demand for both bays and components is a function of the orbital average skin temperature, and the complicated and unnecessary factor of skin temperature variation within an orbit was eliminated.

To correlate flight data with orbital severity, the vehicle thermal model was used to compute average skin temperatures as a function of expected orbital severity, with β angle as the variable. (See figure 3-37.) It should be noted that the distributions shown do not reflect flight altitudes less than 83 nautical miles, where the effects of free molecule heating become extremely significant. Flight data and heater power usage for fly-low conditions are compared later.

3.8.2.3 Orbital Skin Temperature Instrumentation

Orbital skin temperature instrumentation on the Program 206 vehicle is listed in table 3-19. Care was taken in the placement of the flight skin temperature sensors to insure that their outputs were representative of the environmental conditions. It should be noted that the temperature range of the 0° and 180° sensors on the OCV located at station 190 were originally intended for powered flight, and their range was too great for use in the orbital severity study. Determination of OCV orbital severity therefore had to be based on the response of only four sensors. Figure 3-37 (part A) illustrates the relationship between the arithmetic average of the four OCV skin sensors, the total mid-OCV skin temperatures and orbital severity. The correlation between the over-all bay skin and average sensor response was determined from ground test. Part B of figure 3-37 shows a similar plot used to determine Adapter orbital severity. The 3σ hot case calculated for the Adapter assumed a thermal accommodation coefficient (α_{TH}) of 1.0, while flight data indicates the effective α_{TH} is

64SD4760
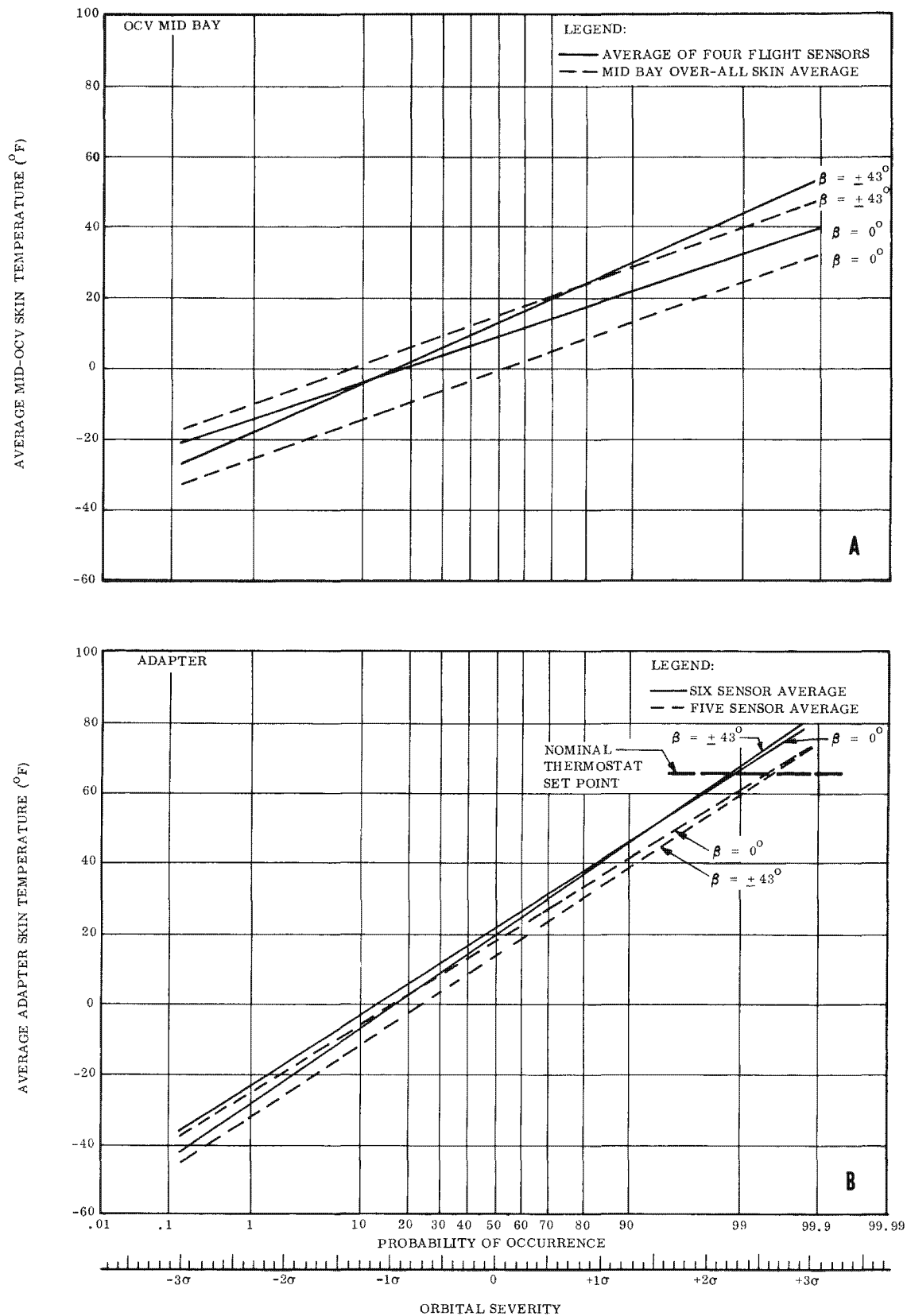
Figure 3-37. Skin Temperatures Versus Orbital Severity

64SD4760

3-102

around 0.7. Correction of the $+3\sigma$ point would lower the entire curve; that is, a particular average temperature would represent a hotter orbit than is shown. No attempt has been made to revise the curves, because of the extant uncertainties in α_{TH} determination.

Table 3-19. Orbital Severity Instrumentation

Bay	Station	Angle	Sensor Ranges (^{o} F)	Comments
Adapter	64	0	−80 to 200	
	64	60	−80 to 200	
	64	120	−80 to 200	
	64	180	−80 to 200 − − − − {	Removed, SV 956
	64	240	−80 to 200	
	64	300	−80 to 200	
Mid-OCV	190	0	40 to 540	Inadequate range
	190	60	−80 to 200	
	190	120	−80 to 200	
	190	180	40 to 540	Inadequate range
	190	240	−80 to 200	
	190	300	−80 to 200	

3.8.2.4 <u>Flight Data</u>

Figures 3-38 and 3-39 present the complete summary of Adapter and OCV orbital skin temperature flight data used in this analysis. The temperatures of the Adapter and mid-OCV sensors are plotted as a function of orbital position and represent a composite of real-time and playback data taken within a time span of several revs. The zero percent (0%) rev position on the curves corresponds to the ascending node. Good determination of the temperature profiles is strongly dependent upon having a large number of data points (both real-time and playback surveys). Playback data are critical to orbital severity determination since they heavily affect the average response of a given sensor. In general,

64SD4760

3-103

Figure 3-38. Summary of Adapter Orbital Skin Temperatures, Sheet 1 of 2

Figure 3-38. Summary of Adapter Orbital Skin Temperatures, Sheet 2 of 2

64SD4760

Figure 3-39. Summary of OCV Orbital Skin Temperatures, Sheet 1 of 2

64SD4760

C05099047

Figure 3-39. Summary of OCV Orbital Skin Temperatures, Sheet 2 of 2

64SD4760
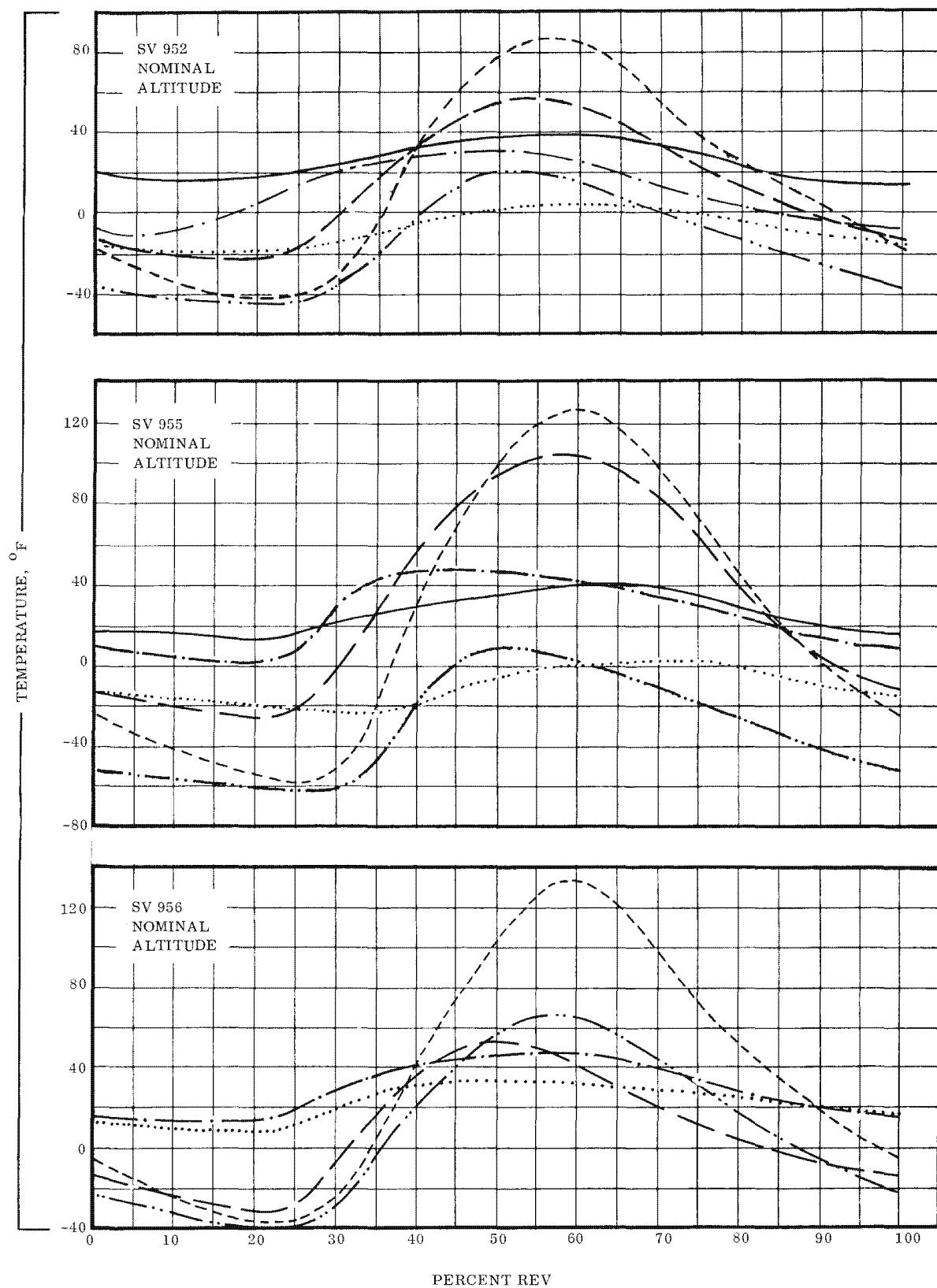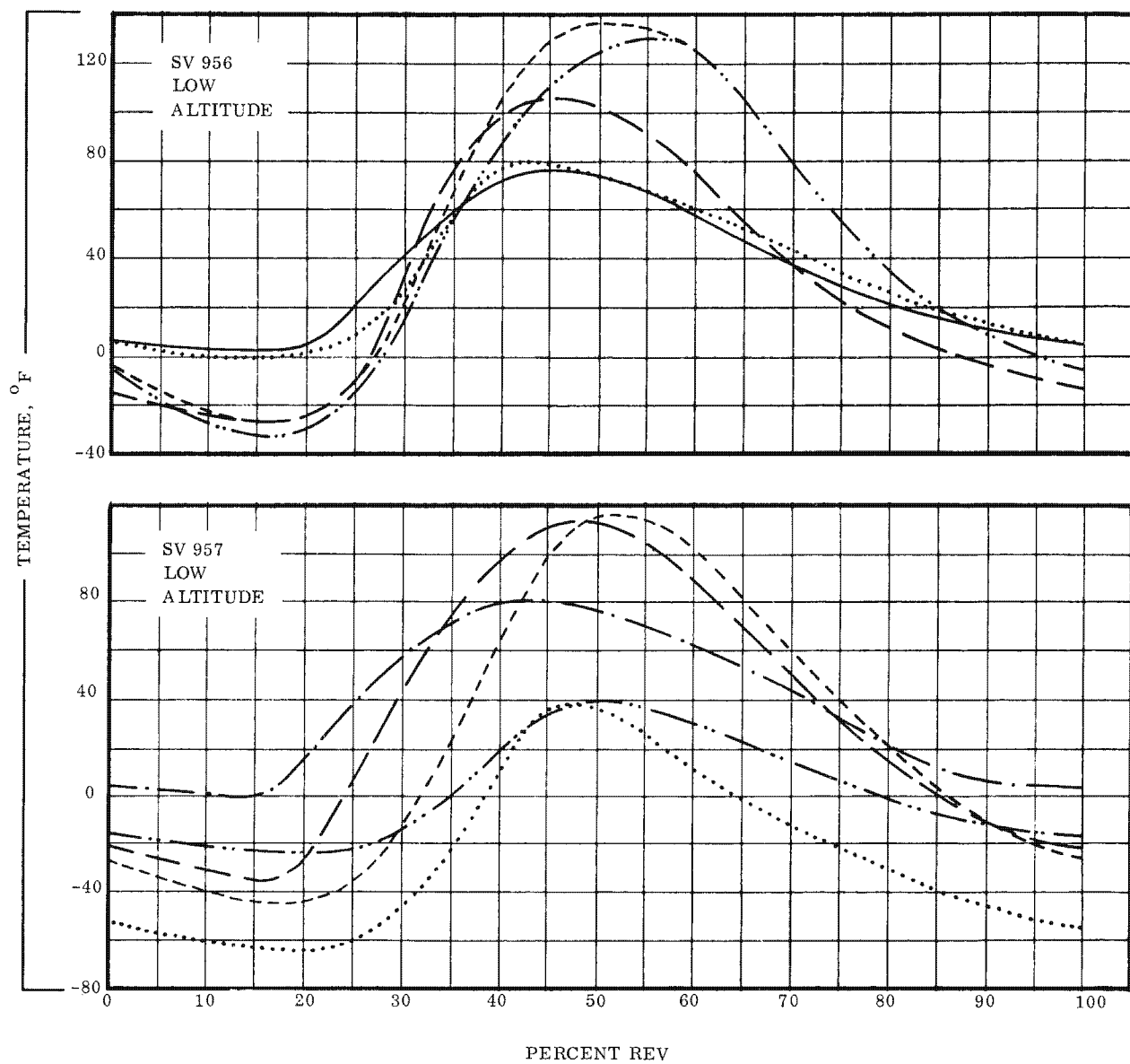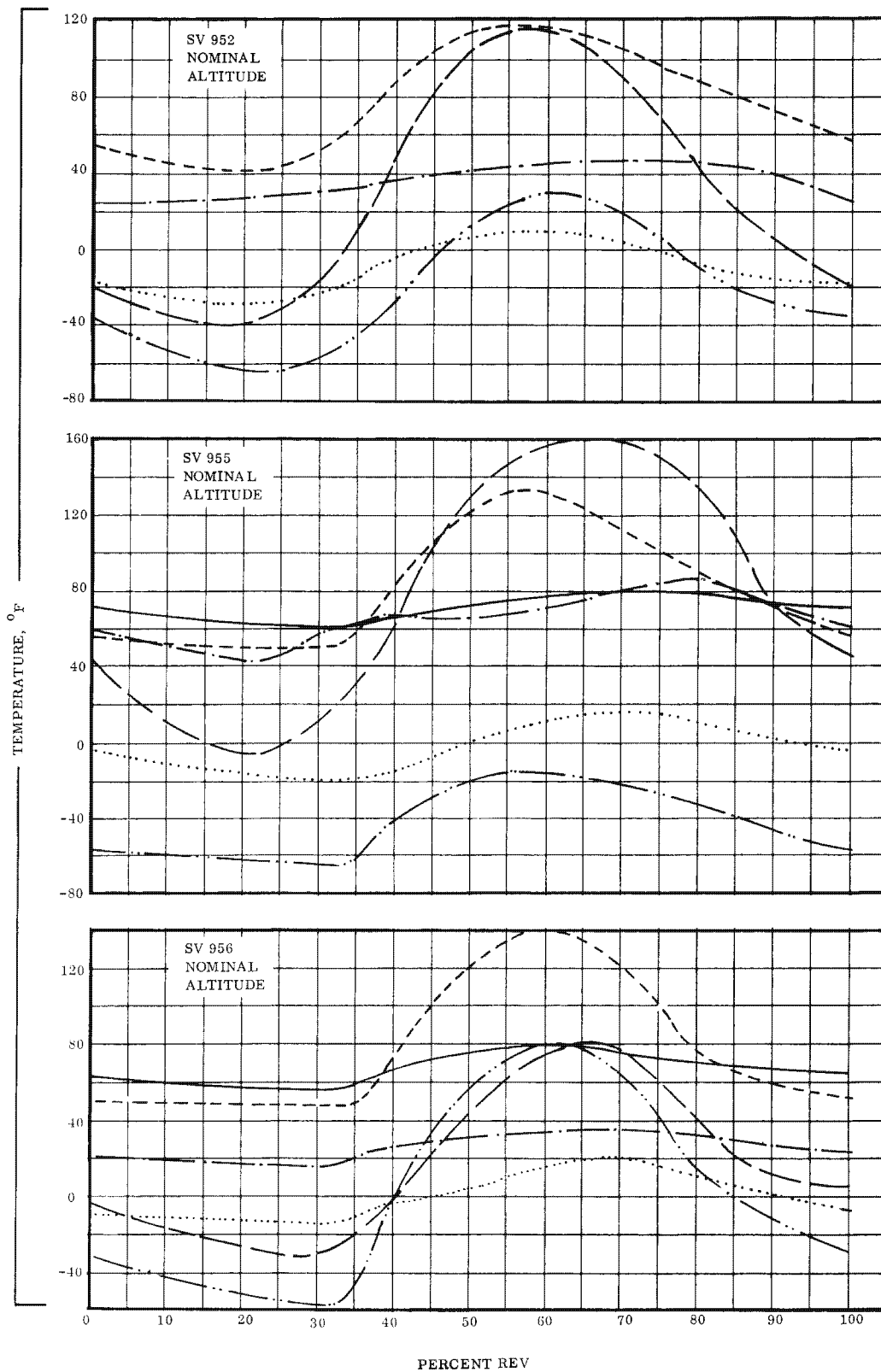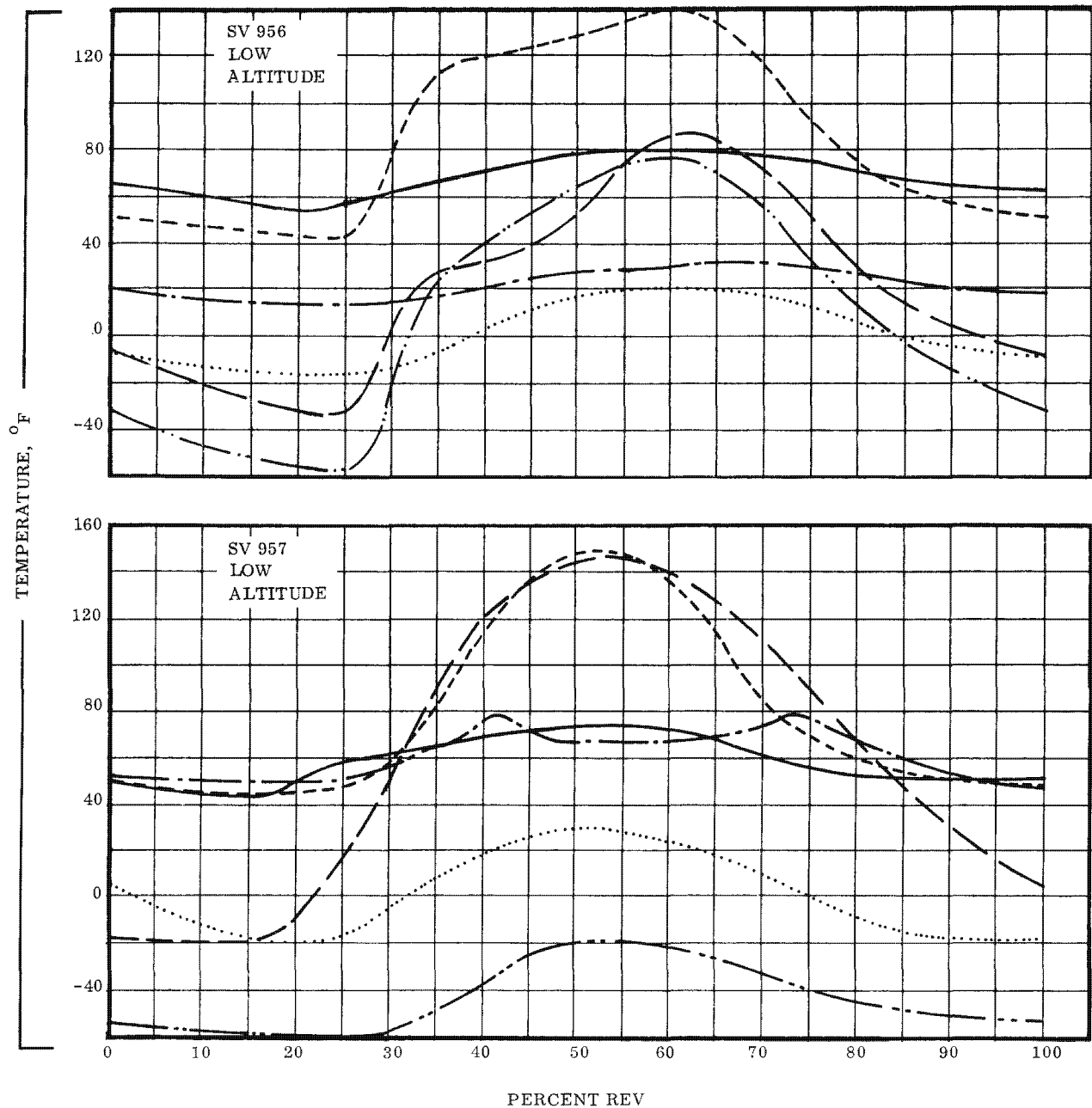
3-107

it can be said that sensor response is fairly descriptive of the environmental influences, that is, entering and leaving the earth's shadow, peak solar exposure on sensor position, perigee location, and vehicle orientation. Various malfunctions have precluded the attainment of the necessary data for this analysis on all ten flights.

The mean temperature for each flight thermistor and the corresponding arithmetic average representing the respective bay temperature were calculated and are summarized in table 3-20. The corresponding orbital severity is also given. The equivalent orbital severity determined from the Adapter skin sensors differed significantly from that determined from the OCV sensors. This difference was expected and is readily explained by the difference in molecular heating between the Adapter and OCV, radiation view factors, and α/ϵ coating. The correction of the orbital severity curves for a lower α_{TH} would also have the effect of reducing the differences in orbital severity determination from the Adapter and OCV sensors.

3.8.2.5 Vehicle Orbital Heaters and Power Usage Estimation

Table 3-21 specifies the location and pertinent characteristics of each heated area in the vehicle. The heater systems in the vehicle can be classified in two general categories: those heaters which provide essentially isothermal component or bay temperature control, and those heaters which activate only under extreme environmental conditions. In the former case, flight temperature sensors located on the component indicate very little about the power demand since the heaters maintain component temperatures fairly constant over a wide range of environment. The deduced orbital severity must be used to estimate power usage of these heaters. In the latter case, flight temperatures are generally expected to be above the thermostat activation point and therefore environment control power demand will be less significant in those areas for the vast majority of flights. Local component flight thermistors are used to estimate heater usage in these areas. Since the Adapter thermal environment was never as cold as the 4° F. thermostat setpoint, the heaters situated on the forward and aft racks did not activate in any of the four flights which were analyzed in detail. Power usage by the compartment heaters in vehicle Section 5 are significantly

64SD4760

3-108

C05099047

64SD4760

Table 20. SV Flight – Mean Orbital Temperatures

Sensor Location	Nominal Altitudes (°F)			Low Altitudes (°F)	
	SV 952 β = 11 deg	SV 955 β = 20 deg	SV 956 β = 2 deg	SV 952 β = 2 deg	SV 957 β = 22 deg
Adapter Sta 64 @ 0 deg	15.5	22	15.2	45.9	22.1
Adapter Sta 64 @ 60 deg	-16.3	-32	-12.3	41.1	-24.9
Adapter Sta 64 @ 120 deg	- 8.5	-12	2.2	33.6	0.9
Adapter Sta 64 @ 180 deg	24.9	30	No Sensor	No Sensor	No Sensor
Adapter Sta 64 @ 240 deg	10.3	24	9.3	32.9	35.7
Adapter Sta 64 @ 300 deg	12.1	32	-10.6	29.3	30.9
Adapter – Average	6.3	10.7	0.8	36.6	12.9
Equivalent Orbital Severity	- 0.7σ	- 0.5σ	- 1.0σ	+1.1σ	-0.1σ
OCV Sta 190 @ 60 deg	-21.6	-42.7	1.0	12.5	-42.8
OCV Sta 190 @ 120 deg	-10.7	- 3.6	- 1.5	1.5	0.1
OCV Sta 190 @ 240 deg	36.1	63.8	25.7	23.0	61.3
OCV Sta 190 @ 300 deg	28.8	75.6	16.0	21.9	64.6
OCV – Average	8.2	23.3	10.3	14.7	20.8
Equivalent Orbital Severity	- 0.2σ	+ 1.1σ	+ 0.2σ	+0.6σ	+ 0.9σ

3-109

Table 3-21. SV Environmental Control Subsystem: Orbital Heaters

Heated Component or Area	Heater Unit No.	Nominal Heater Output at 28V	Nominal Thermostat Setting ($^{\circ}$F)	Overload Thermostat Setting ($^{\circ}$F)
SRV				
Capsule	A1724	32.4	67±3	--
Recovery Battery	Internal	32.4	57±3	67±3
Thrust Cone	A1634, 1635	16.2	57±3	--
Adapter				
Fwd Rack Quad II (Recorder)	A1358	9.0	4±3	20±5
Fwd Rack Quad III (Recorder	A1357	9.0	4±3	20±5
Aft Rack Hi Volt P.S. 1	A1350	8.0	4±3	20±5
Aft Rack Hi Volt P.S. 2	A1351	9.0	4±3	20±5
Aft Rack Pwr. Controller	A1355	8.5	4±3	20±5
Aft Rack Pulse Pos. Demod.	A1354	8.5	4±3	20±5
Torque Box Quad III RF Xmtr	A1353	18.8	4±3	20±5
Torque Box Quad III Pwr. Amp	A1352	22(954-961) 11(962&Sub)	4±3	20±5
Fwd OCV (Section 5) Heater Zones 1-4, 8-11	A1122-1125 A1129-1132 A1372	} 83	70.2±.2	82 max thermostat 59 min thermostat
Mid OCV (Section 6				
Primary Battery 1	A1111	13.7	33±3	72±3
Primary Battery 2	A1112	13.7	33±3	72±3
Primary Battery 3	A1113	13.7	33±3	72±3
Primary Battery 4	A1114	13.7	33±3	72±3
Primary Battery 5	A1115	13.7	33±3	72±3
Prog. B/U Battery	A1121	10.7	72±3	110±5
RAGS	Internal	13.6	165±2.5	152±3 (on block)
Fuel Tank	A1109	9.2	50±3	110±5
Oxidizer Tank	A1161	9.2	50±3	110±5
Nitrogen Tank	A1117	13.7	33±3	110 ±5
Pneumatic Tray	A1168	7.4	33±3	110±5
BUSS Freon Tank Regulator	A1961	16.0	45±5 ON 75±5 OFF	

64SD4760

3-110

Table 3-21. SV Environmental Control Subsystem: Orbital Heaters (Cont)

Heated Component or Area	Heater Unit No.	Nominal Heater Output at 28 V	Nominal Thermostat Setting (^{o}F)	Overload Thermostat Setting (^{o}F)
Aft OCV (Section 7)				
TARS	Internal	51.0	165$\pm$2.5	--
Cold Gas Tank Quad I	A1398	20.1	110$\pm$5	--
Cold Gas Tank Quad IV	A1397	20.1	110$\pm$5	--
Cold Gas Line Quad II	A1349	10.1	33$\pm$3	110$\pm$5
Cold Gas Line Quad III	A1165	10.1	33$\pm$3	110$\pm$5
Rocket Nozzle Solenoids Quad I	A1167	5.5	33$\pm$3	110$\pm$5
Rocket Nozzle Solenoids Quad IV	A1166	5.5	33$\pm$	110$\pm$5
Miscellaneous, GFE	--	150.0	--	--

64SD4760

3-111

affected by variations in thermal environment. The relationship between vehicle Section 5 heater power usage and average bay skin temperature (or orbital severity) was determined directly from the thermal test program, and is illustrated in figure 3-40.

Of the remaining vehicle heaters as listed in table 3-21, those whose power demands are rather difficult to determine are the BUSS tank, the cold gas tanks, and the cold gas lines. This is because of poor instrumentation, a secondary sensitivity to the thermal environment, or internal thermodynamic transients taking place within the component. An estimated range of heater power demand must be assumed in these areas.

3.8.2.6 Total Power Usage Evaluation

The total average heater power demand together with the most influential SV thermal parameters are summarized in table 3-22. Both the specification and below-specification altitude SV temperature data were correlated to an orbital severity applicable only to altitudes in excess of 83 nautical miles (figure 3-32). The effect therefore is to state a fictitous orbital severity for the fly-low data of SV 956 and 957. This comparison is, however, important in terms of the apparent changes in environment during lower altitude flight.

Those vehicle heaters which, based on local flight temperatures, never activated for the five flight cases given in table 3-20 and were therefore not a contributing item to the total demand, were the SRV recovery battery, OCV primary batteries 1 through 5, programmer back-up battery, propellant tanks, nitrogen tank, pneumatic tray, and rocket nozzle solenoids. Of the heaters which were active, the total heater power demand is based on the equivalent orbital severity, local component temperatures and/or an estimated power demand. The estimation required setting limits of operation based on analysis for some heaters, such as the BUSS tank regulator; hence the minimum/maximum power figures.

The orbital severity based on Adapter skin sensors was used in evaluating heaters in the SRV and Adapter sections because of their higher responsiveness to free molecular heating.

64SD4760

3-112
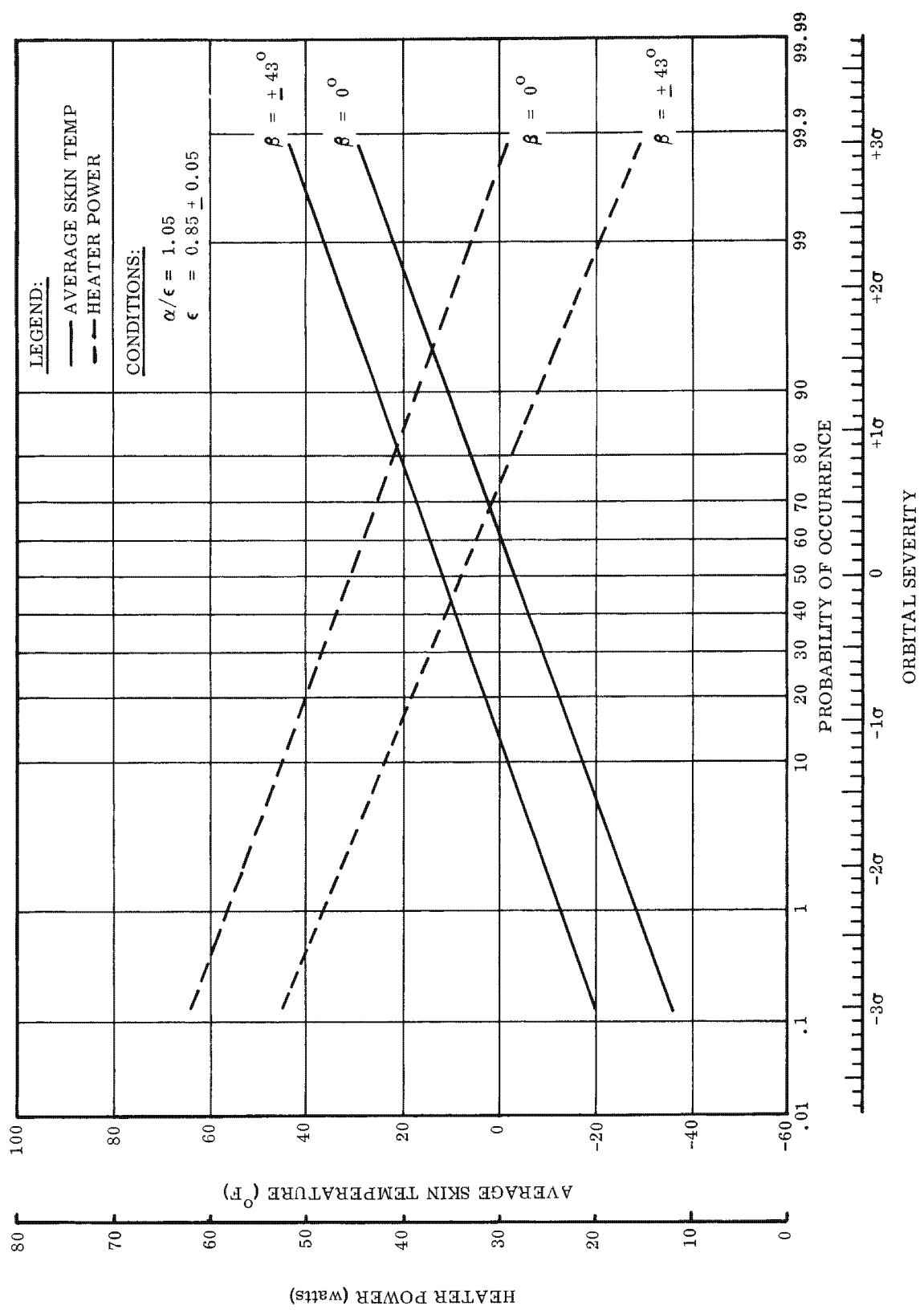
Figure 3-40. OCV Forward Bay Skin Temperatures and Heater Power Usage Versus Orbital Severity

64SD4760

3-113

Table 3-22.   Thermal Environment Summary

SV	β Angle (deg)	Nominal Altitudes (> 83 n mi)						Low Altitudes (< 83 n mi)					
		h_p/h_a (n mi)	Equivalent Orbit Severity		Heater Power (watts)		EP&SD Estimate of Power Usage (watts)	h_p/h_a (n mi)	Equivalent Orbit Severity		Heater Power (watts)		EP&SD Estimate of Power Usage (watts)
			Adapter	Mid OCV	Min	Max			Adapter	Mid OCV	Min	Max	
952	11	98/164	0.7σ cold	0.2σ cold	136	155	118	NO LOW ALTITUDE OPERATION					
953	20	89/118	0.5σ cold	1.1σ	116	163	88						
956	2	93/126	1.0σ cold	0.2σ	152	200	106	70/197	1.1σ hot	0.6σ hot	88	140	55
957	22	INSUFFICIENT DATA						73/202	0.1σ cold	0.9σ hot	116	164	100

This excludes those heaters whose operation was determined from local component temperature sensors. Similarly, the mid-OCV sensor equivalent orbit severity was used to determine the duty cycles of operating heaters in the forward, mid and aft-bays.

The information in table 3-22 shows very good consistency with flight parameters. For the specification altitude flights the smaller β - angle orbits required more heater power, consistent with previous analysis which showed a 0 degree-β case provided less average external flux to the vehicle. The significant warming effect of adjusting to lower than specification altitudes is illustrated by the SV 956 data. The Adapter orbital severity changed from 1σ cold to 1.1σ hot and was attributable solely to the change in free molecule heating rates. The OCV, under this same change in altitude, experienced much less of a change (from 0.2σ hot to 0.6σ hot) illustrating the lesser effects of molecular heating on the OCV. This is of course due to the lower molecular impingement rate received by a body whose surface is parallel to the direction of flight rather than having an angle of attack relative to this direction. The higher perigee and apogee fly-low altitudes of SV 957 compared to the lower altitudes of SV 956 with their associated higher molecular heating rates, are also illustrated by the lesser power demands of SV 956 during fly-low. The only quantitative inconsistency appears to be in the high (1.1σ hot) OCV orbital severity from SV 955 temperature data. No specific reason for this response has been determined, however the skin sensor at the 300° position on the OCV indicated a disproportionately high average orbit temperature. It is possible that the sensor was not properly calibrated and was giving erroneous readings, thereby increasing the apparent orbital severity. SV 955 did experience a large yaw attitude error, however this was corrected following rev 18 and the skin temperature data used in determining orbital severity were from rev 24 on.

3.8.2.7 Comparison to Electrical Power Subsystem Data

The SV is instrumented to measure system power and current demands upon the primary power supply, but no current or power monitors are available to sense the individual subsystem demands. To assess the power usage of a given subsystem, it is necessary to go through a process of deduction. It has been determined from the battery ampere hour

64SD4760

3-115

readings that nominal usage for all subsystems is 20.4 ampere hours per rev, at an approximate bus voltage of 28 volts (380 watts average). It has further been determined by subtracting the estimated demands of all other subsystems that average environmental control demand is 5.5 ampere hours per rev or approximately 100 watts, and ranges between 88 and 118 watts for the five cases discussed here. The estimated environmental control demands based on electrical data are shown in table 3-22 beside the corresponding power figures determined from thermal data. Certain observations may be made in comparing the electrical and thermal estimates:

a. Although the electrical power estimates are consistently lower than those derived from temperatures, they are in general agreement with the minimum heater power figures.

b. The data from SV 956 nominal altitude flight displays the greatest difference between electrical and thermal estimates of heater power (152 - 106 = 46 watts). Considering the relatively coarse orbital severity instrumentation and the necessary estimation and deduction processes involved, the agreement is reasonable, i.e., 39% vs. 27% of total power usage.

c. The electrical power data is based upon the average battery energy demand during the flight. The environmental power demand calculated from skin temperature is based upon orbital severity after all initial thermal transients are damped out. The thermal data therefore describes the stable demand for environmental control power. Because prelaunch conditions provide a warmer ambient to the vehicle, full heater usage is not necessary until a number of orbits have been completed. This is perhaps a strong reason for the difference between the estimates.

d. The absence of the SRV during the SV 956 low altitude flight contributed to the difference in that case since its demand for heater power was not included in the electrical estimate but was projected from thermal data.

e. The electrical demand of the Stabilization Subsystem was based upon laboratory measurements which included some unknown quantity for the TARS and RAGS gyro heaters. The thermal figures include estimates of TARS and RAGS gyro heater demands as part of the environmental control total. This "double-accounting" would increase the apparent gap between the differently derived power demands.

3.8.2.8 Conclusions

a. The ability to determine the heater power demands of the 206 Environmental Control Subsystem based upon post-flight analysis of skin temperature has been demonstrated with reasonable accuracy.

b. The general agreement between thermal and electrical estimates of heater power usage gives confidence to present knowledge of local heater demands as a function of environment. Improvements in local energy management may therefore be assessed with greater accuracy.

c. Vehicle improvements, if further study of thermal orbital severity is desirable, would consist of the addition of a flight radiometer (radiant flux meter) and densitometer, more comprehensive temperature surveys during all flight modes to improve knowledge of skin temperature responses, the addition of an electrical power or energy monitor on an environmental power bus and the further improvement in temperature instrumentation on the skin and at heated component locations.

d. It is felt therefore, that temperature data from early in a mission, would be of marginal value in predicting total mission demand since many points are required to accurately define orbital severity with the present instrumentation. The environmental control power demands determined from the four vehicle samples examined are not conclusive enough upon which to base mission life at this time.

64SD4760

3.9 ORBIT ADJUST SUBSYSTEM

The Orbit Adjust Subsystem was provided so that precise changes in the vehicle's orbit could be accomplished by increasing or decreasing orbital velocity. The accuracy of estimating changes in the orbital parameters resulting from an orbit adjust is dependent upon two factors: combined engine thrust and vehicle weight at engine ignition. It has been the objective of the Orbit Adjust Subsystem capability analysis to determine the level of thrust of the engines expected during a given firing, thereby permitting greater accuracy in the prediction of velocity change.

The thrust of each engine may be anywhere within the specification limit of 45.5 to 50.5 pounds, since propellant injectors are selected to make thrust fall within this limit. Therefore, the combined thrust of any pair of engines can be anywhere between 91 and 101 pounds. This thrust is expected to remain constant throughout a flight, since the characteristics of this subsystem are such that, once a set of components has been put together to form the subsystem, the thrust delivered will not vary more than one-tenth pound (excepting the occurrence of a malfunction).

It is apparent that precise predictions depend on being able to determine what thrust is being delivered during a particular flight. If sufficient instrumentation (for example, thrust chamber pressure taps) were made available, thrust could be determined directly early in the mission by means of a short "calibration" firing. Since this instrumentation does not now exist, no primary sensing is available during the flight to determine thrust accurately.

In lieu of being able to determine thrust on a real-time basis, it would be helpful to be able to use thrust information from previous flights to predict performance on succeeding flights. This can be done by computing the Program mean and standard deviation of the thrust levels achieved by combining the data from the previous vehicles. The point estimate of the mean value is normally the thrust level most likely to be expected on subsequent flights. Additionally, a confidence interval can be established within which the true mean value is expected to lie.

64SD4760

3-118

Unfortunately, considerable difficulty has been experienced in determining thrust for each flight. The lack of appropriate instrumentation required that the thrust measurement be done by evaluating the change in velocity obtained as a result of each firing. Using this method, thrust values were calculated for SV 955, SV 956, and SV 957, and are presented in table 3-23. The large standard deviation associated with each flight indicates that the measurement method was not precise. However, it has been assumed (with little justification) that measurement errors have tended to compensate, and that the calculated means are representative of the demonstrated thrust levels. The Program mean thrust is then just the average of the individual flight levels.

Based on these three data points, the point estimate of the Program mean thrust was found to be 96.8 pounds, very close to the specification nominal of 96.0 pounds. The 95% confidence interval of the mean thrust level was determined to be between 91.9 and 101.7 pounds. Since data is very limited, this wide range is inconclusive for improving prediction capability. Therefore, the best estimate of the expected thrust level remains the specification nominal of 96.0 pounds. As data is obtained from each succeeding flight, it is possible that this interval will become smaller, allowing more confidence in precise predictions of the thrust expected from the system.

Several methods have been used to obtain a measurement of ΔV, all of which have been based on the best fit ephemeris as the source of data. The following equation was felt to yield the most precise results, and was used to compute the velocity increments for all vehicles.

$$\Delta V_E = V_a \left[1 - \frac{2\,\Delta P}{3P} \right] \left[\frac{1+\epsilon}{1-\epsilon} \cdot \frac{1+\epsilon - \dfrac{\Delta P}{3P}}{1-\epsilon+\dfrac{\Delta P}{3P}} \right]^{1/2} \left[\frac{\Delta P}{3P} \right] \quad \text{at apogee}$$

64SD4760

3-119

$$\Delta V_E = V_p \left[1 - \frac{2\,\Delta P}{3P}\right] \left[\frac{1-\epsilon}{1+\epsilon} \cdot \frac{1-\epsilon-\dfrac{\Delta P}{3P}}{1+\epsilon+\dfrac{\Delta P}{3P}}\right]^{1/2} \frac{\Delta P}{3P} \qquad \text{at perigee}$$

where:

ΔV_E = effective change in velocity, ft/sec

V_a = velocity at apogee, ft/sec

V_p = velocity at perigee, ft/sec

P = orbital period, seconds

ΔP = change in orbital period, seconds

ϵ = orbital eccentricity

(All parameters are taken either before or after the adjust, but are consistent within a computation.)

Following the SV 958 flight, it was possible to validate under controlled conditions this "ΔP - method" of evaluating the imparted velocity change by applying it to the results of a KUPDATE post-adjust calculation which was available for the first time. (See reference 12.) Good agreement between the two processes was obtained (0.1 ft/sec difference in 23.1 ft/sec).

The equation by which average effective engine thrust (T_E) was derived from the velocity change (ΔV_E) is:

$$T_E = \frac{\dfrac{\Delta V_E}{\Delta t} \cdot \dfrac{W_c}{g_0}}{1 + \dfrac{\Delta t}{2\,W_c}\left|\dot{\omega}_c\right| + \ldots}$$

where

W_c = Post flight estimate of vehicle weight

Δt = Engine firing time

g_0 = 32.172 ft/sec^2

$\dot{\omega}_c$ = Propellant flow rate, based on telemetered propellant temperatures and pressures.

This equation is valid under the assumptions of a constant I_{sp} and a thrust vector aligned along the flight path, (both of which are reasonable for this Program) and is in optimum form for use with available information.

Table 3-23. Summary of Orbit Adjust Performance[1]

SV	Cumulated Firing Time (seconds)	Effective Thrust (pounds)[3]	
		Mean	Std Dev
953[2]	33.8	100.7	3.14
955	237.5	97.1	1.16
956	309.0	99.0	2.05
957	193.8	94.2	3.68

Notes:

1) OCV de-orbit operations are not included.

2) SV 953 operations are not included in Program mean calculations.

3) Point estimate of Program mean effective thrust is 96.8 pounds

64SD4760

3-121

3.10 STRUCTURES SUBSYSTEM

The maximum loading conditions experienced by the vehicle structure during the ascent phase of flight occur prior to and at Atlas booster-engine cutoff (BECO). Maximum pressure differentials across the vehicle skin and bulkheads occur at approximately the time of transonic flight. The combined bending moment and axial loads are the highest when the product of the dynamic pressure and total angle of attack is maximum; the combined thermal and axial loads are maximum at BECO.

The flight data presented in this section is representative of an Atlas pitch attenuation factor of .92, which was programmed for the first ten flights.

3.10.1 STRUCTURAL CAPABILITY

The margins inherent in the vehicles' structural design are illustrated in figures 3-41 and 3-42. As shown in figure 3-41, the structure exhibits a satisfactory positive margin when exposed to maximum differential pressure loads.

The calculated bending moment and axial loads determined from flight data at the time of maximum $q\gamma$, when compared with the associated design capability at the critical stations, indicate that the structure provides a large positive margin (figure 3-42). These large margins can be attributed to the small total angles of attack experienced in flight as compared to the design angle of 9.25 degrees. The estimated maximum total angle of attack experienced on any flight has been 2.0 degrees or less. Maximum upper atmosphere wind shears have been approximately 128 feet/second or less, resulting in these low total angles of attack.

The axial loads and temperatures calculated from flight data at booster-engine cutoff have been well within the design capability of the critical stations (figure 3-42).

Tables 3-24 through 3-26 show comparisons of the design criteria for the various powered flight load conditions with a typical set of flight parameters. From this comparison, it can be seen that the design parameters exceed the flight parameter values in most cases.

64SD4760
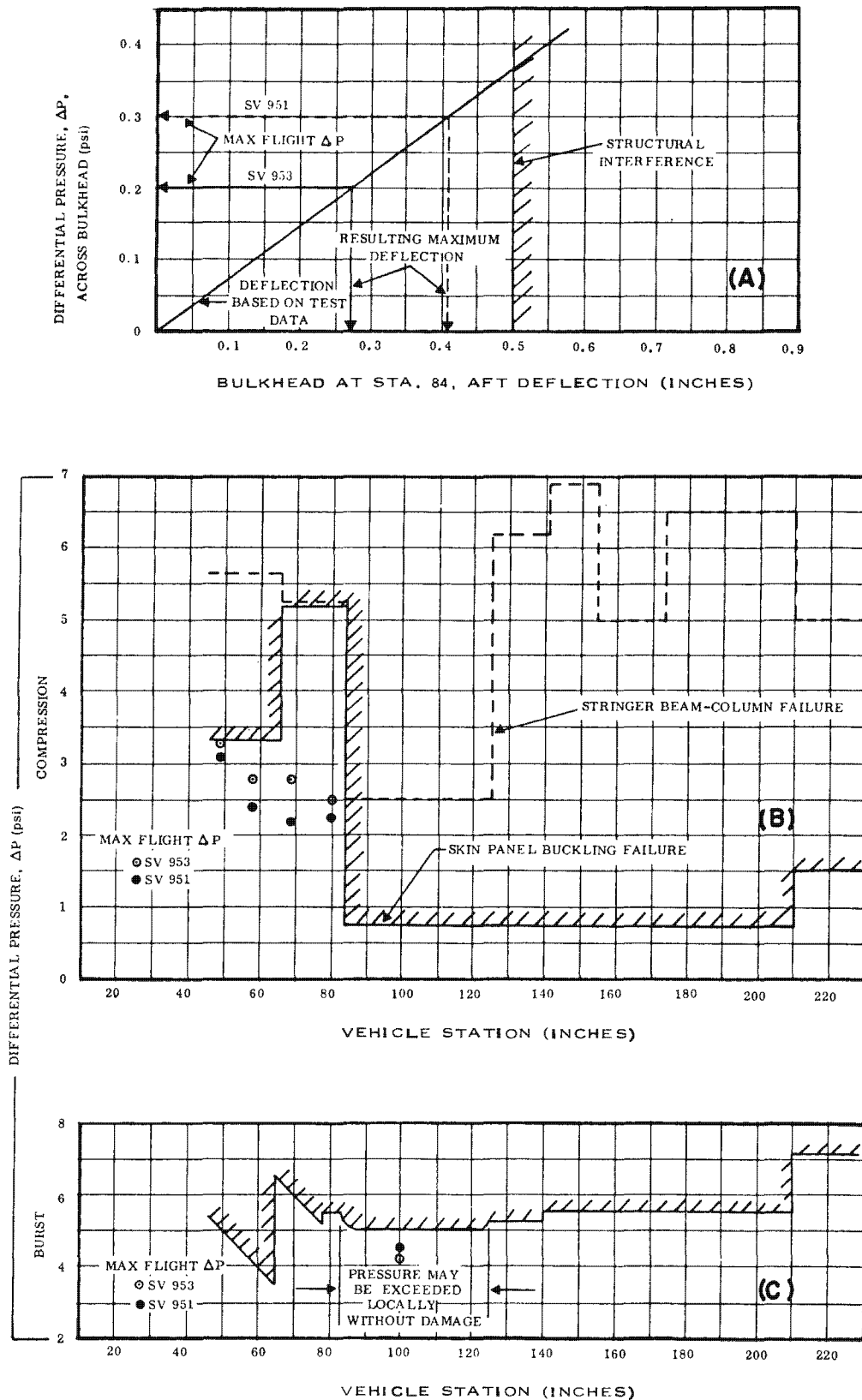
Figure 3-41. Representative SV Ascent Structural Differential Pressure Capabilities

64SD4760
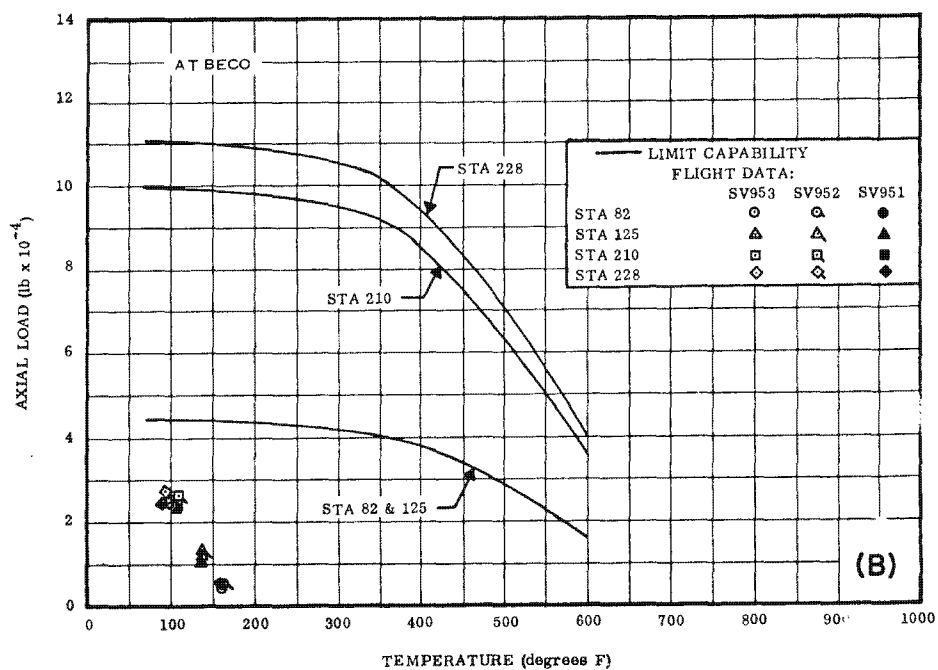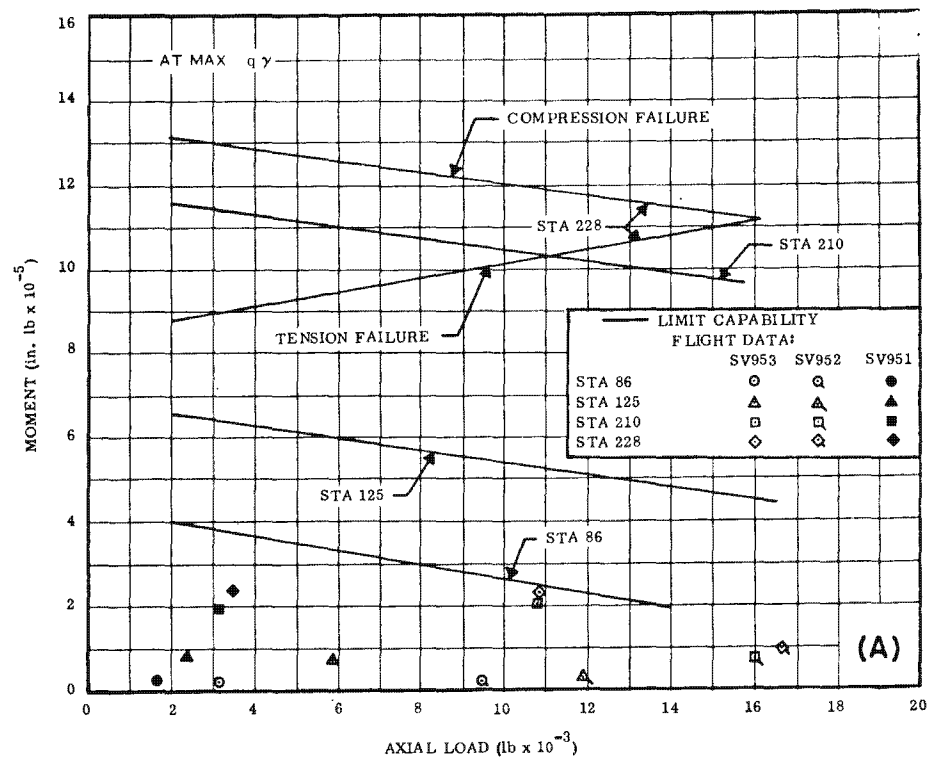
Figure 3-42. Representative SV Ascent Structural Load Capabilities

64SD4760

Table 3-24. Parameters at Max qγ

Parameter	Value	
	Design	Flight
Altitude	30,000	40,000 ft
Time from two-inch motion	62 sec	68 sec
Mach no.	1.42	1.75
Axial acceleration	2.01G	2.28G
Lateral acceleration	0.430G	0.093G (Est from aero data)
Dynamic pressure	858 psf	850 psf
Angle of attack	9.25 deg	2.00 deg

Table 3-25. Parameters at BECO

Parameter	Value	
	Design	Flight
Altitude	171,000 ft	204,000 ft
Time from two-inch motion	143 sec	136 sec
Mach no.	8.64	8.3
Axial acceleration	7.5G	6.2G
Lateral acceleration	0.10G	0.08G (Est from aero data)
Ring temperatures:		
Sta 82	203°F	160°F
Sta 125	167°F	135°F
Sta 210	118°F	105°F
Sta 228	110°F	95°F

64SD4760

3-125

Table 3-26. Peak Skin Temperatures

Structure	Temperature (^{o}F)	
	Design	Flight
Adapter skin	860	660
OCV skin	433	310

3.10.2 VIBRATION ANALYSIS

The vibration data presented herein is considered to be representative of the powered flight vibration responses of the Block II vehicles. The vehicle station locations and sensitive axis of each sensor used to monitor the environment are shown in figure 3-43.

Axial vibration responses, as shown in figures 3-44 and 3-45, were obtained from the sensor mounted on the TARS "bent" section at station 225.
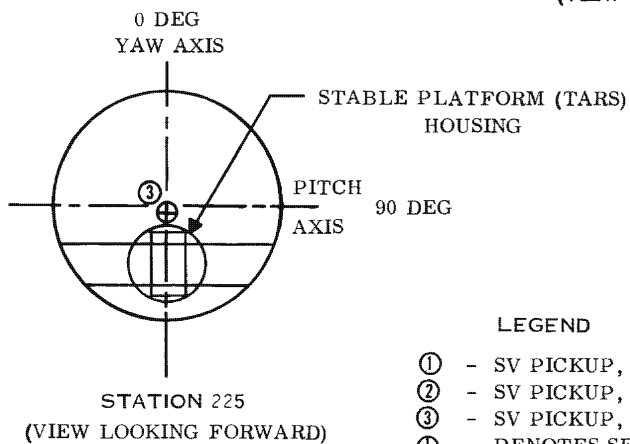
The random-plus-sine vibration Operability Assurance test level is shown in figure 3-45 to facilitate comparison of the flight and ground test levels. As shown, the responses are significantly lower than the ground test environment except for the narrow-band peak in the flight spectral densities at 300 cps.

Lateral vibration responses, obtained from the sensor located at station 210, are shown in figure 3-44 and 3-46. These vibration data were compared to similar data obtained from earlier Block I vehicles and were found to be higher for the Block II vehicles. This has been attributed to relocation of the aft bulkhead. The removal of the bulkhead from the structural ring at station 210 removed the snubbing effect provided by the bulkhead which caused the vibration amplitude to become higher. This conclusion was further substantiated by the fact that the increase in level occurred in the high frequency (800-1000 cps) range which is in the vicinity of the ring mode frequencies, and by the fact that the levels correspond well to those occurring at the station 247 ring on the Block I vehicles which were sensed by Agena instrumentation.

64SD4760

3-126

64SD4760

0 DEG
YAW AXIS

90 DEG

PITCH
AXIS   90 DEG

292°

STATION 125
(VIEW LOOKING FORWARD)

0 DEG
YAW AXIS

PITCH
AXIS   90 DEG

153°

②

STATION 210
(VIEW LOOKING FORWARD)

0 DEG
YAW AXIS

STABLE PLATFORM (TARS)
HOUSING

③

PITCH
AXIS   90 DEG

STATION 225
(VIEW LOOKING FORWARD)
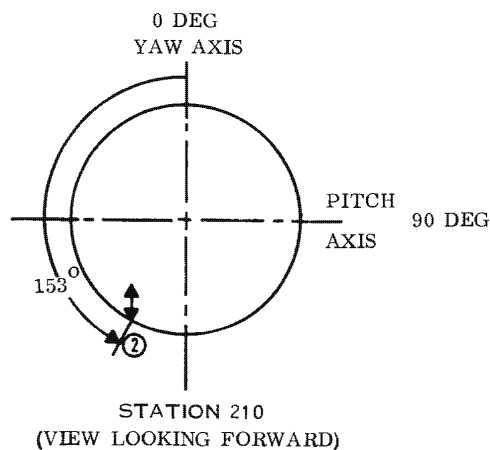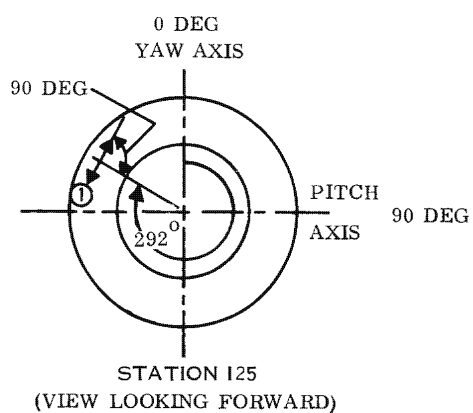
LEGEND

① – SV PICKUP, BAND 17
② – SV PICKUP, BAND C
③ – SV PICKUP, BAND A
⊕ – DENOTES SENSOR SENSITIVITY PARALLEL TO LONGITUDINAL AXIS
↔ – DENOTES DIRECTION OF SENSOR SENSITIVITY IN PITCH-YAW PLANE

Figure 3-43. Location and Sensitive Axes of Vibration Detectors

C05099047
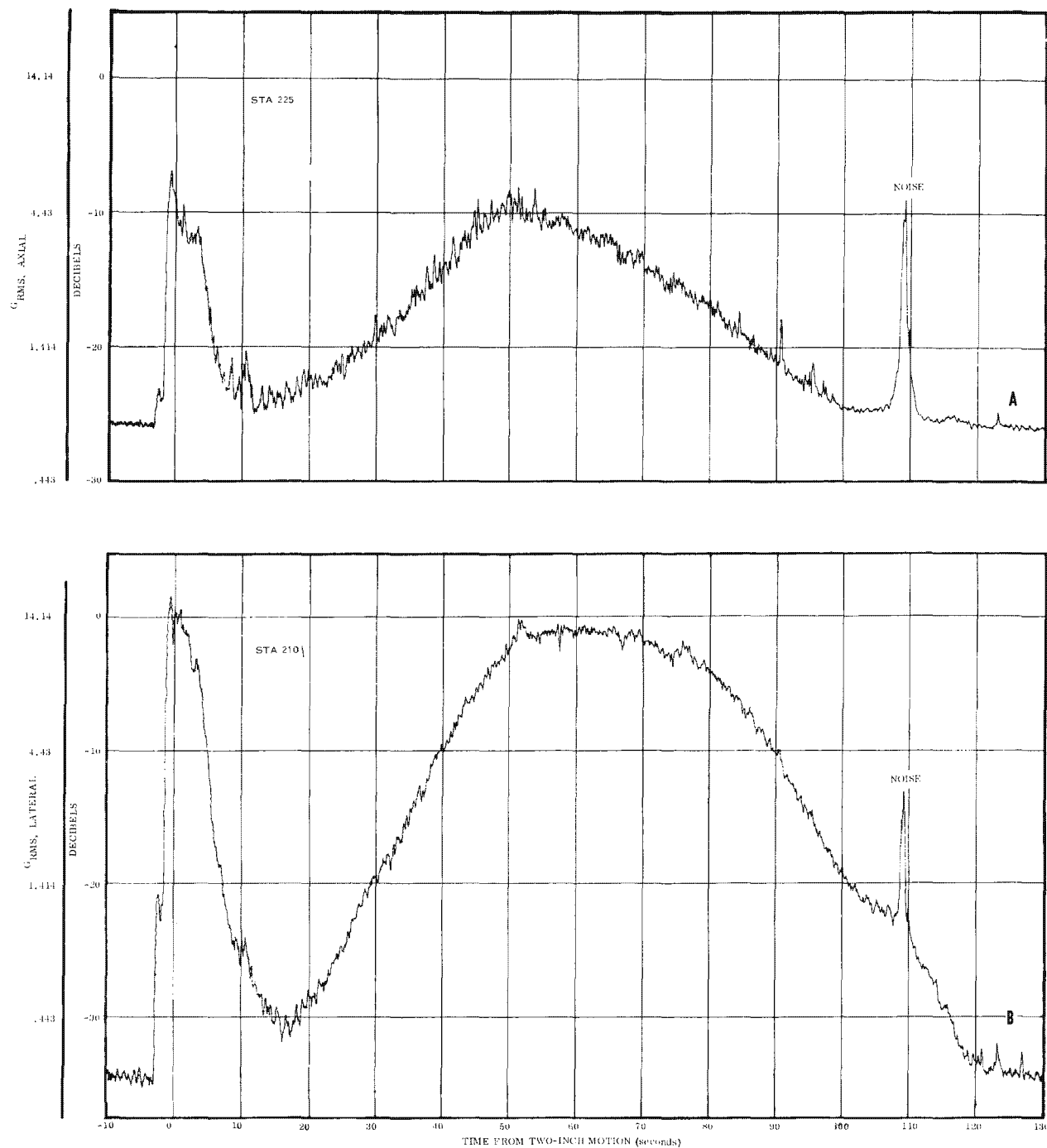
Figure 3-44. Representative Time Histories of Ascent Axial and Lateral Vibration, G_{RMS}

64SD4760

3-128
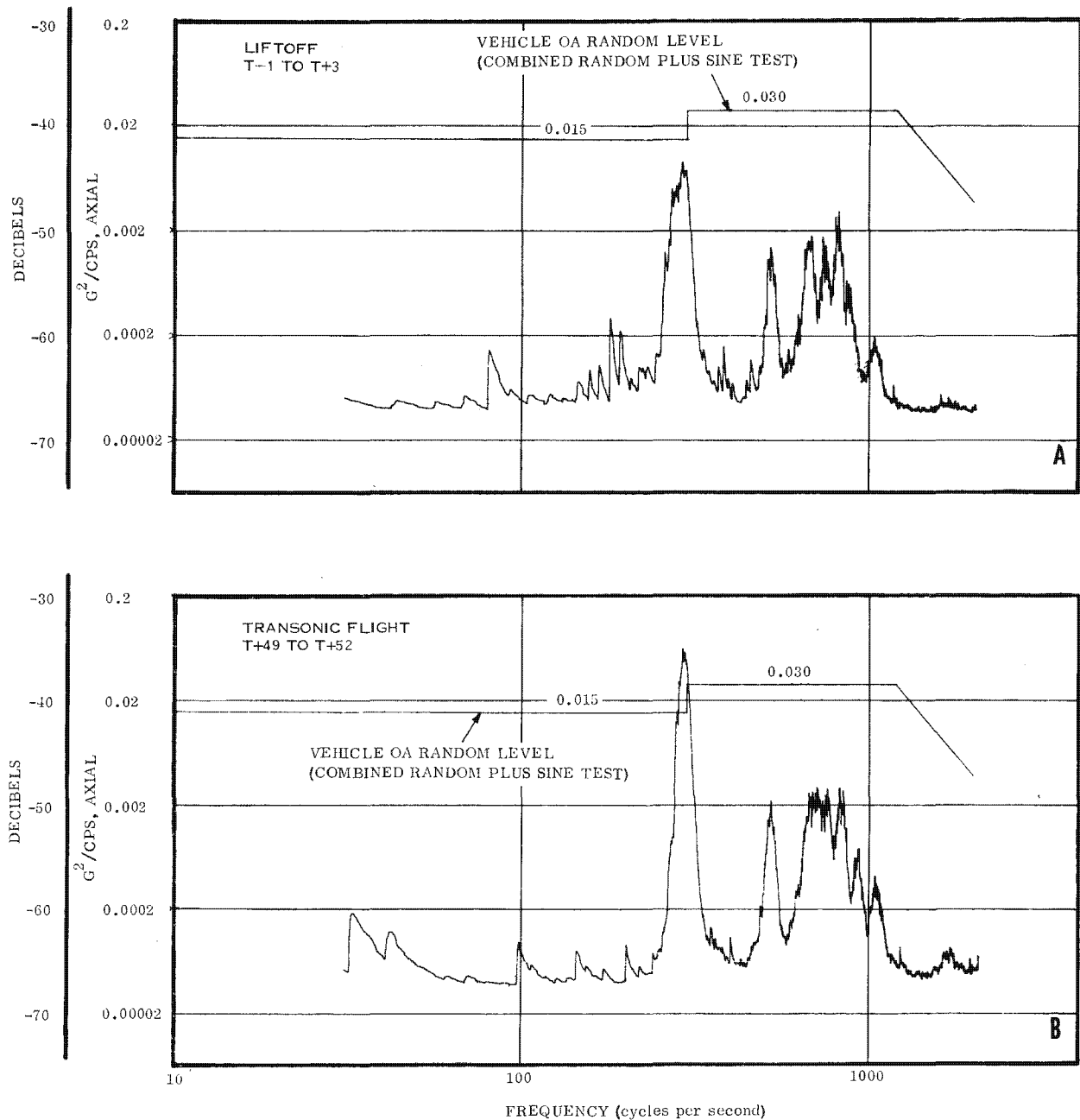
Figure 3-45. Representative Axial Vibration, Power Spectral Densities (Station 225)

64SD4760

3-129
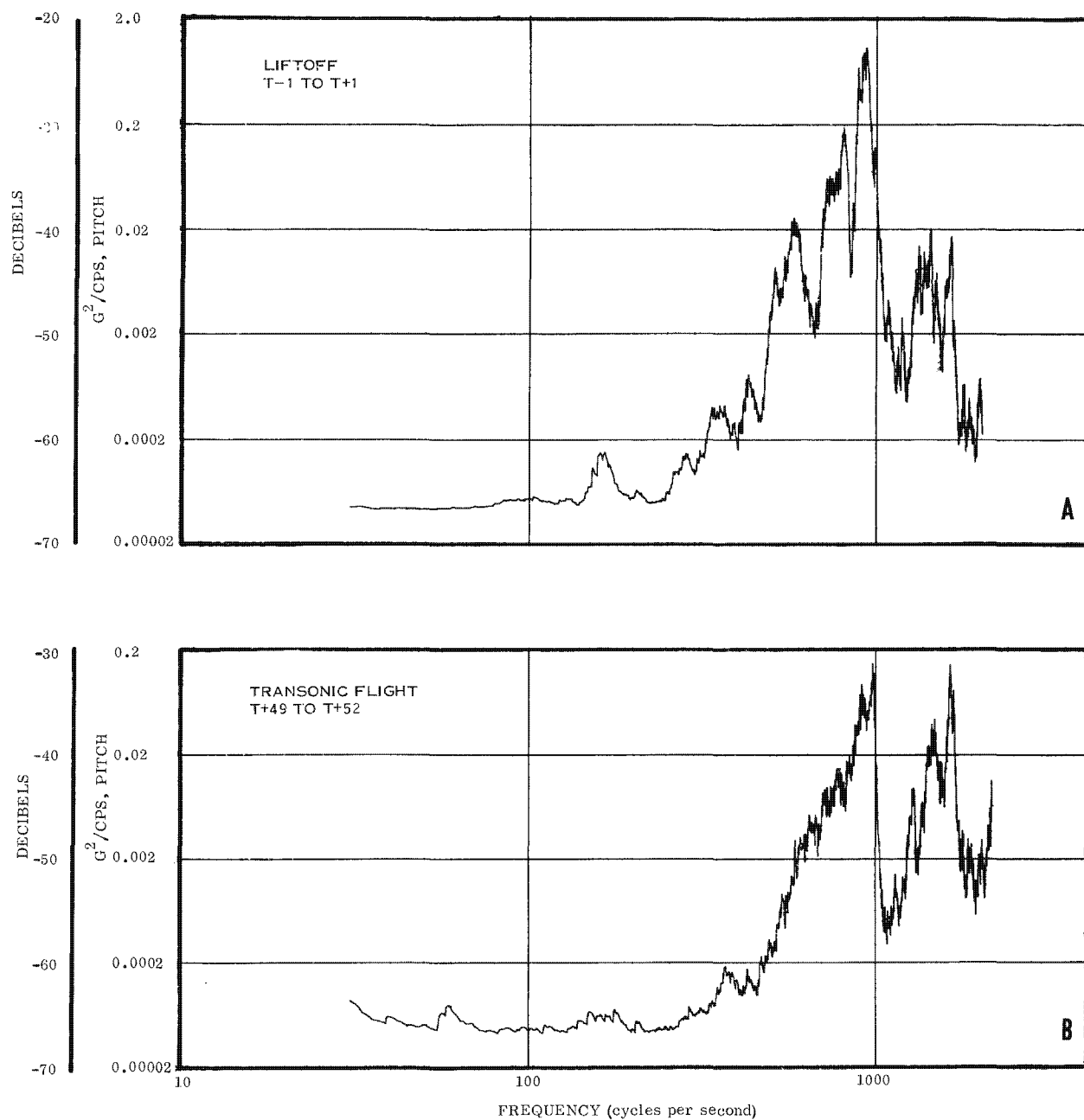
Figure 3-46.   Representative Ascent Lateral Vibration, Power Spectral
Densities (Station 220)

64SD4760

The torsional vibration responses, shown in figure 3-47, were obtained from the sensor located at station 125. The torsional vibration input at the SV-Agena interface, expected to occur at BECO, was of predominant interest on this program. The level of the low frequency component was expected to have been on the order of between 4.5 and 5.0 g's. Flight data has indicated that the disturbance, which is in the 70 cps range, normally occurs 0.2 second after BECO is initiated and lasts for approximately 0.2 second with peak amplitudes not exceeding 2.0 g's.

64SD4760

64SD4760

STATION 125

TIME FROM TWO-INCH MOTION (seconds)

DECIBELS

G_{RMS} (TANGENTIAL)

3-132
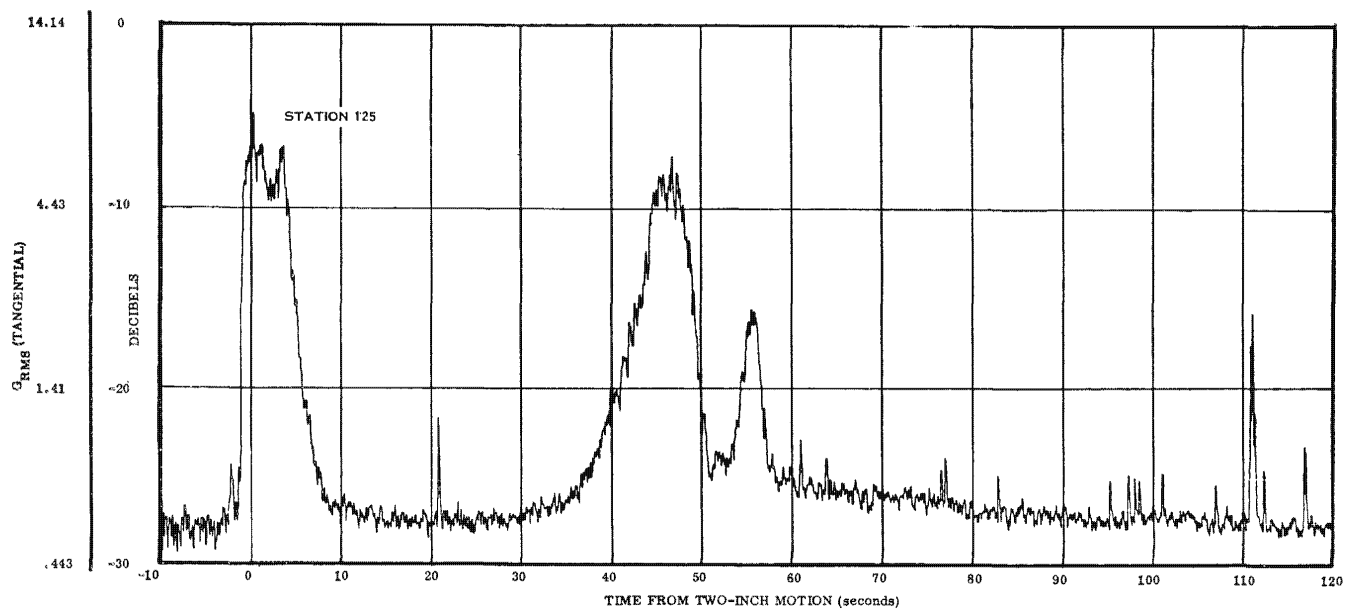
Figure 3-47. Time History of Ascent Tangential Vibrations. G_{RMS}

SECTION 4

SPECIFICATION MATRIX

This section is comprised of a specification matrix which shows the outcome of the observed performance of those subsystem functions which are considered to exemplify vehicle performance. The outcome of those functions whose performance is evaluated in the individual subsystem capability analyses does not appear in the matrix but in the appropriate subsystem sections.

The following key is used in the matrix to denote the outcome of the observed performance of the functions:

M — The performance of each function was observed to meet its specification requirement without exception, given the opportunity to perform.

DNM — The performance of the function was observed not to meet its specification requirement.

N/A — Not applicable or the function did not have an opportunity to perform.

UNK — The outcome was unknown.

For a detailed discussion of the observed performance of each function, refer to the appropriate Final Flight Evaluation Reports (references 5 through 13).

64SD4760

4-1

SPECIFICATION MATRIX

64SD4760

4-2

Subsystem	Function	Specification Requirement	Satellite Vehicle									
			951	952	953	954	955	956	957	958	959	960
Telemetry, Tracking & Command (TT&C)	S-Band PRF	410-612 PPS	M	M	M	M	M	M	M	M	M	M
	Stored Command Execution	As Required	DNM	M	M	M	DNM	M	M	DNM	M	N/A
	Stored Command Timing	± 0.2 sec	M	M	M	M	M	M	M	M	M	M
	Real Time Command Execution	As Required	M	DNM	M	M	M	M	M	M	M	M
	Hybrid Command Execution	As Required	M	M	M	M	M	M	M	M	M	DNM
	Secure Command Execution	As Required	N/A	N/A	M	M	M	M	M	M	M	N/A
	Timer Accuracy	360 ± 45 sec	M	M	M	M	M	M	M	M	M	M
		720 ± 90 sec	M	M	M	M	M	M	M	M	M	M
	Vehicle Clock Offset	± 5.0 cps	M	M	M	M	M	M	M	M	M	M
	Vehicle Clock Drift	± 50.4 ms/24 hr	M	M	M	M	M	M	M	M	M	M
Stabilization	Coarse Mode Attitude Errors											
	Pitch	± 2.0 deg	M	N/A	M	M	M	M	M	M	M	M
	Roll	± 2.0 deg	M	N/A	M	M	M	M	M	M	M	M
	Yaw	± 2.0 deg	M	N/A	M	M	M	M	M	M	M	M
	Coarse to Fine Transfer Time	15.0 sec (max)	M	N/A	M	M	M	M	M	M	M	M
	Pitch Attitude											
	Level Flight	-0.6 deg	M	N/A	M	M	M	M	DNM	N/A	N/A	M
	Pitched Down	-58.6 deg	M	N/A	M	N/A	M	M	DNM	N/A	M	N/A
	Roll Maneuver Rates											
	Low	± 0.25 deg/sec (min)	M	N/A	M	M	M	–	–	–	N/A	M
	Medium	± 1.50 deg/sec (min)	M	N/A	M	M	M	–	–	–	N/A	M
	High	± 3.00 deg/sec (min)	M	N/A	M	M	UNK	–	–	–	N/A	M

C05099047

64SD4760

4-3

SPECIFICATION MATRIX (Cont)

Subsystem	Function	Specification Requirement	Satellite Vehicle									
			951	952	953	954	955	956	957	958	959	960
	Settling Time	6.0 sec (max)	M	N/A	M	M	M	–	–	–	N/A	M
	Cold Gas Impulse	8000 lb-sec (min)	DNM	DNM	M	N/A	M	M	M	N/A	N/A	M
	Mission Life – Pneumatics	5 days	DNM	DNM	M	N/A	M	M	M	N/A	N/A	N/A
Back-Up Stabilization (BUSS)	Temp, F/C Elec.	-30 to +165°F	N/A	N/A	N/A	UNK	M	M	M	M	M	M
	Temp, Pneu. Supply	-100 to +165°F	N/A	N/A	N/A	UNK	M	M	M	M	M	M
	Supply Voltage	22.0 to 29.5 VDC	N/A	N/A	N/A	UNK	M	M	M	M	M	M
	Time to Acquire Attitude	90 sec (max)	N/A	N/A	N/A	UNK	N/A	DNM	M	M	M	M
	Attitude Maintenance	105 sec (min)	N/A	N/A	N/A	UNK	N/A	DNM	M	UNK	M	M
	Sequence of Events	Occur as Required	N/A	N/A	N/A	M	DNM	M	M	UNK	M	M
Electrical Power & Signal Distribution (EP&SD)	Operational Bus Voltage	27.0 to 32.5 VDC	M	M	M	M	–	–	–	M	M	M
	Programmer B/U Battery Voltage	25.5 to 32.4 VDC	M	M	M	M	M	M	M	M	M	M
	Mission Life-Ampere Hours	5 days	M	M	M	M	–	–	–	N/A	N/A	N/A
Satellite Recovery Vehicle (SRV)	Ejection Events	Occur as Required										
	Recovery Events	Occur as Required										
	Retrieval	Air Snatch or Water Recovery				Refer to SRV S/S Section						
	Inhibit Timer Execution	1000 n. mi. (min)										
	Impact Dispersion	±75 n. mi. intrack ±7.7 n. mi. crosstrack										

SPECIFICATION MATRIX (Cont)

Subsystem	Function	Specification Requirement	Satellite Vehicle									
			951	952	953	954	955	956	957	958	959	960
Separation	Baroswitch Closure	55,000 to 95,000 ft	M	M	M	M	M	M	M	M	M	M
	Computer Prearm	Occur as Commanded	M	M	M	M	M	M	M	M	M	M
	SV Separation	Occur as Commanded	M	M	M	M	M	M	M	M	M	M
	BUSS Antenna and Mag. Boom Erection	Occur as Commanded	N/A	N/A	N/A	M	M	M	M	M	M	M
	SRV Separation	Occur as Commanded	M	M	M	M	M	M	M	M	M	M
	Disconnect 1	Occur as Commanded	DNM	M	M	M	M	M	M	M	M	M
	Disconnect 2	Occur as Commanded	M	M	M	M	M	M	M	M	M	M
	SV/Agena Separation Velocity	0.5 to 1.5 FPS	M	M	M	M	M	M	M	M	M	UNK
	SRV/OCV Separation Velocity	1.5 to 1.9 FPS	M	M	M	M	M	UNK	M	UNK	M	M
Environmental Control	Temp. RF Pwr Amp	0 to 160°F	M	M	M	M	M	M	M	M	M	M
	Temp., A/B Recorder	0 to 120°F	M	M	M	M	M	M	M	N/A	M	M
	Temp., Dec/Prog. Mount Plate	30 to 110°F	M	M	M	M	M	M	M	N/A	M	M
	Temp., DCPS	-20 to 160°F	M	M	M	M	M	M	M	M	M	M
	Temp., TARS E/P Int.	18 to 135°F	M	M	M	M	M	M	M	N/A	M	M

SPECIFICATION MATRIX (Cont)

Subsystem	Function	Specification Requirement	Satellite Vehicle									
			951	952	953	954	955	956	957	958	959	960
	Temp., RAGS Gyros	162.5 to 167.5°F	UNK	UNK	M	DNM	DNM	M	M	N/A	M	M
	Temp., TARS Gyros	162.5 to 167.5°F	M	M	M	M	M	M	M	N/A	M	M
	Temp., Operational Batteries	40 to 100°F	UNK	UNK	M	M	M	M	M	M	M	M
	Ox/Fuel Diff. Temp.	±20°F	N/A	N/A	M	M	M	M	M	M	M	M
Orbit Adjust (O/A)	Total Impulse	60,000 lb-sec (min)	N/A	N/A	M	N/A	M	M	M	N/A	N/A	N/A
	Accuracy	±1/2 FPS or 5% whichever is larger	N/A	N/A	M	N/A	M	M	M	M	UNK	N/A
	Thrust	48 ±2.5 lbs	N/A	N/A	-	N/A	-	-	-	-	UNK	N/A
	Acceleration	.67 ft/sec² (min)	N/A	N/A	M	N/A	M	M	M	M	UNK	N/A

64SD4760

4-5/4-6

REFERENCES

1. "System Test Objectives", Aerospace Corporation, DIN AS-64-0000-00555.

2. "Field Test Processing Summary, SV 960", GE-ASPD, FTPS - SV 960.

3. "Preliminary Flight Evaluation Report", Aerospace Corporation, DIN AS-64-0000-03073.

4. "Next Flight Analysis Summary Report (TWX), SV 960", GE-ASPD, DIN 6035-42-4.

5. "Final Flight Evaluation Report, SV 951", GE-ASPD, DIN 63SD4751.

6. "Final Flight Evaluation Report, SV 952", GE-ASPD, DIN 63SD4752.

7. "Final Flight Evaluation Report, SV 953", GE-ASPD, DIN 63SD4753.

8. "Final Flight Evaluation Report, SV 954", GE-ASPD, DIN 64SD4754.

9. "Final Flight Evaluation Report, SV 955", GE-ASPD, DIN 64SD4755.

10. "Final Flight Evaluation Report, SV 956", GE-ASPD, DIN 64SD4756.

11. "Final Flight Evaluation Report, SV 957", GE-ASPD, DIN 64SD4757.

12. "Final Flight Evaluation Report, SV 958", GE-ASPD, DIN 64SD4758.

13. "Final Flight Evaluation Report, SV 959", GE-ASPD, DIN 64SD4759.

14. "Subsystem Design Requirements - TT&C", GE-ASPD, DIN SVS 3969D.

15. "Post Flight Best Fit Ephemeris, FTV 3802", Aerospace Corporation, DIN VE-64-0000-00487.

64SD4760

R-1/R-2